"Design and Application of Continuous Magnetic Extraction"

zur Erlangung des akademischen Grades eines
DOKTORS DER INGENIEURWISSENSCHAFTEN (Dr.-Ing.)

der Fakultät für Chemieingenieurwesen und Verfahrenstechnik des
Karlsruher Instituts für Technologie (KIT)

genehmigte
DISSERTATION

von
Dipl.-Ing. Ingo Fischer
aus Pforzheim

Referent: Prof. Dr.-Ing. Matthias Franzreb

Korreferent: Prof. Dr. rer. nat. Christoph Syldatk

Tag der mündlichen Prüfung: 24. Juli 2013

„Der Mensch hat drei Wege, zu lernen:
Erstens durch Nachdenken, das ist der edelste. Zweitens durch Nachahmen,
das ist der leichteste und drittens durch Erfahrung, das ist der bitterste.“

Konfuzius

Danksagung

Die vorliegende Arbeit entstand in den Jahren 2009 – 2013 am Institut für Funktionelle Grenzflächen am Karlsruher Institut für Technologie – Campus Nord. An dieser Stelle möchte ich mich bei allen Personen bedanken, die zum Gelingen dieser Dissertation beigetragen haben.

Ganz besonderer Dank gilt meinem Betreuer Prof. Dr. –Ing. Matthias Franzreb für die hervorragende Betreuung, die freundschaftliche Arbeitsatmosphäre, das große Vertrauen und den Freiraum eigene Ideen zu verfolgen.

Herrn Prof. Dr. Christoph Syldatk danke ich herzlich für die Übernahme des Korreferats.

Bei den Mitgliedern des EU Projektes MagPro²Life möchte ich mich für die gute Zusammenarbeit bedanken, insbesondere bei Prof. Owen Thomas für die schöne Zeit während des Aufenthalts als Gastwissenschaftler an der Universität Birmingham.

Großer Dank gebührt Anna-Lena Walde, Christian Morhardt und Markus Gärtner, die im Rahmen ihrer Praktika bzw. Diplomarbeiten einen großen Beitrag zum Gelingen dieser Arbeit geleistet haben. Desweiteren möchte ich mich bei Mike Füssler für die technische Umsetzung von manch schräger Idee bedanken.

Den Menschen aus meiner Arbeitsgruppe, die mich innerhalb der 3 Jahre ein Stück weit begleitet haben, möchte ich für viel Spaß, witzige Gespräche und ab und an sogar fachliche Diskussionen danken, insbesondere bei Birgit Hetzer, Christine Müller, Jens Bolle, Martín Silvestre, Tobias Müller, Stephanie Ewert, Jonas Wohlgemuth, Nils Danckwardt, Anja Paulus und Ellen Biegert.

Besonders bedanken möchte ich mich bei Ebru Diler für intensives Korrekturlesen und eine außergewöhnliche Zeit im und außerhalb des Labors.

Letztlich möchte ich mich bei allen hier nicht genannten Freunden und meiner Familie für ihre langjährige Unterstützung bedanken.

Abstract

The application of magnetic particles has been considered a promising alternative to conventional primary capture processes in downstream processing throughout the last years. By use of the particles, solid-liquid separation and the primary capture step can be integrated into one process. Up to now, however, the separation of magnetic particles in technical scales has only been possible through High Gradient Magnetic Fishing (HGMF) in a batch-wise fashion.

In this work, a continuous process for the separation of functionalized magnetic particles has been developed based on the combination of magnetic nanoparticles and aqueous micellar two-phase systems (AMTPS). This combination is referred to as *magnetic extraction*. AMPTS consist of micellar solutions and exhibit thermoresponsive behavior, which means that they split into a micelle-rich and a micelle-poor phase upon temperature increase. Components added to an AMTPS partition between the two phases based on their unique physico-chemical properties.

In the course of magnetic extraction, a target protein is first bound to the magnetic particle. Then, the temperature is raised to induce phase separation. The magnetic carriers partition completely into the micelle-rich phase of the AMTPS due to their physico-chemical properties. The time required for phase separation is thereby fundamentally increased by means of an external magnetic field. The micelle-poor phase is withdrawn, and thus all components which neither bound to the particles nor partitioned into the micelle-rich phase. In the subsequent step, the target protein is eluted from the magnetic particle. During the elution, the system remains under single-phase conditions. Afterwards, the system is split again. The target proteins then partition into the micelle-poor phase while the magnetic carriers partition into the micelle-rich phase. As a result of this process, a magnetic particle-free phase with a low micelle concentration containing the target protein and a magnetic particle-concentrated phase containing most of the micelles are obtained. While the target protein can be withdrawn, the magnetic particle and micelle-rich phase can be recycled within the next process step and used again.

In the first part of the thesis, the analytics of the AMTPS-forming nonionic surfactants - which are required for a proper process control and optimization - were established. Considering a continuous process, fast reliable process monitoring of the phase-forming surfactant in the presence of proteins and magnetic carriers is required. A titration method was established that rendered possible both a robust detection of the temperature-dependent phase diagram and the off-line monitoring of the surfactant concentration in a continuous process.

In the next step of the process development, optimal combinations of magnetic carriers and AMTPS were investigated. As ideal AMTPS-forming surfactant, Eumulgin ES was identified in combination with 100 nm-sized magnetic cation exchange particles. AMTPS based on Eumulgin ES exhibit advantageous partitioning characteristics: Due to a high concentration of the surfactant in the micelle-rich phase (up to 70%), dissolved biological components were almost completely excluded from the micelle rich-phase. The model proteins ovalbumin and lysozyme exhibited partitioning coefficients of < 0.1 and 0.12, respectively. This partitioning behavior is favorable in two ways: During separation of the particles following the binding step, almost all undesired components are withdrawn in the micelle-poor phase as waste. During phase separation after the elution of the target protein, it is partitioned into the micelle poor-phase and excluded from the micelle-rich phase, leading to both, high yields and high purities in the eluate. The particles were characterized by means of adsorption isotherms in the presence and absence of the phase-forming surfactant, revealing an influence of the surfactant onto the maximum particle capacity. This influence was, however, attributed to unspecific binding, as the amount of eluted protein remained the same.

At the beginning of this work, the mechanism which drives the particles exclusively into the micelle-rich phase of an AMPTS was mainly unclear. In order to gain insight into this mechanism, the surface interactions between the particles and the phase-forming surfactants were investigated by means of modern surface analytical methods. The aim of the investigation was to reveal the varying partitioning behavior of the magnetic particles with varying buffer conditions. Therefore, the "online" monitoring of surfactant adsorption onto model surfaces was performed by means of Quartz Cristal Microbalance

with Dissipation (QCM-D). Furthermore, the surface of the particles was investigated using non-invasive Attenuated Total Reflectance Fourier Transform Infrared Spectroscopy (ATR-FTIR). In order to correlate the results obtained from these physico-chemical experiments with particle experiments more practically relevant, classic adsorption and elution experiments were performed. The results from all methods led to the same conclusion: The partitioning behavior of the particles is dominated by the adsorption of the hydrophilic head of the surfactants to the particle surface. When the surfactants were adsorbed to the particle surface, these particles were completely enriched in the micelle-rich phase. If the surfactants were not adsorbed, the particles partitioned completely into the micelle poor phase. The adsorption of the surfactants to the hydrophilic surface was attributed to hydrogen bonds between the surface of magnetic particles and the hydroxyl or oxygen groups of the surfactants.

Finally, an apparatus for the continuous processing of magnetic extraction was designed. The core of this apparatus is a settling tank with a volume of 2.28 liters surrounded by a permanent magnet. To maintain the required phase separation temperature, these components are placed in the inside of a temperature-controlled, isolated box. The binding step is accomplished in a large temperature-controlled mixer at single-phase conditions outside of the separator. Then, the broth is heated by passing a heat exchanger. This leads to the formation of a dispersed surfactant-rich and a continuous surfactant-depleted phase, and the stream is injected into the settling tank. The phases separate while passing through the magnetic field-surrounded separator. The removal of the top phase is realized by means of a weir, while the bottom phase is withdrawn by a pump directly connected to the settler, and both phases are collected separately. This continuous magnetic separator allows the continuous separation of magnetic particles having mean diameters ranging from 100 nanometers to 2 micrometers at flow rates up to 9 liters per hour with particle separation efficiencies of > 99 %. Finally, continuous magnetic extraction was applied for purification of the antibody fragment Fab α33 from a "real" biosuspension. The purification was performed with a total initial feed volume of 14.8 liters with a fab purity of 16 %. Three consecutive process steps were performed: Binding of the target product, intermediate washing of the phases, and elution of the Fab α33. The elution yielded in a fraction of 5 liters with a Fab purity of > 98 % and a total

yield of 67 %. The cumulative loss of magnetic particles was approximately 1 % of the initial amount.

In order to remove the remaining phase-forming surfactant from the magnetic extraction eluate phase, its removal by means of cross-flow ultrafiltration was investigated. Upon applying polyethersulfone membranes, the nonionic surfactant was almost entirely removed from the proteinaceous solution. Although the molecular weight cut-off (MWCO) of the membranes was smaller than the size of a theoretical micelle, the surfactants passed the membranes unhindered. This effect was attributed to the adsorption of single surfactant molecules to the membrane pores, which was confirmed by a rapid congruent decrease of the flow rate through the membrane. By means of a PES membrane with a MWCO of 10 kDa, a further purification of the Fab α33 from the continuous magnetic extraction was obtained. While > 96 % of the remaining surfactant could be removed in the filtrate, the antibody fragment Fab α33 was retained in the retentate.

Zusammenfassung

Die Verwendung von funktionalisierten magnetischen Partikeln wird bereits seit einigen Jahren als vielversprechende Alternative zu konventionellen Prozessen im Downstream Processing gesehen. Durch die Partikel lassen sich die Fest-flüssig Trennung und ein primärer Aufreinigungsschritt zu einem einzigen Prozessschritt zusammenfassen. Allerdings war die Abtrennung der magnetischen Partikel im technischen Maßstab bisher lediglich absatzweise durch Hochgradienten-Magnetseparatoren möglich.

Im Rahmen der vorliegenden Arbeit wurde ein kontinuierliches Verfahren zur Abtrennung funktioneller Magnetpartikel entwickelt, das auf der Kombination des Einsatzes der Partikel mit dem Einsatz von mizellaren wässriger Zweiphasensysteme (AMTPS) beruht. Diese Kombination wird als *magnetische Extraktion* bezeichnet. AMTPS bestehen aus einer Lösung eines nichtionischen Tensids und zeigen ein temperatursensitives Verhalten, d.h. sie zerfallen bei der Überschreitung einer kritischen Temperatur in zwei wässrige Phasen, wobei eine mizellreiche und eine mizellarme Phase entsteht. Substanzen, die in ein AMTPS eingebracht werden, verteilen sich anhand ihrer physikochemischen Eigenschaften zwischen den beiden entstehenden Phasen.

Im ersten Schritt des Verfahrens der magnetischen Extraktion wird ein Zielmolekül über einen selektiven, reversiblen Mechanismus an den Magnetpartikel gebunden. Anschließend wird die Temperatur derart erhöht, dass das Gesamtsystem in eine mizellreiche und eine mizellarme Phase zerfällt. Aufgrund der Eigenschaften der magnetischen Partikel reichern sich diese in der mizellreichen Phase an. Durch das Anlegen eines externen Magnetfeldes wird zudem die Zeit, die für die Phasentrennung benötigt wird, stark verkürzt. Die mizellarme Phase wird nun entfernt und damit alle Komponenten, die nicht an den Magnetpartikeln gebunden sind oder sich in der mizellreichen Phase befinden. Im nächsten Schritt wird das Zielprotein im einphasigen Systemzustand wieder vom den magnetischen Partikeln eluiert und die Phasen anschließend abermals durch Temperaturerhöhung getrennt. Das Zielprotein kann nun in der mizellarmen Phase abgezogen werden, während sich die Magnetpartikel wiederum in der mizellreichen Phase sammeln. Die mizellreiche Phase inklusive Magnetpartikel

können daraufhin rezykliert und zu unbehandelter Biorohsuspension gegeben werden, wobei die Partikel zur Bindung der Zielproteine und die Mizellen für die Phasenseparation genutzt werden.

Im ersten Teil dieser Dissertation wurde die für die Prozesskontrolle und -optimierung notwendige Analytik der phasenbildenden Tenside etabliert. Die Erfassung der Tensidkonzentrationen im Verlauf des Prozesses erfordert eine robuste Methode, die nicht durch die Präsenz von Proteinen oder magnetischen Sorbentien gestört wird. Eine Methode, die auf potentiometrischer Titration beruht, erfüllt diese Kriterien und ließ sich dabei sowohl zum Erstellen des temperaturabhängigen Phasendiagrams als auch zum offline Prozess-Monitoring verwenden.

Während der Prozessentwicklung wurden geeignete Kombinationen aus magnetischen Partikeln und AMTPS untersucht. Als ideales phasenbildendes Tensid wurde dabei das nichtionische Tensid Eumulgin ES in Verbindung mit 100 Nanometer großen magnetischen Kationenaustauschpartikeln identifiziert. AMTPS, die mit diesem Tensid gebildet werden, zeichnen sich durch extreme Verteilungskoeffizienten aus. Aufgrund des extrem hohen Tensidanteils in der mizellreichen Phase (mehr als 70 %) werden gelöste Proteine beinahe vollständig aus dieser Phase ausgeschlossen. Der Verteilungskoeffizient der Modellproteine Ovalbumin und Lysozym in einem Eumulgin ES basierten AMTPS belief sich dabei auf < 0,1 beziehungsweise 0,12. Dieses extreme Verteilungsverhalten ist für den Prozess der magnetischen Extraktion in doppelter Hinsicht von Vorteil: Während der Phasentrennung im Anschluss an den Bindeschritte werden beinahe alle kontaminierenden Proteine aus der mizellreichen Phase ausgeschlossen und somit mit der mizellarmen Phase verworfen. Im Verlauf der Phasentrennung nach der Elution reichert sich das Zielprotein dann nahezu vollständig in der mizellarmen Phase an und wird somit in einer hohen Ausbeute und mit einer hohen Reinheit aus dem Prozess abgeführt. Die Adsorptionseigenschaften der magnetischen Kationenaustauschpartikel wurden für den Fall der Proteinbindung in An- und Abwesenheit der phasenbildenden Tenside verglichen. Es stellte sich heraus, dass die Tenside die Bindekapazität der Partikel zwar herabsetzen, dies jedoch auf unspezifische Wechselwirkungen an der

Partikeloberfläche zurückzuführen ist, denn die Proteinmenge, die sich von den Partikeln eluieren ließ, blieb unverändert.

Der Mechanismus, der die Partikel dazu veranlasst, sich ausschließlich in der mizellreichen Phase des AMTPS anzureichern, war zu Beginn der Arbeit weitgehend ungeklärt. Um Aufschluss darüber zu erhalten, wurden die Interaktionen der phasenbildenden Tenside mit der Oberfläche der Magnetpartikel mit modernen oberflächenanalytischen Methoden untersucht. Ziel war die Aufklärung des stark pufferabhängigen Verteilungsverhaltens der Magnetpartikel in AMTPS. Dazu diente einerseits das „online"-Monitoring des Anlagerungsvorgangs der Tenside an Modelloberflächen mittels einer Quarzkristall-Mikrowaage mit Dissipationsmodul. Andererseits wurde die Oberfläche von Magnetpartikeln nach Anlagerungsversuchen unter verschiedenen Bedingungen mittels der Fourier Transformierten Infrarotspektroskopie unter Abgeschwächter Totalreflektion untersucht. Zur Korrelation der Ergebnisse der physikochemischen Untersuchungsmethoden mit anwendungsnahen Versuchen erfolgten schließlich klassische Adsorptions- und Elutionsversuche. Alle verwendeten Methoden ließen dabei denselben Schluss zu: Das Verteilungsverhalten der Partikel basiert auf der Adsorption der Tenside auf der Oberfläche der Partikel. Unter Bedingungen, bei denen die Tenside an den Partikel- bzw. Referenzoberflächen adsorbierten, wanderten die Partikel vollständig in die mizellreiche Phase des AMTPS. Im Umkehrschluss wanderten die Partikel bei Bedingungen, bei denen die Tenside nicht an deren Oberfläche adsorbierten vollständig in die mizellarme Phase. Die Adsorption der nichtionischen Tenside an die hydrophilen Partikel wurde dabei auf die Entstehung von Wasserstoffbrückenbindungen zwischen den hydrophilen Oberflächengruppen der Partikel und den Hydroxyl- oder Sauerstoffgruppen des hydrophilen Anteils der Tenside zurückgeführt.

Zur technischen Umsetzung der magnetischen Extraktion wurde eine Anlage für den kontinuierlichen Betrieb der Separation entwickelt. Das Herzstück der Anlage besteht aus einem 2,28 Liter fassenden Abscheider. Dieser ist in einen Permanentmagneten eingebracht. Abscheider und Magnet befinden sich in einer temperaturregulierten, isolierten Kammer, um die für die kontrollierte Phasentrennung benötigte, konstante Temperatur zu gewährleisten. Der Adsorptionsschritt erfolgt in einem gekühlten

Doppelmantelreaktor unter Rühren außerhalb dieser Apparatur. Innerhalb des Reaktors wird die Temperatur so eingestellt, dass es nicht zur Phasentrennung kommt. Vom Reaktor wird der Strom dann durch einen Wärmetauscher in den Abscheider gepumpt, wodurch es zu einer raschen Ausbildung einer fein dispergierten, tensidreichen Phase sowie einer tensidarmen kontinuierlichen Phase kommt. Beim Durchlaufen des Magnetfeld-unterstützten Abscheiders werden diese beiden Phasen kontinuierlich getrennt. Die Ausschleusung der Oberphase erfolgt durch ein Überlaufwehr, während die Unterphase abgepumpt wird. Der Separator ermöglichte eine kontinuierliche Prozessführung und die Abtrennung von magnetischen Partikeln mit einer Abscheideeffizienz von über 99,8 % - bei Flussraten bis zu 9 Litern pro Stunde. Diese Abscheideeffizienz wurde für verschiedene Partikelchargen mit mittleren Durchmessern von 100 Nanometern bzw. 2 Mikrometern erreicht. Abschließend wurde die Apparatur zur magnetischen Extraktion des Antikörperfragments Fab α33 aus einer Biorohsuspension verwendet. Das Volumen der Ausgangslösung zur Reinigung dieses Fragments betrug dabei 14,8 Liter mit einer Reinheit von 16 %. Drei aufeinanderfolgende Prozessschritte wurden durchgeführt: Das Binden des Zielproteins an magnetische Kationenaustauschpartikel, ein Waschschritt zur Entfernung der restlichen Unterphase aus dem Bindeschritt und letztlich die Elution des Antikörperfragments in die neu gebildete Unterphase. Das Volumen der Elutionsfraktion belief sich letztlich auf 5 Liter. Die erzielte Reinheit in der Elutionsfraktion betrug über 98 % und die Gesamtausbeute 67 %. Der kumulative Partikelverlust aus allen 3 Prozessschritten betrug dabei 1 % der ursprünglich eingesetzten Partikelmenge.

Die Entfernung der verbliebenen phasenbildenden Mizellen aus der erhaltenen Elutionsfraktion wurde mittels Cross-Flow Ultrafiltration untersucht. Beim Einsatz von Membranen aus Polyethersulfon konnten die Tenside die Membran vollständig permeieren, obwohl die theoretische Mizellgröße deutlich größer als die molekulare Ausschlussgröße der Membran war. Dieser Umstand deutet auf die Adsorption der einzelnen Tensidmoleküle an die Membranoberfläche und die Poren der Membran hin. Diese Annahme wird bekräftigt durch die Tatsache, dass der Transmembranfluss beim Kontakt mit tensidhaltigen Lösungen drastisch sinkt. Dieser Effekt ist jedoch reversibel. Durch den Einsatz einer PES Membran mit einem molekularen Größenausschluss von

10 kDa wurde das verbleibende Tensid von dem Antikörperfragment Fab α33 getrennt. Während das Antikörperfragment von der Membran zurückgehalten wurde, ließen sich mehr als 96 % der Tenside entfernen.

Index

1 Introduction

Today, a vast number of pharmaceutical active ingredients are biotechnologically fabricated proteins or polypeptides, like antibodies or enzymes. Due to their molecular structure, these molecules are as much complex as they are fragile. The maintenance of their three-dimensional structure, however, during the processing is crucial for their biological activity. Especially, when it comes to purification (downstream processing) of such bioactive substances after their production, this is a challenging task. Unit operations that would require high temperatures, pressure or the use of organic solvents cannot be applied due to the instability of the target product. In addition to this, the molecule of interest is often accompanied by a huge number of molecules having similar properties, as, e.g. during the fermentative production of a protein, also the housekeeping genes are expressed by the host cells. In addition to that, the final purities of biopharmaceuticals required are very high. For these reasons the cost of the downstream processing usually makes up the lion´s share (up to 80 %) of the total cost in biopharmaceutical productions.

Up to now, multi-stage liquid column chromatography is the state of the art process for gentle purification of biomolecules. Chromatography has been applied for more than 100 years now and allows high resolutions and, concomitant, high purities of the target product. Chromatographic separations, however, require the preceding clarification of the initial feed, as solids can block the chromatographic column, leading to extreme pressure drop, and in the end failure of the whole process. For that reason preceding decantation, centrifugation and filtration steps have to be integrated, with each additional unit operation reducing the total yield of the target protein. In addition to that, large amounts of buffers and water are consumed in the course of chromatographic processes.

Given these challenges, alternative routes for the direct purification or capture of the target protein from the initial feed streams have been under investigation for many years. One of these alternative routes, discussed since the 1950´s, is the use of so called aqueous two-phase systems (ATPS) or aqueous micellar two-phase systems (AMTPS).

These systems are generated by mixing polymers and/or salts (ATPS) or by the addition of certain classes of surfactants and increasing the temperature (AMTPS). They are composed mainly of water providing a gentle environment for biomolecules. The biphasic systems can be applied to selectively extract target molecules into one of the two emerging phases, with the accumulation of the (solid and dissolved) contaminants in the other phase or at the interphase. Another route for the direct capture of a molecule of interest is the application of functionalized magnetic particles. These particles can exhibit the same functional groups used in column chromatography. Functionalized magnetic particles can be added directly to the initial feed and selectively separated by means of magnetic forces. The adsorbed components are subsequently eluted into a new, clarified stream.

A combination of both of these promising routes has been demonstrated for ATPS by a workgroup in Japan in 1995. For AMTPS, it has been demonstrated by our workgroup in batch mode in 2009, and termed magnetic extraction. Magnetic extraction benefits from the synergy effects of both, the simple scalability of AMTPS and the versatility of functionalized magnetic particles.

1.1   Outline of the Thesis

The goal of this work was the design and the application of a process for continuous magnetic extraction (CME). The principle of CME is based on the addition of functionalized magnetic sorbents and AMTPS forming surfactants to a particular biological feed solution that contains a target protein (or macromolecule). AMTPS form a single phase at low temperatures but upon temperature increase they split into two phases – a surfactant rich and a surfactant depleted phase.

In the first step, the target protein binds to the magnetic nanoparticle due to the functional ligand at the particle surface. In the subsequent step the magnetic sorbents are separated from the remaining feed solution by selective partitioning in the micelle rich phase of the AMTPS. The separation is hereby performed in a continuous fashion: The broth is heated to induce phase separation and subsequently injected into a separator. The separator is set up so as to maintain the temperature, therefore it is isolated by a

polystyrene case and additionally supplemented with a heater. Due to the elevated temperature the system undergoes phase separation while passing through the separator. The magnetic carriers are enriched in the dispersed phase due to the formation of magnetic particles-doped micellar droplets form by the splitting of the phase. An external magnetic field is applied in order to enhance both the migration velocity of the micellar droplets and the droplet coalescence. Finally, two streams leave this magnetic settler- the magnetic particle clarified and surfactant depleted phase and the surfactant enriched phase which contains the magnetic carriers. In order to perform an entire bio-purification procedure, the separation is repeated twice - to wash the particles and to elute the target protein from the particles into the micelle poor phase. Finally, the elution step yields in two streams: The micelle depleted stream which contains the target protein and the micelle rich phase containing the magnetic sorbents. The latter can subsequently be applied to the next binding step. The principle of one CME step is depicted by Figure 1.1.
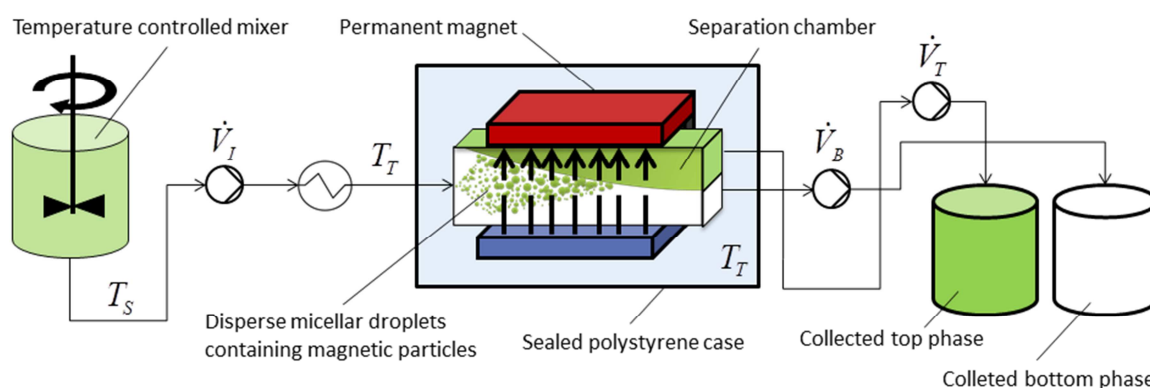
Figure 1.1: Principle of Continuous Magnetic Extraction. In the temperature controlled mixer adsorption of the target protein to the magnetic sorbent is performed at a temperature of single-phase conditions. The broth is processed through a heat exchanger in oder to induce phase separation and subsequently injected into the settler. The settler is surrounded by a permanent magnet. Within the settler the phases separate. Both, magnetic particle and micelle rich top phase and micelle and particle depleted bottom phase are collected.

In order to achieve the goal of a robust CME process, the first step was the establishment of appropriate surfactant analytics from which the required process phase diagrams can be obtained in a rapid, reliable fashion. Additionally, a possibility for online or at least rapid off-line detection needed to be realized. The next step was the detection of suitable combinations of magnetic sorbents and phase forming surfactant. This combination

required: a) complete partitioning of the magnetic sorbents into the micelle enriched phase of the AMTPS independent from the binding and elution conditions and b) exclusion of other feed components from the micelle rich phase. For the establishment of such a reliable combination, a further task was the investigation of the mechanisms of the partitioning of the magnetic sorbents in the AMTPS. With this knowledge, an apparatus was to be developed that allowed continuous operation of the CME with flow rates in the liters-per-hour scale. The hydrodynamic properties in terms of maximum throughput, separation efficiency and stability of the separation process had to be investigated. Using the optimized process parameters, CME was applied to target a real bioseparation, in particular the purification of the antibody fragment Fab α33 produced from an *E. coli* fermentation. As CME results in a target product stream that contains remaining phase forming surfactants, the final task of this thesis was to establish a procedure for the separation of the phase forming surfactant from the target protein.

2 Theoretical Basics

2.1 Magnetic Separation in Downstream Processing

2.1.1 Application of Functionalized Magnetic Beads in Protein Separation

The isolation and purification of proteins, peptides or other specific molecules by means of magnetic particles is a simple and versatile technique. Due to the magnetic character of the particles and the diamagnetic properties of the aqueous bio-feedstock, the particles can be selectively separated by the application of a magnetic field. By means of magnetic separation target molecules bound onto a magnetic bead can be separated directly, e.g. from cell lysates, whole blood, plasma, milk, whey, urine or cultivation media [1]. The striking advantage of magnetic separation cf. traditional packed bed chromatography is that no preceding clarification is required, thus magnetic separation is a splendid example for process integration. In addition to this, relatively little equilibration and washing buffer is required in contrast to column chromatography. The biochemical binding mechanisms, however, follow the same principles than those in conventional packed bed chromatography, therefore, all combinations of ligands and magnetic particles are possible for the surface modification of the magnetic carriers, e.g. ion exchange, affinity or hydrophobic interactions. Among the products purified are enzymes, antibodies, DNA, whole cells or peptides. Detailed reviews about the application of magnetic sorbents in bioseparation can be found e.g. from Safarik [1] or Franzreb [2].

Due to the non-porous character of the small magnetic particles, the adsorption of the target protein to the particle surface is not limited by pore diffusion and therefore the particles exhibit fast binding kinetics and high loading capacities. The binding properties of magnetic carriers are usually described by the binding model according to Langmuir [3]:

The model accounts for a process where the rate of sorption and desorption of a specific component have reached equilibrium (described with *). Furthermore it is stated that the surface is covered with a monolayer of the compound. In this state, the correlation

between the coverage of the surface, or loading q^* and the equilibrium concentration c^* is described by:

$$q^* = q_{max} \cdot \frac{c^*}{K_L + c^*}$$

[Eq. 2.1]

In Equation 2.1 q_{max} describes the maximum capacity of the component and the constant K_L describes the affinity of the component to the surface. In a sorption process the mass balance of the target component in solution and bound to the particle at any time is given by:

$$q = q_0 + \frac{c_0 - c}{c_P}$$

[Eq. 2.2]

The initial loading of the particle is given by q_0, actual loading of the particle is described by q, the initial concentration c_0 and the actual concentration in the solution is c.

When the sorption equilibrium is achieved both, Equation 2.1 and 2.2 are valid. The equilibrium concentration can then be calculated by combining 1 with 2 (based on [4]) to:

$$c^* = -\frac{a}{2} + \sqrt{\frac{a^2}{4} - b}$$

[Eq. 2.3]

with:

$$a = c_P \cdot (q_{max} - q_0) + K_L - c_0$$

[Eq. 2.4]

$$b = -K_L \cdot (c_P \cdot q_0 + c_0)$$

[Eq. 2.5]

These equations deliver practical information for adsorption experiments, as from the assumption of e.g. the K_L value and q_{max}, the required particle concentration can be estimated.

For the further understanding of magnetic separation processes, the next chapter deals with the fundamental principles required in magnetic separation technology. The chapter is based on [5].

2.1.2 Magnetism and Magnetic Fields

Magnetism is an inherent characteristic of all matter. It arises from the spin magnetic moments of the electrons and nuclei of the atoms. *Magnetic fields* are generated by moving electric charges. These can occur either macroscopically as currents in wires or in a microscopic fashion associated with the electrons movement in the orbits of atoms. The force which is generated in vacuum by a magnetic field is characterized by its vector field H. The impact of the magnetic field onto matter is described by the magnetic flux density B:

$$B = \mu_r \cdot \mu_0 \cdot H$$ [Eq. 2.6]

The magnetic flux density takes into account the influence of the magnetic properties of the particular material to the magnetic field, described as the magnetic permeability. In Equation 2.6 μ_0 is the permeability constant of the vacuum and μ_r is the permeability of the particular material affected by the magnetic field. In vacuum μ_r equals 1.

2.1.2.1 Polarization and Susceptibility

If a particular substance is introduced into a magnetic field, the magnetic flux density inside the substance increases from the initial value B_{vac} to the value B_{sub}. This difference ΔB is called *magnetic polarisation* J:

$$J = \Delta B = B_{sub} - B_{vac}$$ [Eq. 2.7]

Except for ferro- and ferrimagnetic substances, the magnetic polarisation is proportional to the applied magnetic flux density with a proportionality constant κ:

$$\Delta B = \kappa \cdot \mu_0 \cdot H \qquad\qquad\qquad\qquad \text{[Eq. 2.8]}$$

The proportionality constant κ is called magnetic susceptibility:

$$\kappa = \mu_r - 1 \qquad\qquad\qquad\qquad \text{[Eq. 2.9]}$$

The magnetic character of a substance can be classified according to its susceptibility, if

- $\mu_r > 1$ and $\kappa > 0$, the substance is paramagnetic. This substance increases the impact of the magnetic field
- $\mu_r < 1$ and $\kappa < 0$, the substance is diamagnetic. This substance decreases the impact of the magnetic field

In case of ferro- and ferrimagnetic substances, μ_r is a function of the magnetic field strength. The magnetic polarisation is not increased proportionally with the applied magnetic field, but reaches a saturation J_S at very high magnetic field strengths. The saturation magnetization can be seen from the *magnetisation curve*.

2.1.2.2 Magnetisation Curve

In practice, the impact of a magnetic field on ferro- or ferrimagnetic substances is described by the increase of the magnetic field strength, the magnetization M in order to be consistent with Equation 2.7:

$$M = \Delta H = H_{sub} - H_{vac} \qquad\qquad\qquad\qquad \text{[Eq. 2.10]}$$

The saturation magnetisation M_S is reached when all atomic dipoles are aligned by means of the influence of an external magnetic field. When the polarisation is plotted versus the applied magnetic field, a magnetisation curve is obtained. From this curve the magnetic

properties of ferro- or ferrimagnetic substances can be deduced. Exemplarily, a magnetisation curve for a ferromagnetic substance is shown in Figure 2.1.
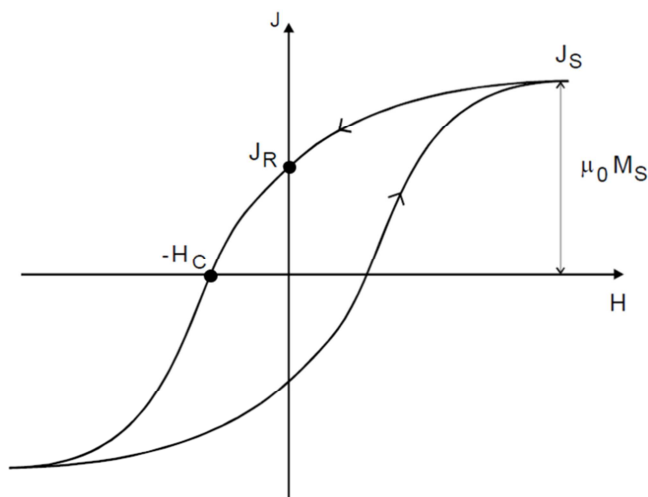
Figure 2.1: Magnetisation curve of a ferromagnetic substance. From the curve, the coercive field strength H_C, the magnetic remanence J_R, and the saturation magnetisation M_S can be derived as characteristic magnetic properties of the substance.

The saturation polarization J_S can be seen as the Y-axis value at the right end of the magnetisation curve. When the magnetic field strength is decreased to zero or the external magnetic field is removed, starting from this point, for non-superparamagnetic substances a remanence J_R remains. The material retains this polarization until a magnetic field pointing into the opposite direction reaches a certain strength - the so-called coercive field strength H_C. In other words, the coercive field strength is the strength required to remove the remaining polarization of the ferro- or ferrimagnetic material.

2.1.2.3 Influence of Particle Form and Size

Magnetic susceptibility is not only a characteristic of the particular material, but also a characteristic of the form and size of the material. For a finite particle, an external magnetic field induces a counter-directed magnetic field within the particle, dependent of size and shape of the particle which attenuates the overall magnetic field. The dependency is described by the demagnetization factor D_m:

$$\kappa = \frac{\kappa_i}{1 + D_m \cdot \kappa_i}$$ [Eq. 2.11]

with $0 < D_m < 1$.

In Equation 2.11, κ_i is the intrinsic magnetic susceptibility of the particular substance, which is measured with a sample that does not exhibit any demagnetization, e.g. a very long cylinder or an annulus consisting of the particular material.

The magnetic behavior of very small ferro- or ferrimagnetic particles that contain only of one or few magnetic domains is fundamentally different to the behavior of macroscopic material: Large particles have many magnetic domains and thus their value of remanence magnetisation is virtually constant. For particles smaller than approximately 100 µm the total number of magnetic domains is consequently reduced and as a result of this reduction, the coercive field strength increases and the susceptibility decreases, as can be seen in Figure 2.2.
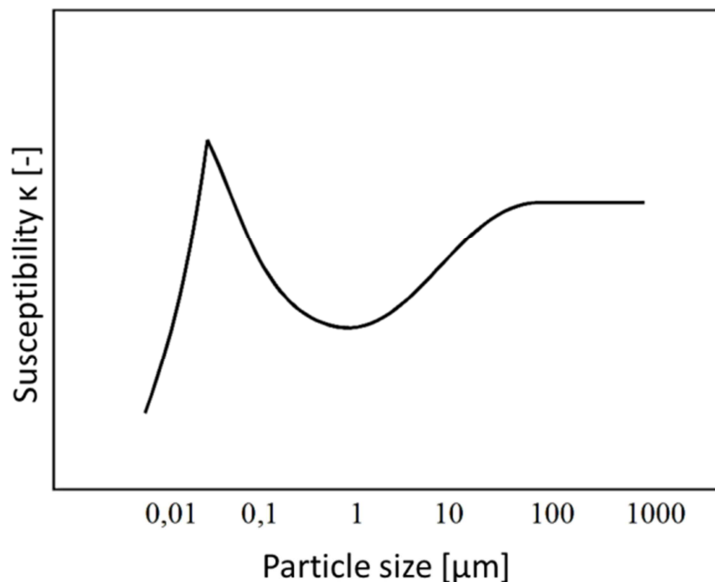
Figure 2.2: Dependency of the susceptibility of the particle size of magnetite from [6].

If the particle size is reduced so that only a single magnetic domain remains, the coercive magnetic field strength reaches a maximum and the susceptibility a minimum. In the case of magnetite particles, this transition is around 1 µm. When the particle size is further

reduced, the coercive field strength is reduced until it reaches zero [7]. Ferromagnetic particles with these sizes show on the one hand the magnetic behavior of paramagnetic substances, on the other hand, their magnetisation is profoundly higher. Therefore their magnetic character is called superparamagnetic. For magnetite particles of spherical shape the transition to superparamagnetism is reached at particles sizes of approximately 10 nm [6].

2.1.3 Technical Separation of Magnetic Particles

The fundamental principle of magnetic separation is based on a magnetic field exerting a force on magnetic and magnetizable material. The relationship between the magnetic force F_M, the particle volume V_P, the magnetic field H, and the particle magnetisation M_P is given by Equation 2.12:

$$F_M = \mu_0 \cdot V_P \cdot M_P \cdot \nabla H \qquad\qquad \text{[Eq. 2.12]}$$

As can be seen, for constant magnetic particle characteristics, F_M can only be increased by the increase of the magnetic field gradient ∇H. Thus, for bioseparation applications where small particles in the range of nano- to micrometers are applied, a steep gradient is crucial. Steep magnetic field gradients are realized up to now only by means of High Gradient Magnetic Separators (HGMSs).

2.1.3.1 High Gradient Magnetic Separation

The principle of HGMS originates from the minerals industry [8], yet, the adaptation of this principle to protein separation came up in the beginning for the 21st century at the Technical University of Denmark (DTU) and was termed High Gradient Magnetic Fishing (HGMF) [9-13]. Further development has been made at the Research Center Karlsruhe (Forschungszentrum Karlsruhe) and the potential of this technique has been proven for various biological feedstocks, e.g. cell homogenisate, whey, fermentation broth or horse serum [14-18]. The centerpiece of an HGMF apparatus is a magnetisable separation matrix, which is placed in an external magnetic field. In Figure 2.3 the principle of the separation is depicted by means of the cross section of a single ferromagnetic wire. The

wire is exemplarily for magnetisable material. In the simplest cases, this material is loosely packed steel wool. The recent generation of HGMS uses as stack of ordered wire meshes. Due to the wires, the external magnetic field is concentrated with a gradient towards sections on the wire. Para-, ferri- and ferromagnetic particles are highly attracted to the wire.
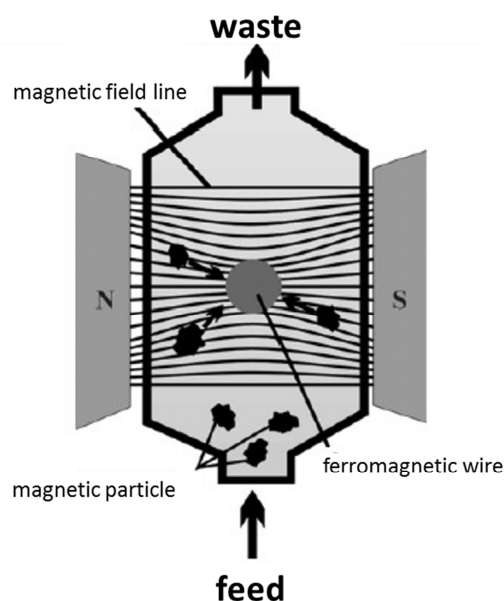
Figure 2.3: Principle of the separation of magnetic particles in HGMF. The application of an external magnetic field to a magnetisable wire leads to high magnetic field gradients. Particles are drawn toward the wire and separated from the feed.

If the capacity of the magnetic wires is saturated, the feed flow is stopped, the external magnetic field is switched off and the magnetic particles are back-flushed out of the separator.

2.1.3.2 Magnetic Field Enhanced Centrifuge

Recently, the application of a magnetic field enhanced centrifuge (MEC) has been reported [19]. The principle of the magnetic centrifuge is shown in Figure 2.4. The basic principle is similar to the one of HGMS: A separation chamber with magnetisable wires is placed inside an electromagnet. The difference between MEC and HGMS is that the particles are removed from the magnetisable wires by centrifugal forces that drive the particles from the wire to the wall of the centrifuge. The feed is injected into the

separation chamber under low rotational speed in order to prevent removal of large nonmagnetic contaminants [19].
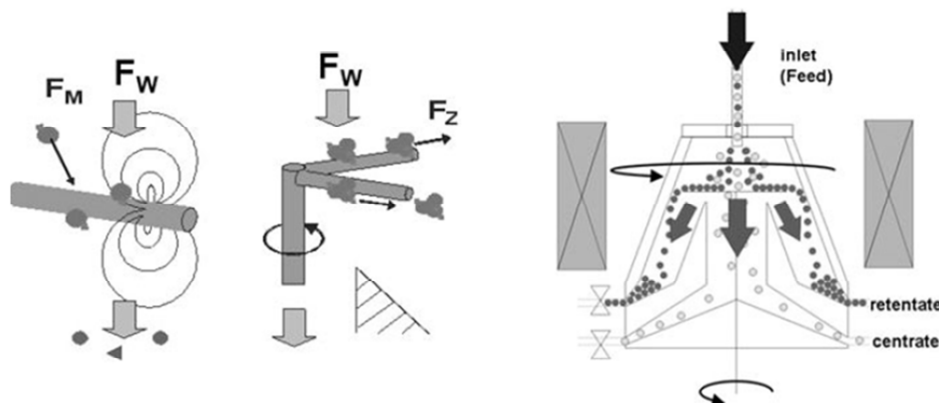
Figure 2.4: Principle of magnetic field enhanced centrifugation. Left: The magnetic particles are attracted to the magnetized wires. The particles are then separated by centrifugal force F_Z as agglomerates and accumulate at the wall of the centrifuge. Right: Set-up of magnetic enhanced centrifugation by adjusting a bowl centrifuge inside an electromagnet. (From: [19])

MEC and HGMS can both be applied for the continuous separation of magnetic particles from a particle-containing feed until the saturation of the wires - in case of HGMS - or centrifugal wall - in case of the MEC - is reached. Thus both unit operations have to be processed batch wise, because back-flushing of the particles is necessary. An interesting alternative for the continuous processing of magnetic sorbents is presented in the next chapter: the selective partitioning of the particles within aqueous (micellar) two-phase systems.

2.2 Partitioning in Two-Phase Systems

Ever since the integration of bioseparation processes was postulated, the particular partitioning of a target molecule between two phases has arisen more and more interest. With the affinity of insoluble components, e.g. cell debris, to the opposite phase, solid-liquid separation and initial capture of the protein can be integrated into one extractive process step. Small biomolecules can be partitioned between organic and aqueous phases, between two organic phases or between two aqueous phases. As for large molecules like proteins and polypeptides, aqueous phases exhibit the gentlest

environment, therefore, aqueous two-phase systems and aqueous micellar two-phase systems have been examined for several years in the context of bioseparation.

2.2.1 Aqueous Two-Phase Systems

When two hydrophilic polymers are mixed in water, the system can undergo spontaneous phase separation. The phase separation results in two aqueous phases of whom one phase contains most of the one kind of polymer and the other phase contains most of the other polymer. The demixing and macroscopic emerging of two aqueous phases has originally been described by Beijerinck [20] in a system of starch, agar and gelatine. It was, however, Albertsson in 1956 who discovered the potential of these so called aqueous two-phase systems (ATPS) for the selective enrichment of biological components in one of the two phases [21, 22]. The ATPS described by Albertsson were aqueous solutions consisting of polyethylene glycol (PEG) and Dextran or PEG and phosphate salts. These ATPS split in two aqueous phases – one of them containing PEG to a large extent and the other most of the dextran or phosphate. The main component in both phases is still water - usually more than 80% [22].

Several other combinations of phase forming components have been described up to now, e.g. systems composing of phosphate-salts and ethanol, ionic liquids and phosphate-salts [23], acrylamide-modified starch and phosphate-salts [24] or a chaotropic and a cosmotropic salt [25]. In Table 2.1 additional compositions of APTS described in the literature are depicted. ATPS based on micellar interactions are described in chapter 2.2.2 separately.

Table 2.1.Combinations of substances that lead to ATPS formation. From: Huddelston [26].

Polymer-polymer systems

Poly(ethylene glycol)	and	Dextran
		Poly (vinyl alcohol)
		Poly (vinyl pyrolodine)
		Ficoll
		Hydroxyl propylstarch
Poly(vinyl alcohol)	and	Methyl cellulose
		Hydroxipropyl dextran
		Dextran
		Poly (acrylic/methacrylic acid)

Polymer-salt systems

Poly(ethylene glycol)	and	Sodium/potassium phosphate
		Citrate, Tartrate, Succinate
		Al/Na/Mg/Cu/Fe/Zn/Li-sulphates

When certain components are added to the ATPS, they partition unevenly between both phases, based on their unique phyico-chemical properties. The partition behavior is described by the partitioning coefficient K:

$$K = \frac{c_{Top}}{c_{Bottom}}$$ [Eq. 2.13]

Where c_{Top} is the concentration of the particular component in the top phase and c_{Bottom} its concentration in the bottom phase. Ever since their first discovery, a vast number of applications of ATPS has been described for the selective separation of e.g. proteins [27], nanoparticles [28], dyes [29], DNA [30], inclusion bodies [31], antibodies [32] or ions [33] in one of the two phases. For this enumeration is far away from being comprehensive, the reader is referred to one of the - also numerous - reviews published in the last years [26, 32, 34-38].

2.2.1.1 ATPS Phase Diagram

The composition of the emerging two phases of an ATPS can be seen from its phase diagram. The phase diagram is valid only for a specific combination of phase forming components (and a fixed temperature) of the system. Exemplarily, a phase diagram can be seen in Figure 2.5. In the phase diagram the X- and the Y- axis describe the (weight-) concentrations of the two phase-forming components, the third component is water by convention [22]. The binodale separates the single phase region from the two-phase region. When a solution is prepared resulting in concentrations in the two-phase region above the binodale (e.g. point M in Figure 2.5) this solution system splits into two phases. The compositions of the emerging light phase L and heavy phase H are determined by the specific tie line which runs through M and ends at the binodale.
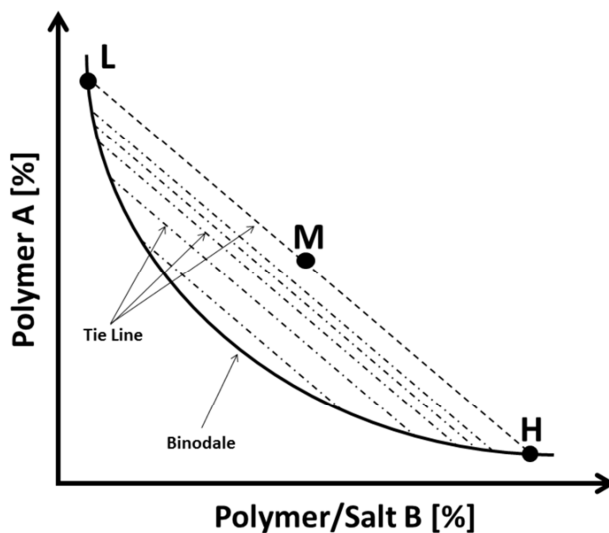
Figure 2.5. Generic phase diagram of an ATPS. The binodale separates the stable single phase regime from the two-phase region. A mixture M splits spontaneously in two phases, where the composition of light phase is described by point L and the composition of the heavy phase is described by point H. L, M and H are localized on the same tie-line.

The mass fractions w_i of the components, defined by Equation 2.14, can be directly obtained from the phase diagram:

$$w_i = \frac{m_i}{m_{total}}$$

[Eq. 2.14]

Because the densities of the initial and emerging phases are almost equal to that of pure water, their differences are neglected. Therefore, from the mass fractions, the phase volume ratio R of the resulting phases can be determined according to the lever rule [22, 39]:

$$R = \frac{V_{Top}}{V_{Bottom}} = \frac{V_L}{V_H} = \frac{w_H - w_M}{w_M - w_L} = \frac{\overline{MH}}{\overline{LM}}$$

[Eq. 2.15]

Here, V_{Top} and V_{Bottom} are the volumes of the resulting phases. For the calculation however, the knowledge of which polymer forms the top – and which forms the bottom phase of the ATPS is necessary.

2.2.2 Aqueous Micellar Two-Phase Systems

In contrast to "classical" ATPS, AMTPS consist only of one phase forming component - commonly a surfactant. When the temperature of the micellar solution is increased above a certain point, spontaneous phase separation occurs. The system splits in a micelle rich (or coacervate) phase and a micelle depleted (or aqueous) phase [40]. At the temperature where the phases start to separate (at a certain concentration), the system becomes turbid or "cloudy" and thus this point is often denoted as cloud point [41]. Various types of surfactants have been applied as phase forming surfactant for the generation of an AMTPS, among these zwitterionc surfactants e.g. dioctanoyl phosphatidylcholine (C-8-lecithin) [42], triblock copolymers of PEG and polypropylene glycol (PPG) (called pluronics) [43, 44], as well as mixtures of ionic and non-ionc surfactants [45]. The most frequently applied class of surfactants for the generation of AMTPS however are nonionic surfactants, and especially PEG - alkyl ethers [40, 46]. These surfactants consist of a hydrophilic PEG chain and a hydrophobic alkyl head. They are typically abbreviated C_xE_y, where Y is the length of the alkyl chain and X is the number of PEG units.

2.2.2.1 Physico-chemical background of phase separation of AMTPS

The molecular thermodynamic background of the phase separation of AMTPS has been fundamentally investigated by the workgroup around Blankschtein [47, 48]. In their

theory increasing the temperature leads to the growth of the (spherical or cylindrical) micelles due to an increase of the intermicellar attractions. If the resulting loss in entropy is larger than the win in enthalpy, phase separation will follow. In Figure 2.6 the temperature induced phase separation based on the growth of the micelles is depicted.
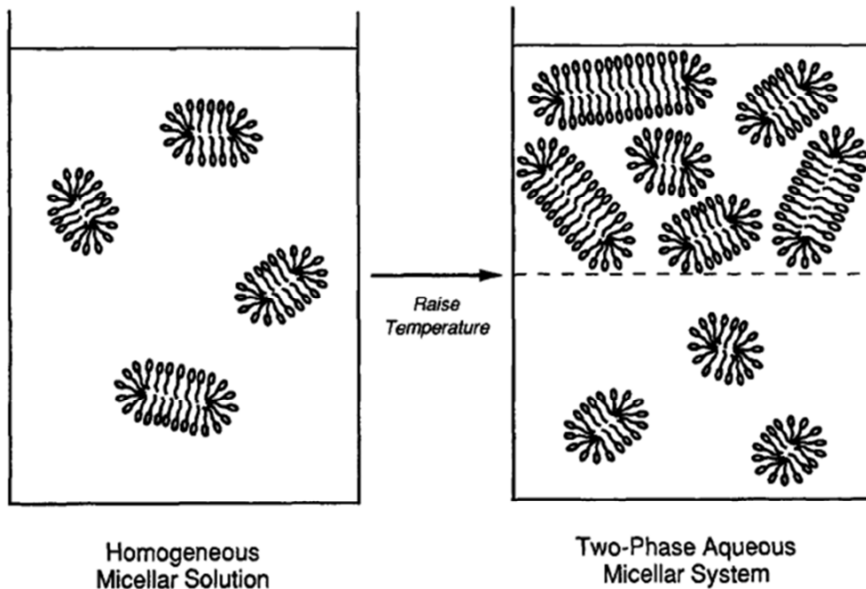
Figure 2.6: Temperature induced phase separation. Each of the resulting coexisting phases contains cylindrical micelles but possesses different micellar concentrations. The cylindrical micelles in the micelle-rich (top) phase are larger than those in the micelle depleted (bottom) phase. From: [42].

According to Blankschtein´s theory the coexistence curve of an AMTPS can be modeled using two physically relevant parameters: C as the measure for the magnitude of the attractive intermicellar free energy and Δμ as free energy gain from micellar growth, which means Δμ increases with increasing micellar size and micellar polydispersity [49, 50].

With the usage of the Equation 2.16 for the mole fraction of the surfactant χ_i, the parameters C and Δμ are given by Equations 2.17 and 2.18:

$$\chi_i = \frac{n_i}{n_{total}}$$
[Eq. 2.16]

$$C(\chi_{aq}, \chi_{co}, T) = \frac{k \cdot T}{\gamma} \cdot \left(1 + \frac{3 \cdot \gamma - 2}{3} \right)$$
$$\cdot \left[2 \cdot \left(\sqrt{\chi_{aq}} + \sqrt{\chi_{co}} \right)^2 - 3 \cdot \sqrt{\chi_{aq} \cdot \chi_{co}} \right]$$

[Eq. 2.17]

$$\Delta\mu(\chi_{aq}, \chi_{co}, T) = k \cdot T \cdot \ln \left[\frac{\left(\frac{6}{3 \cdot \gamma - 2} \right)^2}{\chi_{aq} \cdot \chi_{co} \left(\sqrt{\chi_{aq}} + \sqrt{\chi_{co}} \right)^6} \right]$$

[Eq. 2.18]

Here, k_B is the Boltzmann constant, T is the absolute temperature, χ_{aq} and χ_{co} are the mole fractions of the aqueous and the coacervate phase, while γ is the ratio of the effective volume of a surfactant molecule to a water molecule, which according to Lam can be approximated by the ratio of the molecular weight of the surfactant to that of water. With knowledge of these parameters the phase separation curve which separates the single phase area from the two-phase region was successfully calculated [49].

2.2.2.2 Phase diagram
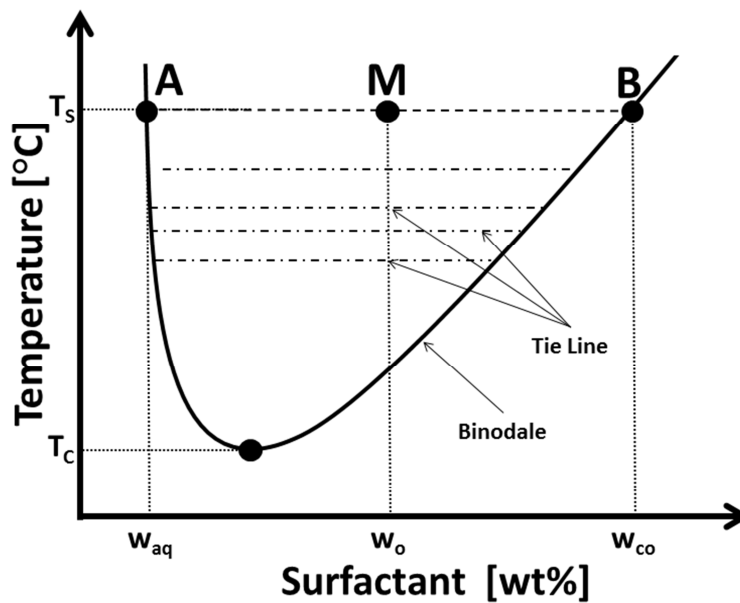
Figure 2.7: Phase diagram of an AMTPS.

The phase diagram of an AMTPS characterizes the phase separation region based on the temperature and the surfactant concentration. Therefore the axes differ from the phase

diagram of a classic ATPS. On the Y-axis the temperature is depicted, while the X-axis shows the weight fraction of the phase forming surfactant. At the lower consolute (critical) temperature T_C the system system begins to split in two phases. For a constant temperature T_S, e.g. a solution M with the initial composition w_0 separates in an aqueous phase A with a composition of w_{aq} and a micelle rich or coacervate phase B with the surfactant concentration w_{co}. Usually, AMTPS based on nonionic surfactants split on warming, as shown in Figure 2.7. Other AMTPS have been described which split when the temperature is decreased e.g. the zwitterionic surfactant C8-lecithin, thus these system exhibit an upper consolute critical temperature [41, 51]. The volume ratio R in AMTPS can be calculated by the lever rule similar to ATPS based on the mass balance around the initial and the resulting phases [52]:

$$w_o \cdot \rho_0 \cdot V_0 = w_{aq} \cdot \rho_{aq} \cdot V_{aq} + w_{co} \cdot \rho_{co} \cdot V_{co} \qquad \text{[Eq. 2.19]}$$

With

$$V_0 = V_{aq} + V_{co} \qquad \text{[Eq. 2.20]}$$

If the e.g. top phase is the coacervate phase R is given by:

$$R = \frac{V_T}{V_B} = \frac{V_{co}}{V_{aq}} = \frac{w_0 \cdot \rho_0 - w_{aq} \cdot \rho_{aq}}{w_{co} \cdot \rho_{co} - w_0 \cdot \rho_0} \qquad \text{[Eq. 2.21]}$$

In AMTPS the density differences of the initial, aqueous and the coacervate phase are approximately equal [52]:

$$\rho_{aq} \cong \rho_{co} \cong \rho_0$$

Thus Equation 2.21 is simplified to:

$$R = \frac{w_0 - w_{aq}}{w_{co} - w_0} = \frac{\overline{AM}}{\overline{MB}} \qquad \text{[Eq. 2.22]}$$

If the bottom phase is the coacervate phase, this changes to:

$$R = \frac{w_{co} - w_0}{w_0 - w_{aq}} = \frac{\overline{MB}}{\overline{AM}} \qquad \text{[Eq. 2.23]}$$

From R the hold-up of the dispersed phase ε can be calculated with

$$\varepsilon = \frac{V_{co}}{V_{co} + V_{aq}} \qquad \text{[Eq. 2.24]}$$

If the top phase is the coacervate phase:

$$\varepsilon = \frac{R}{R + 1} \qquad \text{[Eq. 2.25]}$$

And if the coacervate phase is the bottom phase:

$$\varepsilon = \frac{1}{R + 1} \qquad \text{[Eq. 2.26]}$$

2.2.2.3 AMTPS as tool for (bio)-separation

When substances are added to the micellar solution and the solution is heated, the substances partition between the two emerging phases. The selective extraction of substances into one of the two phases was termed cloud point extraction (CPE) or micelle-mediated extraction (MME) [53]. CPE was initially applied for the concentration of metal ions [54] in 1978. In 1981, Bordier employed AMTPS for the recovery of hydrophobic membrane proteins in the micelle rich phase of an AMTPS based on the nonionic surfactant Triton X-114 [55]. This was the beginning for CPE being exhaustively exploited as the primary isolation step of proteins. Numerous studies were published

proposing specific extraction and back extraction schemes of organic and inorganic substances [56-58]. Especially in the field of protein downstream processing several articles have been published by e.g. the workgroups of Kula [59-64] and Watanabe and Tani [40, 43, 44, 53, 65].

2.2.2.4 Moleculardynamic background of the Partitioning Behavior in AMTPS

The partitioning behavior of proteins in AMTPS was theoretically described by the workgroup of Blankschtein and termed "Excluded Volume Theory" in a molecular-dynamic approach [66]. The theory is fundamentally based on steric, excluded volume interactions between globular hydrophilic proteins and the micelles. The steric interactions lead to the exclusion of certain substances from the micelle rich phase. With the definition for the volume fraction given in Equation 2.27, the expression for the partitioning coefficient from the excluded volume theory K_{EV} was determined to:

$$\Phi_i = \frac{V_i}{V_{total}}$$

[Eq. 2.27]

$$K_{EV} = exp\left[-(\Phi_T - \Phi_B) \cdot \left(1 + \frac{R_{Prot}}{R_{Mic}}\right)^n\right]$$

[Eq. 2.28]

In Equation 2.28 Φ_T and Φ_B are the surfactant volume fractions in the top and bottom phases of the resulting AMTPS, R_{Prot} is the hydrodynamic radius of the protein and R_{Mic} the cross sectional radius of each micelle. For cylindrical micelles the exponent n is 2 and for spherical micelles n is 3. Figure 2.8 shows the prediction plot for the K_{EV} as a function of the quotient of the hydrodynamic radii of the micelles and the target protein.
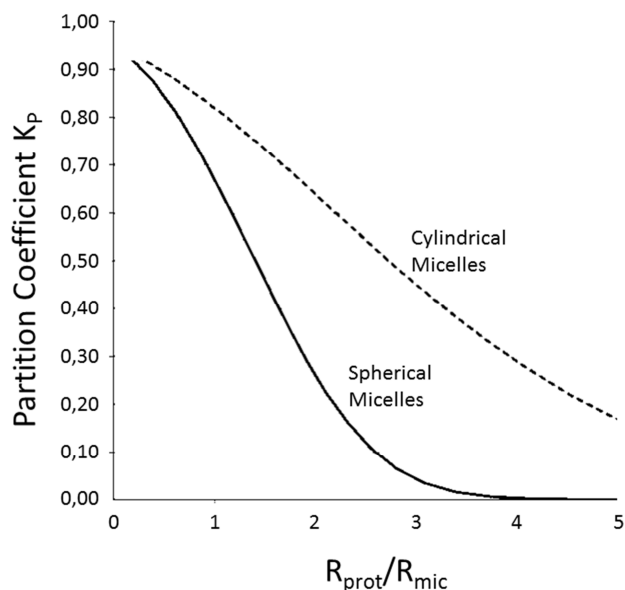
Figure 2.8: Predicted protein partition coefficient based on the excluded volume theory as a function of the ratio of the hydrodynamic radius between the target protein and a cylindrical or spherical micelle. The curves are based on a micellar radius of 1.78 nm and a volume fraction difference of 5%. (From: [66])

As can be seen from Equation 2.28, for static radii of the micelles and the target protein, the excluded volume interactions are solely dependent on the volume fraction difference of the surfactant between both phases. As can be easily seen from the title of the theory, large proteins are excluded from the micelle rich phase, while the effect is more prominent in spherical micelles than in cylindrical micelles. In the course of their work, the authors were able to obtain reasonable correlations for the protein ovalbumin and the nonionic surfactant n-decyl tetra(ethylene exide) – $C_{10}E_4$ with the theory [66]. The first version of the excluded volume theory took into account only hydrophilic and steric interactions. Later, the authors extended the theory further and added terms for the electrostatic and affinity interactions between the surfactants [49, 52, 67], which resulted in reasonable correlations between the theory and their experimental results. Despite the clearly fundamental physical background, the theory was only adapted to the experimental results and the prediction of partitioning of unknown proteins in unknown systems has not been tried yet.

2.2.2.5 Continuous Application of ATPE or CPE

One of the major advantages of the application of ATPS and AMTPS is that the partitioning behavior of proteins and particles is independent of the volume size [22]. Once the partitioning behavior of a certain substance has been determined in a small scale, an upscaling to large volumes can be performed theoretically to any volume of choice. This is one of the most striking arguments for the application of A(M)TPS in downstream processing cf. traditional packed bed chromatography. The large-scale application of ATPE has been described as early as 1978 in a disc stack centrifuge [68]. As many studies described potential targets for large-scale ATPE, only few technical-scale plants have been reported. In the last years, however, different equipment for ATPE and CPE has been described:

Recently, Vazquez-Villegas et al. described a novel separator for the continuous processing of ATPS based on a mixer-settler set-up [69]: Their set up is composed of two peristaltic pumps, a static mixer, a tubular phase separator and a collector with a harvesting port. The authors were able to run the separator with flow rates of 50 - 60 ml per minute while continuously separating a PEG phase from a potassium phosphate phase. The partitioning coefficient of the applied whey protein mixture was 0.5 in the batch experiments and around 0.4 in continuous mode. The separator was run continuously for several hours at almost steady state, therefore, the potential of their set-up is clearly pointed out. The protein recoveries in the continuous system were 90 %, with the remaining 10 % precipitated at the interface. In their previously performed batch experiments 66 % were lost due to precipitation at the interface. The authors explained these differences by "the dynamic nature of the interface of two moving liquids, minimizing protein precipitation". Besides this mixer-settler equipment, extraction columns have been applied. The performance of a Kühni-type extraction column at different impeller speeds was investigated for the partitioning of plasmid DNA in a PEG-potassium phosphate ATPS [70]. The continuous extraction of a human immunogolobulin G (IgG) using ATPS in a packed column was described by a group of Aires-Barros in cooperation with Bayer Technology Services GmbH [71]. In their study the authors performed a complete characterization of the hydrodynamic properties and the mass

transfer of IgG. A recovery of the target protein of 85 % was obtained with more than 85 % of the contaminating proteins being removed and 50 % of the total contaminants [71]. This application is to the knowledge of the author the first industrial application of a continuous APTS process.

Continuous CPE has been reported so far only by means of temperature regulated rotating disc contactors (RDCs). The first application of continuous CPE for the extraction of (aromatic) organic molecules which partitioned to the dispersed, micelle rich phase of a Triton X-114 AMTPS has been described by a group around Osuwan [72-74]. The authors used a RDC with a column of 1000 mm height. A similar RDC was also used for the continuous separation of vanillin. The authors reported an optimum of the stirrer speed: a low stirred speed resulted in a low mass transfer due to the large droplets, while a high stirrer speed resulted in extreme back mixing and therefore led to loss of the surfactant [75]. Thus it can be seen that CPE faces the same limitations than conventional extraction.

2.2.3 Enhancing the Partitioning in ATPS – From Affinity ATPS to Magnetic Extraction Phases

Despite the large-scale applicability of APTS and AMTPS, a major hurdle is the insufficient partitioning behavior of the molecule of interest in one of the two phases. For example, the enrichment of a protein in the bottom phase of a two-phase system even with an extreme partition coefficient of 0.2 and a phase ratio of 1 leads to a loss of 20 % of the target protein in the top phase. Especially for high-value proteins in, e.g. biopharmaceutical industry, this loss is economically unacceptable. Therefore the idea to modify an aqueous two-phase system to increase the partitioning coefficient has come up early and was termed affinity partitioning. Reviews about can be found e.g. from Koppenschlaeger [76], Xu [34] or Ruiz-Ruiz [36]. Basically, three routes have been followed to increase the partitioning:

a) *Modification of one of the phase forming components*

In 1974 Takerkart covalently attached p-aminobenzamidine (PAB) to PEG for the selective partitioning of trypsin into the PEG phase [77]. In 1975 the term *affinity partitioning* was

created by Flanagan [78], who synthetized dinitrophenyl to PEG for the separation of the S-23 myeloma protein to the PEG phase of an PEG/dextran system. Both authors reported an increase of the partitioning coefficient of the target proteins by the synthetisation of the affinity ligand to the polymer. Dye ligands, e.g. Cibacron bue, F3GA or Procion Yellow HE-3G, have often been used as affinity ligands coupled to polymers to enhance the partitioning [79-81]. In Table 2.2 an excerpt from Ruiz-Ruiz [36] of modified polymer/polymer or polymer/salt affinity ATPS is summarized.

Table 2.2: Affinity ATPS applied for the selective enrichment of a target product. (Excerpt from [36])

Product	Basic ATPS	Modification	Reference
IgG	Dextran T500/PEG 3350	PEG-benzyl	[82]
IgG	Dextran T500/PEG 3350	PEG-diglutaric acid	[83]
S-23 myeloma protein	Dextran T500/PEG 6000	PEG-dinitrophenyl	[78]
IgG	Dextran T500/PEG8000	PEG-Protein A	[84]
Trypsin	Dextran T500/PEG8000	PEG-trypsin-inhibitor	[84]
Lysozyme	Dextran T500/PEG 8000	Dextran-benzoyl	[85]
Thaumatin	PEG 8000/phosphate	PEG-gluthatione	[84]
Penicillin acylase	PEG 4000/phosphate	PEG-benzoate	[86]
Penicillin acylase	PEG 4000/phosphate	PEG-phenylacetamide	[86]

In the case of AMTPS, mostly the embedding of ionic surfactants and thus the generation of charged mixed-micelles was accomplished instead of the modification of the nonionic surfactants themselves [45, 52, 63, 67]. In all cases the authors were able to successfully increase the partitioning coefficient as a consequence of the electrostatic attraction. An affinity co-surfactant was added to a $C_{10}E_4$ AMTPS by Lee to increase the partitioning of vancomycin by a factor of 16 at pH 4 [87].

b) Modification of the Target Protein

Besides the modification of the phase forming polymer, the target protein can be modified in order to increase its affinity to one of the two emerging phases. The modification can be realized either chemically or genetically by co-expression of a fusion tag or a complete fusion protein. The introduction of hydrophobic and charged groups by

acylation of the amino residues of the proteins BSA and ß-lactoglobulin for instance lead to a higher affinity to the hydrophobic PEG phase [88, 89]. The enhancement of the partitioning efficiency of recombinant fusion proteins has been described by Berggren [90] or Fexby [91]. The modification of the target protein can also be combined with the modification of the polymer. For instance Ekblad et al. combined biotinylated liposomes and avidin coupled to dextran: In a system without dextran-avidin 90% of the liposomes partitioned to the PEG phase, whereas in its presence more than 95% partitioned into the dextran phase [92].

As examples for affinity AMTPS, Lam et al. used a fusion protein consisting of the green fluorescent protein (GFP) and a "family 9 carbohydrate-binding module" (CBM9-GFP) [49]. The AMTPS was formed with the nonionic surfactant n-decyl beta-D-glucopyranoside, which acted simultaneously as the affinity ligand. In this case the partitioning coefficient was more than six-fold higher (3.1 cf. 0.47) as in the "control" case, where the affinity interactions were inhibited by the addition of glucose [49].

c) Addition of Free Ligands or Insoluble Particles

Instead of modifying either the phase forming components or the target molecule, the third way of improving and steering the partition of substances is to add free ligands as affinity components to the system. If these free ligands accumulate in one phase, the affinity for the target product drives it to same phase, despite its initial orientation. The benefit obtained from the application of free ligands is that they are usually cheaper compared to the elaborative chemical modification of polymers or proteins. Among these cheap free ligands applied, are Cibacron blue[93], starch [94], chitosan [95], butyrate [96] or alginate [97] added to ATPS. In the case of AMTPS, no significant difference in the partitioning behavior of glucose-6-phosphate dehydrogenase was discovered by Lopes [98] when affinity ligands were added in AMTPS based on Triton X-114 or $C_{10}E_4$. The author attributed this effect to the strong influence of the excluded volume effect described in chapter 2.2.2.4. Saitoh on the one hand confirmed these findings, but upon the usage of the zwitterionic surfactant 3-(nonyldimethylammonio) propylsulfate and the addition of affinity ligands he was able to extract the large, hydrophilic protein

hexokinase into the micelle rich phase of this AMTPS [99] despite the excluded volume effect. The partitioning was strongly dependent on the pH-level.

Besides free *soluble* ligands, the usage of *insoluble* particles with affinity functionalization has been demonstrated. The advantage of insoluble affinity components is their simple removal and regeneration from the two-phase system whereas the separation of soluble components in order to re-use them may become cost intensive. In 1984, pioneering work in this field was conducted by Hedman and Gustafsson who investigated the partitioning and protein binding characteristics of modified Sepharose and Sephadex materials in PEG-phosphate systems [100]:

The authors demonstrated that cell fragments – in this case homogenized *S.cerevisiae* – partitioned to the bottom phase of a PEG-phosphate ATPS, while the affinity sorbents partitioned to the top phase, thus no precedent clarification step was necessary in order to remove the target proteins from the cell debris. In his work, Hedman bound the target proteins (BSA, IgG, Albumin and ADH) in the affinity system, collected the particles afterwards and eluted them in a column. By doing this, the author circumvented the issue of the redistribution of the target proteins between the two phases after eluting them from the particles. Additionally, the author emphasized on the influence of the ionic strength in PEG-Phosphate systems: Due to the high salt concentration, e.g. in PEG-phosphate ATPS, the binding step is limited to salt-tolerant affinity mechanisms. Following this publication, several workgroups have described the integration of functionalized affinity sorbents to ATPS [101-104] with Ku being the first authors who eluted the target proteins back into the other phase (in their case dextran), while the particles remained in the PEG phase [105, 106]. In all the cases the application of affinity particles led to an improved separation performance of the target proteins cf. the application of the ATPS alone.

Considering the current thesis, an important process concept was introduced in 1995 by Suzuki et al.: The use of magnetic particles as affinity sorbents in ATPS [107]. Suzuki hereby combined the affinity enhanced separation of proteins – in this case Protein A – and magnetically enhanced phase separation. Initially, basic magnetite particles with sizes

ranging between 7 and 15 nm were coated with aminosilane, and subsequently with Eudragit S-100. Then, the particles were further functionalized with human IgG to capture staphylococcal Protein A from an *E. coli* crude extract. The particles and the cell extract were added to a PEG-phosphate ATPS, in which the particles accumulated in the upper phase. After mixing, the phase separation of the two-phase system was accelerated due to the application of a hand magnet. Protein A, which was excluded from the top phase (K = 0.39) in the absence of the magnetic particles, was enriched in the top phase of the affinity system (K = 11.4). Approximately 90 % of the Protein A was bound to the particles. The target protein was eluted from the particles by 3.5 M KSCN and 39 % of the protein was recovered from the particles with a purity of 45 %. In summary the partition coefficient increased 35-fold and the purity 4-fold in the system compared to a traditional ATPS [107]. Despite the fact that the elution efficiency of the target protein was unsatisfactory, a novel bioseparation process scheme was proposed by the authors, shown in Figure 2.9. Recently, the same approach was used by for the separation of lysozyme and BSA by using carboxyl modified magnetic particles [108].
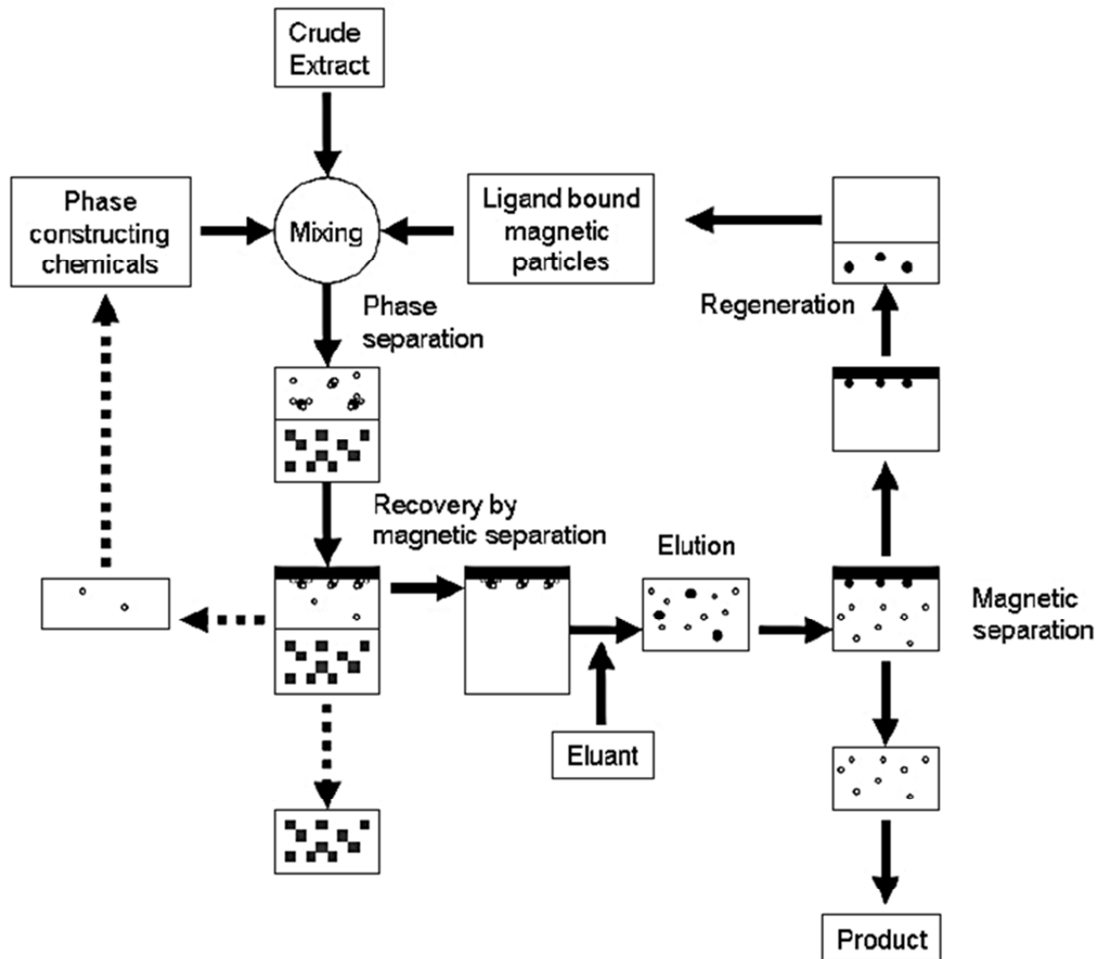
Figure 2.9: Process scheme from Suzuki et al. [107]. Functional magnetic sorbents, crude extract and ATPS forming components are mixed for the selective binding of a target protein. The phase separation is afterwards accelerated by means of a magnetic field. The particle containing phase is withdrawn and the target protein is eluted from the magnetic particles. After a regeneration step, the particles can be reintroduced to the mixing chamber

One seminal result that can be found from the publication of Suzuki is that the phase separation rate can be increased by the application of an external magnetic field when magnetic particles are added to an ATPS. Thus in this work the integration of affinity ATPS and the increase of the phase separation rate is described for the first time.

The integration of magnetic particles to APTS in order to speed up the phase separation alone had already been discussed by a group from the University of Lund [109-111]: The authors could show that the addition of magnetic particles in PEG/Dextran and PEG/phosphate ATPS significantly increase the phase separation rate under the influence of magnetic fields. The particles were required to partition the dispersed phase of the

system. Based on the combination of selective magnetic separation and magnetically enhanced phase separation, the concept of Magnetic Extraction Phases (MEP) was introduced.

2.2.4 Magnetic Extraction Phases

2.2.4.1 Principle

The term MEP was introduced by Becker et al. [112]. The principle of MEP is based on the combination of AMTPS and functionalized magnetic sorbents that partition into the disperse, coacervate phase, shown in Figure 2.10:

The first step of MEP is the adsorption of the target protein to the particle. The target protein containing feed is mixed together with the functionalized particles and the phase forming surfactant at conditions below the phase separation temperature. After the adsorption is complete, the temperature is raised and the phases begin to split. The magnetic particles together with the target protein are enriched in the coacervate phase of the system. The speed of phase separation is hereby increased by the application of an external magnetic field. After the phase separation is complete, the aqueous phase is removed and subsequently elution buffer is added to the coacervate phase to elute the target protein from the particles. During this desorption step, the system remains in the single-phase state. After desorption, the temperature is raised to induce phase separation again and a magnetic field is switched on. The target protein partitions between both phases, unaffected by the magnetic sorbents, and is withdrawn from the aqueous phase. The coacervate phase comprises the regenerated magnetic sorbents. At this step, the MEP cycle is complete. The magnetic sorbents and the coacervate phase can be reinjected into the next adsorption step. Assuming a high separation efficiency, only little phase forming surfactants and magnetic sorbents have to be added to the next cycle.
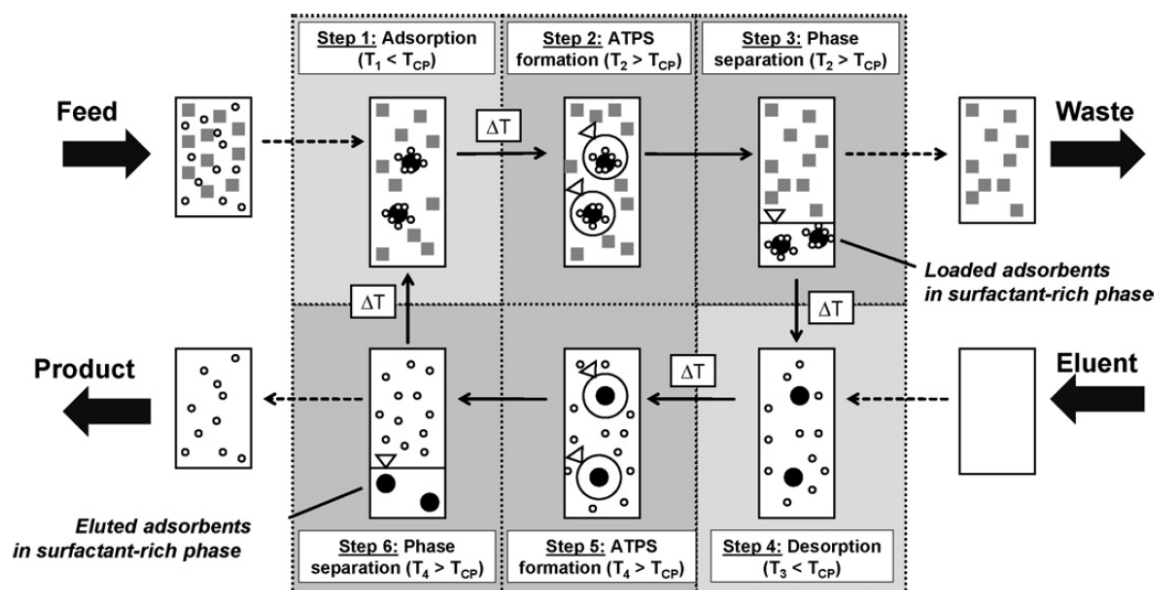
Figure 2.10: Proposed MEP Process from [112]. The target protein is bound to the particle at a temperature which corresponds to the single phase regime. The temperature is raised and due to the application of a magnetic field the phase separation is accelerated. The aqueous phase from the phase separation comprises the contaminants and is withdrawn in the next step. Eluent is added to desorb the target protein from the particles and the temperature is increased to split the phases. After magnetically augmented phase separation, the aqueous product stream contains the target protein, while the coacervate phase contains the particles. The micelle and particle rich phase can be reused in the next cycle, minimizing the cost for particles and phase forming surfactant.

In contrast to the ATPS, described in the work of Suzuki, the application of AMTPS bears striking advantages:

- Only one phase forming component is required

- The coacervate phase contains the particles, thus most of the phase forming component is recycled together with the particles

- Only little phase forming component remains in the product stream. This not only minimizes the loss of the component, but also maximizes the product purity

- By the help of the temperature, the system is tunable between the single-phase and the two-phase regime. Thus, the adsorption of a target molecule can be performed in single phase state omitting the negative influence of the two-phase system to the adsorption kinetics of the target protein

- An AMTPS can be selected with extreme partitioning coefficients for the target protein, thus the elution step results in a high protein yield and concentration in the aqueous phase

- The remaining target protein which is eluted from the particles and partitions to the micelle rich phase is recycled together with particles and surfactant and therefore is not lost but stays in the process

2.2.4.2 MEP - State of Knowledge

In the following, important results from Becker are summarized [112]:

Within this work, two different phase forming surfactants were investigated for their applicability in MEP. In general the applicability is dependent on the fact that the applied magnetic sorbents partition exclusively to the micelle rich phase of the AMTPS.

The first candidate was the nonionic surfactant Aethoxal B ($C_{12}PEO_{4,5}PPO_5$). AMTPS based on Aethoxal B were characterized by extreme partitioning coefficients K. The investigated protein solutions (Lysozyme, 6xHis-GFP, Soy Protein) partitioned almost completely to the aqueous bottom phase (K<<1). In addition to this, the surfactant was economically beneficial due to its low cost. On the other hand, unfavorable partitioning of a range of magnetic particles with different functionalities (e.g. cation-exchange, hydrophobic, metal-chelate) was investigated. Most of the particles partitioned to the interface of this AMTPS. In addition the partitioning was strongly (and unpredictably) dependent on the degree of particle functionalization. This led to the exclusion of this promising MEP candidate.

The second AMTPS investigated was based on the nonionic surfactant Triton X-114. Using this system, the partitioning coefficients of two model proteins, lysozyme and ovalbumin, were rather moderate cf. the ones in the Aethoxal B system: For a temperature of 30°C and a protein concentration of 0.1 g/L the partitioning coefficients were determined to $K_{Lys} = 1.53$ and $K_{Ova}=2.72$. In this case, the top phase was the aqueous phase. A combination of this AMTPS and magnetic particles functionalized with polyacrylic acid lead to the successful demonstration of a MEP process. With a particle concentration >2.5 g/L, the target protein lysozyme was transferred from the aqueous to the coacervate phase, while the contaminating protein ovalbumin remained in the aqueous phase.

A semi technical-scale MEP was conducted in a 200 ml batch reactor and three consecutive MEP cycles were performed. The magnetic field gradient was realized by means of an electromagnet. Figure 2.11 shows the phase separation of the MEP in the 200 ml separation chamber. In this set of experiments, the phase separation was initiated by turning of the stirrer and simultaneously switching on the electromagnet for 20 minutes. As can be seen, the aqueous top phase is still "cloudy" which means that the phase separation is not fully completed. On the other hand, the magnetic particles were separated completely within this timeframe. The total particle separation in the three cycles was quantified to > 99 %, the estimated loss in phase forming surfactant was 6 % per cycle.
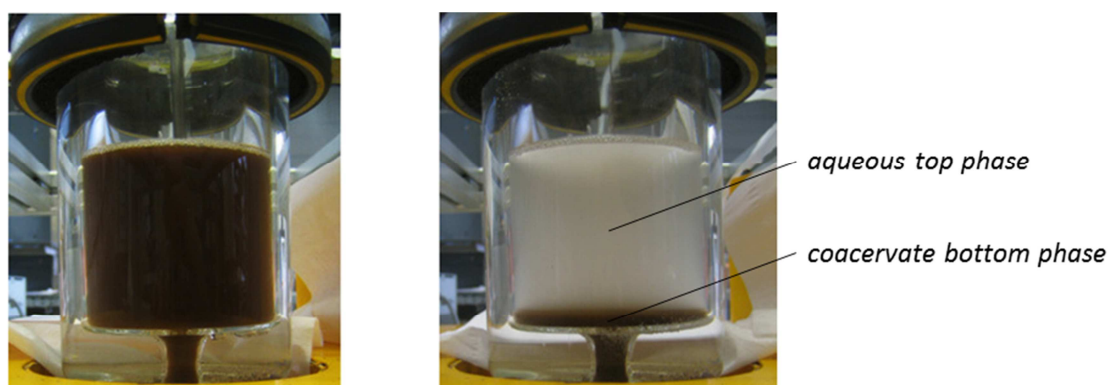
Figure 2.11: 200 ml batch MEP: 1.33 % Triton X-114 AMTPS with a magnetic particle concentration of 2 g/L. Left: Single-Phase System. Right: Two-Phase System after 20 min at T = 30 °C, ΔB=30 T/m and B_{max}=0.4 T. From [112].

The protein separation performance however left room for improvement.In the course of the three cycles 50 – 70 % of the target protein was obtained in the product stream. The separation performance can be increased by: i) Increasing the K-value of the target protein between the phases or ii) Optimization of the binding mechanism of the magnetic particles. The protein binding and protein elution performance of the particles highly influences the overall performance of the MEP process. On the one hand, the adsorptive properties of magnetic sorbents can be fully optimized independent from the AMTPS but on the other hand, the particles are required to partition exclusively to the coacervate phase. Therefore, the optimization of the particle functionalization is challenging.

In summary it was shown by Becker, that MEP is a promising concept for the technical-scale separation of proteins. From an economical point of view, the utilisation of cheap permanent magnets instead of expensive electromagnets is favorable. In addition to this, an economic MEP process will require optimized AMTPS and – more importantly - magnetic particles with excellent binding and elution properties and proper partitioning behavior. Therefore the need in understanding mechanisms of the partitioning of the magnetic particles between the two phases is crucial for the further development of the MEP process.

2.2.5 Partitioning of Colloids and Particulates

2.2.5.1 Energetic Considerations

When colloids and insoluble small particules are added to a two-phase system, these substances partition between the two phases or accumulate at the interphase. A theoretical consideration of such a small particle partitioning between two phases was early described by Albertsson and Walter [113]. The model is based on the following assumptions:

- The adsorption of particles at the interface reduces the free interfacial area between the two phases by the area of the cross sectional radius of the particle.
- This reduces the Gibbs free energy of the system compared to a system where the particles are suspended in one of the two phases.

A particle which is located at the interface between two phases is depicted in Figure 2.12.
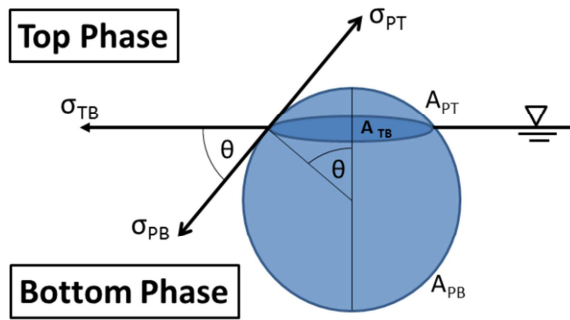
Figure 2.12: A particle accumulated at the interface between the top and the bottom phase of a biphasic system.

The total free interfacial energy of such a particle is given by the product of the surface tension σ_i of the phase and the total interfacial area A_i within this phase. For energetic considerations the interfacial area of a particle at a certain interface has to be calculated. From Figure 2.12 the surface areas of the particle in the bottom phase A_{PB}, the top phase, A_{PT} and of the interface A_{TB} are given by the following equations:

$$A_{PB} = 2 \cdot \pi \cdot R^2 \cdot (1 + cos\,\theta) \qquad \text{[Eq. 2.29]}$$

$$A_{TB} = 2 \cdot \pi \cdot R^2 \cdot (1 - cos^2\,\theta) \qquad \text{[Eq. 2.30]}$$

$$A_{PT} = 2 \cdot \pi \cdot R^2 \cdot (1 - cos\,\theta) \qquad \text{[Eq. 2.31]}$$

The total change in free energy is then given by the equation

$$F = \sigma_{PB} \cdot A_{PB} + \sigma_{PT} \cdot A_{PT} - \sigma_{TB} \cdot A_{TB} \qquad \text{[Eq. 2.32]}$$

For given surface tensions, a particle will then be located at a position with the minimum free energy. As an illustration, Figure 2.13 shows the course of the free energy for values σ_{PT} = 0.02 J m^{-2}, σ_{PB} = 0.01 J m^{-2} and σ_{TB} = 0.015 J m^{-2}. The free energy is hereby normalized by the particle surface area $4\,\pi\,R^2$.
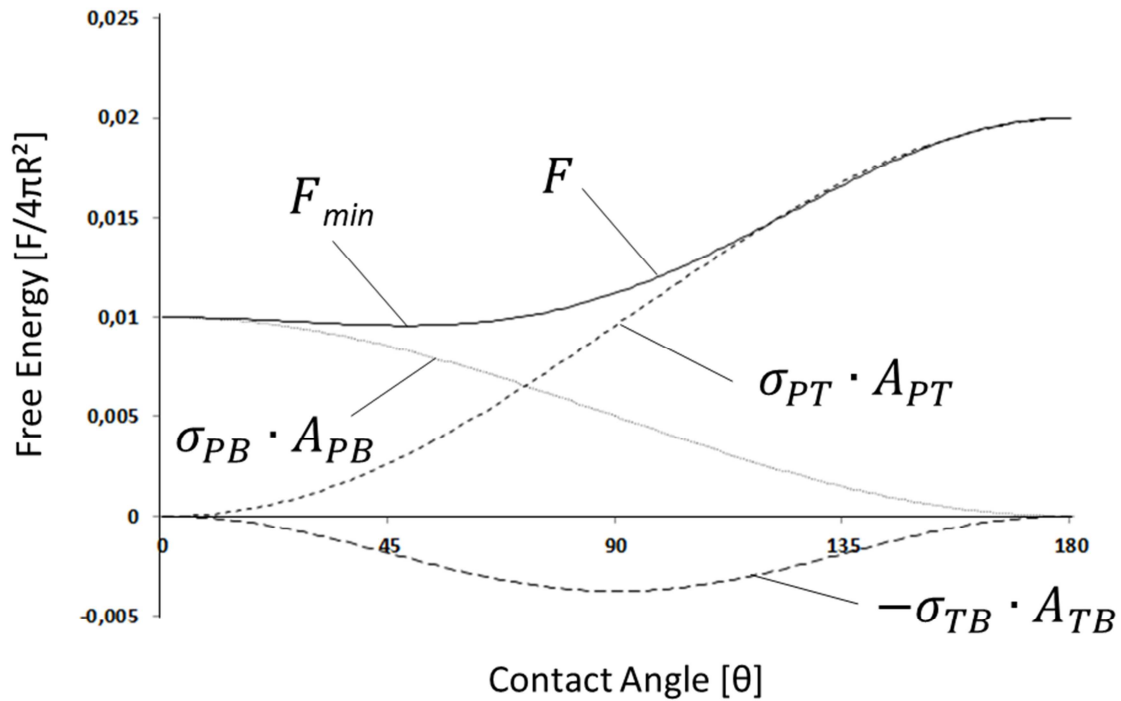
Figure 2.13: Course of the total free surface energy as a function of the contact angle θ. At θ ≈ 48° the total free surface energy reaches a minimum.

Differentiating Equation 2.32 with respect to θ results in the Young equation, from which θ can be calculated directly:

$$\frac{\sigma_{PT} - \sigma_{PB}}{\sigma_{TP}} = cos\,\theta$$

[Eq. 2.33]

Based on Equation 2.33, Albertsson classified the partitioning behavior of particles in five categories [22]:

$$\frac{|\sigma_{PT} - \sigma_{PB}|}{\sigma_{TP}} \geq 1 \quad \text{with} \quad \sigma_{PT} > \sigma_{PB} \quad \textit{Particles partition to the bottom phase}$$

$$\frac{|\sigma_{PT} - \sigma_{PB}|}{\sigma_{TP}} \geq 1 \quad \text{with} \quad \sigma_{PT} < \sigma_{PB} \quad \textit{Particles partition to the top phase}$$

$$\frac{|\sigma_{PT} - \sigma_{PB}|}{\sigma_{TP}} < 1 \quad \text{with} \quad \sigma_{PT} > \sigma_{PB} \quad \textit{Particles at the interphase with 0° < θ < 90°}$$

$$\frac{|\sigma_{PT} - \sigma_{PB}|}{\sigma_{TP}} < 1 \quad \text{with} \quad \sigma_{PT} = \sigma_{PB} \quad \textit{Particles at the interphase with } \theta = 90°$$

$$\frac{|\sigma_{PT} - \sigma_{PB}|}{\sigma_{TP}} < 1 \quad \text{with} \quad \sigma_{PT} < \sigma_{PB} \quad \textit{Particles at the interphase with } 90° < \theta < 180°$$

As can be seen from this classification, the partitioning behavior is considered as a function of the surface tensions only. The gravitational force (thus the particle size), as well as the Brownian motion, which tends to the randomly distribution of the particles in both phases [22], are not considered. These effects are considered in the work of Hoeben [114]:

In case of spherical particles, a planar interface between the two phases and neglection of the gravitational force, the free interfacial energy is described by the equation:

$$\Delta E_{Ads} = -\frac{1}{4}\pi \cdot d_P^2 \cdot \sigma_{TB} \cdot (1 + \cos\theta)^2 \qquad \text{[Eq. 2.34]}$$

Here, d_p is the particle diameter, σ_{TB} is the interfacial tension between the two phases and θ is the contact angle between the liquid-liquid interface and the solid-liquid interface measured through liquid B.

For a high interfacial tension σ_{TB} ΔE_{Ads} becomes negative, thus the particle will remain attached to the liquid-liquid interface.

If there is a significant density difference between the particles and the surrounding liquid, the gravitational force F_G will significantly influence to the particle behavior. If F_G is large enough, the particle will be pulled from the interface to the bottom phase of the system. In order to be removed from the interface, a particle has to be moved a distance of approximately half its diameter. The change in gravitational energy of the whole system can be then be calculated to:

$$\Delta E_G = \pm \frac{1}{12}\pi \cdot d_P^3 \cdot (\rho_P - \bar{\rho}_I)^2 \cdot g \qquad\qquad \text{[Eq. 2.35]}$$

Where ρ_P is the density of the particle, $\bar{\rho}_I$ is the average density of the liquid phases and g is the gravitational constant.
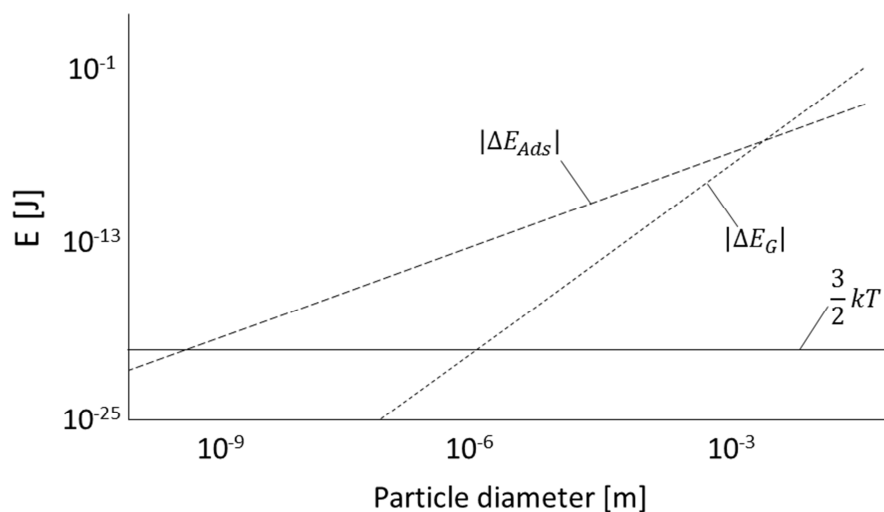
Figure 2.14: Energetic Considerations of a particle partitioning between two phases. ΔE_G is defined as the change in gravitational energy and ΔE_{Ads} is the change in total interfacial energy of the system. The density difference between the particle and the average density of the liquids is 200 kg m^{-3}, the interfacial tensions between the two liquids σ_{ab} is 30 mN m^{-1}, the contact angle θ is 90° and the absolute temperature T is 298 K. From: [114]

It can be seen from Figure 2.14 that for the given system parameters, ΔE_G exceeds ΔE_{Ads} if the particle diameter is larger than 1 mm. Particles with sizes larger than 1 mm will therefore sediment from the interface due to a win of the gravitational energy. For particles with sizes of 1 nm up to 1 mm, ΔE_{Ads} is the dominating factor, thus it is energetically favorable to remain at the liquid-liquid interface. For very small particles with sizes below 1 nm, the impact of the Brownian motion due to the thermal energy, which is equal to 3/2 k T is predominant. Therefore spontaneous desorption from the interface due to Brownian motion is likely to occur [114].

2.2.5.2 Practical Investigations

In practice, the direct determination of the free energy of particles and interfaces is difficult. Therefore, several authors investigated the partitioning of particles in ATPS and AMTPS from an experimental point of view:

Colloidal polymeric acrylic latex particles and TiO_2 particles were partitioned in PEG/Dextran ATPS [115]. The authors investigated the partitioning of a variety of chemically modified beads with sizes from 100 to 450 nm. In their work they found a fundamental influence of the surface chemistry and the pH level of their system. For lower pH levels, they observed a preferable partitioning of the particles to the PEG phase and explained this effect by the creation of hydrogen bonds [115]. At higher pH levels the partitioning of carboxylated particles was reversed. In another study, Helfrich et al. applied PEG/Dextran ATPS for the selective separation of Au and Ag nanoparticles. At a particle size of approximately 14 nm, the Au particles partitioned to the upper, PEG rich phase, while the Ag particles were enriched in the lower dextan phase [28]. Increasing the Au particle size up to 250 nm did not change their partitioning behavior, the authors describe the settling of the larger particles to the interphase after 96 hours, thus, showing, that the interfacial tension in this ATPS is large enough to overcome the gravitational force [28]. The partitioning of inorganic silica and hematite particles in biphasic systems of Triton X-100/dextran was investigated [116, 117]. The authors described a pH-dependent reaction of the silica particles. At low pH these particles partitioned to the surfactant rich phase and with an increase of the pH the partitioning behavior was turned around. In contrast to this, the partitioning of the hematite was not pH dependent and the hematite particles partitioned to the bottom, dextran phase at pH 3, 7, and 11. In both studies, the addition of ionic surfactants to the system, had significant influence on the partitioning of the particles: The addition of the cationic surfactant dodecyltrimethylammonium bromide (DTAB) fundamentally changed the partitioning behavior of the silica particles from the surfactant phase to the dextran phase of the system. The anionic surfactant sodium dodecyl sulfate (SDS) did not change the partitioning behavior of the silica particles [116]. In case of the haematite particles the addition of DTAB transferred them from the bottom to the top phase [117]. The difference in the partitioning behavior was explained by adsorptive and electrostatic interactions between the polymers of the biphasic system and the particles.

In summary, all experimental studies investigating the behavior of insoluble particles in ATPS explain the particular partitioning of the components by attractive interactions between the polymers of the two-phase system and the particle. These may be either

attributed to (pH-dependent) hydrogen bonds as in the case of silica particles, or due to electrostatic interaction between oppositely charged polymers and particles.

2.3 Surfactants

AMTPS are formed on the basis of nonionic or mixed surfactant solutions. It is therefore crucial to keep in mind, that – besides thermodynamic considerations – the attractive interactions between the surfactants and the solubilized components and the interactions between the surfactants and insoluble colloids (in this case the magnetic particles) play a dominant role. Besides these interactions, this chapter deals with important process considerations, specifically the detection and analysis of surfactants as well as their removal from aqueous solutions.

In general a surfactant (from: SURFace ACTive AgeNT) molecule consists of a hydrophilic head and a hydrophobic tail schematically shown in Figure 2.15. A convenient way for their classification is based on the electrostatic charge to cationic, anionic, zwitterionic and nonionic surfactants. In solutions, surfactants can form a variety of different structures depending on the particular conditions and their processing. In Figure 2.16 different forms of surfactant aggregates are depicted.
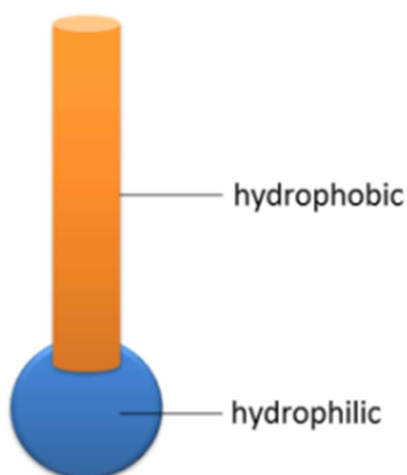
Figure 2.15: Scheme of a surfactant molecule with hydrophilic head and hydrophobic tail.
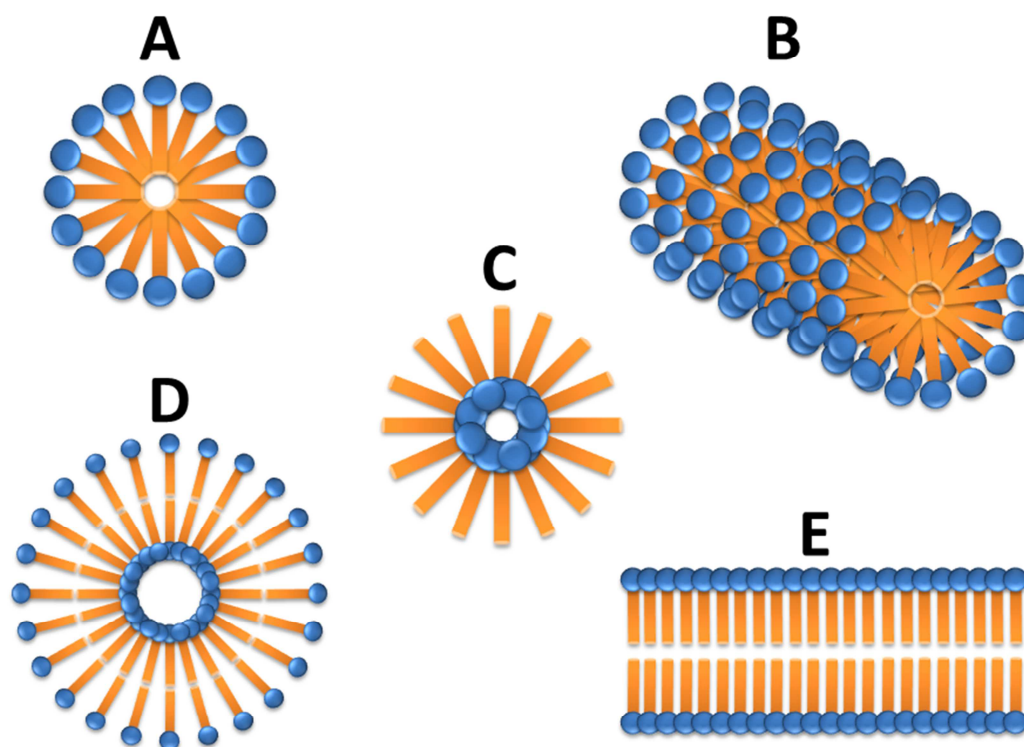
Figure 2.16: Forms of surfactant aggregates. A: Spherical micelle, B: Cylindrical micelle, C: Reversed micelle, D: Liposome, E: Bilayer

2.3.1 Analysis of Nonionic Surfactants

Magnetic Extraction is based on AMTPS created by nonionic surfactants. In order to monitor the surfactant concentrations during this process, a fast, robust and reliable method and, in addition, a wide detection range is required. One issue hereby is the variation of the chain length of the surfactant species themselves: For instance, the well-known Triton X-114, depicted in Figure 2.17 varies in the number of the PEG-units in its hydrophilic head. Only the average number (n=7.5) is provided.
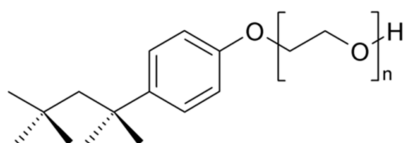
Figure 2.17: Molecular Structure of Triton X-114 with the average number of PEG subunits: n=7.5.

The nonionic surfactant Eumulgin ES will play a dominant role in this thesis. The chemical formula of Eumulgin ES is $C_{12\text{-}14}PEO_5PPO_5$. Besides the varying hydrophobic carbon chain, it is produced by copolymerization of PEG and PPG. The copolymerization results in a variety of possible chain configurations. These examples demonstrate, that surfactants cannot be classified as "a" defined molecule, but a range of very similar molecules. In addition, the influence of large organic macromolecules, such as proteins, must be considered. These macromolecules can exhibit similar properties than the surfactants and therefore interfere their analysis. For example surfactants of the Triton X series exhibit an absorbance maximum at 283 nm due to their aromatic character. Therefore, UV-Vis spectroscopy can be exploited as rapid method for their quantification in aqueous solutions. Protein quantification, however, is typically performed at 280 nm. Thus, both substances interfere the quantification of the other. The absorbance spectrum of Eumulgin ES is shown in Figure 2.18 for varying Eumulgin ES concentrations at wavelengths from 200 nm to 500 nm. As can be seen, Eumulgin ES exhibits an absorbance peak maximum at 213-216 nm. A similar maximum has been reported for the non-ionic detergent pluronics F68, a PEG-PPG copolymer surfactant. In the given context, the quantification of a surfactant protein solution by photometric detection has to be waived for the same reasons than in the Triton X case.
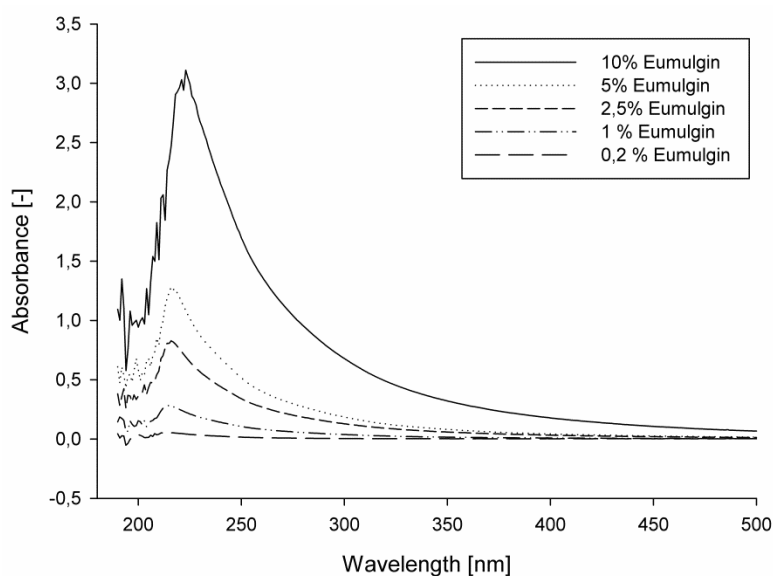
Figure 2.18: UV-VIS absorbance spectrum of Eumulgin ES. The spectra show an absorbance maximum at 213-216 nm.

Besides direct spectrophotometric assays, precipitating reactions with the surfactant molecules have often been applied for their quantification. The precipitation by ammonium cobaltothiocyanate, following extraction of the precipitate into ethylene dichloride has been reported [118]. This precipitation is not interfered by proteins and the author was able to detect Triton X-100 in the range down to 40 µg. The chemicals used however are toxic thus complicating the assay. Other analytical procedures are based upon the precipitation of the surfactant with e.g. phosphotungstic acid [119], silicotungstic acid [120] or Triolein [121]. The amount of surfactant is then determined directly by turbidity of the solution or by subsequent gravimetric, volumetric or photometric determination [118]. Most of these described methods are rather exotic and a lot of experimental effort is required making them impracticable for fast process monitoring. A fast method for the detection of nonionic surfactants was developed based on potentiometric titration [122-125]: The principle of the method is the complexation of barium ions with the hydrophilic chain of the surfactants and the subsequent precipitation using sodium tetraphenylborate. Figure 2.19 shows the principle of this reaction.
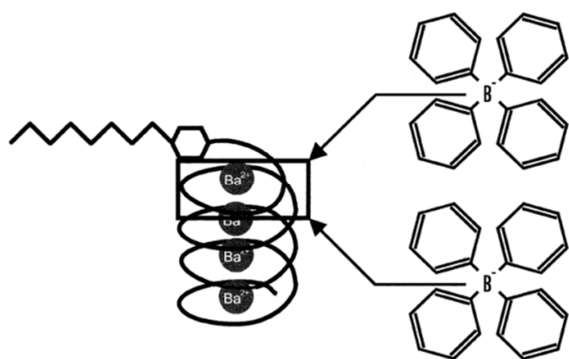
Figure 2.19: Precipitation of a nonionic surfactant upon the complexation with Ba²⁺ ions and precipitation with sodium tetraphenylborate. From [122].

The titration is then performed by: a) addition of barium chloride to a surfactant solution, b) titration of the solution with sodium tetraphenylborate, and c) detection of the quantitative precipitation of sodium tetraphenylborate by a particular electrode (NIO-electrode from [122]**.** Table 2.3 summarizes candidates for the process monitoring of nonionic surfactants in a magnetic extraction process, the detection limits of each method and their limitations. For concentrations above 200 mg/L and in absence of

interfering substances, the determination of the Eumulgin ES concentration by UV-spectroscopy is a fast, convenient method. For very low concentrations surface tension can be applied by back-titration of the solution with milliQ water until the cmc is deceeded and the surface tension begins to increase. Although this method has been successfully applied [126], sufficient amount of sample is required and the detection method is laborious. For samples that do not contain other carbon sources, the determination of the total organic carbon (TOC) is best suited, as the detection limit is very low. For determinations of nonionic surfactants in presence of interfering carbon sources (proteins, DNA, peptides etc.) potentiometric titration is a robust, reliable method.

Table 2.3: Comparison of different surfactant detection methods, their detection limits and limitations

Method	Detction Limit	Drawback
UV-Spectroscopy	300 mg/L	Adsorbance of other components
Potentiometric Titration[a]	20 mg	-
Surface Tension[b]	9 mg/L	Components influencing the surface tension
Total Organic Carbon[c]	2 mg/L	Influence of other carbon sources

[a]Potentiometric Titration is a method based on the total mass of surfactant. The volume used can vary thereby from 40 ml to approximately 1 liter with a detection limit of 20 mg total surfactant.

[b]Surface Tension measurement based on results presented in Chapter 8.4.1.

[c]TOC measurement based on experimental data from Chapter 6.3.3.1.

2.3.2 Adsorption of (Non)Ionic Surfactants to Solid Surfaces

2.3.2.1 Mechanism and Orientation

As described in Chapter 2.2.5.2, the interactions of phase forming components in A(M)TPS and particles supposedly play a dominant role for their partitioning behavior. However, in most articles addressing partitioning phenomena in AMTPS the contribution of adsorption of the phase forming component is neglected. In this context, this chapter deals with the interactions of nonionic surfactants in solutions with solid interphases. Surfactants are surface active by definition. Thus, their interaction with all kinds of

surfaces is obligatory. In industrial processes the interactions of surfactants and colloidal particles are of importance as adsorption phenomena directly influence the colloidal stability of the dispersion [127]. An example for the interaction of surfactants and dispersed particles is the cationic surfactant CTAB which was shown to adsorb to anionic silica particles by measuring the reduction of the surface tension upon increasing particle concentration [128]. The mechanisms of the adsorption of (non)ionic surfactants to surfaces are as versatile as the properties of the surfactants. A review of experimental studies of surfactant adsorption at hydrophilic interfaces can be found from Paria and Khilar, who divide the adsorption mechanisms of ionic and nonionic surfactants as follows: [129]:

- Ion Exchange: Replacement of counter ions adsorbed on the substrate equally charged surfactant ions

- Ion Pairing: Adsorption of surfactant ions from solution onto oppositely charged sites unoccupied by counter ions

- Hydrophobic bonding: Adsorption by an attractive hydrophobic force

- Adsorption by polarization of π-electrons: Attraction between an electron rich aromatic nucleus in the surfactant and the solid adsorbent having strongly positive sites

- Adsorption by dispersion forces: Van der Waals forces between adsorbate and adsorbent increases with increasing molecular weight of the adsorbate

The adsorption kinetics of nonionic surfactants to hydrophilic surfaces, especially silica surfaces, has been investigated thoroughly. A basic model for the adsorption kinetics of surfactants to silica layers from ellipsometry measurements is provided from Brinck [130, 131] in Figure 2.20.
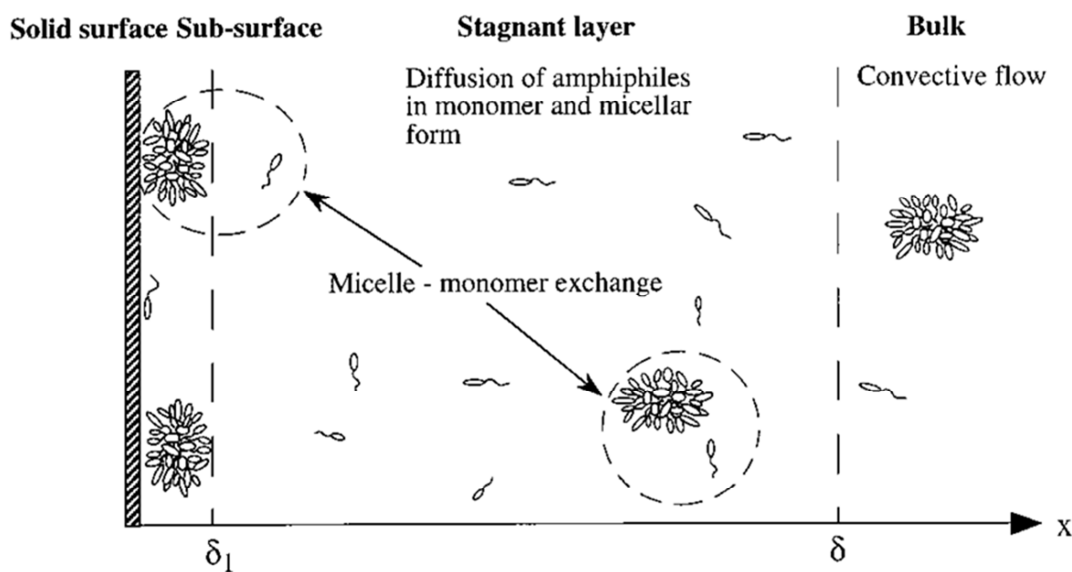
Figure 2.20: Schematic solution profile in the bulk surfactant solution. The adsorption and desorption process are considered to proceed in two consecutive steps. In case of adsorption: 1) Diffusion of the surfactant monomers or micelles from the bulk to the stagnant layer. 2) Passage from the stagnant layer to the sub-surface and adsorption. Both steps happen simultaneously. From [131].

The model is based on monomer diffusion, micellar diffusion and micellar dissociation, whereas it is assumed that only single surfactant molecules adsorb to the surface.

Early studies were performed in order to investigate the adsorption of the surfactants by adsorption isotherms e.g. at hydrophobic surfaces [132, 133]. The *orientation* of surfactant adsorption to hydrophilic silica surfaces has recently aroused much attention. Using ellipsometry and atomic force microscopy (AFM) the group around Tiberg showed that hydrophobic surfaces were mainly covered with surfactant monolayers or sub-monolayers while hydrophilic surfaces are covered with surfactant bilayer-type aggregates that were identified as globular structures similar to bulk micelles [134-136]. Figure 2.21 depicts the experimental results from the oriented adsorption of nonionic surfactants of the class of $C_X E_Y$ onto hydrophobic and hydrophilic surfaces.
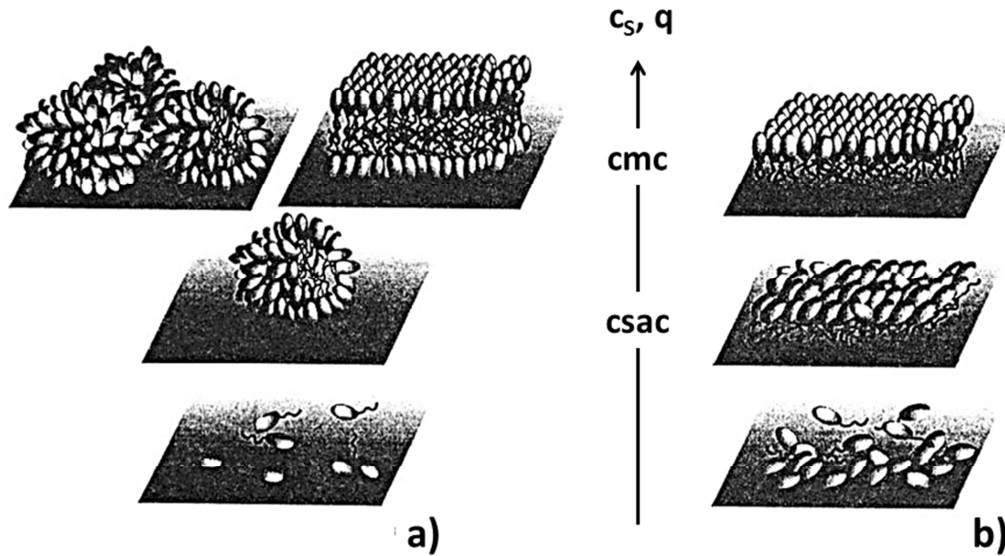
Figure 2.21: Orientation of C_NE_M surfactants at a) bare silica and b) hydrophobic silica with increasing surfactant concentration c_S and surface coverage q. When the concentration reaches the critical surface aggregation concentration (csac) aggregates are formed. A plateau in q is reached for c_S > cmc. From [134].

Globular, ordered micelle structures rather than bilayers were also found by ^{2}H-NMR investigations [137] and additionally by the group around Oberdisse, who investigated the adsorption of nonionic surfactants onto colloidal silica particles by small angle neutron scattering (SANS). This phenomenon was termed "micelle decorated silica" [138-141].

Besides SANS, AFM and Ellipsometry, detection methods like Attenuated Total Reflection Fourier Transferred Infrared Spectroscopy (ATR-FTIR) and Quartz Crystal Microbalance with Dissipation (QCM-D) were used to provide rapid, noninvasive data to monitor surfactant adsorption to solid surfaces e.g. [142-144].

2.3.2.2 Role of pH on the Adsorptive Behavior of Nonionic Surfactants

The binding of surfactants to hydrophobic surfaces arises from interactions between the carbon chain of the surfactant and the surface. The binding to hydrophilic surfaces however is assumed to be related to hydrogen bonding between the ether or terminal hydroxyl group of the surfactants and the surface [145]. This assumption is confirmed by the increase of surfactant adsorption with decreasing pH as the number of protonated OH groups (of the surface or the surfactant) capable for hydrogen bonding increases [146]. This was also shown for resins with carboxyl groups [147]. The same effect was

shown for PEG polymers alone (PEG is often the hydrophilic part of a surfactant): Dynamic light scattering was used to monitor the adsorptive behavior of the PEG onto colloidal silica particles of 22 nm size: The amount of adsorbed PEG was constant up to pH 10 and then sharply dropped to zero [148].

In summary, nonionic surfactants are capable of adsorbing to hydrophilic as well as hydrophobic interfaces. The impact of pH on the adsorptive behavior of nonionic surfactants onto hydrophilic surfaces however is striking. As the adsorption of the surfactants is supposedly involved in the partitioning behavior of magnetic carriers during the magnetic extraction process, the pH is a crucial criterion of process feasibility.

2.3.3 Removal of Nonionic Surfactants

Bioseparation processes making use of surfactant systems, for instance magnetic extraction, require the subsequent removal of the surfactant from the target product. In the best case, magnetic extraction leads to a product stream with a surfactant concentration close to the cmc. This however requires complete phase separation (as described in chapter 2.2.2). Due to process limitations the surfactant concentration is therefore likely to exceed the cmc more or less. Solid-phase extraction techniques can be applied for the removal of surfactants, e.g. by nonpolar hydrophobic beads [149]. The separation performance, however, depends on the properties of the target molecule. Besides adsorptive methods, the separation of surfactants can be realized in terms of filtration techniques: Surfactants with a high cmc have been removed by dialysis and more efficiently by gel filtration [150]. Especially in technical scale, dialysis is unfavorable due to the large dialysis volumes (typically 1000 times the volume of the feed) and prolonged process times. On the other hand, the removal of surfactants can be realized by means of ultrafiltration.

2.3.3.1 Ultrafiltration

Ultrafiltration (UF) is based on the hydrostatic transmembrane pressure between two liquids separated by a permeable membrane. It is classified by a membrane pore size of $1-100$ nm. In Table 2.4 the classification of membrane based filtration techniques is summarized.

Table 2.4: Classification of transmembrane pressure based filtration processes

Process	Pore Size	Transmembrane Pressure
Microfiltration	0.05 – 10 µm	< 2 bar
Ultrafiltration	1 – 100 nm	1 – 10 bar
Nanofiltration	< 2 nm	10 – 25 bar
Reverse Osmosis	-	20 – 100 bar

UF can be operated either in "dead-end" mode where the direction of the feed flow is orthogonal to the filter or in cross-flow mode, where the feed is pumped in a tangential manner to the membrane. If the volumetric flux J_V through an UF membrane is limited by the membrane only, it is described by the Hagen-Poiseuille equation:

$$J_V = \frac{V}{A \cdot t} = \frac{r^2 \cdot \varepsilon \cdot \Delta p}{8 \cdot \eta \cdot \Delta \chi \cdot \tau} \qquad \text{[Eq. 2.36]}$$

Here V is the volume, A is the membrane surface area, t is the time, r the radius of the pore, ε the porosity of the membrane, Δp is the transmembrane pressure, η the viscosity of the fluid, Δχ is the length of the channel and τ the tortuosity. For cylindrical pores orthogonal to the membrane surface, τ equals 1. As can be seen from Equation 2.36, the flux is a linear function of the transmembrane pressure.

In technical applications the flux is often not fully independent of the pressure. In these cases as the pressure is increased the flux is asymptotically approximating a maximum flux J_∞ as shown in Figure 2.22.
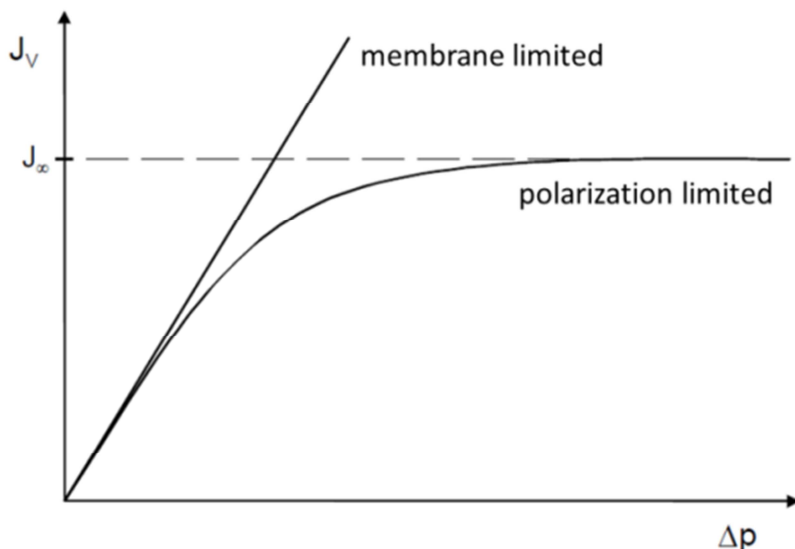
Figure 2.22: Dependency of the flux on the transmembrane pressure. If the flux is only dependent on the membrane properties, the correlation to the pressure is linear. For the development of a gel layer, the flux is limited to J_∞.

This effect is due to the accumulation of retained material and subsequent depletion of the (permeating) components in the boundary layer adjacent to the membrane surface. A second layer called gel or cake is formed at the membrane surface. The principle of this so-called *concentration polarization* model [151, 152] is depicted in Figure 2.23.
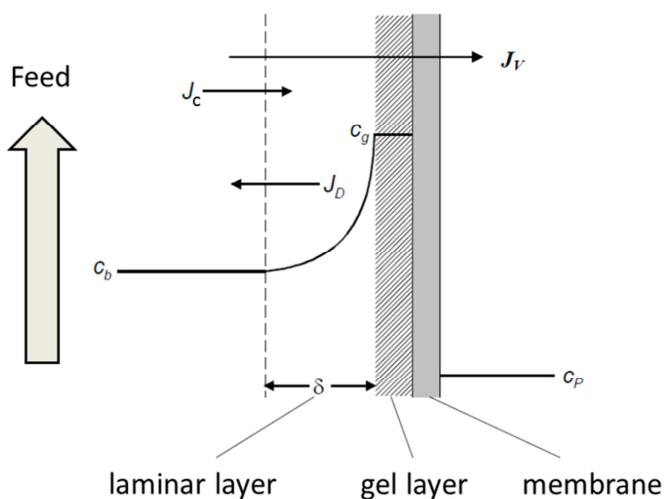
Figure 2.23: Concentration Polarization model at a cross-flow ultrafiltration membrane. Due to accumulation of a component at the membrane surface, a gel layer is formed by which the flow through the membrane is decreased.

The convective transport of a particular substance S (with the bulk concentration c_b) from the bulk towards the membrane is given by:

$$J_{S,con} = \frac{\dot{N}_S}{A} = J_V \cdot c_b$$

[Eq. 2.37]

The flux of S through the membrane is given by:

$$J_{S,mem} = J_V \cdot c_p$$

[Eq. 2.38]

Due to the relative decrease of solvent in the vicinity of the membrane c_b is increased to the maximum gel concentration c_g. The concentration gradient $dc/d\delta$ leads to a diffusive transport of the substance from the membrane to the bulk solution. The diffusive flux $J_{S,diff}$ is described by Equation 2.39:

$$J_{S,diff} = \frac{\dot{N}_D}{A} = -D \frac{dc}{d\delta}$$

[Eq. 2.39]

Here, D is the diffusion coefficient of the target component in the solvent. At steady-state conditions one finds:

$$J_{S,mem} = J_{S,con} - J_{S,diff}$$

[Eq. 2.40]

Integration around the boundary conditions ($c = c_g$ and c_b; $x = 0$ and δ) results in the equation for the flux through the membrane:

$$J_V = \frac{D}{\delta} \cdot ln \frac{c_g - c_P}{c_b - c_P}$$

[Eq. 2.41]

For complete retention of the substance ($c_P \rightarrow 0$), the equation is simplified to:

$$J_V = \frac{D}{\delta} \cdot ln\frac{c_g}{c_b}$$

[Eq. 2.42]

From the linear graph $J_V = f\,(ln\,c_b)$ the maximum gel concentration can then be obtained by its extrapolation to the intercept of the X-axis and the quotient D/δ as its slope.

2.3.3.2 Ultrafiltration of Surfactants

The removal of nonionic surfactants by means of UF has already been described to purify surfactants from solutions in 1964 by Schott [153]. Nonionic surfactants have been separated in UF using dead end filtration [154] or cross-flow filtration [155]. It is generally assumed that, by means of UF, the large micelles can be separated from the small single surfactant molecules [156]. This is heavily exploited in the concept of micellar enhanced ultrafiltration (MEUF): MEUF is used to remove traces of heavy metal ions by their entrainment in oppositely charged micelles. The metal ion containing micelles are subsequently separated from the solution by means of UF, resulting in a heavy metal ion depleted permeate stream [157]. In several UF studies, however, the concentration of the surfactants in the permeate exceeds the cmc e.g. [155, 158-160]. In addition to this, for filtration of surfactant solutions above their cmc a harsh flux decline is generally reported. For instance, for the filtration of nonionic surfactants of the Triton X series or $C_{10}E_x$ through a 10 kDa polyethersulfone (PES) membrane, a reversible flux decline up to 86 % during filtration was detected. This could however not directly be attributed to the standard concentration polarization model - as increasing the transmembrane pressure from 0.5 – 2 bar consequently increased the flux in a linear fashion [161]. The flux decline in surfactant filtration is explained not only by the formation of a gel, but also by adsorption of surfactant molecules to the membrane surface or "creeping" of single molecules to the membrane pores [158]. A concentration polarization model was proposed by Jönsson to describe the mechanisms of nonionic surfactants ultrafiltration [162], shown in Figure 2.24.
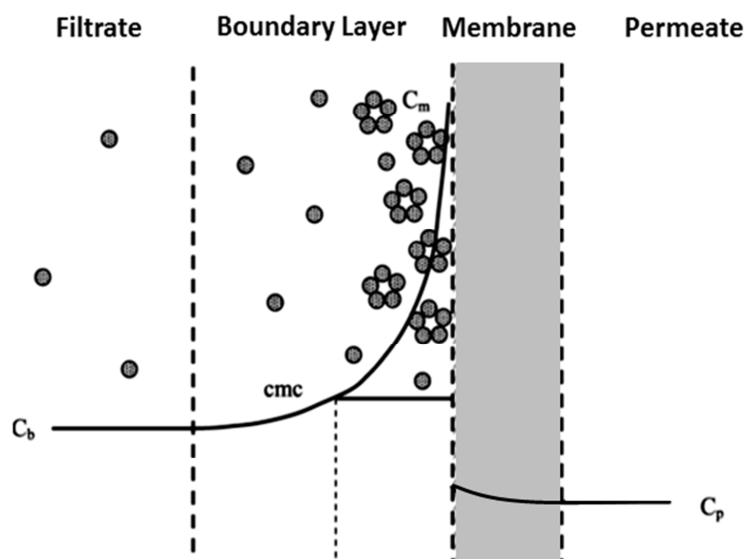
Figure 2.24: Model of concentration polarization of nonionic surfactants at the filtrate side of an UF membrane. The concentration of the nonionic surfactant monomers is increased above the cmc close to the membrane. In addition to this, the surfactant molecules adsorb to the membrane. A boundary layer is formed containing micelles and surfactant monomers. In this model dots symobolize surfactant molecules and the clusters symbolize micelles.

As surfactants can adsorb to the membrane, it is obvious that the surfactant retention is dependent from the *type of membrane*. Further understanding of the mechanisms of surfactant removal via UF with different membranes, can be achieved from the following studies:

I)   It was reported that the retention of nonionic surfactants is much higher (93 % for a MWCO of 200) for hydrophilic surfaces whereas hydrophobic PES membranes led to a very low retention of the surfactants (46 % for MWCO of 400 and 1000 respectively) in solutions below their cmc [163].

II)   It was also shown that the adsorption of nonionic surfactants to a more hydrophobic PES membrane is more pronounced, than the adsorption to a hydrophilic cellulose acetate membrane by static adsorption experiments [164].

III)   Hydrophobic PES membranes showed a flux reduction for the filtration of nonionic surfactants at concentrations even below the cmc, whereas no flux reduction was observed for the same conditions with a hydrophilic cellulose membrane [159].

From these evidences it can be hypothesized, that nonionic surfactants adsorb to hydrophobic membranes due to hydrophobic interactions. The adsorption at the membrane and especially inside the membrane pores as well as the micelle formation adjacent to the membrane lead to a drastic flux reduction. The surfactants localized inside the membrane pores can pass the membrane unhindered, thus their concentration in the permeate stream can exceed the cmc.

2.4 Liquid-liquid Extraction

In general, liquid-liquid extraction is a separation process based on the different distribution of the target component between the two phases. Two physical processes determine the overall process performance.

- The mass transfer of the target component from the initial to the target phase. For a fast mass transfer, small droplets (thus large contact areas) are desired.
- The phase separation rate.

For magnetic extraction, the binding of the target component to the beads takes place under single phase conditions. After the adsorption of the target component is completed, the phase separation is initiated by an increase of the temperature. Therefore it can be concluded that during magnetic extraction, the influence of the mass transfer is neglectable. Thus, after protein binding to the particle is complete, the phase separation rate is dominating the remaining process time.

2.4.1 Phase Separation of two immiscible Fluids

A typical phase separation profile of a batch experiment can be seen from Figure 2.25 for a disperse light phase and a continuous heavy phase. In the sedimentation zone where no coalescence occurs, the phase separation curve shows typically linear behavior. If the droplet separation rate is faster than the rate of coalescence, a zone of dense-packed droplets forms. Within this zone, the droplets grow by droplet-droplet coalescence and eventually coalesce into the top phase. At the time t_e the phase separation process is complete [165].
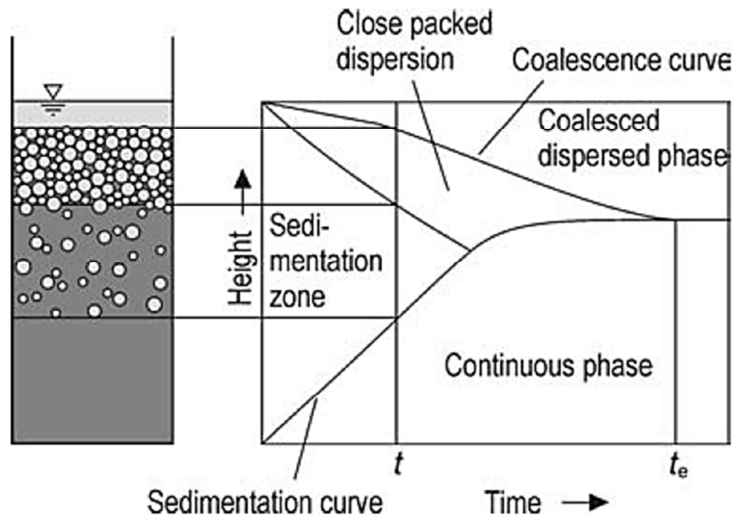
Figure 2.25: Typical phase separation curve in batch experiments. The disperse droplets float to the interphase and form a dense package. From this package, the disperse droplets coalesce to the top phase. From [166].

For a continuous system, typically a dispersion wedge or dispersion band is formed as illustrated in Figure 2.26. The length of the dispersion wedge equals the minimum required length of the separator. Besides the creation of a dispersion wedge or band, very small droplets are formed, that are difficult to separate [167].
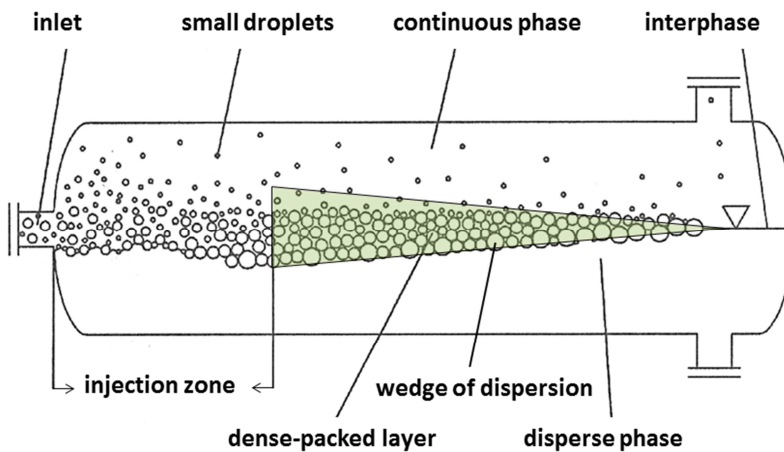
Figure 2.26: Continuous liquid liquid extraction. A wedge of dispersion is formed depending on the flow of the feed. Modified from [167].

The phase separation can be divided into two processes steps: Sedimentation (or flotation) of the droplets to the interface and coalescence effects between the single droplets and the disperse phase. The basic principles of these interactions are explained in the next chapters.

2.4.1.1 Sedimentation of Single Droplets

The velocity of the sedimentation of a single, spherical particle (or a spherical liquid droplet without deformation) surrounded by a continuous viscous liquid is described by the Stokes´ law:

$$v_{St} = \frac{g \cdot \Delta\rho \cdot d^2}{18 \cdot \eta_C} \qquad \text{[Eq. 2.43]}$$

Where $\Delta\rho$ is the density difference of the particle and the surrounding liquid and d is the droplet diameter, g is the gravitational force and η_C the viscosity of the fluid. With the given equations for the Reynolds number and the Archimedes number:

$$Re = \frac{d \cdot v \cdot \rho_C}{\eta_C} \qquad \text{[Eq. 2.44]}$$

$$Ar = \frac{\rho_C \cdot \Delta\rho \cdot g \cdot d^3}{\eta_C^2} \qquad \text{[Eq. 2.45]}$$

Equation 2.43 can be expressed as:

$$\text{Re}_{St} = \frac{Ar}{18} \qquad \text{[Eq. 2.46]}$$

Stokes´ law is only valid for a single solid particle and laminar flow. In this case, laminar flow is, however, only valid for a Reynolds number < 0.25 [168]. For turbulent flow during sedimentation the Reynolds number can be calculated according to Zimmels [168]:

$$Re_{zi} = \left(\frac{-4.8 + \sqrt{23.04 + 2.91 \cdot \sqrt{Ar}}}{1.26} \right)^2 \qquad \text{[Eq. 2.47]}$$

2.4.1.2 Internal Circulation

Besides the effects of turbulent and laminar flow, for a liquid droplet sinking or floating in the surrounding fluid the "Marangoni convection" has to be considered. The Marangoni convection is caused by surface tension gradients between the droplets and the surrounding liquid. This gradient can lead to the circulation of the fluid in the inside of the droplets, which can result in an increase of the droplet velocity in comparison to a solid particle. The effect is diminished, however, by the presence of surfactants at the droplet surface, as the surfactants decrease the mobility of the droplet interphase [167]. A simple mathematical correlation was developed by Hadamard and Rybcynski (from [167]) based on viscosities of the continuous and disperse phase: for a single droplet, the Stokes velocity v_{st} is multiplied with the correction factor K_{HR}:

$$K_{HR} = \frac{1 + \dfrac{\eta_D}{\eta_C}}{\dfrac{2}{3} + \dfrac{\eta_D}{\eta_C}}$$

[Eq. 2.48]

For very large viscosities of the disperse phase cf. the continuous phase, K_{HR} approximates 1 thus no internal circulation occurs (e.g. an extreme case would be a solid particle). For very small viscosity differences K_{HR} converges to 1.5.

2.4.1.3 Effect of Hold-Up

The considerations above are only valid for a single droplet. The influence of interaction of a large amount of hold up, resulting in many droplets and the interactions of these droplets with the continuous phase, is neglected. Sinking droplets lead to a counter-directed flow of continuous phase that is displaced by the droplets, which in consequence leads to a reduced phase sedimentation velocity. Correction factors describing this effect as a function of the total hold-up can be found e.g. from Zimmels [168] or Jeelani [169]:

$$K_{Swarm,Zi} = \frac{(1 - \epsilon)}{\left(1 + \epsilon^{1/3}\right) exp\left(\dfrac{5}{3} \cdot \dfrac{\varepsilon}{1 - \varepsilon}\right)}$$

[Eq. 2.49]

$$K_{Swarm,Je} = \frac{(1 - \varepsilon)^2}{1 + 4.56 \cdot \varepsilon}$$ [Eq. 2.50]

2.4.1.4 Coalescence

As shown in Figure 2.25 droplet sedimentation leads to the accumulation of the droplets in a dense-packed zone next to the interphase. The droplets either coalesce during sedimentation, which leads to larger drops with increased sedimentation speed, or the drops coalesce at the dense layer. The basic scheme of coalescence is depicted in Figure 2.28 and divided into three stages:

I: Approaching of the droplet to the interphase.

II: Droplet deformation at the interface due to the interfacial tension between the disperse phase and the continuous phase. A thin film is formed. The gravity (or buoyancy) affecting the droplet leads to film drainage between the droplets. When the thickness of the thin film reaches its critical value, the van der Waals forces cause it to rupture [170].

III: The droplets coalesce with the interphase. The total time of coalescence is dominated by the film drainage. However, no generally accepted model for calculation of the film drainage has been developed yet [167].
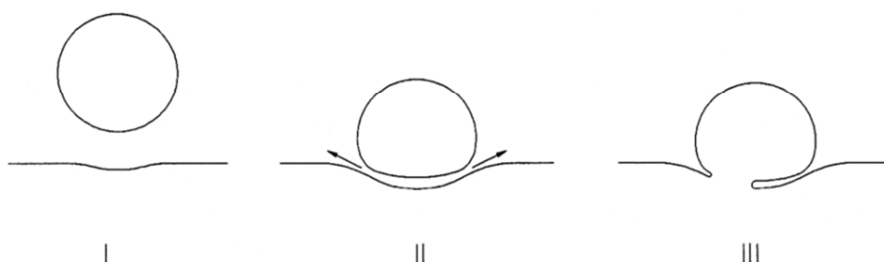
Figure 2.27: Principle of droplet coalescence. A droplet approaches the interface. A thin film is formed in between the droplet and the interphase. The film drains until the layers rupture and the droplet coalesces. From [167].

The mechanism of film drainage is even more complex in the presence of surfactants. As shown in Figure 2.28 the film drainage between a droplet and the interface leads to the

generation of a surfactant gradient (Figure 2.28 left). The surfactant gradient causes a surface tension gradient which provokes Marangoni convection (Figure 2.28 right). Thus the reflux of the continuous phase between the droplet and the interphase is induced and the coalescence of the droplet is impeded.
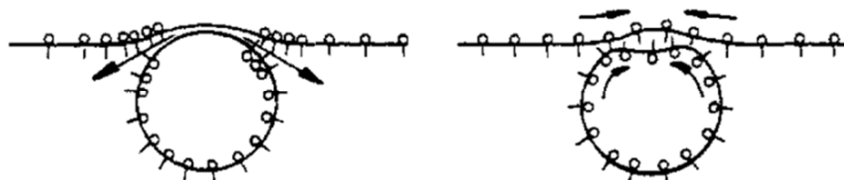
Figure 2.28. Induction of Marangoni convection during coalescence of a droplet in surfactant systems. The film drainage leads to the establishment of a surface tension gradient that leads to marangoni convection and reflux of the continuous phase between the droplet and the interphase. From [171]

2.4.2 Phase separation in MEP – State of Knowledge

A model was developed by Becker for the phase separation velocity in Magnetic Extraction [112]. The model is based on the following assumptions:

- The magnetic particles are completely integrated into the micellar droplets of the AMTPS
- The magnetic particles are homogeneously dispersed throughout the micelle rich droplets
- The increase in volume of the micellar droplets related to the uptake of magnetic particles is neglectable
- The friction can be calculated according to Stokes
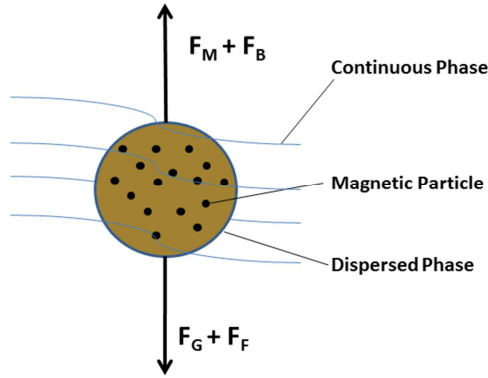
Figure 2.29. Force balance around a magnetic particle doped micellar droplet in an AMTPS at steady state. The magnetic field gradient is directed upwards. The particles are enriched in the droplet.

At steady state conditions, the mass balance is then given by:

$$F_G + F_F = F_B + F_M \qquad \text{[Eq. 2.51]}$$

With the applied forces given by the equations:

Gravity:
$$F_G = \frac{1}{6} \cdot \pi \cdot g \cdot \left(\rho_D + \frac{c_P}{\varepsilon} \right) \cdot d^3 \qquad \text{[Eq. 2.52]}$$

Friction:
$$F_F = \pi \cdot \eta_c \cdot v \cdot d \qquad \text{[Eq. 2.53]}$$

Buoyancy:
$$F_B = \frac{1}{6} \cdot \pi \cdot g \cdot \rho_C \cdot d^3 \qquad \text{[Eq. 2.54]}$$

Magnetic Force:
$$F_M(x) = \mu_0 \cdot \frac{c_P}{\varepsilon} \cdot \frac{1}{6} \pi \cdot d^3 \cdot M(x) \cdot gradH(x) \qquad \text{[Eq. 2.55]}$$

Equation 2.51 can be solved for the velocity to:

$$v_{ME}(x) = \frac{1}{18} \cdot d^2 \cdot \frac{g \cdot (\rho_D - \rho_C) + \gamma(x) \cdot \frac{c_P}{\varepsilon}}{\eta_C} \qquad \text{[Eq. 2.56]}$$

With

$$\gamma(x) = g + \mu_0 \cdot M((H(x)) \cdot gradH(x) \qquad\qquad \text{[Eq. 2.57]}$$

From Equation 2.56 the velocity of a single droplet can be calculated. Besides the physical properties of the AMTPS and the magnetic particles, the knowledge of the geometry of the magnetic field is required, as both magnetic field gradient as well as magnetic strength at the X-coordinate influence the magnetic force. These can be obtained without elaborative sedimentation experiments. The droplet diameter remains as only process dependent parameter. This parameter, however, is independent from the process volume and needs to be either estimated or determined in small-scale experiments.

2.4.3 Mixer Settler Devices

All technical devices applied for liquid-liquid extraction are based on the same tasks. The first task is the dispersion of one of the liquids in the other in order to enlarge the contact area to maximize the mass transfer. In the mixer the energy input is ideally directly related to the resulting drop size. The second task is the demixing of the fluids. The technical apparatus can be classified into extraction columns, centrifugal extractors and mixer settlers. The choice of the separator is based on the process requirements whose basic criteria can be seen from Figure 2.30.
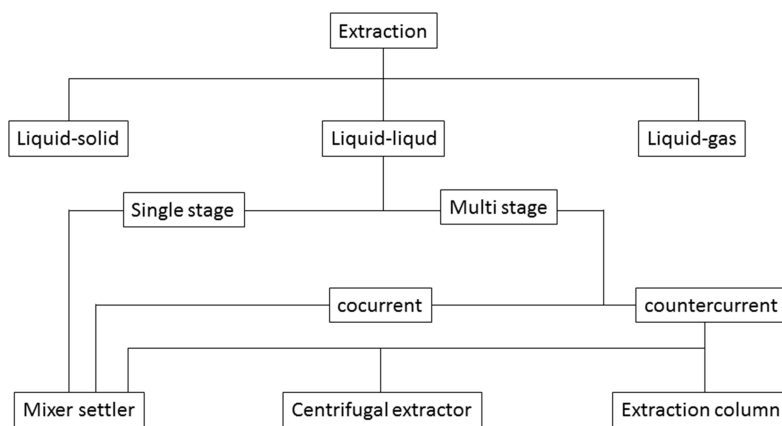
Figure 2.30: Criteria for the choice of separation apparatus for liquid liquid separation. Modified from [172].

In case of the concept of CME (described in chapter 2.2.4) the mass transfer plays a minor role. The separation is conducted under the influence of the magnetic field generated by a plain permanent magnet and the phases are injected in a concurrent fashion. The appropriate apparatus for this separation is therefore a mixer settler. For this reason a detailed illustration of centrifugal extractors and extraction columns is spared. Further information about these apparatus can be found e.g. in [172-174].

2.4.3.1 Mixer Settlers

The advantage of mixer settlers in comparison to other extraction equipment is that efficiencies of nearly 100 % can be reached [173]. These high efficiencies can be retained even for large throughputs. The simple technical installation of a cascade of mixer settler batteries has led to their broad industrial use. A mixer settler unit consists of a mixer area (e.g. a stirred vessel) followed by a settling vessel where the phases are separated. At the end of such a unit the heavy and the light phase are withdrawn. Usually additional valves are installed to remove sludge at the interphase or from the bottom of the heavy phase. The basic concept can be seen in Figure 2.31.
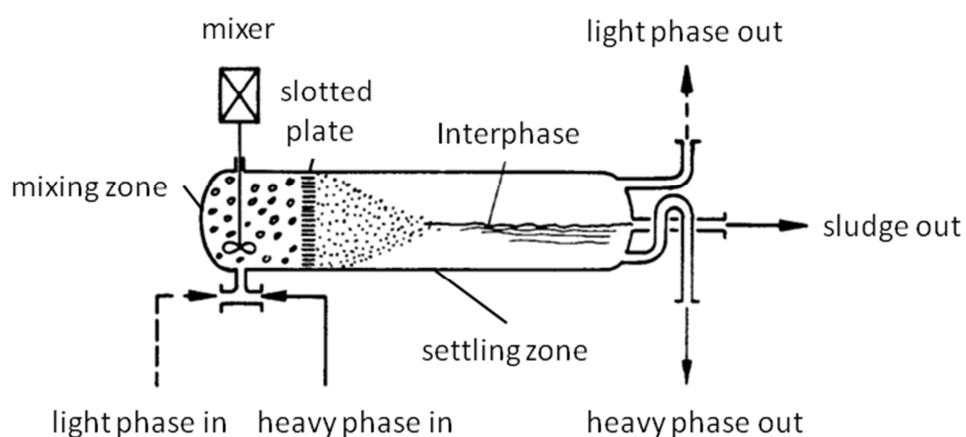
Figure 2.31: Principle of a mixer-settler unit. Modified after [175].

Due to the horizontal arrangement of the settlers large areas are required in order to achieve high throughputs in industrial applications. Thus for industrial applications, special mixer-settler arrangements have been created to spare space. In a *box-type* mixer settler, shown in Figure 2.32 the mixing and separating areas are integrated into one unit.

The phases are separated by an overflow weir for the light phase, while the heavy phase underflows a slit. The agitator disperses and conveys the liquid phases [173].
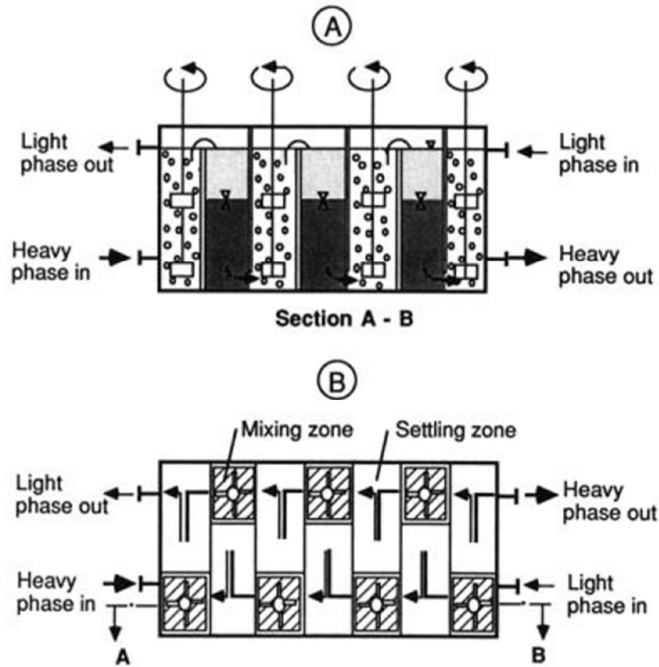
Figure 2.32. Box-type mixer settler. A: Side view; B: Plain view. From [173]

Another space-saving design composes of a tower-like arrangement of the mixer settler battery. This arrangement is called Lurgi tower extractor and depicted in Figure 2.33.
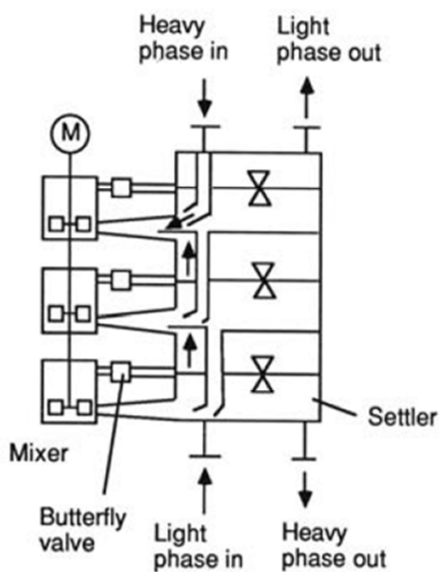
Figure 2.33. Principle of the Lurgi tower as mixer settler. From [173].

2.4.3.2 Coalescence Aids

The coalescence time of the disperse phase determines the residence time of the liquid in the settler, thus, governing the area required for the separator. Therefore, mixer settler units are often supplied with coalescing aids to decrease the coalescence time [176]. Coalescing aids provide contact area inside the mixer, where the small droplets can form lager droplets. Usually, but not necessarily, the droplets wet the surface of the coalescing aid. By the use of coalescence aids the length of the separator (or the residence time) can be reduced by a factor 2-5 [173, 177]. The most important coalescing aids are inclined packages of plain (or corrugated) plates shown in Figure 2.34-A and fiber bed filters shown in Figure 2.34-B.
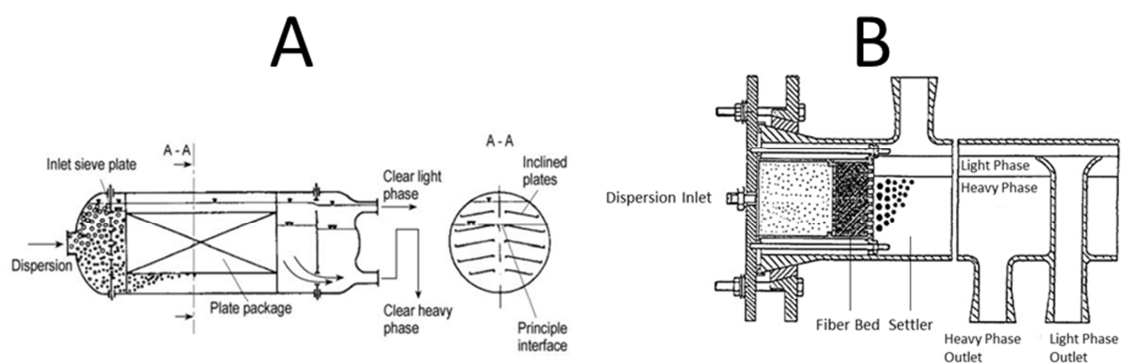
Figure 2.34. A: Inclined plates in a mixer settler to increase the coalescence of the droplets. B: Fiber bed as coalescing aid of a settler unit from [173],

The influence of various coalescing aids onto the separation performance is summarized by [173] form several scientific reports:

- Thin laminar films should flow on the plates, as the coalescence of drops is promoted by shear stress of film flow near the plate. The larger the flow rate of the concurrent continuous phase, the smaller the film thickness and the better is the coalescence
- The plate should preferably be wettable by the disperse phase
- The drop swarm has to be distributed equally over the width of the plates
- Constructions that can thin the trickling film increase the overall settler performance

- Short lengths of plates of approximately 400 mm are sufficient for coalescence of drops atop the film

- Surfactants hardly influence coalescence and settling performance up to medium flow rates of the disperse phase

- Depending on the liquids involved, the drop coalescence leaves very small droplets, due to partial coalescence. This leads to droplet entrainment at the settler exit

- The optimum of plate inclination is within the range between 10° and 15°

3   Publications and Manuscripts

Direct Determination of the Composition of Aqueous Micellar Two-phase Systems (AMTPS) Using Potentiometric Titration – A Rapid Tool for Detergent-based Bioseparation

Ingo Fischer and Matthias Franzreb

Colloids and Surfaces A: Physicochemical and Engineering Aspects, 377 (2011) 97-102

Nanoparticle Mediated Protein Separation in Aqueous Micellar Two-Phase Systems

Ingo Fischer, Matthias Franzreb

Solvent Extraction and Ion Exchange, 30 (2012) 1-16

Partitioning behavior of silica-coated nanoparticles in Aqueous Micellar Two-Phase Systems: Evidence for an adsorption driven mechanism from QCM-D and ATR-FTIR measurements

Ingo Fischer, Christian Morhardt, Stefan Heissler, Matthias Franzreb

Langmuir, 28 (2012) 15789-15796

Continuous Protein Purification by Combination of Functional Magnetic Nanoparticles and Aqueous Micellar Two-phase Systems

Ingo Fischer, Markus Gärtner, Chia-Chang Hsu, Christine Müller, Timothy W. Overton, Owen R.T. Thomas, Matthias Franzreb

Journal of Chromatography A, December 2012, submitted

Removal of the nonionic surfactant Eumulgin ES from protein solutions by means of adsorption and ultrafiltration

Ingo Fischer, Matthias Franzreb

4 Direct Determination of the Composition of Aqueous Micellar Two-phase Systems (AMTPS) Using Potentiometric Titration – A Rapid Tool for Detergent-based Bioseparation

Ingo Fischer*, Matthias Franzreb

Karlsruhe Institute of Technology, Herrmann von Helmholtz Platz 1, 76344 Eggenstein-Leopoldshafen, Germany

*Corresponding author: Email: Ingo.Fischer@kit.edu

4.1 Abstract

Coexistence curves of two different aqueous micellar two-phase systems (AMTPS) were determined by potentiometric titration. The nonionic surfactants Triton X-114 and Eumulgin ES were quantified by means of the Metrohm NIO Surfactant Electrode with excellent correlations coefficients. The influence of different media on the titration end-point was ascertained. Measurement in the presence of commonly used biotechnological buffers 2-(N-morpholino)ethanesulfonic acid (MES), sodium phosphate, and 2-(Bis(2-hydroxyethyl)amino)acetic acid (bicine) as well as in the supernatant of an *E. coli* fermentation exhibited deviations below 5 %. Coexistence curves of Triton X-114 AMTPS and Eumulgin ES AMTPS were investigated in a temperature range of 25 °C to 40 °C by measuring the surfactant concentration of both, the detergent-rich (coacervate) and the detergent-depleted (aqueous) phase after phase separation. The resulting coexistence curves are in good agreement with those published by authors who have employed the cloud point method. Yet, potentiometric titration outranges the cloud point method as it provides direct information about the compositions of the coacervate and the aqueous phase, which form when an AMTPS is shifted up to a temperature at which it splits.

Keywords: Aqueous micellar two phase system, Potentiometric titration, Cloud point, Phase separation, Triton X-114, PPG-5-Laureth-5

4.2 Introduction

Polyoxyethylene-based detergents, typically abbreviated C_iE_j, belong to the class of nonionic surfactants (NIS). Aqueous solutions containing NIS concentrations above their critical micelle concentration (cmc) form a single clear phase. Upon temperature increase, at a certain point called the cloud point, the single phase separates into two phases, one surfactant-rich phase, the other surfactant-depleted yet still above the cmc [1].

Bordier was the first who, using the NIS Triton X-114, demonstrated that proteins added to such a detergent-based Aqueous Micellar Two Phase Systems (AMTPS) partition selectively between the phases, based on their hydrophobicity [2]. Since then, the application of AMTPS as liquid-liquid extraction technique has created a large field of interest and several AMTPS have been identified for the purification of, e.g. biomolecules [3-5], aromatic hydrocarbons [6], metal ions [7], and azo-dyes [8].

With regard to large-scale purification by continuous or cyclic application of AMTPS, respectively, accurate knowledge of detergent concentrations in both phases is required. The detergent concentrations of the top and bottom phases at a certain temperature and in a certain buffer system are located on a tie line depicted by the coexistence curve.

The most common procedure for mapping the coexisting curve is the cloud point method introduced by Huang et al. [9]. This method is based on the micellar solution becoming turbid at the transition from single-phase to two-phase regime and vice versa. The principle of the cloud point method is depicted in Figure 4.1. A solution containing a certain concentration of surfactant (S1 to S4 in Figure 1) is set up in a temperature-controlled bath. The stirred clear solution is slowly heated until it becomes turbid. The temperature is noted and the solution is allowed to cool down until it becomes transparent. The average temperature at both points of transition is taken as the cloud point, marking one spot of the coexisting curve (marked with a cross in Figure 4.1). In order to set up a coexisting curve, this procedure has to be repeated for numerous surfactant concentrations.
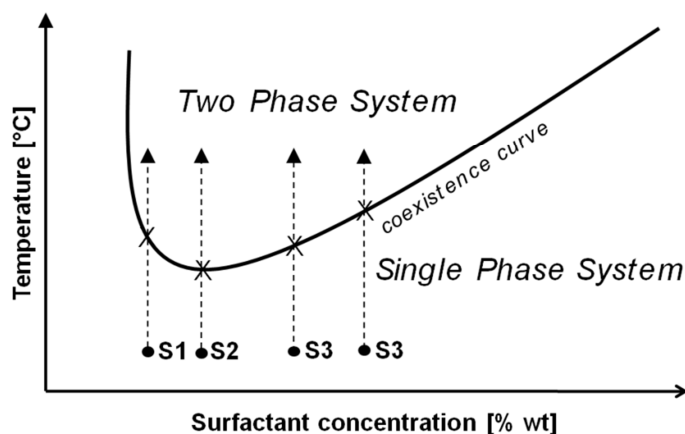
Figure 4.1: Principle of the cloud point method for determination of the coexistence curve. **Soultions with surfactant concentrations S1-S4 are heated until the solution becomes "cloudy" (marked with a cross). The coexistence curve is obtained by connecting the cloud points**

The cloud point method is the method of choice for the characterization of many recently discovered AMTPS, e.g. tri-block polymers [10] or alkyldimethylohosphodine oxide [11] although it comes with several drawbacks. The most severe one consists in the fact that this method cannot provide direct information about the length of a tie line and the NIS concentrations corresponding to a certain temperature, something which is essential when performing a partitioning experiment. The cloud point method only marks the point of transition from a single- to a two-phase system. In addition, the cloud point obtained from heating up the solution can differ from the cloud point derived from cooling the solution by up to 2 °C [12].

In the following, an alternative method for determining coexistence curves will be reported, which directly measures the concentration of polyoxyethylated NIS. The principle of the method is illustrated by Figure 4.2. An AMTPS is adjusted to a certain temperature. At this temperature both, the detergent-rich and the detergent-depleted phase, are in equilibrium, which is described by their corresponding tie line. The direct determination of the surfactant concentrations provides information about the tie line marking two spots of the coexisting curve. This procedure can be repeated at several temperatures resulting in the complete coexisting curve including the knowledge of tie line lengths. Moreover, most of the, e.g. protein partitioning experiments are performed at defined temperatures because of the thermal stability of proteins [13]. In this case, knowledge of the coexistence curve is unnecessary; in fact, a single phase separation

experiment at the given temperature followed by the determination of the surfactant concentration is sufficient.
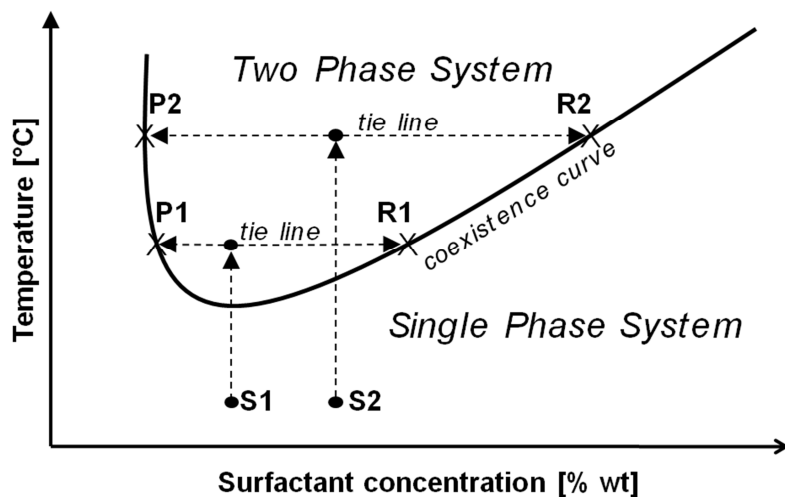
Figure 4.2: Principle of the determination of the coexistence curve by direct determination of the surfactant concentration. Solutions with the surfactant concentrations S1 and S2 are heated to a certain temperature located in the two-phase region. After phase separartion is completed, the concentration of the surfactant- poor P1-P2 and surfactant-rich R1-R2 phases is determined by potentiometric titration

The determination of the surfactants is based on a potentiometric end-point titration using the Metrohm NIO surfactant electrode. This electrode has been specially designed for the determination of polyoxyethylated NIS [14]. The basic principle of the determination is the formation of a pseudocationic complex of the NIS´s polyoxyethylene moiety with barium ions followed by precipitation via sodium tetraphenylborate. The potentiometric titration of polyethylene glycols has been introduced by Levins in 1965 [15]. The mechanism of complexation of polyoxyethylene groups and metal ions is extensively reviewed by Okada [16].

Potentiometric titration by means of the Metrohm NIO electrode has already been applied for the determination of NIS in industrial biological wastewaters [17, 18]. Furthermore, it has been shown to be sensitive up to a micromolar surfactant level [19]. This makes it a promising instrument for AMTPS research.

In this paper, we report coexistence curves for two different AMTPS varying in their polyoxyethylene moiety. The surfactants used were Trion X-114, which is well-known in

membrane protein purification [20], as well as the hitherto unknown Eumulgin ES, a laurymistrylether with a polyoxyethylen-polyoxypropylen moiety.

For quantification, calibration curves are used, giving information about the relation of the titration end-point volume and NIS mass. Afterwards, we demonstrate the general applicability of the potentiometric titration by determining several coexistence curves for NIS in different buffer systems as well as in an *E. coli* fermentation broth supernatant.

4.3 Material and Methods

4.3.1 Material

4.3.1.1 Titration Equipment

The equipment for titration was purchased from Metrohm AG, Herisau, Switzerland. The NIO surfactant electrode was connected to a Titrino 902 SM for the potentiometric end-point detection of several polyethoxylated NIS. As reference electrode, an Ag / AgCl electrode was used; the reference electrolyte was KCl (c=3 mol/L).

4.3.1.2 Detergents

We performed our experiments using the following polyoxethylated surfactants: the polyethylene glycol *tert*-octylphenyl ethers (t-Oct-C_6H_4-$(OCH_2CH_2)_x$OH) Triton X-100, **x** = 9 or 10; Triton X-114, **x** = 7 or 8 (Sigma-Aldrich, Germany); Eumulgin ES (Cognis, Germany), $C_{12}/C_{14}PEO_5PPO_5$.

4.3.1.3 Buffers

All buffers and chemicals were from buffer or p. A. grade. Water was deionized and purified by a Millipore Milli-Q Ultrapure system. The buffers used for the potentiometric titrations were made according to Metrohm, Switzerland [14]. Sodium tetraphenylborate (Fluka, Germany) was used as titrant solution with a concentration of 0.01 mol/L. 10 mL of borate buffer, pH 10, and 10 g polyvinyl-alcohol (Merck, Germany), average MW 60.000, were added to 1 liter of titrant solution. Barium chloride solution (Fluka,

Germany) (c = 0.1 mol/L) was used to create a pseudocationic complex preceding titration as described.

4.3.1.4 AMTPS Systems

Detergents were dissolved in buffers buffering different pH levels, thus creating AMTPS spanning a wide range of possible applications. The following buffers were made: MES (Carl Roth, Germany), 50mM, pH 5; sodium phosphate (Fluka, Germany), 50mM, pH 7; bicine (Applichem, Germany), 50mM, pH 8.8.

4.3.1.5 *E. coli* Fermentation Supernatant

Supernatant of the bacterial *E. coli* strain BL21(DE3)RIL was provided by D. Wiese from the group of Dr. K. Schmitz, Institute of Functional Interfaces, after cultivation in LB medium at 37 °C. The cells were separated from the supernatant by centrifugation.

4.3.2 Methods

4.3.2.1 Titration

The Titrino 902 SM titration device was controlled by TiNet software, v. 2.4, (Metrohm) installed on a Fujitsu Siemens Lifebook, C-Series, connected to it via RS 232 interface. The TiNet program was run in MET (monotone end-point titration) mode and the following parameters were adjusted: Dosing increments were set up depending on the end-point between 0.15 mL and 0.5 mL; drift control was set to 5 mV / min with a maximum time delay of 120 seconds; the end-point criterion was set to 15 mV. An initial pause of 360 seconds was kept preceding each titration in order to equilibrate the electrodes within the given media.

At the beginning of a titration, a given sample was weighed in to a glass beaker. 10 mL of barium chloride solution and 60 mL of water were added. The solution was steadily stirred by the Metrohm Magnetic Swing Out Stirrer 728 while the titrant was added. The response of the NIO electrode towards titration with sodium tetraphenylborate was recorded by the TiNet software, which simultaneously performed end-point analysis. As a

result, a characteristically s-shaped titration curve was obtained including the end-point volume derived from software analysis.

Both electrodes were rinsed with water after each titration. After multiple titrations, the NIO electrode was rinsed with methanol or wiped with a methanol moistured wipe to remove precipitated surfactant sticking to it and to prolong its lifetime.

4.3.2.2   Calibration Curves

Varying quantities of pure (laboratory grade) surfactant were weighed into a glass beaker and titrated as described. The end-points of each titration were put in relation to the total surfactant mass weighed by using linear regression. In order to examine the selectivity of the potentiometric titration, different buffers were added to the surfactant solutions and the end-points were compared to those containing the same amount of surfactant without interfering substance.

4.3.2.3   Phase Separation Experiments / Mapping the Coexistence Curve

A temperature-controlled water bath (RC 20 S, Lauda) was set up with an external temperature control. In order to keep the temperature preferably constant, the water bath was sealed with a polystyrene lid. Using this setup, the temperature remained constant with a temperature variation of less than 0.1 °C.

Mass fractions of surfactants and buffer systems were weighed into 15 mL centrifuge tubes. The centrifuge tubes were tempered using the water bath until the phase separation was completed for at least 12 hours. Subsequently, top and bottom phase of the resulting two-phase system were quickly removed, in order to avoid a sudden shift in phase equilibrium by the influence of the ambient temperature resulting in alteration of surfactant concentration in the phases. Surfactant concentrations of both phases were detected by potentiometric titration as described. This procedure was repeated for various temperatures and buffer / surfactant combinations.

4.3.2.4 Derivation of regression lines

Based on a theory originally developed by Blankschtein [21, 22] a regression line fitting the complete coexistence curve was calculated for each of the experimental data sets. According to this theory the coexistence curve of an AMTPS can be modeled using two physically relevant parameters: C is the measure for the intermicellar attractions and Δμ is the tendency for micellar growth. The parameters are given by Equations 4.1 and 4.2:

$$
\begin{aligned}
C(\chi_{aq}, \chi_{co}, T) = \frac{k \cdot T}{\gamma} \cdot \left(1 + \frac{3 \cdot \gamma - 2}{3}\right) \\
\cdot \left[2 \cdot \left(\sqrt{\chi_{aq}} + \sqrt{\chi_{co}}\right)^2 - 3 \cdot \sqrt{\chi_{aq} \cdot \chi_{co}}\right]
\end{aligned}
$$

[Eq. 4.1]

$$
\Delta\mu(\chi_{aq}, \chi_{co}, T) = k \cdot T \cdot ln\left[\frac{\left(\frac{6}{3 \cdot \gamma - 2}\right)^2}{\chi_{aq} \cdot \chi_{co}\left(\sqrt{\chi_{aq}} + \sqrt{\chi_{co}}\right)^6}\right]
$$

[Eq. 4.2]

Here, k_B is the Boltzmann constant, T is the absolute temperature, χ_{aq} and χ_{co} are the surfactant mole fractions in the surfactant depleted and surfactant rich phases, respectively, and γ is the ratio of the effective volume of the surfactant molecule to a water molecule, which according to Lam [23] can be approximated by the ratio of the molecular weight of the surfactant to that of water. In this work Lam´s method is applied to solve Equations 4.1 and 4.2: First, a linear regression analysis of $C(T)/k_B$ and $\Delta\mu(T)/k_B$ using the temperature dependent surfactant fractions obtained by potentiometric titration is performed. Second, the surfactant poor and surfactant rich concentrations at any given temperature and therefore the complete coexistence curves are obtained by solving Equation 4.1 and 4.2 using the C and Δμ values derived from the linear regression analysis. In this way, for all experimentally examined system a best-fit coexistence curve is generated.

4.4 Results and Discussion

4.4.1 Calibration

Different quantities of surfactant were weighed into a glass beaker and titrated as described. Figure 4.3 shows a titration curve obtained by plotting titration volume versus response of the NIO electrode. The curve shape exhibits a precise inflection point. The volume related to the inflection point of the titration curve is denoted as end-point volume.
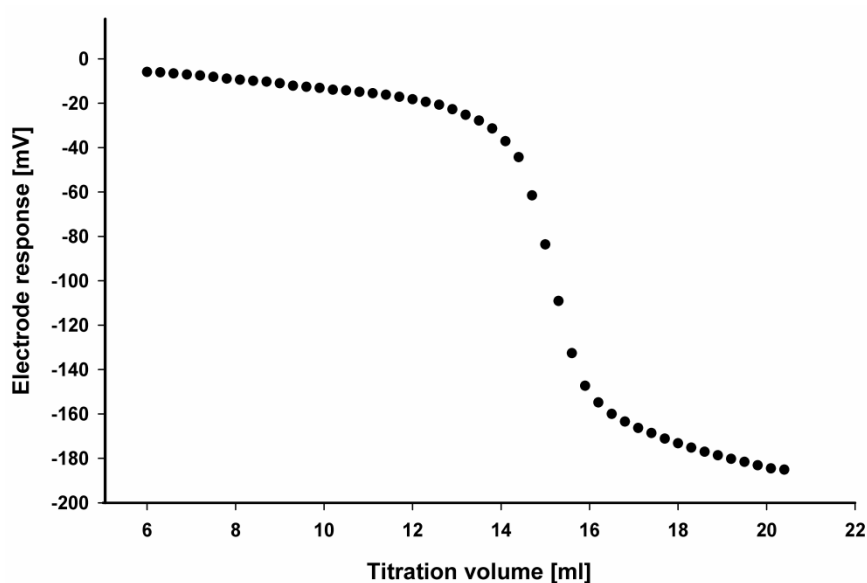
Figure 4.3: Titration curve of 53 mg Eumulgin ES dissolved in 60 mL H2O; coordinates of the inflection point are 15.19 mL / - 100.1 mV

In order to obtain calibration curves, the end-point volume was put in relation to the amount of surfactant applied. Figure 4.4 shows the results for Triton X-114 and Eumulgin ES.
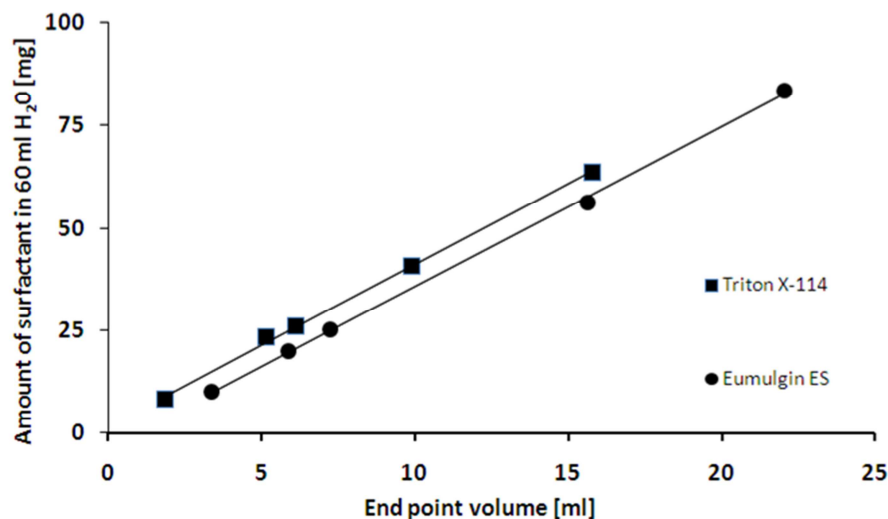
Figure 4.4: Titration end-point volume versus surfactant mass of Triton X-114 and Eumulgin ES dissolved in 60 mL H2O

The calibration graphs obtained for both Eumulgin ES and Triton X-114 were strictly linear with correlation coefficients for Eumulgin ES of 0.9994 and of 0.9985 for Triton X-114, respectively. The increased end-point volume of Eumulgin ES in contrast to that of Triton X-114 may be attributed to the difference of the hydrophilic moiety of the surfactants. A larger amount of titration solution is necessary to form a complex with the polyoxyethylen - polyoxypropylen moiety of Eumulgin ES in contrast to the polyoxyethylene branch of the Triton X-114 molecule. The increasing ability of hydrophilic polyoxyethylene chains to "trap" bivalent ions with increasing chain length has already been described by Toei et al. for potassium ions [24]. A minimum amount of surfactant weighed in was 7 mg for Triton X-114 and 10 mg for Eumulgin ES in 60 mL titration solution following the standard protocol; this results in a lowest detectable concentration of 0.116 g/L of Triton X-114 and 0.166 g/L of Eumulgin ES. This detection limit has turned out to be sufficient for our experiments; however, the sensitivity can be increased by dilution of the titrant solution up to 20 times [19], if necessary.

4.4.1.1 Influence of Buffers

The influence of several commonly used biotechnological buffers spanning a range of pH levels from 5 to 8.8 onto the end- point volume was examined. For this, buffers

containing a distinct surfactant concentration were titrated as described above. Experimental deviations are shown in Table 1 for Triton X-114.

Table 4.1. Influence of buffers on potentiometric titration of Triton X-114

Buffer	Surfactant concentration [%wt]	Concentration determined by titration [% wt]			Average deviation [%]
50mM MES, pH 5	2.05	1.94	1.92	2.03	4.26
50mM sodium-phosphate, pH 7	2.02	1.95	1.99	2.03	1.75
50mM bicine, pH 8.8	2.01	1.96	1.94	1.91	3.93
E. coli fermentation supernatant	2.64	2.54	2.6	2.53	3.27

Deviations of the measurement of the surfactant concentration in the presence of the tested buffers were below 5%. Therefore, the deviation is practically within the error of the calibration curve of Triton X-114. From Table 1 it can also be seen that, as in the case of buffers, the measurement within *E. coli* fermentation supernatant which contains various salts and proteins does not interfere with the end- point titration.

4.4.1.2 Mapping the Coexistence Curve for Triton X-114

Determination of the coexistence curve was performed by quantification of the surfactant concentrations of the top and bottom phases of several Triton X-114 / buffer systems by potentiometric titration after phase separation. Subsequently, the curves were fitted using Lam´s method. Experiments were performed in a temperature range of 25 °C up to 35 °C. Figure 4.5 shows the resulting phase diagram of Triton X-114 in water. In accordance with the cloud point method, each measured value also represents the point of transition from the single-phase (below) to the two-phase (above) regime, thus marking one cloud point.
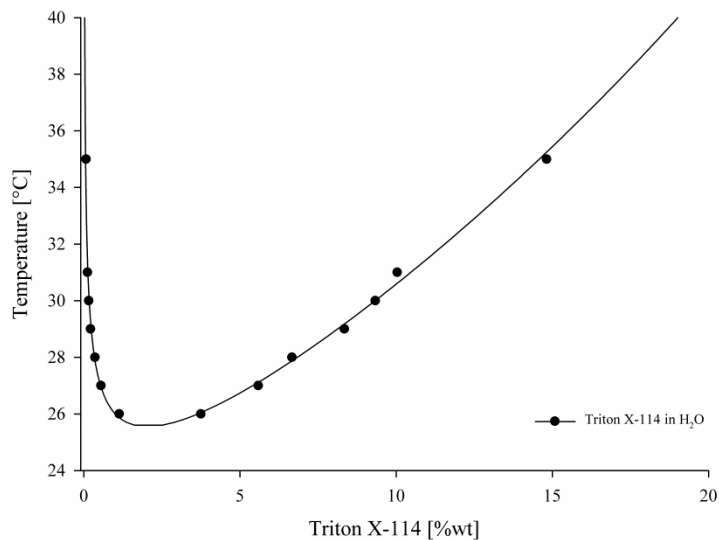
Figure 4.5: Coexistence curve of Triton X-114 in H$_2$O

Additionally, coexistence curves were set up for several commonly used biotechnological buffers. Figure 4.6 shows coexisting curves of MES, sodium-phosphate and bicine, while in Figure 4.7 the coexistence curve of the supernatant of an Triton X-114/*E. coli* fermentation broth AMTPS is shown.
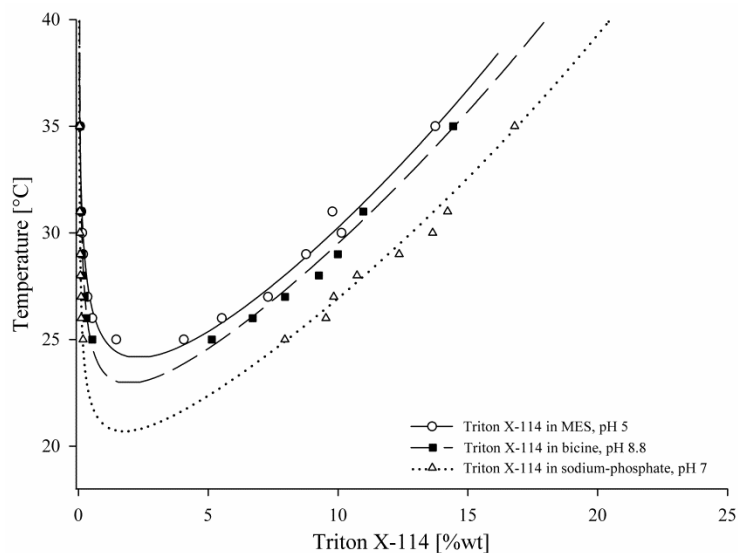
Figure 4.6: Coexistence curve of Triton X-114 in MES at pH 5, in bicine at pH 8.8 and in sodium-phosphate at pH 7.
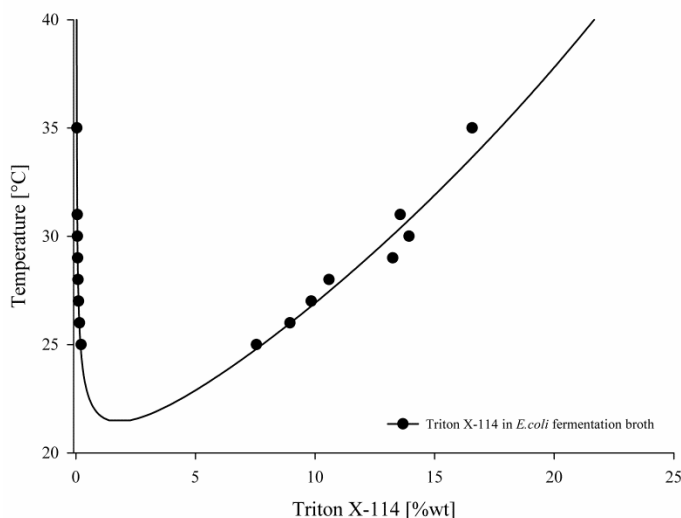
Figure 4.7: Coexistence curve of a Triton X-114 in *E. coli* fermentation supernatant AMTPS.

Although it was not our intention to investigate the influence of salts or pH level on the phase separation behavior of AMTPS, it becomes evident that upon addition of salts, the complete coexistence curve is moved towards lower temperatures. This effect has already been intensively studied, e.g. [9, 10, 25, 26], and is related to salting-out effects of chaotropic ions following the Hofmeister series. The shapes of the coexistence curves are in good accordance with those published by authors using the cloud point method, e.g. [27]. The quantification of surfactants of both phases results in the immediate knowledge of the ends of the tie line for a given phase equilibrium. In applications which are performed at certain fixed temperatures, e.g. protein partitioning experiments [27], this information is advantageous compared to the one which results from the cloud point method. Here, the identification of a tie line requires laborious mapping of cloud points followed by fitting the coexistence curve precedent to tie line identification.

4.4.1.3 Coexistence Curves of Eumulgin ES

Coexistence curves of Eumulgin ES were set up in water and 100mM sodium-phosphate buffer depicted by Figure 4.8.
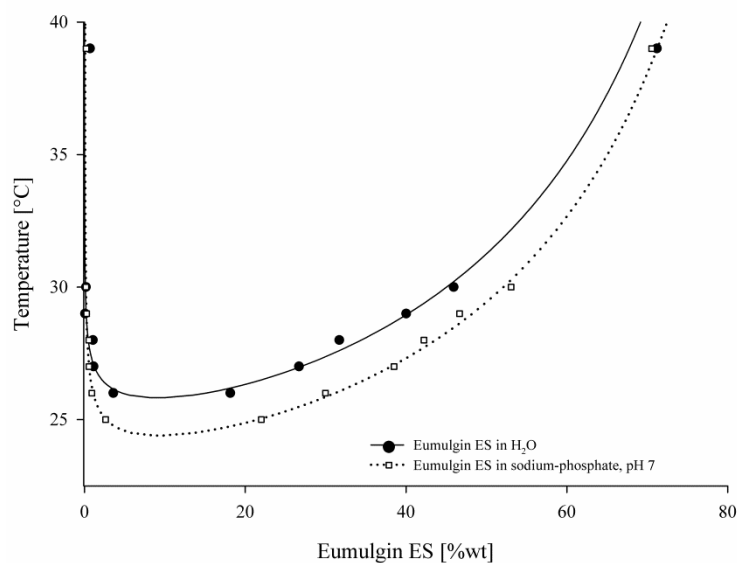
Figure 4.8: Coexistence curve of Eumulgin ES in H2O and in sodium-phosphate at pH 7.

As can be seen, phase separation in the Eumulgin ES/H$_2$O AMTPS occurs at ambient temperatures. Phase separation is induced at a temperature above 25.8 °C at about 10% wt. Basically, the shape of the coexistence curves resemble that of the Triton X-114 but the surfactant concentrations in the micelle-rich and micelle-depleted phases are clearly elevated compared to the concentration in Triton X-114 AMTPS. According to the best-fit curve, at 30 °C, the concentration of the micelle-rich phase is 45% wt; upon increasing the temperature to 39 °C it is concentrated to 68% wt in the ES/H$_2$O AMTPS. The coexistence curve of sodium-phosphate / Eumulgin ES AMTPS shows a concentration of the micelle-enriched phase of 52% wt at 30 °C pointing out the effect of sodium-phosphate on the dislocation of the coexisting curve. Eumulgin ES was firstly introduced to AMTPS research as *Aethoxal B* by Becker [28], who determined coexistence curves based on the *Lever rule* measuring the phase volume ratio after complete phase separation. The coexistence curves obtained by potentiometric titration are in good accordance with the coexistence curves set up by Becker.

4.5 Conclusion

Coexistence curves of Eumulgin ES and Triton X-114 in several buffers have been determined. The AMTPS were kept at constant temperatures until separation of micelle-rich and micelle-depleted phase was completed. Potentiometric titration using a NIO

surfactant electrode has been applied to quantify the surfactant concentrations of both phases. The coexistence curve was obtained by plotting the resulting surfactant concentrations versus their equilibrium temperatures. This method outmatches the *cloud point* method which is commonly used for the characterization of AMTPS as one experiment renders not only one point of transition from the single-phase to the biphasic state, but at once information about the surfactant concentrations of both phases in equilibrium. For many applications in which equilibrium concentrations at fixed temperatures are needed, it will no longer be necessary to set up a complete coexistence curve, but a single-phase separation experiment followed by quantification via potentiometric titration will provide sufficient information. It has been shown that the method is suitable for the detection of polyoxyethylated NIS in buffers of different compositions and pH levels as well as biological feeds making potentiometric titration not only a tool for the detection of coexistence curves but also a promising instrument for polyoxyethylated detergents research in general.

4.6 References

[1] H. Watanabe, H. Tanaka, Nonionic Surfactant as a New Solvent for Liquid-Liquid - Extraction of Zinc(Ii) with 1-(2-Pyridylazo)-2-Naphthol, Talanta, 25 (1978) 585-589.

[2] C. Bordier, Phase-Separation of Integral Membrane-Proteins in Triton X-114 Solution, Journal of Biological Chemistry, 256 (1981) 1604-1607.

[3] G.C. Terstappen, R.A. Ramelmeier, M.R. Kula, Protein Partitioning in Detergent-Based Aqueous 2-Phase Systems, Journal of Biotechnology, 28 (1993) 263-275.

[4] H. Tani, T. Kamidate, H. Watanabe, Aqueous micellar two-phase systems for protein separation, Analytical Sciences, 14 (1998) 875-888.

[5] A. Sanchezferrer, R. Bru, F. Garciacarmona, Phase-Separation of Biomolecules in Polyoxyethylene Glycol Nonionic Detergents, Critical Reviews in Biochemistry and Molecular Biology, 29 (1994) 275-313.

[6] J.L. Li, B.H. Chen, Equilibrium partition of polycyclic aromatic hydrocarbons in a cloud-point extraction process, Journal of Colloid and Interface Science, 263 (2003) 625-632.

[7] H. Reffas, T. Benabdallah, M.H. Youcef, H. Ilikti, Study on the Cloud Point Extraction of Copper(II) from an Aqueous Sulfate Medium with N,N '-Bis(salicylideneaminoethyl)amine Polydentate Schiff Base into a Nonionic Surfactant Phase, Journal of Chemical and Engineering Data, 55 (2010) 912-918.

[8] V.O. Doroschuk, S.A. Kulichenko, S.O. Lelyushok, The influence of substrate charge and molecular structure on interphase transfer in cloud point extraction systems, Journal of Colloid and Interface Science, 291 (2005) 251-255.

[9] Y.X. Huang, G.M. Thurston, D. Blankschtein, G.B. Benedek, The Effect of Salt Identity and Concentration on Liquid Liquid-Phase Separation in Aqueous Micellar Solutions of C-8-Lecithin, Journal of Chemical Physics, 92 (1990) 1956-1962.

[10] K. Patel, B. Bharatiya, Y. Kadam, P. Bahadur, Micellization and Clouding Behavior of EO-PO Block Copolymer in Aqueous Salt Solutions, Journal of Surfactants and Detergents, 13 (2010) 89-95.

[11] G.C. Kresheck, Z. Wang, A new micellar aqueous two-phase partitioning system (ATPS) for the separation of proteins, Journal of Chromatography B-Analytical Technologies in the Biomedical and Life Sciences, 858 (2007) 247-253.

[12] T. Gu, P.A. Galeragomez, Clouding of Triton-X-114 - the Effect of Added Electrolytes on the Cloud Point of Triton-X-114 in the Presence of Ionic Surfactants, Colloids and Surfaces a-Physicochemical and Engineering Aspects, 104 (1995) 307-312.

[13] D.T. Kamei, D.I.C. Wang, D. Blankschtein, Fundamental investigation of protein partitioning in two-phase aqueous mixed (nonionic/ionic) micellar systems, Langmuir, 18 (2002) 3047-3057.

[14] Metrohm, Titrimetric/potentiometric determination of non-ionic surfactants based on polyoxyethylene adducts using the NIO electrode, Application Bulletin 230/1 e.

[15] R.J. Levins, R.M. Ikeda, Direct Potentiometric Titration of Polyethylene Glycols and Their Derivatives with Sodium Tetraphenylboron, Analytical Chemistry, 37 (1965) 671-&.

[16] T. Okada, Complexation of Poly(Oxyethylene) in Analytical-Chemistry - a Review, Analyst, 118 (1993) 959-971.

[17] H. Feitkenhauer, U. Meyer, On-line titration of non-ionic surfactants in wastewater treatment plants using a specific electrode, Water Science and Technology, 45 (2002) 61-68.

[18] H. Feitkenhauer, Effiziente Überwachung biotechnologischer Prozesse mittels Titration, Chemie Ingenieur Technik, 74 (2002) 1759-1753.

[19] M. Sak-Bosnar, D. Madunic-Cacic, R. Matesic-Puac, Z. Grabaric, Sensitive potentiometric method for determination of micromolar level of polyethoxylated nonionic surfactants in effluents, Tenside Surfactants Detergents, 44 (2007) 11-18.

[20] A. Helenius, K. Simons, Solubilization of Membranes by Detergents, Biochimica Et Biophysica Acta, 415 (1975) 29-79.

[21] D. Blankschtein, G.M. Thurston, G.B. Benedek, Phenomenological Theory of Equilibrium Thermodynamic Properties and Phase-Separation of Micellar Solutions, Journal of Chemical Physics, 85 (1986) 7268-7288.

[22] D. Blankschtein, G.M. Thurston, G.B. Benedek, Theory of Phase-Separation in Micellar Solutions, Physical Review Letters, 54 (1985) 955-958.

[23] H. Lam, M. Kavoosi, C.A. Haynes, D.I.C. Wang, D. Blankschtein, Affinity-enhanced protein partitioning in decyl beta-D-glucopyranoside two-phase aqueous micellar systems, Biotechnology and Bioengineering, 89 (2005) 381-392.

[24] K. Toei, S. Motomizu, T. Umano, Extractive Spectrophotometric Determination of Non-Ionic Surfactants in Water, Talanta, 29 (1982) 103-106.

[25] H. Schott, Effect of inorganic additives on solutions of nonionic surfactants - XVI. Limiting cloud points of highly polyoxyethylated surfactants, Colloids and Surfaces a-Physicochemical and Engineering Aspects, 186 (2001) 129-136.

[26] L. Koshy, A.H. Saiyad, A.K. Rakshit, The effects of various foreign substances on the cloud point of Triton X 100 and Triton X 114, Colloid and Polymer Science, 274 (1996) 582-587.

[27] A.M. Lopes, A. Pessoa, C.D. Rangel-Yagui, Can affinity interactions influence the partitioning of glucose-6-phosphate dehydrogenase in two-phase aqueous micellar systems?, Quimica Nova, 31 (2008) 998-1003.

[28] J.S. Becker, Einsatz magnetischer Extraktionsphasen zur Bioproduktaufarbeitung, PhD Thesis, (2009).

5 Nanoparticle Mediated Protein Separation in Aqueous Micellar Two Phase Systems

Ingo Fischer, Matthias Franzreb*

Institute of Functional Interfaces, Karlsruhe Institute of Technology, Herrmann von Helmholtz Platz 1, 76344 Eggenstein-Leopoldshafen, Germany

*: Corresponding author: Email: Matthias.Franzreb@kit.edu

5.1 Abstract

Magnetic nanoparticles with cation exchange functionality (MNCX) are combined with an Aqueous Micellar Two-Phase System (AMTPS) based on the nonionic surfactant Eumulgin ES for the purpose of protein separation. As proof of principle the positively charged protein lysozyme is separated from the negatively charged protein ovalbumin with a purity of approximately 100%. In comparison with the application of the MNCX alone, the presence of Eumulgin ES reduced the amount of lysozyme bound, however, the amount of eluted lysozyme stays the same. The advantage of applying the AMTPS is that the MNCX are easily handled as they partition utterly into the dispersed phase of the system while the applied proteins partition almost entirely to the continuous phase.

Keywords: Magnetic nanoparticles, protein purification, cation exchange, aqueous micellar two-phase system, magnetic extraction

5.2 Introduction

In small scale, the separation of biomolecules by means of magnetic sorbents is a widely used and well-established procedure. In the course of the procedure a molecule of interest is directly sorbed from a crude feedstock onto selective ligands at the surface of the sorbent. After complete separation of the protein-loaded magnetic sorbents from the feed by application of a magnetic field gradient, following washing and elution steps will deliver the target in a purified form. The application of magnetic sorbents as tool in bioseparations therefore integrates several unit operations including clarification, preconcentration and initial purification.

At larger scales, the magnetic separation of especially micro- or nanosized sorbents is more delicate. High-Gradient Magnetic Separation (HGMS), however, an operation originating from the industrial treatment of minerals, which was introduced to biotechnological research in 2001 [1], has been demonstrated to be an effective approach for the processing of magnetic sorbents. An exciting alternative to the handling of magnetic micro- and nanosized sorbents by means of HGMS is their processing in a liquid phase using Aqueous Two-Phase Systems (ATPS) or Aqueous Micellar Two-Phase Systems (AMTPS).

AMTPS emerge from the addition of particular classes of surfactants to water. When reaching a certain characteristic temperature, denoted as cloud point, the single phased system splits into two phases, one containing a high surfactant concentration, whilst the other comprises a low surfactant concentration, yet still above the critical micelle concentration (cmc). Ever since it was reported by Bordier that proteins partition selectively between the phases based on their hydrophobicity AMTPS have drawn much attention in terms of bioseparation [2-6]. Another advantage in processing ATPS as well as AMTPS is its simple scalability, which has often been demonstrated by successful large-scale protein purification [7-9].

A limiting factor in processing ATPS and, in particular, AMTPS concerning industrial application is the phase separation rate, which essentially determines the overall process time. In AMTPS the density difference between the micelle rich and the micelle depleted

phase is often very small leading to phase separation rates of several hours [8]. Therefore, efforts have been made to increase the phase separation rate. Apart from the successful implementation of disc stack centrifuges [9], external magnetic fields were used to speed up the phase separation rate [10-12]. Magnetically enhanced phase separation is achieved by adding inert magnetic particles to the two-phase system. Assuming the complete partitioning of the particles into the dispersed phase of the system, the velocity of the migration of the particle-doped droplets is considerably augmented by a magnetic field gradient.

It were Suzuki et al. who successfully combined both magnetically enhanced phase separation and selective protein separation making use of functionalized magnetic sorbents in ATPS [13]. Recently, at our lab Becker et al. introduced the concept of Magnetic Extraction Phases (MEP). MEP transfers the idea of functionalized magnetic particles and magnetically enhanced phase separation from ATPS to "temperature-tunable" AMTPS Systems [14]. In MEP, the sorption of the target molecule takes place at a low temperature in the single phase regime. The temperature is subsequently increased, which leads to the protein-loaded particles being accumulated into in the micelle rich phase of the resulting AMTPS. After removal of the micelle depleted phase, an AMTPS is set up with elution buffer and the former micelle rich phase of the sorption step. The proteins are consequently eluted from the particles and while the magnetic sorbents partition completely to the micelle rich phase, the target protein partitions in the AMTPS based on its partitioning coefficient K. A proper MEP system therefore should exhibit a partition coefficient which drives the protein to the micelle poor phase, while the magnetic particles (in loaded as well as in unloaded state) are required to accumulate to the micelle rich phase.

The first generation MEP was a combination of the well known nonionic surfactant Triton X-114 AMTPS and superparamagnetic ion exchange particles with a size range from 1 to 3 µm. Basically, the system met the requirements of a proper MEP - complete partitioning of the magnetic sorbents into the micelle rich phase, yet lacked a proper partitioning coefficient of the proteins.

Here, we introduce a novel MEP system. It is based on an AMTPS consisting of the nonionic surfactant Eumulgin ES and nanosized magnetic particles, which are functionalized with cation exchange groups (denoted henceforth magnetic nano cation exchangers - MNCX). The novel AMTPS is characterized in terms of protein partitioning coefficients as well as the influence of the surfactant in particle-protein interaction. A mixture of lysozyme and ovalbumin was chosen as model system in order to achieve comparability with recent AMTPS experiments applying magnetic micro-particles and data of conventional ion exchange chromatography using the same proteins. It is illustrated that the MNCX can be easily processed in a protein purification process by means of MEP.

5.3 Materials and Methods

5.3.1 Materials

Ferrimagnetic nanosized particles (MNCX) were obtained from Merck KGaA (Darmstadt, Germany). The particles with a mean diameter of 25nm had been coated with a silica layer and grafted with sulfonate groups. Because of this surface functionality the nanoparticles exhibit the characteristics of a strong acid cation exchanger.

All chemicals were from buffer or p. A. grade. Water was deionized and purified in a Millipore Milli-Q Ultrapure system. The proteins ovalbumin from hen egg white (Molecular weight: 44.2 kDa, grade >98%) and lysozyme from chicken egg white (Molecular weight: 14.6 kDa ~70000 units/mg) were purchased from Sigma-Aldrich (St. Louis, USA-MO) as well as the chemicals sodium tetraphenylborate and barium chloride.

Polyvinylalcohol (av. MW 60.000) and Comassie Brilliant Blue R250 were obtained from Merck KGaA (Darmstadt, Germany). Disodium-hydrogen phosphate and sodium-chloride were supplied by Carl Roth (Karlsruhe, Germany). Bicine was reviewed from Applichem (Darmstadt, Germany). The nonionic surfactant Eumulgin ES (PPG-5-Laureth-5, CAS-No.: 68439-51-0) was purchased from Cognis (Düsseldorf, Germany). 12% precast mini-PROTEAN® TGX™ and Precision Plus Protein All Blue Standards were supplied from Bio-Rad (Hercules, USA-CA).

5.3.2 Experimental Section

5.3.2.1 Characterisation of the AMTPS

Preparation of the AMTPS

Aqueous Micellar Two Phase Systems were prepared using the nonionic surfactant Eumulgin ES. A 10% Eumulgin ES solution containing 0.2 g/L lysozyme and ovalbumin, respectively, was set up in 20 mM sodium-phosphate with pH adjusted to 6.8. The phase separation was induced by heating up the accordant solution to 26° C and maintaining this temperature until the phases were completely separated. The phase separation resulted in a surfactant rich top phase while the bottom phase remained surfactant depleted. Samples from both phases were taken and analyzed for their surfactant concentration.

Partitioning of Ovalbumin and Lysozyme in the AMTPS

0.5 g/L ovalbumin and lysozyme were added to a 10% Eumulgin ES AMTPS and the phases were allowed to separate at 26°C for at least 12 hours. The protein concentrations in the top and bottom phases were investigated by SDS-PAGE afterwards. If the protein concentrations were high enough to identify a proper band in a Coomassie stained gel, the concentration was quantified by densiometric analysis.

Additionally, the partitioning of a 0.2 g/L lysozyme and ovalbumine solution was investigated in AMTPS ranging from 5% up to 25% Eumulgin ES based AMTPS.

5.3.2.2 Protein Sorption Studies

Protein binding studies were performed in 1.5 ml microcentrifuge tubes in a total volume of 150 µl and a MNCX concentration of 1 g/L. Protein concentrations were prepared in a range from 2 g/L to 0.1 g/L in 20mM sodium-phosphate buffer at pH 6.8. The MNCX were equilibrated in the same buffer before the protein solution was added. Sorption was performed for 300 seconds in a thermomixer (Eppendorf, Hamburg, Germany) at 25° C and 1400 rpm. Sorption in presence of surfactant was performed with a concentration of 10% of Eumulgin ES in the protein solution before the solution was brought into contact

with the magnetic sorbents. Sorption equilibrium was achieved in less than 60 seconds (data not shown).

After the sorption step, the nanoparticles were removed by use of a permanent magnet and the particle-free supernatants were subsequently analyzed as described above. The nanoparticles were then washed three times with sodium-phosphate buffer.

5.3.2.3 Protein Desorption Studies

Protein desorption was achieved by incubation of the loaded MNCX in 100 µl elution buffer consisting of 50 mM bicine and 1 M sodium-chloride, adjusted to pH 8.8. Incubation was performed for 600 seconds at 25°C and 1400 rpm. Afterwards, the eluate was separated from the sorbents and analyzed for its protein content. A second elution step did not result in additional protein elution. To maintain comparability of the results from sorption and elution experiments, the eluates obtained from the sorption experiments which were carried out in presence of Eumulgin ES were analyzed by densiometry.

5.3.2.4 Magnetic Extraction using MNCX

MNCX were processed in Magnetic Extraction experiments by concentrating them in the micelle rich phase of an Eumulgin ES based AMTPS at the end of each process step. The concept of MEP is that positively charged proteins are dragged from the micelle depleted into the micelle rich phase by MNCX. Afterwards the micelle depleted phase together with the majority of the contaminants can be removed. The protein is released from the MNCX by mixing them with elution buffer and splitting the mixture again into a new micelle depleted phase that contains the target protein and a micelle rich phase containing the unloaded MNCX. In between sorption and elution a wash step is integrated following the pattern described. The principle of MEP is depicted in Figure 5.1.
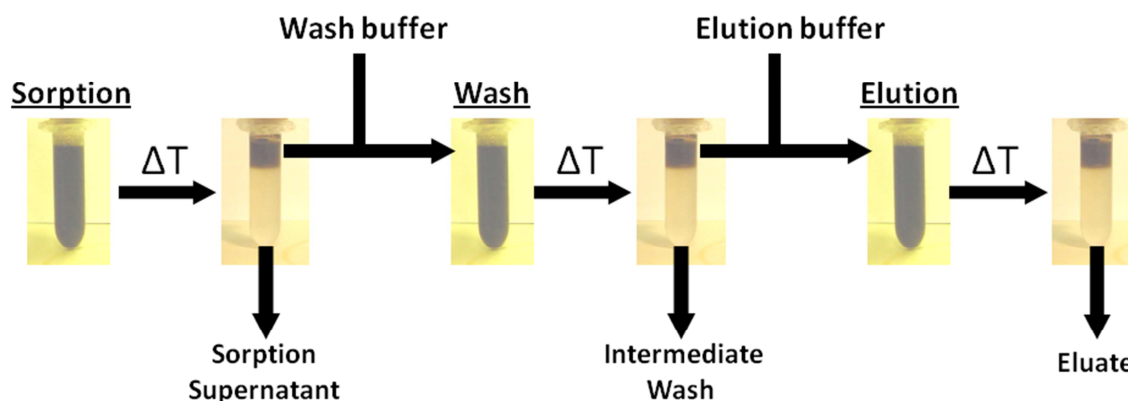
Figure 5.1: Principle of Magnetic Extraction. The main components of Magnetic Extraction Phases are functionalized magnetic sorbents (MNCX) and the AMTPS forming nonionic surfactant Eumulgin ES. By raising the temperature, the single phase system splits into a micelle rich and a micelle depleted phase. The sorbents accumulate completely in the micelle rich top phase. When applying a protein solution to the MEP, the proteins accumulate – depending on their partitioning coefficient - in the micelle depleted phase. In the first step of a Magnetic Extraction the protein of interest binds to the magnetic sorbent. The temperature is raised so that the AMTPS splits. The sorbents accumulate to the micelle rich phase while the sorption supernatant forms to the micelle depleted phase. The sorption supernatant is removed and wash buffer is added to the micelle rich phase which contains the sorbents with the target protein bound to them. The wash step is again performed in the single phase regime. After another temperature induced phase separation the intermediate wash is separated together with the micelle depleted phase from the micelle rich phase. For the elution of the target protein, suitable buffer is applied to the micelle rich phase and elution takes place in the single phase regime before the system is split again by increasing the temperature. Finally, the eluted protein can be withdrawn in the micelle depleted phase, while the unladed sorbents accumulate in the micelle rich phase.

The MEP was set up using a protein feed of 0.2 g/L lysozyme and ovalbumin, respectively. The particle concentrations varied from 2 g/L up to 8 g/L. The Eumulgin ES concentration was kept constant at 10%. The sorption was performed at 20° C in the single phase regime for 15 minutes. Afterwards the temperature was increased to 26°C to induce phase separation. Phases were separated by gravity for at least 4 hours.[1] After phase separation the micelle and particle rich top phase was removed and sodium-phosphate containing 1.2 % Eumulgin ES was added to it to wash loosely bound proteins from the particles and to remove remaining sorption supernatant. This was done at 20° in the single phase regime, followed by another phase separation step and removal of the resulting wash-phase. Elution buffer was added to the particle containing micelle rich

---

[1] In order to keep the comparability to ATMPS experiments without the addition of magnetic nanosorbents, gravimetric phase separation was applied in all experiments, although the superimposition of a magnetic field would have increased the phase separation rate considerably.

phase followed by incubation at 20° C for 15 minutes. Afterwards the temperature was raised to 26° C and the phases were allowed to separate. In the resulting eluate-AMTPS, the target protein remained in the surfactant depleted phase, while the magnetic supports were completely accumulated in the micelle rich phase.

Samples were taken before sorption was performed as well as from the micelle depleted, wash and elution phases. The samples were analyzed by SDS PAGE.

5.3.3 Analytical Procedures

5.3.3.1 Determination of the Surfactant Concentration

The Eumulgin ES concentration was measured using potentiometric titration. A given sample was weighed into a glass beaker. 10 mL of barium chloride solution and 60 mL of water were added. This solution was subsequently titrated with sodium-tetraphenylborate using the Metrohm NIO electrode. As result the end-point volume was recorded. The surfactant mass fraction was then obtained by comparing the end point volume with the end point volumes of known surfactant mass fractions using linear regression. The detection limit of this reference method was determined to be 0.01 % (w/w) surfactant.

5.3.3.2 Determination of the Protein Concentration

Quantitative protein determination was performed depending on the composition of the sample. Protein concentrations in samples free of surfactants were measured spectrophotometrically at 280 nm using a Nanodrop® ND-1000 (Thermo Fisher Scientific, Waltham, USA-MA) photometer. For chicken ovalbumin and lysozyme the mass extinction coefficients of a 10 mg/ml solution were determined to be 5.5 and 26.4, respectively. Samples containing a certain amount of surfactant were analyzed by SDS PAGE following software supported densiometric analysis. The protein loaded TGX gels were Coomassie blue stained and scanned as TIFF image files. The images were afterwards analyzed using the software LumiAnalyst® (Roche Diagnostics GmbH, Media Cybernetics, 1999). Protein band intensities were converted to biochemical light units (BLU) by the software. In order to quantify the protein concentration standards with known protein concentrations were

applied on the same gel. SDS-PAGE was not interfered with Eumulgin ES concentrations up to 5%. Hence, samples containing higher Eumulgin ES concentrations were diluted below this limit.

5.3.4 Equations describing the results

5.3.4.1 Partitioning in AMTPS

The partitioning of molecules in ATPS or AMTPS is usually described by the following characteristics. The ratio of the concentrations of a target protein P in the top ($c_{P,T}$) and bottom phase ($c_{P,B}$) is expressed as the partitioning coefficient K:

$$K = \frac{c_{P,T}}{c_{P,B}}$$
[Eq. 5.1]

The ratio of the volumes of the top (V_T) and bottom phase (V_B) can be described by the parameter R:

$$R = \frac{V_T}{V_B}$$
[Eq. 5.2]

The volume ratio R can also be expressed using the lever rule [15, 16]:

$$R = \frac{V_T}{V_B} = \frac{c_{S,0} - c_{S,B}}{c_{S,T} - c_{S,0}}$$
[Eq. 5.3]

With $c_{S,0}$ being the overall surfactant concentration in g/L precedent phase separation and $c_{S,B}$ and $c_{S,T}$ the surfactant concentrations in the top and bottom phase after phase separation. In AMTPS the densities of the initial single phase and the both resulting phases after phase separation are practically equal, therefore the equation can be rewritten as:

$$R = \frac{V_T}{V_B} = \frac{w_{S,0} - w_{S,B}}{w_{S,T} - w_{S,0}}$$
[Eq. 5.4]

Here, $w_{S,0}$, $w_{S,B}$ and $w_{S,T}$ are the surfactants´ mass fractions of the phases before and after phase separation [3]. With the knowledge of the surfactants mass fractions in the top and bottom phase the phase ratio can be calculated and vice versa.

5.3.4.2 Sorption of Proteins to Surfaces

The amount of protein sorbed to the surface of the particles is be calculated by the mass balance:

$$q = \frac{V_0 \cdot (c_0 - c_s)}{m_P}$$

[Eq. 5.5]

where q (mg/g) is the amount of bound protein onto the particle, m_P (g) the amount of particles, V_0 is the volume of the experiment and c_0 and c_S are the concentrations of the protein in the supernatant before and after the sorption , assuming an initial particle loading of q_0=0.

The experimental data obtained from the sorption experiments can then be fitted to the Langmuir model:

$$q = q_{max} \cdot \frac{c^*}{K_L + c^*}$$

[Eq. 5.6]

with q_{max} (mg/g) representing the maximum binding capacity of the particles and K_L (in g/L) the Langmuir constant and c^* the equilibrium concentration of the protein in the sorption supernatant. The values for the Langmuir parameters were calculated using SigmaPlot (vers. 11.0, Systat Software, Inc., 2008).

5.4   Results and Discussion

5.4.1 Characterisation of Eumulgin ES based AMTPS

5.4.1.1 System Composition of the Eumulgin ES based AMTPS

An Eumuglin ES based AMTPS was set up with 10% in 20 mM sodium-phosphate and a protein mixture of 0.2 g/L lysozyme and ovalbumin. Phases were allowed to separate for

at least 12 hours until they were transparent. Samples of both phases were taken and analyzed for its surfactant concentration by potentiometric titration. The phase ratio was calculated according to Equation 5.4. Table 5.1 summarizes the given system parameters which result in a phase volume ratio of 0.43.

Table 5.1: System conditions of the Eumulgin Based AMTPS

Surfactant concentration in the single phase state	Phase Equilibrium Temperature	Surfactant concentration of the top phase	Surfactant concentration of the bottom phase	Resulting phase ratio R^a
10% (w/w)	26°C	30.3% (w/w)	1.26% (w/w)	0.43

a: Phase volume ratio calculation based on the lever rule

5.4.1.2 Partitioning of Lysozyme and Ovalbumin in the Eumulgin ES based AMTPS

In ATPS and AMTPS the proteins partition specifically between the top and bottom phase based on their unique physico-chemical properties. In this work, the partitioning coefficients of lysozyme and ovalbumine were determined by performing phase separation experiments at 26°C followed by determination of protein concentration in the top and bottom phase, respectively. Figure 2 shows the protein partitioning behavior of a 0.5 g/L lysozyme and ovalbumine protein solution analyzed by SDS-PAGE. Based on densiometric determination the partitioning coefficients for lysozyme was calculated according to Equation 5.1 to K_{Lys}=0.12. For ovalbumine no protein was recognized in the top phase, hence the partitioning coefficient was approximated to K_{Ova}=0.
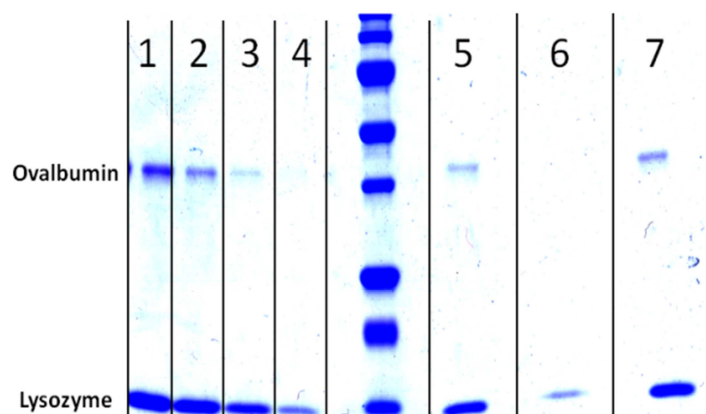
Figure 5.2: Protein partitioning of lysozyme and ovalbumine in a 10% (w/w) Eumulgin ES based AMTPS. Lane 1-4 protein standards with concentrations of: 0.15 g/L; 0.1 g/L; 0.05 g/L; and 0.025 g/L. Lane 5: protein solution in 10% Eumulgin ES in the one-phase regime. Lane 6: micelle rich top phase after phase separation; Lane 7: micelle depleted bottom phase after phase separation.

The small K values indicate that proteins are almost completely excluded from the micelle rich top phase. This exclusion can be related to the high surfactant content in the micelle rich phase (>30%) and the consequently low water content. The higher K value of lysozyme compared to ovalbumin can be explained by the excluded volume theory developed by Nikas et al. which predicts an increasing protein exclusion from the micelle rich phase with increasing protein size [17].

The partitioning of lysozyme and ovalbumine was additionally investigated in AMTPS containing Eumulgin ES concentrations in a range from 5% to 25% at a constant phase splitting temperature of 26° C. According to the lever rule, an increase of the surfactant concentration results in an increasing phase ratio. In Table 5.2 the R values based on the lever rule are listed for starting surfactant concentrations from 5 % to 25% at a phase separation temperature of 26° C.

Table 5.2: Phase ratios of Eumulgin ES based AMTPS resulting from increasing initial surfactant concentrations.

Initial surfactant concentration	5%	10%	15%	20%	25%
Phase Ratio R[a]	0.15	0.43	0.9	1.83	4.57

[a]based on the lever rule

Assuming constant K values of both lysozyme and ovalbumin, the enrichment of the proteins in the micelle depleted phase with increasing surfactant concentration is expected. This effect is approved in Figure 5.3. An initial 0.2 g/L protein solution of lysozyme and ovalbumine is concentrated in the micelle depleted phase with increasing surfactant concentration. It is clearly visible, that both proteins (by means of lane thickness and intensity) are enriched in the micelle depleted phase compared to the initial protein concentration.
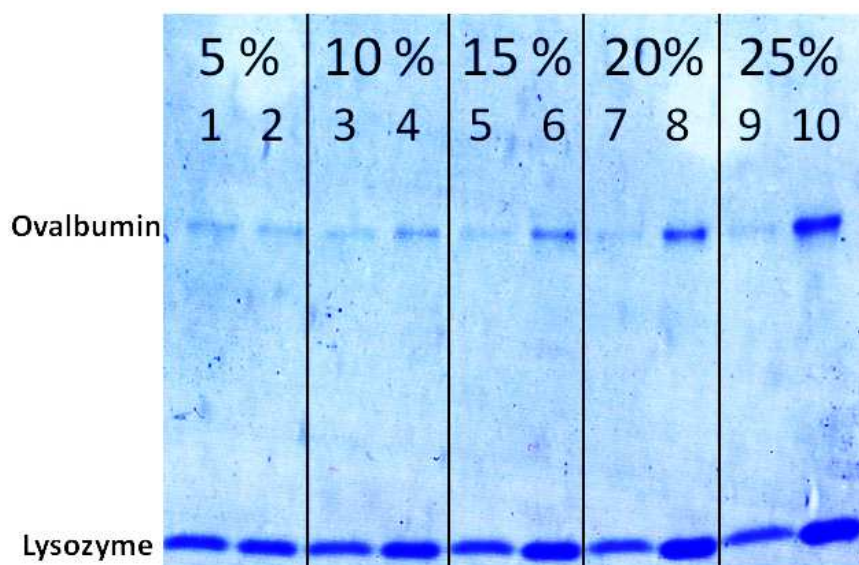
Figure 5.3: Enrichment of 0.2 g/L lysozyme and 0.2 g/L ovalbumin in the micelle depleted phase of an 26° C Eumulgin ES based AMTPS. Lanes 1, 3, 5, 7, 9: Initial protein concentration before phase separation of AMTPS systems containing 5, 10, 15, 20 and 25% Eumulgin ES. Lanes 2, 4, 6, 8, 10: Proteins in the micelle depleted phase after complete phase separation of AMTPS systems containing 5, 10, 15, 20, 25% Eumulgin ES. Equal volumes were applied to each lane

5.4.1.3 Review of an Eumulgin ES based AMTPS as Basis for Magnetic Extraction

Considering the use of an Eumulgin ES based AMTPS as MEP system, the extreme K values are beneficial as in each step the bulk of undesired proteins is removed together with the micelle depleted phase and the micelle rich phase is not "contaminated". Basically, in a MEP process at least two process steps precede the elution of a target molecule from the magnetic support into the micelle depleted phase (sorption - wash - elution). In Figure 5.4 and Figure 5.5 the theoretical protein concentrations of the micelle depleted phases cf.

intial protein concentrations are illustrated for partitioning coefficients of 0.1, 1 and 5 for

R values of 0.43 and 1, respectively.
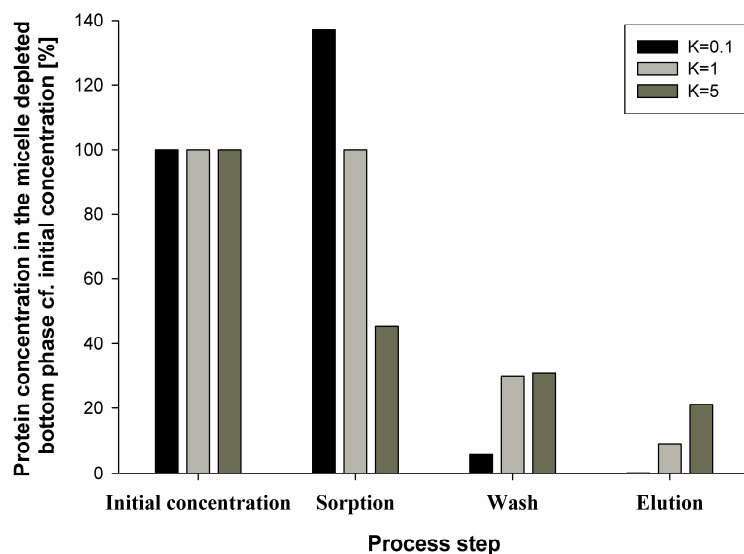
Figure 5.4: Theoretical progress of protein concentration in the micelle depleted phase for a constant phase ratio of 0.43 with varying K values. A three step process is assumed in which in each step the micelle depleted phase is removed and the same volume of protein-free buffer is added. K values of 5, 1 and 0.1 lead to 21.1, 9 and 0.2% of the intial protein concentration remaining in the eluate.
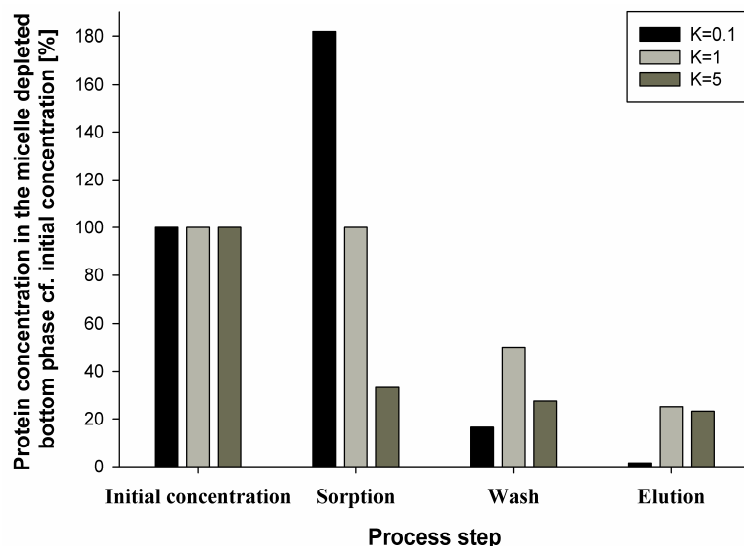
Figure 5.5: Theoretical progress of protein concentration in the micelle depleted phase for a constant phase ratio of 1 with varying K values. A three step process is assumed in which in each step the micelle depleted phase is removed and the same volume of protein-free buffer is added. K values of 5, 1 and 0.1 lead to 23.1, 25 and 1.5 % of the initial protein concentration remaining in the eluate.

With given system parameters of a K value of 0.1 and a volume ratio of 0.43 only 0.23 % of the initial protein feed would be withdrawn to the final elution step. Assuming an even lower partitioning coefficient with increasing protein size, the purity of a target molecule in a MEP process based on an Eumulgin ES AMTPS is only little affected by dissolved proteins which are carried over into the eluate.

5.4.2 Characterisation of the MNCX

5.4.2.1 Sorption of Lysozyme to MNCX

The capability of MNCX to bind and elute proteins was investigated in presence and absence of Eumulgin ES. At first, a sorption isotherm was set up in absence of Eumulgin ES at pH 6.8 in 20 mM sodium-phosphate. In Figure 5.6 the experimental data is fitted to the Langmuir model. For the given system parameters, the fit results in a KL value of 0.03 mg/L and a maximum particle loading of q_{max}= 93 mg/g. Additionally, the sorption of ovalbumin onto the MNCX was investigated. In case of ovalbumin no sorption onto the particles could be observed. This effect is in accordance with the assumed mechanism of cation exchange: at pH 6.8 lysozyme is positively charged, while the charge of ovalbumine is negative [18]. Thus, lysozyme is electrostatically attracted to the MNCX, while ovalbumine is repelled from them.
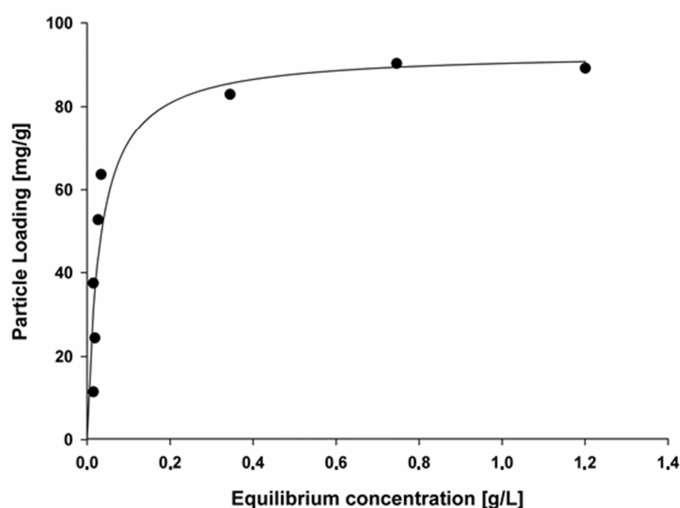
Figure 5.6: Sorption isotherm of lysozyme onto magnetic cation exchange nanoparticles in absence of Eumulgin ES. The solid curve is created by fitting the experimental data to the Langmuir model resulting in parameters of KL=0.03 g/L and qmax=93 mg/g

5.4.2.2 Sorption of Lysozyme to MNCX in Presence of Eumulgin ES

The sorption in presence of 10% Eumulgin ES was investigated in order to determine the influence of this surfactant on the interaction between lysozyme and the MNCX. This influence is of particular interest when considering a MEP process in which the proteins are sorbed in the single phase regime of an AMTPS. In Figure 5.7 a Langmuir curve fitted to the experimental data is depicted. Here, a least square fit of the the Langmuir parameters results in a K_L value of 0.002 g/L and maximal loading of q_{max}= 56 mg/g.
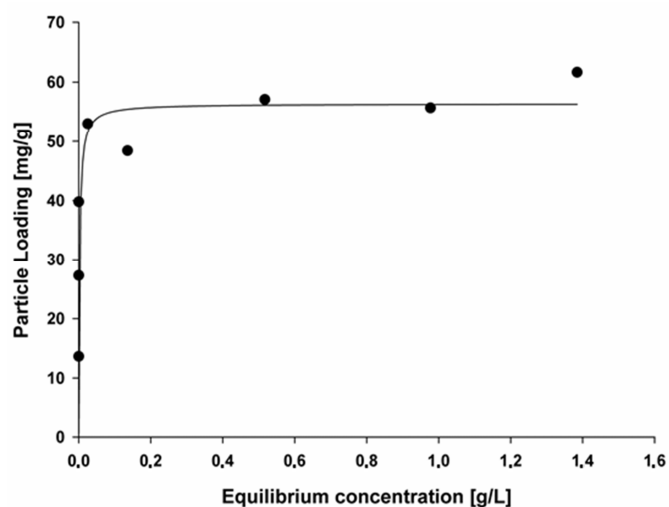
Figure 5.7: Sorption equilibrium isotherm of lysozyme in the presence of 10% Eumulgin ES. The straigt line indicates a Langmuir fit wih KL=0.002 g/L and qmax=56 mg/g

While the improved K_L value needs further confirmation, it is evident, that the presence of Eumulgin ES reduces the q_{max} value for the sorption of lysozyme onto the magnetic supports.The reduction in comparison to the q_{max} value obtained from the sorption isotherm in absence of Eumulgin ES may be attributed to the suppresion of unspecific sorption of lysozyme to the silica surfaces of the nanoparticles. The stronlgy negative charged silica surface of the particles offers attractive binding sites to the positively charged lysozyme in the absence of Eumulgin ES. For it is well investigated that nonionic surfactants adsorb to silica interfaces [19, 20] it is likely that Eumulgin ES adsorbs to the silica surface of the particle, thus reducing the number of (unspecific) binding sites for lysozyme. Additionally, surfactants can form protein-surfactant complexes with proteins adsorbed to a liquid-solid interface and thus lead to an easier desorption of proteins from the surface [21].

5.4.2.3 Desorption of Lysozyme

Desorption of lysozyme from the MNCX was performed by increasing the pH value to 8.8 as well as increasing the ionic strength by addition of 1 M sodium chloride. The particles were washed in sorption buffer three times before the elution buffer was added. A further increase of the pH value or salt concentration as well as repeated elution did not cause additional protein desorption. Protein elution was investigated from samples saturated with lysozyme ($q=q_{max}$). In case of lysozyme sorbed without the presence of Eumulgin ES only 33% of the sorbed protein was eluted from the particles. In contrast to this, when lysozyme is sorbed in the presence of Eumulgin ES, 54% of the bound protein were eluted. In general, the regeneration of bound protein is low, pointing out that the proteins are partly bound to the particles due to unspecific sorption. Figure 5.8 summarizes the amounts of lysozyme sorbed and eluted from the magnetic carriers in equilibrium.
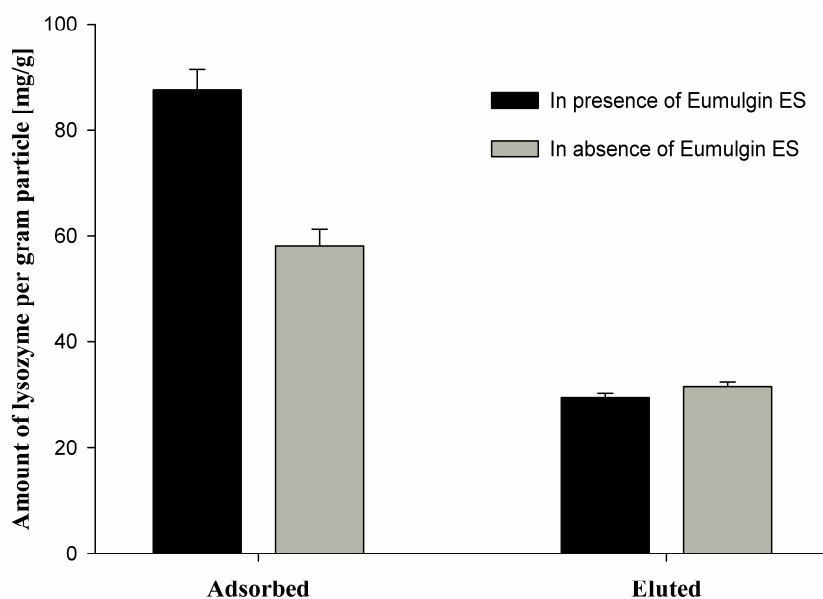
Figure 5.8: Comparison of lysozyme sorbed and eluted from the MNCX in presence and absence of Eumulgin ES

The overall amount of lysozyme eluted from the MNCX in both experiments is virtually equal. Assuming a complete elution of lysozyme from the SO_3^- groups in both cases, the residual difference of sorbed and eluted protein is due to interactions of the silica surface.

The observed difference in elution efficiency supports moreover the hypothesis that the unspecific binding sites are blocked by the surfactant used.

5.4.3 Magnetic Extraction of Lysozyme from an Ovalbumine/Lysozyme Mixture

The Magnetic Extraction Phases were prepared by combining the MNCX, the nonionic surfactant Eumulgin ES and a mixture of lysozyme and ovalbumine in 20mM sodium-phosphate buffer at pH 6.8. By heating up this solution to 26° C phase separation is induced. Figure 9 depicts the proceeding of the phase separation in a 2 ml microcentrifuge vessel at an overall MNCX concentration of 1g/L in 10% Eumulgin ES. The figure clearly shows that the MNCX are concentrated in the micelle rich top phase.
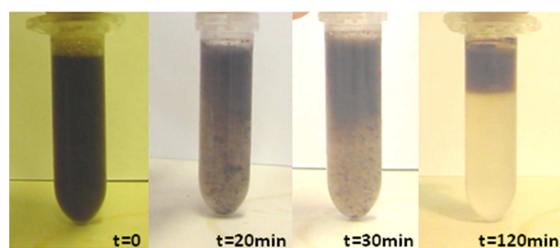
Figure 5.9: Progress of phase separation by gravity in a 10% Eumulgin ES based AMTPS at 26° C in 20mM sodium-phosphate containing 1 g/L MNCX.

Magnetic Extraction Experiments were carried out with increasing particle concentrations (c_P) simultaneously increasing the capacitiy ratio (CR). The capacitiy ratio is given by Equation 5.7:

$$CR = \frac{c_P \cdot q_{max}}{c_0}$$

[Eq. 5.7]

The protein concentrations (c_0) of lysozyme and ovalbumin were kept constant at 0.2 g/L and the Eumulgin ES concentration were adjusted to 10%. The overall volume was 2 mL in a microcentrifuge cup. Capacity ratios were set from 0.28 to 2.24 with an assumed q_{max} value of 56 mg/g. In the course of the experiments samples were taken from sorption supernatant, intermediate wash and eluate, all of them forming the bottom phase of the AMTPS system (see principle of MEP in Figure 5.1). All samples were analyzed by SDS

PAGE depicted in figure 10. The initial protein solution was threefold diluted due to its high surfactant concentration of 10% which otherwise interferes with the protein gelelectrophoresis.
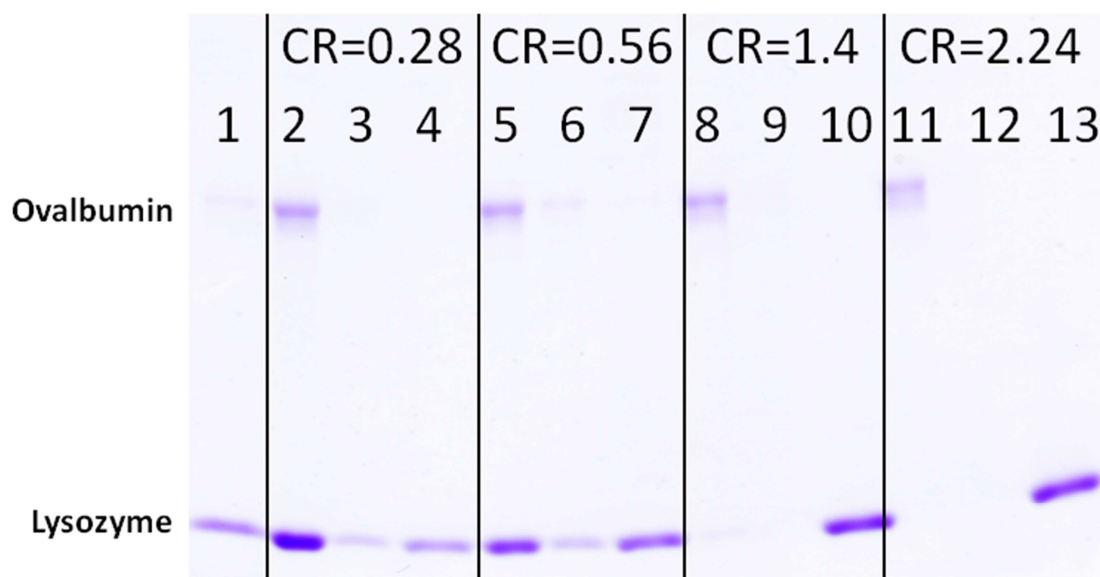
Figure 5.10: Extraction of lysozyme using magnetic nanoparticles in combination with an Eumulgin ES based AMTPS. Lane 1: Initial feed in a threefold dilution. Lanes 2, 5, 8, 11: Supernatants from the sorption experiment with increasing capacitiy ratios: 0.28, 0.56, 1.4, 2,24. Lanes 3, 6, 9, 12: Supernatants from the intermediate wash step. Lanes 4, 7, 10, 13: Resulting eluates with increasing capacity ratios.

With increasing CR, the amount of lysozyme bound increases illustrated by the diminishing lysozyme bands in the supernatnant while the ovalbumin band remains unaffected. During the intermediate wash step not only loosely bound protein is removed, it is also essential to remove remaining supernatant due to incomplete phase splitting at the end of the phase separation step. The amount of sorbed lysozyme (also congruent with the CR) then is eluted from the magnetic particles and consequently separated from them by temperature induced phase separation. Ovalbumin was not detected in the eluate phase. This result can be expected from the results of both, protein partitioning of ovalbumin between the phases and binding experiments. Therefore, the purity of lysozyme can be assumed to be close to 100% in the eluate.

5.5 Conclusion

The feasibility of nanosorbent driven protein purification by Magnetic Extraction Phases has been demonstrated. The positively charged lysozme was bound to a magnetic cation exchange nanoparticle and subsequently- in contrast to the partitioning behavior of the sole protein - co-transferred to the micelle rich phase of an AMTPS. Afterwards lysozyme was released into the micelle depleted phase of another AMTPS by elution from the magnetic sorbent which itself accumulates again in the micelle rich phase. It has been shown, that the presence of the phase forming surfactant Eumulgin ES influences protein sorption without affecting the overall protein elution. In addition to this the bulk protein solution is excluded from the micelle rich phase and thus is concentrated in the micelle depleted phase, which is discarded in the first step.

In conclusion, Magnetic Extraction Phases unite the advantages of both functionalized particles and Aqueous Micellar Two-Phase Systems. The flexibility and selectivity of functionalized magnetic nano particles are combined with thermosensitive AMTPS which can be easily scaled-up for the large scale handling of the sorbents.

Following this promising proof of principle, future work will have to focus on the application of MEP in natural biological system. Due to the complexity of these systems, the application of MEP using MNCX may contribute to the capture step in a protein purification process. To further increase selectivity as well as yield of a MEP based process, the application of magnetic particles grafted with bioaffinity ligands, as well as the modification of this process into a continuous operation may be an exciting alternative to conventional bioseparation processes.

5.6 References

[1] J.J. Hubbuch, D.B. Matthiesen, T.J. Hobley, O.R.T. Thomas, High gradient magnetic separation versus expanded bed adsorption: a first principle comparison, Bioseparation, 10 (2001) 99-112.

[2] C. Bordier, Phase-Separation of Integral Membrane-Proteins in Triton X-114 Solution, Journal of Biological Chemistry, 256 (1981) 1604-1607.

[3] D.T. Kamei, D.I.C. Wang, D. Blankschtein, Fundamental investigation of protein partitioning in two-phase aqueous mixed (nonionic/ionic) micellar systems, Langmuir, 18 (2002) 3047-3057.

[4] A. Sanchezferrer, R. Bru, F. Garciacarmona, Phase-Separation of Biomolecules in Polyoxyethylene Glycol Nonionic Detergents, Critical Reviews in Biochemistry and Molecular Biology, 29 (1994) 275-313.

[5] H. Tani, T. Kamidate, H. Watanabe, Aqueous micellar two-phase systems for protein separation, Analytical Sciences, 14 (1998) 875-888.

[6] G.C. Terstappen, R.A. Ramelmeier, M.R. Kula, Protein Partitioning in Detergent-Based Aqueous 2-Phase Systems, Journal of Biotechnology, 28 (1993) 263-275.

[7] M.J.L. Costa, M.T. Cunha, J.M.S. Cabral, M.R. Aires-Barros, Scale-up of recombinant cutinase recovery by whole broth extraction with PEG-phosphate aqueous two-phase, Bioseparation, 9 (2000) 231-238.

[8] K. Selber, F. Tjerneld, A. Collen, T. Hyytia, T. Nakari-Setala, M. Bailey, R. Fagerstrom, J. Kan, J. van der Laan, M. Penttila, M.R. Kula, Large-scale separation and production of engineered proteins, designed for facilitated recovery in detergent-based aqueous two-phase extraction systems, Process Biochemistry, 39 (2004) 889-896.

[9] T. Minuth, H. Gieren, U. Pape, H.C. Raths, J. Thommes, M.R. Kula, Pilot scale processing of detergent-based aqueous two-phase systems, Biotechnology and Bioengineering, 55 (1997) 339-347.

[10] P. Wikstrom, S. Flygare, A. Grondalen, P.O. Larsson, Magnetic Aqueous 2-Phase Separation - a New Technique to Increase Rate of Phase-Separation, Using Dextran Ferrofluid or Larger Iron-Oxide Particles, Analytical Biochemistry, 167 (1987) 331-339.

[11] S. Flygare, P. Wikstrom, G. Johansson, P.O. Larsson, Magnetic Aqueous 2-Phase Separation in Preparative Applications, Enzyme and Microbial Technology, 12 (1990) 95-103.

[12] P.O. Larsson, Magnetically Enhanced Phase-Separation, Aqueous Two-Phase Systems, 228 (1994) 112-117.

[13] M. Suzuki, M. Kamihira, T. Shiraishi, H. Takeuchi, T. Kobayashi, Affinity Partitioning of Protein-a Using a Magnetic Aqueous 2-Phase System, Journal of Fermentation and Bioengineering, 80 (1995) 78-84.

[14] J.S. Becker, O.R.T. Thomas, M. Franzreb, Protein separation with magnetic adsorbents in micellar aqueous two-phase systems, Separation and Purification Technology, 65 (2009) 46-53.

[15] P.A. Albertsson, Partition of Cell Particles and Macromolecules, John Wiley and Sons, New York, 1986.

[16] W. McCabe, J. Smith, P. Harriot, Unit Operations of Chemical Engineering, Seventh Edition ed., McGraw-Hill, New York, 2005.

[17] Y.J. Nikas, C.L. Liu, T. Srivastava, N.L. Abbott, D. Blankschtein, Protein Partitioning in 2-Phase Aqueous Nonionic Micellar Solutions, Macromolecules, 25 (1992) 4797-4806.

[18] C. Desert, C. Guerin-Dubiard, F. Nau, G. Jan, F. Val, J. Mallard, Comparison of different electrophoretic separations of hen egg white proteins, Journal of Agricultural and Food Chemistry, 49 (2001) 4553-4561.

[19] S. Paria, K.C. Khilar, A review on experimental studies of surfactant adsorption at the hydrophilic solid-water interface, Advances in Colloid and Interface Science, 110 (2004) 75-95.

[20] J. Brinck, B. Jonsson, F. Tiberg, Kinetics of nonionic surfactant adsorption and desorption at the silica-water interface: One component, Langmuir, 14 (1998) 1058-1071.

[21] C. Kotsmar, V. Pradines, V.S. Alahverdjieva, E.V. Aksenenko, V.B. Fainerman, V.I. Kovalchuk, J. Kragel, M.E. Leser, B.A. Noskov, R. Miller, Thermodynamics, adsorption kinetics and rheology of mixed protein-surfactant interfacial layers, Advances in Colloid and Interface Science, 150 (2009) 41-54.

6 Partitioning behavior of silica-coated nanoparticles in Aqueous Micellar Two-Phase Systems: Evidence for an adsorption driven mechanism from QCM-D and ATR-FTIR measurements

*Ingo Fischer, Christian Morhardt, Stefan Heissler, Matthias Franzreb**

Institute of Functional Interfaces, Karlsruhe Institute of Technology, Herrmann von Helmholtz Platz 1, 76344 Eggenstein-Leopoldshafen, Germany

*: Corresponding author: Email: Matthias.Franzreb@kit.edu

6.1 Abstract

Quartz Crystal Microbalance with Dissipation (QCM-D), Attenuated Total Reflectance Fourier Transformed Infrared Spectroscopy (ATR-FTIR) and total organic carbon detection (TOC) are employed to examine the cause of the differences in the partitioning of silica coated nanoparticles in an aqueous micellar two-phase system based on the non-ionic surfactant Eumulgin ES. The particles partition into the micelle rich phase at pH 3 and to the micelle poor phase at pH 7. Our results clearly show that the non-ionic surfactants are adsorbed to the silica surface at pH 3. Above the critical temperature, a stable surfactant bilayer forms on the silica surface. At pH 7 the surfactants do not adsorb to the particle surface; a surfactant-loaded particle is therefore drawn to the micelle rich phase while otherwise repelled from it. These results suggest that the partitioning in aqueous micellar two-phase systems is mainly driven by hydrogen-bonds formed between the surfactants and the component to be partitioned.

6.2 Introduction

Aqueous Two-Phase Systems (ATPS) and Aqueous Micellar Two-Phase Systems (AMTPS) can be used to concentrate proteins and other (in)soluble substances based on their partitioning behavior between the two phases [1]. The mechanism of the partitioning depends on both, system conditions as well as target molecule characteristics and is still unclear.

Much attention has been paid to the partitioning of soluble molecules in AMTPS, and it has been shown, that the partitioning coefficient of a protein can be reasonably predicted by the excluded-volume-theory which is mainly based on the hydrodynamic radius of the particular protein and the (growth of the) cross-sectional radius of the phase-forming micelles [2].

The mechanism of the partitioning of colloids and insoluble particles in aqueous two-phase systems, however, has scarcely been investigated although several publications describe the macroscopic behavior of particles in two-phase systems: PEG/Dextran ATPS have been used to partition Au and Ag nanospheres with sizes less than 100 nm [3]. Here, Au nanospheres partitioned preferentially to the PEG-rich phase while Ag nanospheres were mainly partitioned to the dextran phase. The two-phase behavior of polymeric acrylic latex and colloidal TiO_2 particles was found to be dependent on both surface chemistry and the size of the particles [4]. The authors emphasized the influence of the pH on the partitioning; at low pH, when the carboxylated particles were protonated, they partitioned to the PEG phase. Additionally, it was shown that the addition of silica and polystyrene latex particles to stable PEG/dextran systems induces phase separation by shifting the coexistence curve of the ATPS [5]. The authors explain their results by two different mechanisms, both originating from the adsorption from one polymer to the particles. The addition of magnetic particles as carrier for biomolecules as a tool in biopurification has been shown for ATPS [6, 7] as well as for AMTPS [8, 9]. Recently, the potential of AMTPS to concentrate silver, gold and palladium nanoparticles was shown [10-12]. The authors used the non-ionic surfactants Triton X-114 and Triton X-100 respectively to concentrate the nanoparticles in the micelle rich phase of the two-phase

systems. Despite the practical applicability of these studies, no mechanism of the partitioning of the nanoparticles is explained.

The purpose of our study was to investigate the mechanism of the partitioning of nanoparticles in AMTPS. As described, several authors hypothesize that the partitioning of particles in ATPS is somehow related to adsorption of the phase forming polymer to the particle surface. Our intention was to investigate if the partitioning of particles in AMTPS is based on the same principle – and if so, to investigate the mechanism of adsorption.

Silica coated Fe_3O_4 nanoparticles with a mean size of 100 nm were tested. The partitioning of the particles in an AMTPS based on the non-ionic surfactant Eumulgin ES was investigated at different pH levels as well as in presence and absence of the chaotropic organic molecule urea; the correlation of the partitioning behavior of the particles and adsorption of surfactant to the silica surface was monitored by Quartz Crystal Microbalance with Dissipation (QCM-D). Reference chips with silica surfaces were used at the same conditions than those in the partitioning experiments. In addition adsorptive behavior of the phase forming surfactant onto the particles was directly detected by Attenuated Total Reflectance Fourier Transformed Infrared Spectroscopy (ATR-FTIR) and by surfactant binding studies.

6.3 Experimental

6.3.1 Materials

6.3.1.1 Chemicals

All chemicals were analytical grade and used without further purification. All water used was prepared with MilliQ system (Millipore, USA). Ethanol and citric acid monohydrate were purchased form Merck Millipore (Darmstadt, Germany), disodium phosphate and sodium dodecyl sulfate, hydrochloric acid, and sodium hydroxide form Carl Roth (Karlsruhe, Germany); and sodium-lactate from AppliChem (Darmstadt, Germany). The non-ionic surfactant Eumulgin ES (PPG-5-Laureth-5, CAS-No.: 68439-51-0) was purchased from Cognis (Düsseldorf, Germany). The density of Eumulgin ES was determined by a

DCAT 11 system (Dataphysics, Filderstadt, Germany) and resulted in $\rho = 982$ kg/m³. The average length of an Eumulgin ES molecule C12-(POE)5-(POP)5 was calculated to 5.57 nm using the software Yasara, version 12.4.1 [13]. The hydrodynamic diameter of 0.5 % Eumulgin ES solution in both, 20 mM sodium phosphate at pH 7 and 20 mM sodium citrate at pH 3 was determined by dynamic light scattering (DLS) by means of a Zetasizer 5000 (Malvern Instruments GmbH, Herrenberg, Germany) to 15 nm.

6.3.1.2 Particles

"MagPrep Silica" particles were obtained from Merck Millipore (Darmstadt, Germany). The particles consist of magnetite (Fe_3O_4) monocrystals with a thin silica coating. Scanning electron microscope (SEM) pictures reveal a mean diameter of single particles of 100 nm with a narrow size distribution.

6.3.2 Methodology

6.3.2.1 Partitioning Experiments

Initially, an Eumulgin ES based AMTPS phase diagram was prepared in 20 mM sodium citrate at pH 3 following a protocol described elsewhere [14]. The Eumulgin ES solution was heated to a temperature above the cloud point and the temperature was maintained until the phases were separated. The surfactant concentrations of both emerging phases were determined by potentiometric titration and subsequently plotted in a T, x diagram.

The partitioning of the MagPrep Silica particles in Eumuling ES based AMTPS was investigated with regard to the pH of the AMTPS solution. Therefore, Eumulgin ES AMTPS were set up in 20 mM solutions of sodium citrate, sodium phosphate, and sodium lactate. The pH was titrated to the respective pH with hydrochloric acid or sodium hydroxide. To investigate the influence of urea, an additional AMTPS consisting of 20 mM sodium citrate and 6 M urea was created. In all experiments the Eumulgin ES concentration was 10 %wt.

Initially, the particles were equilibrated in the corresponding buffer and then added to the AMTPS. The final particle concentration in the AMTPS was set to 0.5 g/l. After temperature induced phase separation, the particle partitioning behavior was observed

visually. The phase separation temperature was set to 30° C in all experiments except for the experiments that were carried out with urea; in these experiments the temperature had to be elevated to 35° C to induce phase separation.

6.3.2.2 Quartz Crystal Microbalance

The QCM-D experiments were performed using a Q-Sense E4 system with Qsoft 401 software (Q-Sense, Gothenburg, Sweden). QCM-D exploits the piezoelectric effect in chips composed of an AT-cut, disk-shaped and polished quartz crystal, which has a fundamental frequency of 4.95 MHz. QCM-D monitors the adsorption of molecules onto the surface of the chip due to a negative shift in frequency (f) which is proportional to the mass on the crystal. In addition, there is a positive shift in dissipation (D) proportional to the viscoelastic properties of that mass. QCM-D measurements relate the mass to the frequency shift basis the work of Sauerbrey [15] according to Equation 6.1:

$$\Delta m = -\frac{C \cdot \Delta f}{n} \qquad \text{[Eq. 6.1]}$$

Where m is the adsorbed mass, f the frequency shift, n = 1, 3, 5...13 the observed overtone, C= 17.7 ng Hz^{-1}cm^{-2} the mass sensitivity constant of the crystal. The average thickness of the adsorbed surfactants layer was calculated using Equation 6.2:

$$t_{Eff} = \frac{\Delta m}{\rho_{Eff}} \qquad \text{[Eq. 6.2]}$$

Where ρ_{Eff} is the densitiy of Eumulgin ES and t_{Eff} the thickness of the adsorbed film.

Silica coated chips (QSX 303, Q-Sense, Gothenburg, Sweden) were used for the QCM-D measurements. In order to clean the chips, they were sonicated in ethanol for 10 min, dried with nitrogen and irradiated with UV-ozone (ProCleaner, Bioforce Nanoscience, Ames, US-IA) for 10 min. After the experiments the chips were sonicated in ethanol for 10 min and two times in MilliQ water, dried with nitrogen and stored at ambient conditions. All chips were used multiple times.

During all experiments the flow rate was set to 50 µl/min. All experimental conditions were designed to meet the same conditions than the partitioning experiments: temperatures were either set to 20° C to simulate single phase temperature or to 30° C (to 35° C in case of the urea experiments) to generate phase separation conditions. Buffers used were the same than described in the partitioning experiments. Initially, the chips were equilibrated in the corresponding buffer; after a stable baseline was achieved the buffered 10 %wt surfactant solution was injected. The rinsing with the surfactant solution was performed for at least 45 minutes, afterwards pure buffer was injected until a constant signal was reached. Finally, the system was rinsed with MilliQ water.

6.3.3 Surfactant Binding and Elution Studies

Merck MagPrep Silica solutions were prepared as follows: 10 ml samples containing a particle concentration of 10 g/L were prepared; these samples contained 10 %wt Eumulgin ES either at pH 3 or at pH 7. All solutions were buffered using sodium phosphate. Each sample was kept constant at 4° C or at 30° C. This set up resulted in a total of four different samples: pH 3 or pH 7 at 4° C or at 30° C. All experiments were performed in triplets. The samples were initially incubated in an overhead shaker for 20 minutes in the 10 % Eumulgin ES at the respective pH and temperature. Afterwards the particles were separated from the Eumulgin ES solution using a handmagnet. Then particles were washed in 10 ml of pure buffer at the respective temperature and pH for 20 minutes. The supernatant was again separated from the particles. The washing procedure was repeated for an additional 11 times, resulting in a total wash of 12 times. All samples were analyzed for their Eumulgin ES content by determination of the total organic carbon.

6.3.3.1 Surfactant Determination by TOC

The surfactant concentration in the samples was determined by detection of the total organic carbon using the Multi N/C 2000 (Analytik Jena, Jena, Germany). 15 µl hydrochloric acid was added to each sample before TOC measurement in order to remove dissolved inorganic carbon. The total surfactant concentration was calculated from the

TOC content; the carbon mass makes up for 63.8 % of the total mass of the non-ionic surfactant Eumulgin ES.

6.3.3.2 Surfactant - Particle Investigation with ATR-FTIR

For the ATR-FTIR measurements a Tensor 27 IR spectrometer with a Platinum ATR (single reflecting diamond) accessory (Bruker Optics, Ettlingen, Germany) was used. Each spectrum comprised 64 co-added scans with a spectral resolution of 4 cm^{-1} in the 3600-400 cm^{-1} range. The data was acquired using OPUS 6.5 software (Bruker Optics, Ettlingen, Germany).

The MagPrep Silica particles were equilibrated in a citrate buffer at pH 3 or phosphate buffer at pH 7; and then incubated in the same buffer containing 10 % Eumulgin ES. Afterwards the particles were washed for five times in the pure buffer.

The particle suspensions were applied to the ATR crystal and allowed to dry for 10 min. The spectra of the plain particles were subtracted from spectra of the processed particles. The spectra were baseline corrected by concave rubber band method.

6.4 Results and Discussion

6.4.1 Phase diagram of Eumulgin ES based AMTPS

The unique properties of an AMTPS in a certain buffer are characterized by its phase diagram. Figure 6.1 depicts the phase diagram of an AMTPS of Eumulgin ES in 20 mm sodium citrate. Phase diagrams of Eumulgin ES AMTPS have been determined in water and 100 mM sodium phosphate at pH 7 [14]. From the comparison of the phase diagrams, it can be seen, that the pH and salt concentrations within the investigated range have little influence on the phase diagram, and thus on the intermicellar interactions. It is generally assumed that the phase separation of AMTPS is based on the temperature induced growth of the nonionic micelles. With increasing temperature, the micelles grow until a thermodynamically favored phase separation occurs. This phenomenon has been fundamentally investigated by a workgroup around Blankschtein [16, 17].
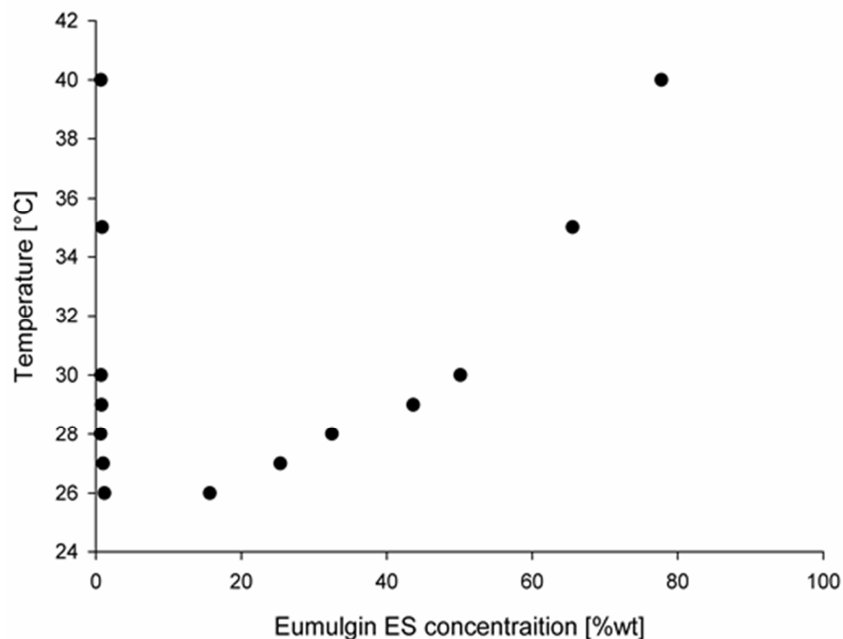
Figure 6.1: Phase diagram of a 20mM sodium citrate Eumulgin ES AMTPS. The points of transition from single phase to two phase state are shown. The phase separation depends on the surfactant concentration and the temperature.

The dots represent the temperature where the system starts to split into two phases.

6.4.2 Partitioning Experiments

The partitioning of silica-coated 100 nm Fe_3O_4 particles in an Eumulgin ES based AMTPS was investigated. At pH 3 and pH 4 the particles partition to the micelle rich phase, independent of buffer used. At pH 7 the particles partition completely to the micelle poor phase.

Figure 6.2 illustrates the difference between magnetic particles in the single phase regime at a low temperature and after phase separation accumulating in the micelle rich top respectively micelle poor bottom phase.
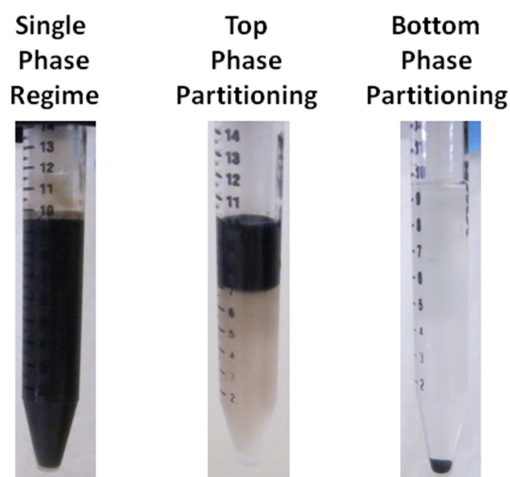
Figure 6.2: Possibilities of the partitioning behavior of 100 nm Silica particles in an Eumulgin ES based AMTPS: left: In single phase state, the particles are homogenously distributed in the solution; middle: the particle partition to the micellar rich top phase; right: the particles partition to the micelle poor bottom phase and sediment to the bottom.

By changing buffer the buffer composition and/or a change of the pH, the ionic strength of the solution changes. The effect of the ionic strength in AMTPS systems, however, results in an increasing or decreasing shift of the phase diagram, depending on the kind and especially the concentration of the applied salt. For chaotrophic agents, the phase separation temperature (the cloud point) is decreased, while for cosmotrophic agents, the cloud point is increased [18]. To exclude the contribution of the particular salt to the partitioning behavior e.g. at pH 3, the partitioning experiments were carried out in presence of two different buffering salts viz. sodium phosphate and sodium citrate. In both cases the partitioning of the particles did not diverge. Phase diagrams of Eumulgin ES have been investigated e.g. in 100 mM sodium phosphate, and in pure water [14]. From these diagrams it can be seen, that the influence of pH and in the investigated range onto the phase diagram and thus onto the aggregation behavior of the surfactants at the investigated salt concentrations even at different pH levels is small. Therefore, the correlation between the non-ionic surfactant, particle surface and pH must be responsible for the partitioning behavior. The interactions of poly(oxyethylated) non-ionic surfactants or poly(oxyethylene) oxide and hydrophilic surfaces however, have been described extensively e.g. [19-21]. It is generally accepted that the interactions are mainly driven by hydrogen bonds that form between the ether oxygens or the hydroxyl end of the non-ionic surfactant and the hydrophilic surface [22]. Therefore, a lower pH level increases the

protonation of the OH groups of either surface or surfactant, leading to the adsorption of the non-ionic surfactants to the surface [23, 24]. For this reason particles in the micellar rich top phase are stabilized by the adsorption of the surfactant onto their surface which prevents particle aggregation, while the particles agglomerate and sediment to the bottom phase when the surfactants do not adsorb.

In order to investigate the role of hydrogen bonds in the mechanism of the partitioning behavior of the silica coated sorbents, an AMTPS containing high concentrations of urea has been set up. Urea is known to have an strong impact on the solvent-solute interaction and the micellar properties of AMTPS, e.g. increasing the critical micelle concentration [25] and the cloud point [18, 26]. In general, the role of urea is related to its direct interaction with the hydrogen bonds between water molecules, or by interaction of urea with the solute. Recent experimental findings support the latter theory, which now has become widely accepted [27, 28].

The addition of urea reverses the partitioning behavior of the 100 nm Fe_3O_4 silica particles from the micelle rich to micelle poor phase in a 20 mM sodium citrate system at pH 3. This effect can be explained by the inference of urea with the hydrogen bonds of the non-ionic surfactant and the silica surface. When the non-ionic surfactants do not adsorb onto the particles, they are excluded from the micellar rich phase of the system.

6.4.3 Surfactant Binding on Reference Surfaces

Quartz Crystal Microbalance signals were recorded in order to monitor the surfactant – SiO_2 interaction at different pH levels at different temperatures. Initially, each silica chip was equilibrated in the respective buffer and then rinsed with the Eumulgin ES solution. Figure 6.3 shows exemplarily the real-time signal curve for the overtones five, seven and nine at 20° C and pH 3.
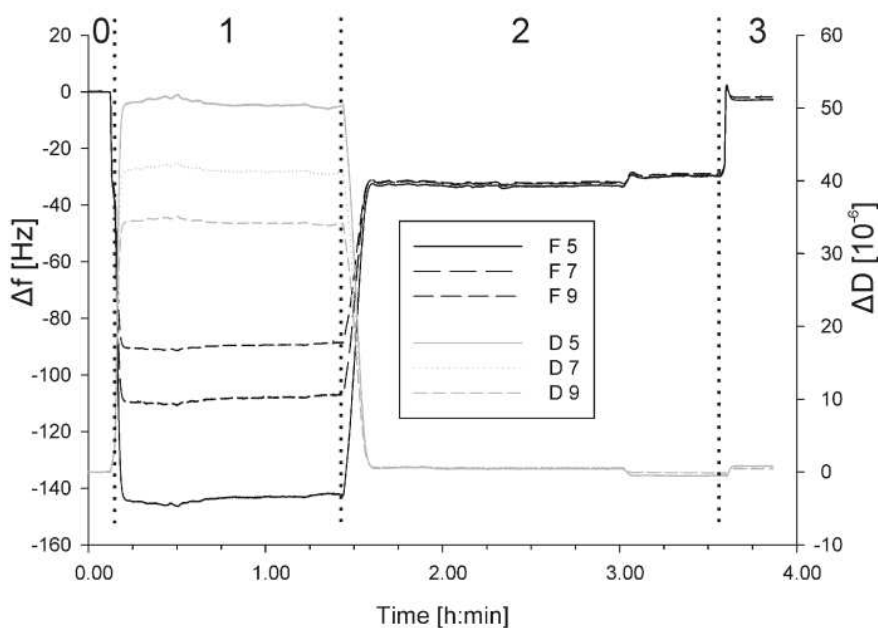
Figure 6.3: QCM-D signal obtained during rinsing a silica chip with sodium citrate and Eumulgin ES at pH 3 and 20° C. The silica chip is rinsed with: 0: sodium citrate; 1: 10 % Eumulgin ES in sodium citrate; 2: sodium citrate; 3: MilliQ water. The signal shift to -35 Hz is generated by a Eumulgin ES monolayer which is adsorbed to the silica surface. When the chip is rinsed with MilliQ water, the Eumulgin ES layer is removed completely.

The signals for Δf decrease and ΔD increase when the chip is being in contact to the surfactant solution, yet the frequency shifts do not run congruently. This is due to the fact that the solution rinsing the chip behaves like a viscoelastic film because of the high surfactant concentration. The increased shift of the energy dissipation also arises from this effect. When the SiO_2 surface is rinsed with buffer containing no surfactant, a stable frequency shift of approximately -35 Hz occurs for all overtones. The dissipation is decreased close to zero. In this state, a stable rigid surfactant layer is adsorbed to the SiO_2 surface. Upon rinsing the surface with MilliQ water, the surfactant layer is desorbed and the signal drops back to zero.

Figure 6.4 displays the QCM-D signal for the experiment at pH 7 at 20°C.
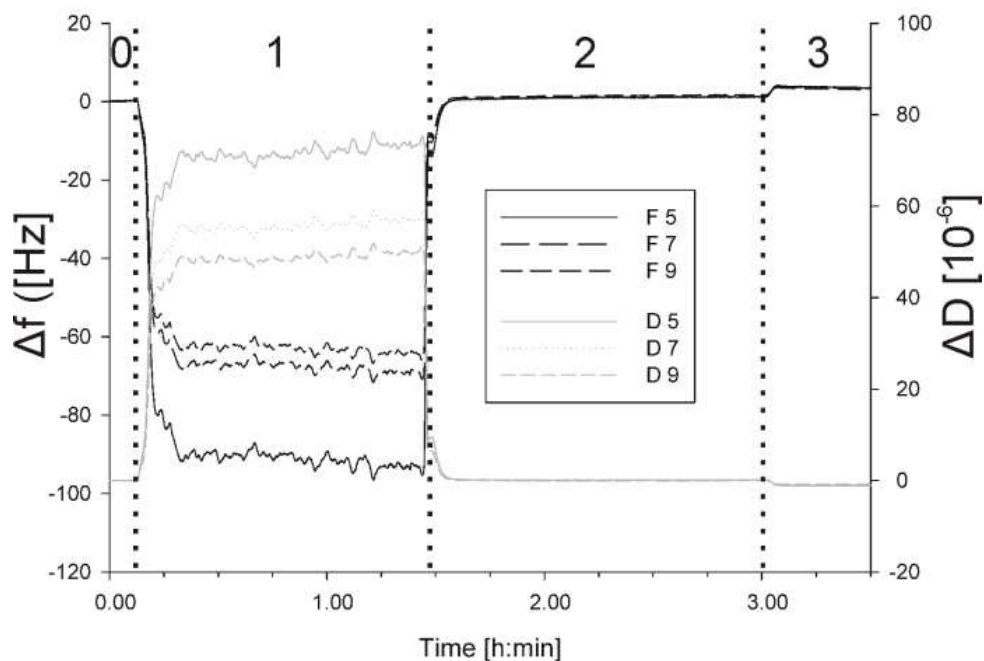
Figure 6.4: QCM-D signal obtained during rinsing a silica chip with sodium phosphate and Eumulgin ES at pH 7 and 20° C. The silica chip is rinsed with: 0: sodium phosphate; 1: 10 % Eumulgin ES in sodium phosphate; 2: sodium phosphate; 3: MilliQ water. Eumulgin ES is completely removed from the chip surface after rinsing with sodium phosphate.

When the silica chip is rinsed with the surfactant solution, the signal change is similar to the signal change at pH 3, yet when the SiO_2 surface is rinsed with pure buffer, the frequency signal drops to zero immediately. Rinsing the silica chip with MilliQ water does not change the signal. In conclusion, at pH 7 no surfactant layer is adsorbed to the SiO_2 surface. The signal change by rinsing with surfactant solution is due to interaction or loose attachment of the surfactant to the silica surface.

When the temperature is increased to 30° C the cloud point of the Eumulgin ES solution is crossed and the system splits. QCM-D signals for a solution heated to 30° C at pH 3 are shown in Figure 6.5.
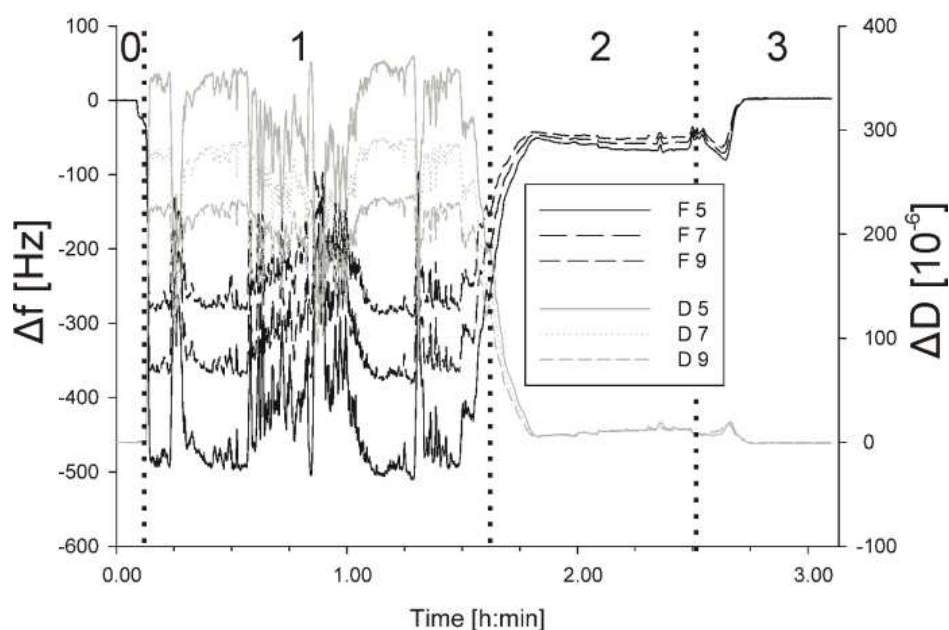
Figure 6.5: QCM-D signal obtained during rinsing a silica chip with sodium citrate and Eumulgin ES at pH 3 and 30° C. The silica chip is rinsed with: 0: sodium citrate; 1: 10 % Eumulgin ES in sodium citrate; 2: sodium citrate; 3: MilliQ water. A signal shift of -55 Hz emerges when the surface is flushed with sodium citrate. The signal comes from a stable surfactant double layer formed on the silica surface at pH 3 and 30°C.

When rinsing with the surfactant solution, fluctuations in the signals can be detected. These occur due to the inhomogeneous solution that is rinsed to the SiO_2 surface. Above the phase separation temperature large micelles are formed that interact with the quartz surface in an uncoordinated manner. When the surface is flushed with pure buffer, however, a constant frequency shift signal of about -55 Hz emerges. Rinsing with MilliQ water decreases the frequency shift to zero. This effect is explained by a two-step mechanism. In the first step, the surfactants adsorb to the SiO_2 surface due to hydrogen bonding (shown in the 20° C experiment). When the temperature is increased, the hydrocarbon chains of the surfactants congregate; the surfactants form a stable double layer on the SiO_2 surface.

In contrast to that, Figure 6.6 shows the signal of the QCM-D when the heated surfactant solution is brought in contact with the silica surface at pH 7. When the chip is rinsed with buffer after contact with surfactant the signal drops to zero. Although the surfactants

congregate, they do not bind to the silica surface, as no hydrogen bonding between polar heads of the surfactant and SiO_2 occurs.

Figure 6.6: QCM-D signal obtained from rinsing a silica chip with sodium phosphate and Eumulgin ES at pH 7 and 30° C. The silica chip is rinsed with: 0: sodium phosphate; 1: 10 % Eumulgin ES in sodium phosphate; 2: sodium phosphate; 3: MilliQ water. Eumulgin ES is completely removed from the chip surface after rinsing with sodium phosphate at 30° C

When urea is added to the buffered solution at pH 3 the QCM-D signal is straight, as can be seen in Figure 6.7.
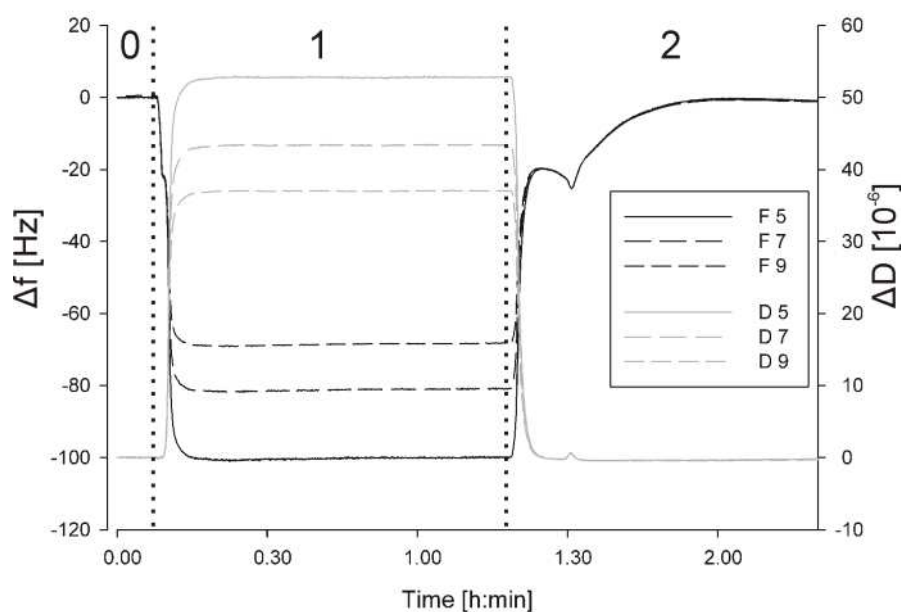
Figure 6.7: QCM-D signal obtained during rinsing a silica chip with sodium citrate, 6 M urea and Eumulgin ES at pH 3 at 20° C. The silica chip is rinsed with: 0: sodium citrate, 6 M urea, pH 3; 1: 10% Eumulgin ES in sodium citrate, 6 M urea, pH 3; 2: sodium citrate, 6 M urea, pH 3. Eumulgin ES is completely removed from the chip surface after rinsing with the buffered urea solution.

Urea stabilizes the micelles; this results in a less staggered QCM-D signal. When rinsed with buffer and urea but without the surfactant at pH 3, the frequency shift drops to zero. When the temperature is increased to 35° C to induce phase separation conditions and the chip is rinsed with buffer and urea after contact with the surfactant solution, the signal of both frequency shift as well as dissipation slowly converges to zero. The signal curve can be seen in Figure 6.8. It can be concluded, that Eumulgin ES does not bind permanently to the silica surface at pH 3 in presence of 6 M urea.
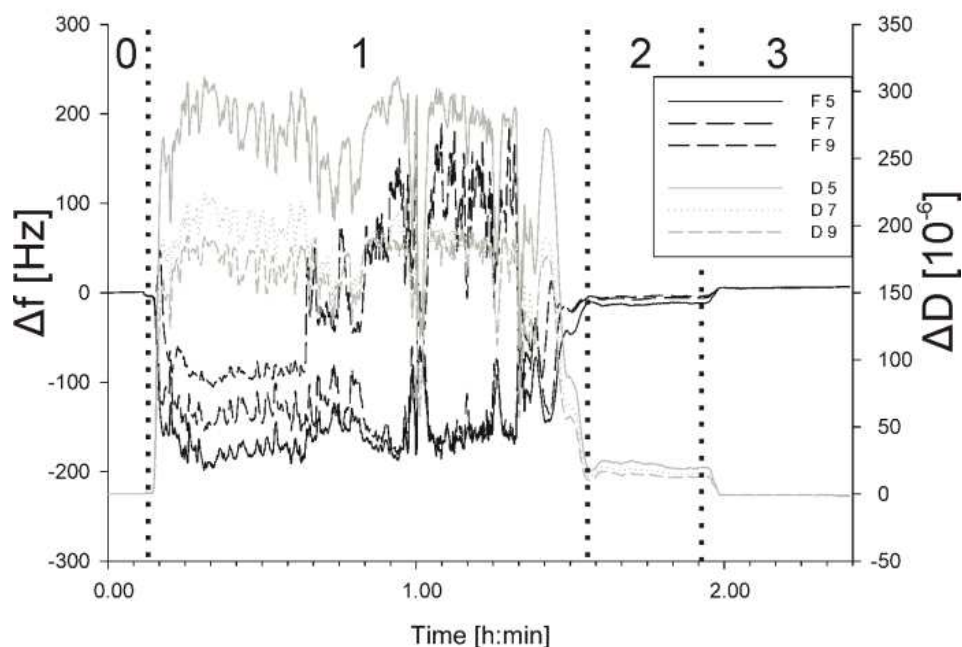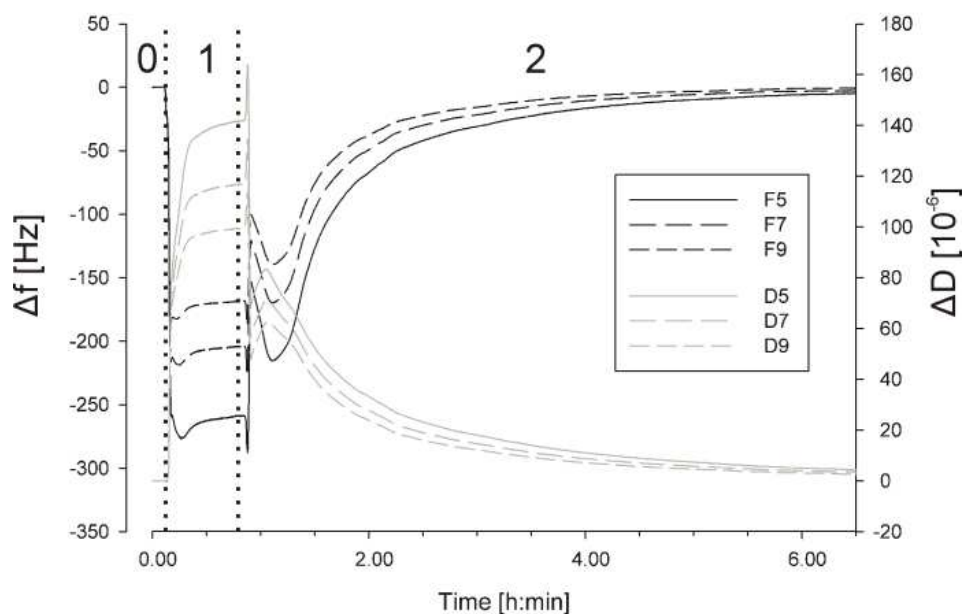
Figure 6.8: QCM-D signal obtained during rinsing a silica chip with sodium citrate, 6 M urea and Eumulgin ES at pH 3 at 35° C. The silica chip is rinsed with: 0: sodium citrate, 6 M urea, pH 3; 1: 10 % Eumulgin ES in sodium citrate, 6 M urea, pH 3; 2: sodium citrate, 6 M urea, pH 3. The obtained signals converge to zero - no surfactant is adsorbed permanently to the silica surface.

The average thickness of the surfactant layers on the silica surfaces were calculated according to Equations 6.1 and 6.2. The results are summarized in Table 6.1 and 6.2.

Table 6.1: Calculated thicknesses of the Eumulgin ES layers on silica chips for different buffer conditions at 20° C. Calculation was done by experimental QCM-D results and Equations 6.1 and 6.2.

Buffer pH / Salt	Thickness of adsorbed surfactant layer [nm]	Standard Deviation [nm]
pH 3	5.50	0.34
pH 3, 6 M Urea	0.23	0.02
pH 7	0.01	0.17

Table 6.2: Calculated thicknesses of the Eumulgin ES layers on silica chips for different buffer conditions at 30° C. Calculation was done by experimental QCM-D results and Equations 6.1 and 6.2.

Buffer pH / Salt	Thickness of adsorbed surfactant layer [nm]	Standard Deviation [nm]
pH 3	11.14	1.04
pH 3, 6 M Urea	0.95	0.04
pH 7	0.01	1.00

For 20° C the average thickness of the surfactant layer is 5.5 nm while at 30° C the thickness was calculated to 11.1 nm. The length of an Eumulgin ES molecule was estimated to 5.5 nm. Therefore, it can be concluded that the surfactant molecules do not adsorb in an outstretched horizontal fashion onto the silica surface but they are oriented vertically, with carbon chains extended towards the liquid and polar heads towards the SiO_2 surface. The addition of urea at pH 3 prevents the permanent surfactant binding completely. As discussed, at pH 7 the surfactants do not bind to the SiO_2 surface, neither at 20° C nor at 30° C.

6.4.4 Surfactant Binding on Particle Surfaces

MagPrep Silica particles were incubated with a buffered surfactant solution of pH 3 and pH 7 and washed with buffer of the respective pH for 12 wash cycles. The surfactant concentrations in the wash fractions were analyzed by TOC. Figure 6.9 shows the concentrations in the wash fractions for wash cycles 4 to 12 performed at 4° C and at 30° C.
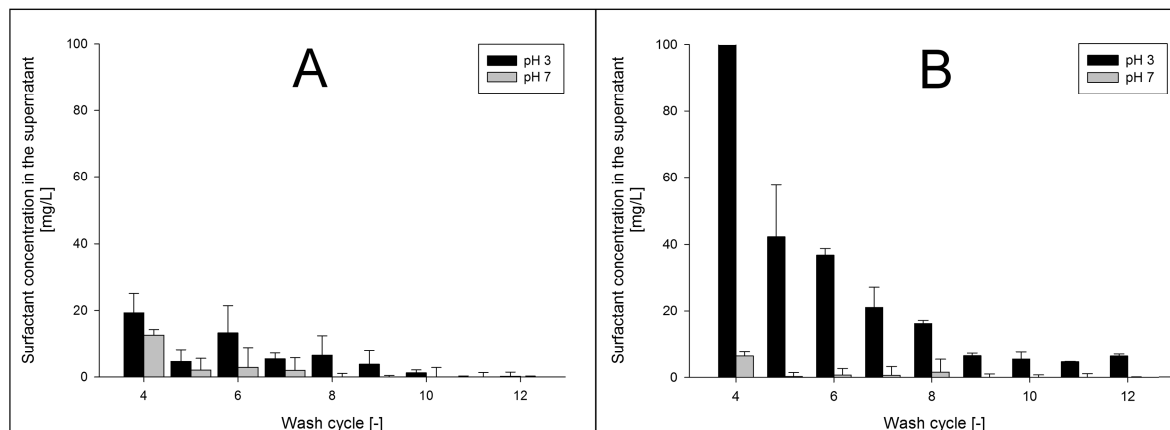
Figure 6.9 A: Eumulgin ES desorbed from MagPrep Silica particles in 12 wash cycles at 4° C. Desorption was performed at 4° C and at pH 3 or pH 7. Surfactant concentrations in the wash solutions are shown from cycle 4-12. At pH 3 the attraction of the surfactant to the SiO2 surface is stronger. B: Eumulgin ES desorbed from MagPrep Silica particles in 12 wash cycles at 30° C. Desorption was performed at 30° C and at pH 3 or pH 7. Surfactant concentrations in the wash solutions are shown from cycle 4-12. At pH 3 the attraction of the surfactant to the surface is much stronger. Eumulgin ES is eluted from the particles after 12 wash cycles, while at pH 7 the surfactant is completely removed from the particles after four wash cycles.

While at 4° C and pH 7 the surfactant is completely eluted from the MagPrepSilica particles after five cycles, at pH 3 the attraction of the silica surface to the surfactant is stronger and up to nine wash cycles are required. This effect is even more prominent when the particles are incubated with surfactant at 30° C as shown in Figure 6.9 B.

At 30° C and pH 7 the surfactant is removed completely after five wash cycles, at pH 3 the Eumulgin ES desorption from the particles is not completed after 12 wash cycles. In summary, at pH 3 the attraction of the non-ionic surfactant to the SiO_2 coated particles is stronger at pH 3 compared to pH 7. These findings are in accordance with the results obtained from the QCM-D experiments and the reference surfaces.

6.4.5 ATR-FTIR Spectroscopy

The sorption of the Eumulgin ES onto MagPrepSilica particles at pH 3 and pH 7 was compared by ATR-FTIR. The particles were first incubated at AMTPS conditions; afterwards particles were washed five times in the same buffer. ATR-FTIR spectra were taken from the plain particles, particles incubated with AMTPS and particles that were washed five times with pure buffer after incubation. The spectra of the plain particles

were subtracted from the spectra of the incubated and rinsed particles and the results are depicted in Figures 6.10 and 6.11.
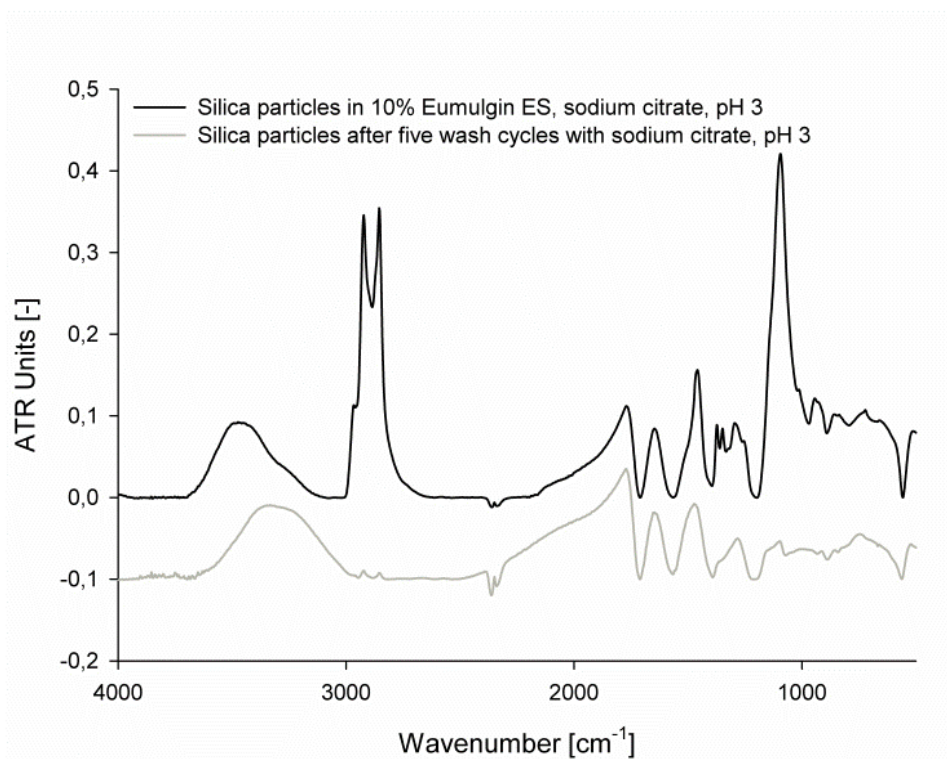
Figure 6.10: ATR-FTIR spectra of MagPrepSilica particles incubated with Eumulgin ES at pH 3. The peaks at 2800-2950 cm^{-1} are generated from CH$_2$ and CH$_3$ stretching caused by surfactants hydrocarbon chain at the particle surface. Peaks can still be observed on the particle surface after five wash cycles at pH 3.
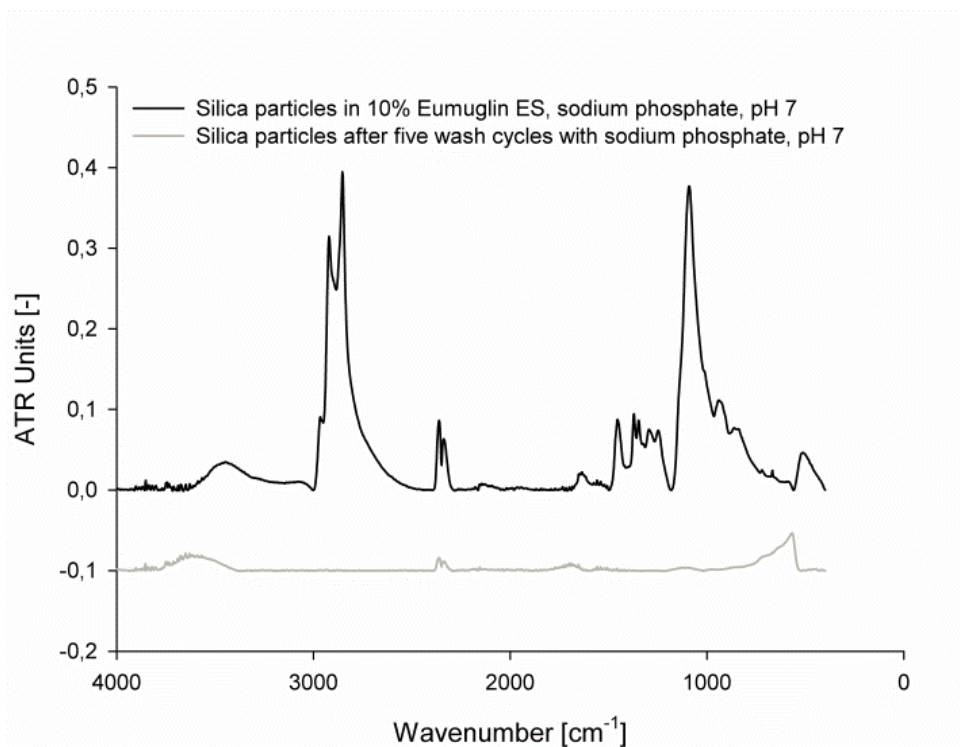
Figure 6.11: ATR-FTIR spectra of MagPrepSilica particles incubated with Eumulgin ES at pH 7. The peaks at 2800-2950 cm^{-1} are generated from CH$_2$ and CH$_3$ stretching caused by surfactants hydrocarbon chain at the particle surface. These peaks cannot be observed on the particle surface anymore after five wash cycles at pH 7.

When the particles are incubated with AMTPS, the surfactants are attached to their surface; this can be observed by the peaks at wavenumber 2800 cm^{-1}, which are caused by stretching vibrations of their CH$_2$ and CH$_3$ groups. Yet, when washed with at neutral pH 7, the surfactants are removed completely, as no peak can be seen in Figure 6.11. At pH 3 however, after five wash cycles, the peaks at 2800cm^{-1} can still be detected. The ATR-FTIR experiments confirm the findings from the QCM-D and direct surfactant elution experiments. The surfactant is completely removed from the SiO$_2$ at pH 7, as the surfactants are not strongly adsorbed to the surface.

6.5 Conclusions

The correlations of pH level, surfactant adsorption and the partitioning of silica coated particles in an AMTPS have been examined.

We have shown that at a low pH, the surfactants physically adsorb to the SiO$_2$ layer of both, particle and reference surface. As the surfactant is of non-ionic nature, these

interactions seem to be hydrogen-bonds formed between SiO_2 and the polar head of the surfactant. The sorption of the surfactant has been investigated using three independent methods: QCM-D, based on a reference silica chip, direct determination of surfactant concentration in solution and ATR-FTIR on the particle surface. QCM-D results suggest, that the non-ionic surfactant adsorbs to the silica surface with its polar head towards the SiO_2 layer. When the temperature is increased, a stable double layer is formed on the silica surface. At the same conditions when the surfactants adsorb onto the silica surface, the particles partition to the micelle rich phase of the system. On the contrary, at conditions when the surfactants only attach loosely to the surface, the particles partition to the micelle poor phase of the micellar two-phase system. We therefore propose that the partitioning of particles in micellar two-phase systems is driven by the adsorption of the phase forming surfactant to the component to be partitioned. Figure 6.12 illustrates the proposed mechanism of the partitioning behavior of particulates in an AMTPS.
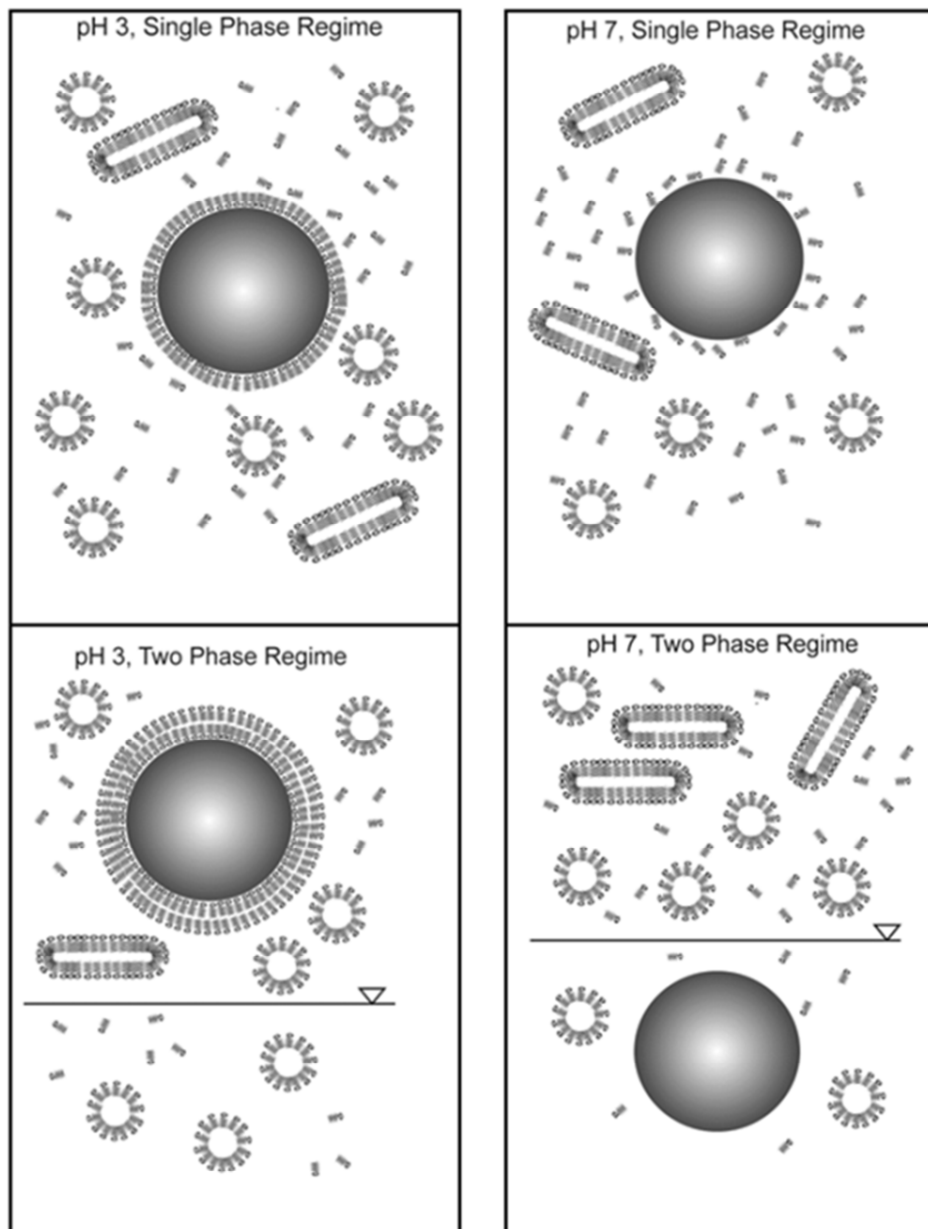
Figure 6.12: Mechanism of the partitioning of an insoluble particle in AMTPS. If the phase forming surfactant adsorbs to the particle, it is drawn to the micelle rich phase. If the surfactant does not adsorb to the particle surface, the particle is expelled from the micelle rich phase.

Whenever the phase forming surfactant covers the particle surface, these particles enter the micelle rich phase; if the surfactant is not adsorbed to the particle surface, the particle is excluded from the micelle rich phase. Similar results have also been discovered for proteinaceous solutions [30]. The authors used negatively charged mixed micelles to increase the partitioning coefficient of positive charged proteins to the micelle rich phase.

Our experimental results suggest that the partitioning of soluble and insoluble nanosized particles are based on the very same principles; hydrogen bonds formed between the phase forming component and the component to be partitioned seem to dominate the partitioning behavior of the component in an aqueous micellar-two phase system.

6.6 References

[1] P.A. Albertsson, Partition of Cell Particles and Macromolecules, John Wiley and Sons, New York, 1986.

[2] Y.J. Nikas, C.L. Liu, T. Srivastava, N.L. Abbott, D. Blankschtein, Protein Partitioning in 2-Phase Aqueous Nonionic Micellar Solutions, Macromolecules, 25 (1992) 4797-4806.

[3] M.R. Helfrich, M. El-Kouedi, M.R. Etherton, C.D. Keating, Partitioning and assembly of metal particles and their bioconjugates in aqueous two-phase systems, Langmuir, 21 (2005) 8478-8486.

[4] S.M. Baxter, P.R. Sperry, Z.W. Fu, Partitioning of Polymer and Inorganic Colloids in Two-Phase Aqueous Polymer Systems, Langmuir, 13 (1997) 3948-3952.

[5] M. Olsson, F. Joabsson, L. Piculell, Particle-induced phase separation in mixed polymer solutions, Langmuir, 21 (2005) 1560-1567.

[6] M. Suzuki, M. Kamihira, T. Shiraishi, H. Takeuchi, T. Kobayashi, Affinity Partitioning of Protein-a Using a Magnetic Aqueous 2-Phase System, Journal of Fermentation and Bioengineering, 80 (1995) 78-84.

[7] P. Vazquez-Villegas, O. Aguilar, M. Rito-Palomares, Study of biomolecules partition coefficients on a novel continuous separator using polymer-salt aqueous two-phase systems, Separation and Purification Technology, 78 (2011) 69-75.

[8] J.S. Becker, O.R.T. Thomas, M. Franzreb, Protein separation with magnetic adsorbents in micellar aqueous two-phase systems, Separation and Purification Technology, 65 (2009) 46-53.

[9] I. Fischer, M. Franzreb, Nanoparticle Mediated Protein Separation in Aqueous Micellar Two-Phase Systems, Solvent Extraction and Ion Exchange, 30 (2012) 1-16.

[10] J.F. Liu, R. Liu, Y.G. Yin, G.B. Jiang, Triton X-114 based cloud point extraction: a thermoreversible approach for separation/concentration and dispersion of nanomaterials in the aqueous phase, Chemical Communications, (2009) 1514-1516.

[11] J.F. Liu, J.B. Chao, R. Liu, Z.Q. Tan, Y.G. Yin, Y. Wu, G.B. Jiang, Cloud Point Extraction as an Advantageous Preconcentration Approach for Analysis of Trace Silver Nanoparticles in Environmental Waters, Analytical Chemistry, 81 (2009) 6496-6502.

[12] M.F. Nazar, S.S. Shah, J. Eastoe, A.M. Khan, A. Shah, Separation and recycling of nanoparticles using cloud point extraction with non-ionic surfactant mixtures, Journal of Colloid and Interface Science, 363 (2011) 490-496.

[13] E. Krieger, G. Koraimann, G. Vriend, Increasing the Precision of Comparative Models with YASARA NOVA - a Self-Parameterizing Force Field, Proteins-Structure Function and Genetics, 47 (2002) 393-402.

[14] I. Fischer, M. Franzreb, Direct determination of the composition of aqueous micellar two-phase systems (AMTPS) using potentiometric titration-A rapid tool for detergent-based

bioseparation, Colloids and Surfaces a-Physicochemical and Engineering Aspects, 377 (2011) 97-102.

[15] G. Sauerbrey, Verwendung Von Schwingquarzen Zur Wagung Dunner Schichten Und Zur Mikrowagung, Zeitschrift Fur Physik, 155 (1959) 206-222.

[16] D. Blankschtein, G.M. Thurston, G.B. Benedek, Theory of Phase-Separation in Micellar Solutions, Physical Review Letters, 54 (1985) 955-958.

[17] D. Blankschtein, G.M. Thurston, G.B. Benedek, Phenomenological Theory of Equilibrium Thermodynamic Properties and Phase-Separation of Micellar Solutions, Journal of Chemical Physics, 85 (1986) 7268-7288.

[18] G. Briganti, S. Puvvada, D. Blankschtein, Effect of Urea on Micellar Properties of Aqueous-Solutions of Nonionic Surfactants, Journal of Physical Chemistry, 95 (1991) 8989-8995.

[19] S. Keith, C.H. Rochester, Infrared Study of the Adsorption of C12e5 on Silica Immersed in Carbon-Tetrachloride, Journal of the Chemical Society-Faraday Transactions I, 84 (1988) 3641-3647.

[20] F. Tiberg, B. Lindman, M. Landgren, Interfacial Behavior of Nonionic Surfactants at the Silica Water Interface Revealed by Ellipsometry, Thin Solid Films, 234 (1993) 478-481.

[21] D.M. Nevskaia, M.L.R. Cervantes, A.G. Ruiz, J.D.L. Gonzalez, Interaction of Triton X-100 on Silica - a Relationship between Surface Characteristics and Adsorption-Isotherms, Journal of Chemical Technology and Biotechnology, 63 (1995) 249-256.

[22] G. Despert, J. Oberdisse, Formation of micelle-decorated colloidal silica by adsorption of nonionic surfactant, Langmuir, 19 (2003) 7604-7610.

[23] N.N. Li, R.K. Thomas, A.R. Rennie, Adsorption of non-ionic surfactants to the sapphire/solution interface - Effects of temperature and pH, Journal of Colloid and Interface Science, 369 (2012) 287-293.

[24] J. Drzymala, E. Mielczarski, J.A. Mielczarski, Adsorption and flotation of hydrophilic and hydrophobic materials in the presence of hydrocarbon polyethylene glycol ethers, Colloids and Surfaces a-Physicochemical and Engineering Aspects, 308 (2007) 111-117.

[25] M.J. Schick, Effect of Electrolyte + Urea on Micelle Formation, Journal of Physical Chemistry, 68 (1964) 3585-&.

[26] S.K. Han, S.M. Lee, M. Kim, H. Schott, Effect of Protein Denaturants on Cloud Point and Krafft Point of Nonionic Surfactants, Journal of Colloid and Interface Science, 132 (1989) 444-450.

[27] L.B. Sagle, Y.J. Zhang, V.A. Litosh, X. Chen, Y. Cho, P.S. Cremer, Investigating the Hydrogen-Bonding Model of Urea Denaturation, Journal of the American Chemical Society, 131 (2009) 9304-9310.

[28] W.F. Li, R.H. Zhou, Y.G. Mu, Salting Effects on Protein Components in Aqueous NaCl and Urea Solutions: Toward Understanding of Urea-Induced Protein Denaturation, Journal of Physical Chemistry B, 116 (2012) 1446-1451.

[29] G. Kopperschlager, G. Birkenmeier, Affinity partitioning and extraction of proteins, Bioseparation, 1 (1990) 235-254.

[30] D.T. Kamei, D.I.C. Wang, D. Blankschtein, Fundamental investigation of protein partitioning in two-phase aqueous mixed (nonionic/ionic) micellar systems, Langmuir, 18 (2002) 3047-3057.

7 Continuous Protein Purification by Combination of Functional Magnetic Nanoparticles and Aqueous Micellar Two-phase Systems

Ingo Fischer[a], Markus Gärtner[a], Chia-Chang Hsu[b], Christine Müller[b], Timothy W. Overton[b], Owen R.T. Thomas[b], Matthias Franzreb[a],*

[a]: Institute of Functional Interfaces, Karlsruhe Institute of Technology, Hermann-von-Helmholtz-Platz 1, 76344 Eggenstein-Leopoldshafen, Germany

[b]: School of Chemical Engineering, College of Engineering and Physical Sciences, University of Birmingham, Edgbaston, Birmingham B15 2TT, England, UK

*: Corresponding author. E-mail address: matthias.franzreb@kit.edu

7.1 Abstract

A novel technique for technical-scale continuous purification of proteins is presented. It is based on the combination of functional magnetic nanoparticles and an Aqueous Micellar Two-Phase System (AMTPS). In the first step, the particles bind the protein of interest. In the next step, the particles are enriched in the micelle-rich phase of the AMTPS. The particle and micelle-rich phases are then continuously separated from the micelle-poor phase in a flowthrough magnetic extractor based on permanent magnets. It is shown that the magnetic extractor can be used to continuously separate magnetic nanoparticles sized 25 nm to 2000 nm with separation efficiencies of up to 99.9 % and surfactant separation rates of up to 98 %. The magnetic extractor is applied in combination with 100 nm sized magnetic cation exchange particles to purify the antibody fragment Fab α33 from a clarified *E. coli* supernatant in a 15 liter scale. Within this process, a yield of 67 %, purity of >98 %, and purification factor of 6.3 were obtained, while the total particle loss summed up to only 1 %.

7.2 Introduction

In times of growing product titers, downstream processing is the bottleneck in biopharmaceutical production processes [1]. The amendment or replacement of traditional downstream operations e.g., column chromatography by integrated and/or continuous separation processes, is certainly a necessity to solve. Aqueous two-phase systems or Aqueous Micellar Two-Phase Systems (AMTPS) have been regarded as such a possible alternative ever since the selective partitioning of (bio)molecules between the two emerging phases of a mixture of polymers and/or salts has been described by Albertsson [2]. In contrast to classical ATPS, AMTPS, introduced by Bordier [3], consist of non-ionic surfactants. These systems undergo temperature-induced phase separation resulting in a micelle-rich (or coacervate phase) and a micelle-depleted phase [4]. Numerous applications and combinations of phase-forming polymers have been proposed since then for the selective enrichment of a protein in one of the aqueous phases (also described as aqueous two-phase extraction ATPE or cloud point extraction CPE) [4, 5]. A striking advantage of ATPE is its easy scalability. Several process schemes have been published recently, which demonstrate the feasibility of continuous bioprocessing in terms of both ATPS [6-8] and AMTPS [9, 10]. Despite these advantages, the cost and loss of phase-forming components in the target protein-depleted phase is still an economic hurdle. The major drawback, however, considering ATPE as an alternative in biotechnological downstream processing, is that the underlying physical principles of the partitioning behavior of a target protein between the phases are still unclear and much experimental effort is required to identify an economic system [11]. In order to circumvent these issues, affinity-enhanced ATPS has been introduced [12]. Here, either the phase-forming polymer is chemically modified or ligands are added to the two-phase system to enhance the partitioning of the molecule of interest into a certain phase of the ATPS [13]. Among these ligands, functionalized magnetic particles constitute a particular class [14-16]. The combination of ATPS and magnetic particles is advantageous, cf. traditional affinity ATPS, as the phase separation rate can be increased drastically by application of an external magnetic field, if these particles partition completely to the dispersed phase of the system [17-19].

Recently, the successful combination of AMTPS and magnetic microsorbents has been described using the well-known non-ionic surfactant Triton X-114 [20]. Here, the sorption of the target molecule was performed in the single-phase regime. The temperature was subsequently increased to induce phase separation. The protein-loaded particles were accumulated in the micelle-rich phase of the resulting AMTPS and the micelle-poor phase was removed. In the following step, an AMTPS was set up with elution buffer and the former micelle-rich phase of the sorption step. The proteins were consequently eluted from the particles and while the magnetic sorbents partitioned completely to the micelle-rich phase, the target protein partitioned in the AMTPS based on its partitioning coefficient K.

This concept – termed Magnetic Extraction Phases (MEP) - was extended to magnetic nano-scaled sorbents and an AMTPS based on the nonionic surfactant Eumulgin ES [21]. The Eumuglin ES-based AMTPS exhibits fundamental improvements, cf. the Triton X-114 AMTPS, for instance extreme protein partitioning coefficients and low surfactant costs, while maintaining a moderate phase separation temperature. Due to the extreme K-value, the target protein was completely eluted to the micelle-poor phase, while the magnetic sorbents were completely accumulated in the micelle-rich phase. The MEP experiments, however, have only been conducted on a lab scale so far.

In this work, the transfer from lab-scale to technical-scale Continuous Magnetic Extraction (CME) is presented. It is based on a novel magnetic extractor set-up, whose principle is depicted in Figure 7.1. The AMTPS containing functional magnetic nanoparticles is injected into a temperature-regulated and magnetically enhanced settler. While passing the settler, the phases are separated. The magnetic field hereby not only speeds up the flotation velocity of the magnetic particle-doped disperse droplets but also increases their coalescence rate. We demonstrate that using this set-up allows the continuous separation of magnetic nanoparticles from the micelle-poor phase at flow rates of several liters per hour. The applied magnetic particles exhibit common surface functionalizations known from chromatographic media. Using cation exchange functionality, CME is applied for the continuous capture of an antibody fragment from a crude *E. coli* cell extract. Applying CME for binding, washing and elution, the final result is a particle-free eluate

phase containing the target antibody fragment, and a concentrated micellar-rich top phase which contains the particles and most of the phase- forming surfactants. As both, the surfactants and the functionalized particles, are concentrated in the top phase, it is possible to directly apply this process stream to a fresh feed.
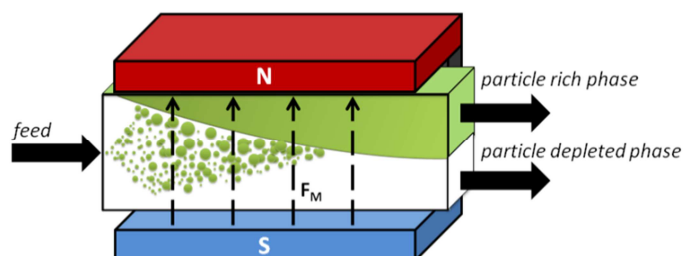
Figure 7.1: Principle of CME. The feed consists of magnetic particles and the AMTPS components. It is injected into a temperature-controlled settler. The settler is surrounded by a permanent magnet. The phases split and separate while passing the settler. The magnetic field increases the phase separation rate by increasing the flotation velocity of the disperse droplets and by enhancing coalescence effects. At the end of the separator, the particle and micelle-rich phases are discharged from the top outlet, while the particle-depleted bottom phases are withdrawn from the lower outlet.

7.3   Material and Methods

7.3.1   General Description of the CME Process

In Figure 2, the process scheme of a continuous magnetic extraction is depicted. The core of the magnetic extraction is the described temperature-controlled, magnetic field-enhanced mixer-settler. In the temperature-controlled mixer, the sorption of the target molecule to the magnetic sorbent occurs at a temperature T_S at which the fluid forms a single phase. In the next step, the AMTPS is heated up to a temperature T_T in which the fluid forms two phases. For phase separation, the fluid is pumped into a separation chamber surrounded by a specially designed permanent magnet which itself is located in the inside of a sealed polystyrene case that is supplemented with a temperature-controlled heater in order to maintain the temperature at T_T. While passing the reactor, micellar droplets doped with magnetic nano- or microparticles form. The external magnetic field of the permanent magnet enhances the migration velocity of these micellar droplets and additionally increases the initial droplet coalescence as well as the coalescence at the interphase of the two- phase system. Finally, a particle-clarified, micelle-depleted bottom phase is discharged from the lower effluent of the separation

chamber, while a micelle and particle-enriched phase is withdrawn from the upper effluent. The single components of the system are shortly explained hereafter.
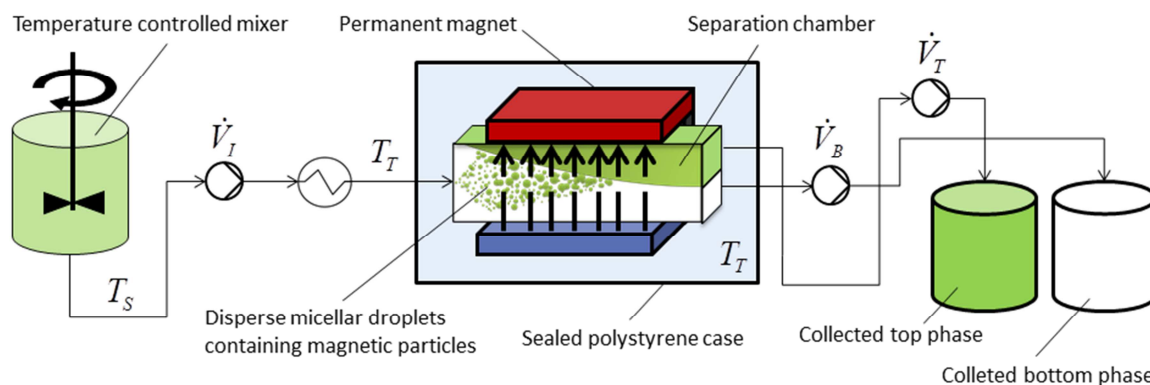
Figure 7.2: Scheme of the magnetic extraction process. AMTPS and magnetic sorbents are mixed in a temperature- controlled mixer at a temperature T_S in the single-phase regime. The solution is pumped through a heat exchanger and enters the magnetic extractor preheated to the two-phase temperature T_T. The extractor consists of a sealed polystyrene case keeping the temperature constant, a permanent magnet, and the separation chamber. Within the extractor, the streams are separated. A micelle-rich phase containing the magnetic particles is discharged from the top phase, while a micelle-poor and particle-depleted phase is removed from the lower effluent of the separator.

7.3.1.1 Separation Chamber

The scheme of the separation chamber is depicted in Figure 7.3. The core of the separation chamber is fabricated in the form of a glass box (10 mm wall thickness) with open front and back. The inner dimensions (length x width x height) of the glass box are: 500 x 120 x 50 mm³. The inlets, outlets and the weir are made from polyvinylchloride and are glued to the open ends of the glass box. The height of the weir was 38 mm, resulting in a liquid volume in the separator chamber of 500 x 120 x 38 mm = 2.28 liters.
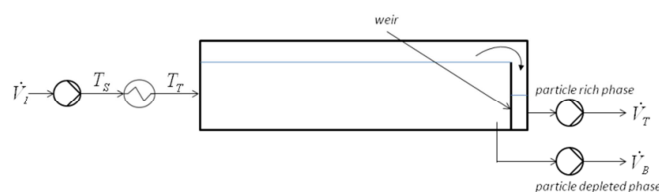
Figure 7.3: Scheme of the separation chamber of the magnetic extractor. After leaving the heat exchanger, the fluid is pumped into the separation chamber, where the phases begin to separate. The particle and surfactant-rich top phase is discharged by a weir in the top phase, while the particle-depleted bottom phase is withdrawn from the lower effluent.

7.3.1.2 Permanent Magnet

A ferrite permanent magnet surrounding the separation chamber was fabricated by Steinert Elektromagnetbau GmbH (Cologne, Germany). The overall size of the magnet is 627x235x306mm. The magnet consists of the magnetic ferrite material (block M in Figure 4) and a surrounding pole shoe. A magnetic field simulation was performed using the FEM software Quickfield 5.7 (Tera Analysis, Svendborg, Denmark). The magnetic characteristics of the ferrite material were supplied by the magnets manufacturer. As can be seen from Figure 4, the pole shoe design results in a vertical magnetic field component which steadily increases towards the upper side of the separator chamber.
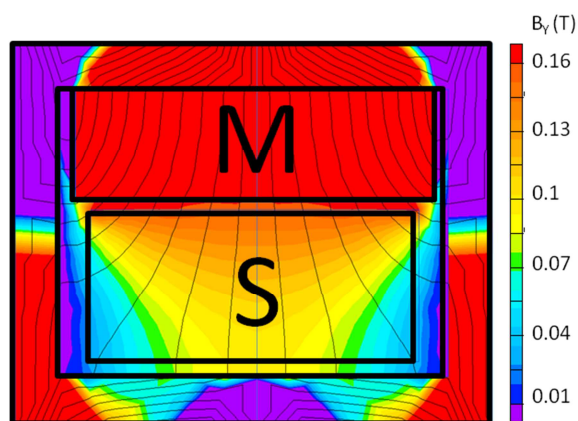
Figure 7.4: FEM simulation of the magnet field generated by the permanent magnet (M). A settler can be installed in the space (S) as in this space, the vertical flux density $B_Y(T)$ is steadily increasing towards the upper side. This results in a lifting force onto magnetic particles in all locations within S.

7.3.1.3 Temperature-regulated Polystyrene Case

As maintenance of a constant temperature during the separation operation is crucial, the magnet and the separation chamber are positioned in a polystyrene case. A radiator (Cirrus 80, DBK, Germany) is installed within the case and connected to a thermostat (LR316, Jumo, Germany). In all experiments, the temperature in the polystyrene case was adjusted to a temperature within the two- phase region of the AMTPS. The sealed polystyrene case containing the permanent magnet and the separation chamber was preheated for at least 2 hours in order to establish a constant temperature.

7.3.1.4 Equations Describing CME Performance

The phase separation curve of the used AMTPS results from plotting the temperature against the corresponding Eumulgin ES concentrations in the phases after complete phase separation.

From the surfactant concentrations, the volume fractions of the surfactant-rich and poor phases can be calculated according to the lever rule [22, 23]:

$$\frac{V_T}{V_B} = \frac{w_{S,0} - w_{S,B}}{w_{S,T} - w_{S,0}} = R$$

[Eq. 7.1]

Here, $w_{S,0}$, $w_{S,B}$ and $w_{S,T}$ are the surfactants´ mass fractions of the phases before and after phase separation and R is denoted as phase-volume ratio. During continuous operation of the magnetic extractor, the phase-volume ratio between the withdrawn top and bottom phase can be expressed as pump ratio P, according to Equation 7.2:

$$P = \frac{\dot{V}_T}{\dot{V}_B}$$

[Eq. 7.2]

As can be seen from Figure 7.3, P is controlled by the feeding rate $\dot{V}_I$ and the discharge rate of the bottom phase $\dot{V}_B$. The amount of liquid removed by the top effluent results from the flow rate difference between the inlet and the bottom effluent. The ratio of the flow rate leaving the top effluent and the inlet flow rate therefore is defined as coacervate ratio C_R:

$$C_R = \frac{\dot{V}_T}{\dot{V}_I} = \frac{\dot{V}_I - \dot{V}_B}{\dot{V}_I} = \frac{P}{P+1}$$

[Eq. 7.3]

with $\dot{V}_T$ being the flow rate of the top phase discharge.

In theory, the ideal operation point of a magnetic extractor would be that the pump ratio P exactly matches the volume ratio R between the surfactant-rich and poor phases determined in batch equilibrium experiments. However, in order to prevent the loss of target component, particles, and surfactant, the CME was operated in a way that

emphasizes the complete removal of the top phase rather than the prevention of contaminating the top phase with traces of bottom phase. In order to achieve the complete removal of the top phase during the CME operation, the theoretical minimal C_R necessary can be calculated from R:

$$C_{R,min} \geq \frac{R}{R + 1}$$

[Eq. 7.4]

The used C_R was derived from this value applying a safety factor of 5 - 10%.

The rate of removal of magnetic particles and surfactant from the initial feed using CME is defined as separation efficiency according to Equation 7.5 for particles and Equation 7.6 for the phase-forming surfactant.

$$S_P = (1 - \frac{\dot{V}_B \cdot c_{P,B}}{\dot{V}_I \cdot c_{P,I}}) \cdot 100$$

[Eq.7.5]

$$S_S = (1 - \frac{\dot{V}_B \cdot c_{S,I}}{\dot{V}_I \cdot c_{S,I}}) \cdot 100$$

[Eq.7.6]

where $c_{P,B}$, $c_{P,I}$ respectively $c_{S,I}$ and $c_{S,B}$ are the concentrations of particles and surfactant in the initial streams and in the discharged bottom phases.

7.3.2 Chemicals

The water used was deionized and purified by a Millipore Milli-Q Ultrapure system. Disodium-hydrogen phosphate and sodium-chloride were supplied by Carl Roth (Karlsruhe, Germany). Citric acid monohydrate and Polyvinyl-alcohol (average MW 60.000), borate and Comassie Brilliant Blue R250 were purchased from Merck Millipore (Darmstadt, Germany). Sodium tetraphenylborate and barium chloride were purchased from Sigma-Aldrich (St.-Louis, US-MO). The chemicals were of buffer or p. A. grade. The nonionic surfactant Eumulgin ES (PPG-5-Laureth-5, CAS-No.: 68439-51-0) was purchased

from Cognis (Düsseldorf, Germany). Precast 15% mini-PROTEAN® TGX™ gels and Precision Plus Protein All Blue Standards were supplied by Bio-Rad (Hercules, USA-CA).

7.3.3 Particles

"Poly-(NIPA-AAc)" particles were provided from the group of Dr. Rodica Turcu from the National Institute for Research and Development of Isotopic and Molecular Technologies (NIIMT). These magnetic particles consist of a magnetite core which is embedded in a poly(N-isopropylacrylamide)-acrylic acid copolymer. The mean diameter of the particles was determined to 200nm by Dynamic Light Scattering (DLS).

"MagPrep Silica 25" and "MagPrep SO_3 100" particles were kindly donated by Merck Millipore (Darmstadt, Germany). The particles consist of magnetite (Fe_3O_4) crystals with a thin silica coating. In the case of the SO_3 particles, the silica coating is further functionalized with sulfonate groups as used in cation exchange chromatography. Scanning Electron Microscope (SEM) pictures revealed a mean diameter of single particles of 25nm for the silica particles and 100nm for the SO_3 particles with a narrow size distribution.

Chemagen DEAP particles were provided from Chemagen (PerkinElmer chemagen Technologie GmbH, Baesweiler, Germany). These magnetic particles with a mean size of approx. 2 μm consist of polyvinylacohol (PVA) with statistically embedded magnetite nanoparticles. PVA is further functionalized with diethylamniopropyl (DEAP) groups which are typically used in anion exchange chromatography.

7.3.4 Determination of the AMTPS Phase Diagrams

The location of the curves separating the two-phase regime and the single-phase regime within a T,x diagram (x being the mass fraction of the surfactant in the mixture) were determined as follows: Different fractions of surfactant and the corresponding buffers were weighed into 15 ml centrifuge tubes. The centrifuge tubes were tempered using a temperature-controlled water bath (RC 20 S, Lauda). The centrifuge tubes were incubated in the water bath until phase separation was completed but for at least 12 hours. Subsequently, top and bottom phase of the resulting two-phase system were quickly

removed and the surfactant concentrations of both phases were measured according to the procedure described in the 'Analytics' section.

7.3.5 Phase Separation Experiments

The phase separation velocity in the magnetic extractor was determined for an operation with and without magnetic particles. An AMTPS was set up which consisted of 10 % wt Eumulgin ES and 90 %wt 50 mM sodium citrate at pH 3. Poly-(NIPA-AAc) particles were chosen for the separation experiments at a temperature of T_S equal to 30°C. The coacervate ratio C_R was kept constant at 0.2, while $\dot{V}_I$ was varied from 0.5 liter per hour to 25 liters per hour. The system was run at the corresponding flow rate until the volume in the separation chamber was exchanged at least twice. Samples were taken from the top and bottom outlet of the magnetic separator and analyzed for their Eumulgin ES concentrations. All experiments were carried out in the absence of the magnetic particles first and afterwards, the same set-up was used with a magnetic particle concentration of 2 g/L.

Long-term continuous operation of the magnetic extractor was investigated by an operation in "loop mode". In loop mode, the leaving top and bottom phases were reinjected into the tempered stirred tank. This set-up allowed the continuous operation of the magnetic extractor for several hours without the exhaustive use of material. The initial particle concentration in the stirred tank was 2 g/L in a total volume of a 9 liter sodium citrate/10% Eumulgin ES AMTPS. The flow rate was set to 9 liters per hour, T_S was set to 30°C and C_R to 0.33. Samples were taken from the initial feed, the top phase and the bottom phase during operation. The samples were analyzed for their magnetic particle and surfactant concentrations.

7.3.6 Purification of Fab α33 by means of CME

For conducting the proof of concept, the CME equipment was shipped to the group of Professor O.R.T. Thomas at the University of Birmingham and applied to capture the antibody fragment Fab α33. For the production of Fab α33, the *E. coli* strain W3110 was used with the α33 Fab' plasmid supplied by UCB Celltech (Slough, UK.) The supernatant was produced by heating the harvested cells to 60° C in 100 mM Tris-HCl, 10 mM EDTA at

pH 7.4. The supernatant was clarified from the cells afterwards and the solution was diluted 10-fold with 20 mM sodium phosphate buffer at pH 5.6. In order to gather the necessary T_S, T_T and C_R, the phase diagram of an AMTPS consisting of Eumulgin ES and the heat shock supernatant was created.

For binding of the Fab α33 protein within the CME process, Merck MagPrep-SO$_3$ particles were applied. An AMTPS was set up, which consisted of the diluted heat shock solution and 10% Eumulgin ES. The total volume of this AMTPS was 14.7 liters. The particle concentration in the binding step was set to 1.4 g/L. The protein binding was performed in a double-jacketed reactor at T_S= 15°C under constant stirring at 140 rpm. T_T was set to 30° C. C_R was set to 0.2 and the flow rate $\dot{V}_I$ was set to 5 liters per hour. The solution was then separated by magnetic extraction and the leaving streams were collected separately. For the washing step, the collected top phase from the experiment was transferred back into the stirred tank. Wash buffer (20 mM sodium phosphate at pH 5.6) was added in a volume ratio of 2:1 and the solution was cooled to T_S. Afterwards, the broth was processed through the magnetic extractor and the leaving streams were collected separately. Finally, the elution step was started by transferring back the collected top phase from the washing step into the stirred tank. Afterwards, elution buffer (750 mM sodium chloride, 20 mM sodium phosphate at pH 5.6) was added in a volume ratio of 2:1. This resulted in a final sodium chloride concentration of 500 mM. The broth was processed through the magnetic extractor and the top and bottom phases were collected separately.

During and after each process step, samples were taken from the top and bottom phases and were analyzed for their particle, surfactant, DNA, total protein, and FAB α33 contents. At the end of each separation, when the top phase withdrawal ran dry, the bottom phase was removed until a turbid solution was noticed. At this time, the bottom valve was closed and the remaining broth was added to the top phase collection tank. Before the next step of the CME was performed, the separation chamber was flushed with buffer, to flush out remaining particles from the separation chamber into the stirred reactor.

7.3.7 Analytics

The concentration of the surfactant Eumulgin ES was determined by potentiometric titration using the NIO surfactant electrode (Metrohm, Birkenfeld, Germany) as described elsewhere [24]. In short, a sample was weighed into a glass beaker and 10 mL of barium chloride solution and 60 mL of MilliQ water were added subsequently. This solution was then titrated with a sodium-tetraphenylborate solution using the Metrohm NIO electrode. As a result, the end-point volume was recorded. The surfactant mass fraction was then obtained by comparing the end point volume with the end point volumes of known surfactant mass fractions using linear regression.

The concentration of the magnetic particles was determined gravimetrically as follows: An adequate volume of particle-containing sample was taken. Particles were separated from the solution by centrifugation for 20 minutes or by using a hand magnet. The supernatant was removed and the particles were washed once with 15ml of methanol and twice with 15ml of MilliQ water. Particles were resuspended in 1ml MilliQ water in HPLC glass vials and dried in an oven at 60°C for at least 16 hours or until all liquid was evaporated. The particle concentration was then determined by the weight of the dry particles and the initial volume of the sample.

The total protein concentration was determined using a micro bichoninic acid (BCA) assay kit (Pierce, Rockford, US-IL). Reagents were prepared according to the manufacturer's instructions. Samples were analyzed using the Cobas Mira (ROCHE) automatic robotic station. In order to eliminate the influence of surfactant on the BCA assay and to concentrate the proteins, a trichloroacetic acid (TCA) precipitation step was performed as follows: 100% TCA was added to the sample to generate a final TCA concentration of 15%. Samples were incubated on ice for 30 minutes. The protein pellet was then separated from the supernatant by centrifugation and decantation. The protein pellet was washed twice with ice-cold acetone and dried afterwards by vacuum centrifugation (Vacufuge, Eppendorf, Hamburg, Germany). The pellet was resuspended in 1% SDS, 0.1M Tris-HCl, pH 8. Protein standards used in the BCA assay were precipitated in the same way as the unknown samples to minimize the influence of protein loss during precipitation to the analytics.

The Fab α33 concentration was determined by densitometric analysis following SDS PAGE. The protein-loaded SDS gels were Coomassie Blue-stained and scanned as TIFF image files. The images were afterwards analyzed using the software ImageJ® [25]. In order to quantify the Fab α33 concentration, standards with known concentrations were applied on the same gel. A linear correlation between the Fab α33 amount on the gel and the protein band intensity was found in a range from 0.1 to 1 μg of Fab α33. Hence, the total volume of the unknown samples applied on the gel was adjusted to match this range.

The DNA concentration was determined using Quant-iT™ PicoGreen® dsDNA kit according to the manufacturer's specifications. The samples were measured in 96-well plates and analyzed by an Ascent Fluoroskan Fluorometer (Thermo Labsystems; Waltham, MA) with excitation at 480nm and emission at 535 nm.

7.4   Results

7.4.1 Part I: Physico-chemical and Hydrodynamic Characterization

The phase diagram of an Eumulgin ES-based AMTPS in sodium citrate, pH 3 buffer can be found in [26]. In comparison with a phase diagram of an Eumulgin ES-based AMTPS in water and sodium phosphate at pH 7, which has already been described in [24], the phase diagram is practically similar. Therefore, it can be concluded that in the observed range, the influence of pH and buffer composition onto the phase separation temperature in Eumulgin ES-based AMTPS is negligible. From the phase diagram in [26], the process parameters R and $C_{R,min}$ were deduced.

Table 7.1: Volume ratio R and minimal coacervate ratio $C_{R,min}$ calculated from Equations 7.1 and 7.4.

T [°C]	R [-]	$C_{R,min}*100$ [%]
29	0.27	22
30	0.23	19
35	0.16	14
40	0.14	12

Table 7.1 shows the calculated values for R and $C_{R,min}$ in an AMTPS consisting of 10% Eumulgin ES. As can be seen from Table 7.1, a minimum C_R of 0.19 has to be adjusted in order to achieve complete phase removal for an Eumulgin ES-based AMTPS at 30°C. The phase separation efficiency of the Eumulgin ES-based AMTPS was monitored during the CME operation by analyzing the concentrations in the top and bottom-phase effluents for different feed flow rates. The Eumulgin ES concentration of the feed was 9.6% wt, the phase separation temperature was set to 30°C, and C_R was set to 0.2. Figure 7.5 depicts the Eumulgin ES concentration profiles of the top and bottom phases. When operating the CME with flow rates of > 15 L/h, no phase separation can be observed. Both streams leave the separator at the same concentrations as those they had when injected. When the flow rate is decreased below 15 L/h, the phases start to separate and reach a plateau at approximately 2 L/h. In steady state, this mode of operation accomplishes a surfactant concentration of 32% in the top phase. Further decrease in the flow rate does not increase the surfactant concentration in top phase.
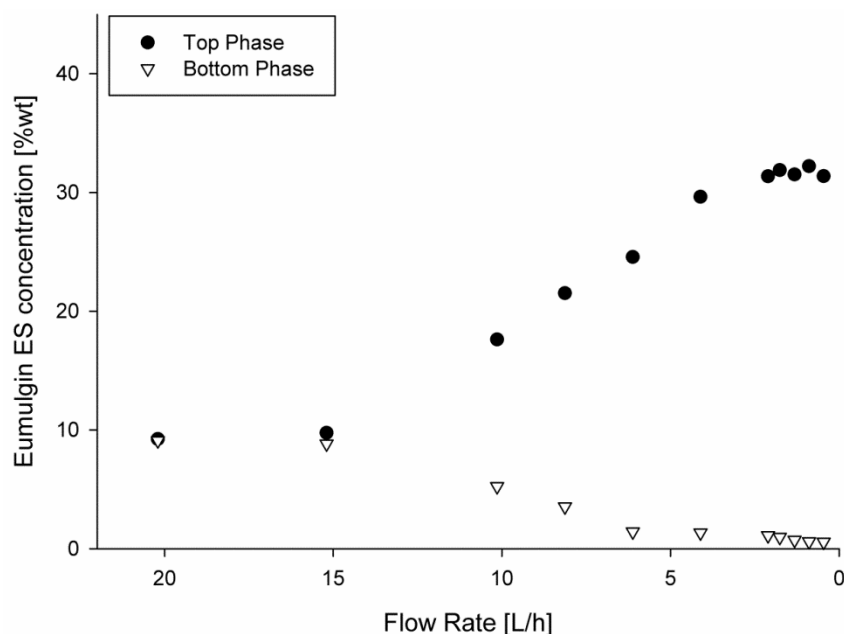
Figure 7.5: Eumulgin ES phase separation achieved in the magnetic extractor during continuous operation at different flow rates. A plateau of 32% wt Eumulgin ES in the micelle-rich top phase and 0.7% in the clarified bottom phase is reached below 2 liters per hour.

When magnetic particles are added to the extractor, the phase separation rate is drastically improved, as can be observed from Figure 7.6.
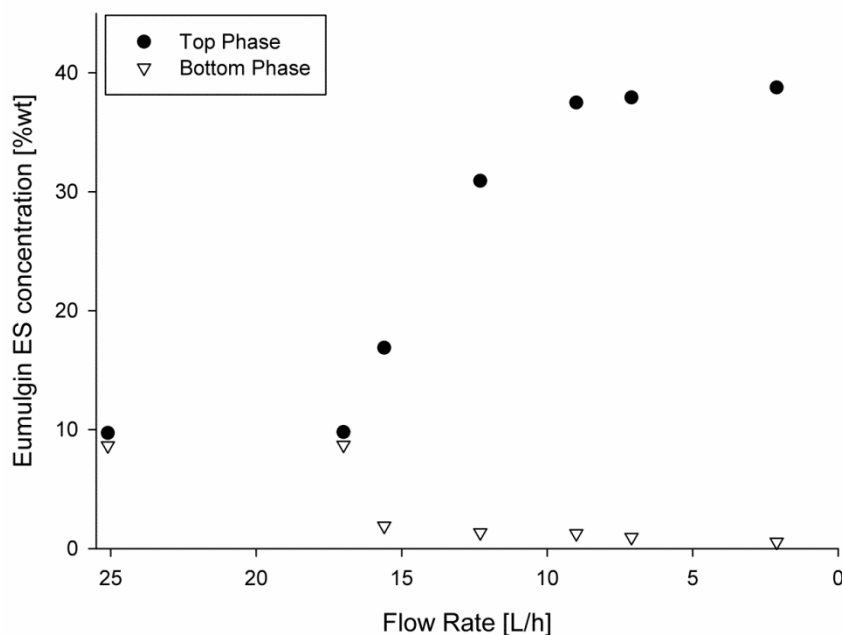
Figure 7.6: : Eumulgin ES phase separation achieved in the magnetic extractor during continuous operation at different flow rates. Poly-(NIPA-AAc) magnetic particles were added to the system with a concentration of 2 g/L. For flow rates less than 10 liters per hour, a plateau phase is reached, with an average Eumulgin ES concentration of 38% wt in the top phase and 0.7% wt in the clarified bottom phase.

The phases start to separate at a flow rate of 17 liters per hour and the maximum phase separation rate is reached already at approximately 9 liters per hour. The benefit from the addition of the magnetic particles to the AMTPS, cf. traditional AMTPS, is clearly visible. By addition of magnetic particles that partition exclusively to the dispersed micellar droplets of the emerging two-phase system, the magnetic force directly impacts the phase separation. On the one hand, the flotation velocity of a "magnetic droplet" is increased by the magnetic field gradient in the separator chamber, which results in a magnetic force pointing upwards. On the other hand, the coalescence rate of the droplets is increased. As a consequence, the maximum surfactant concentration in the micelle-rich top phase increases from 32% in the experiments without particles to 38% in the case of the addition of magnetic particles. However, in both cases the maximum Eumulgin ES concentration in the top phase is lower than the Eumulgin ES concentration of 50%, which results from a complete phase separation temperature of 30°C obtained from the phase diagram. The difference to the experimental data for a continuous operation is likely due to incomplete phase separation – AMTPS usually undergo complete phase separation in 16-20 hours in batch experiments. In the magnetic extractor, the maximum

residence time is 55 minutes in the case of a CME operation with magnetic particles and 5 hours in the case of an operation without particles. A mass balance of the total surfactant in the ingoing and effluent streams of the extractor, however, cannot be solved completely especially for low flow rates. It can be assumed that the micelle-rich phase is accumulated in the reactor in front of the weir. When operating the CME without particles, the effect is more pronounced than when operating it with particles. The applied magnetic field supports the crossing of the magnetic particle-doped surfactant-rich phase over the weir. Nevertheless, the surfactant mass balance of the CME still shows a discrepancy of around 8% which is why long-term CME behavior has to be studied further in order to guarantee stable continuous operation.

In order to study the long-term stability of CME, the magnetic extractor was operated continuously for several hours and the Eumulgin ES and the particle concentrations were monitored. Figure 7 shows the course of the particle concentration profiles in the injected feed, the concentrated top phase and the particle-depleted bottom phase.

The magnetic particles are continuously separated from the feed and the clarified bottom phase is discharged with a remaining particle concentration of 0.02 g/L. On the other hand, the particles are concentrated in the micelle-rich top phase of the system. The injected particle concentration is constant during the complete process (2.7 hours). Due to the fact that the effluents are recycled back into the stirred feed tank in the case of the long-term experiments, particle accumulation within the separation chamber would result in a reduced particle concentration in the effluent and therefore dilute the recycled feed. Hence, it can be concluded that the particles are not held back and accumulated in the reactor but are continuously discharged.
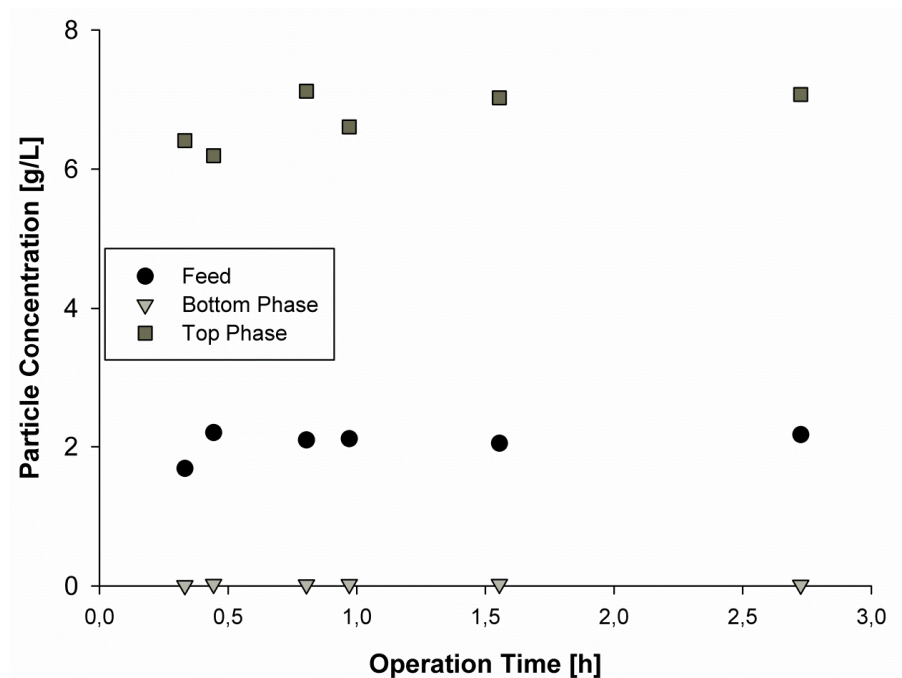
Figure 7.7: Continuous separation of magnetic particles in the magnetic extractor at a flow rate of 9 L/h. The feed contains an initial particle concentration of 2 g/L. The average particle concentration in the bottom phase is 0.02 g/L and the average particle concentration in the top phase is 6.6 g/L.

In addition to the results on particle separation, Figure 8 depicts the progress of the phase-forming surfactant concentrations. As can be seen, the concentrations of the initial and leaving streams are constant. The initial concentration of 10 wt % of phase-forming surfactant is steadily separated and a remaining surfactant concentration of 0.9 wt % Eumulgin ES is discharged in the bottom phase, while the concentration of surfactant in the top phase is 29 wt %. Therefore, in the case of a C_R = 0.33, the total mass balance of the applied surfactant sums up to practically 100 %.
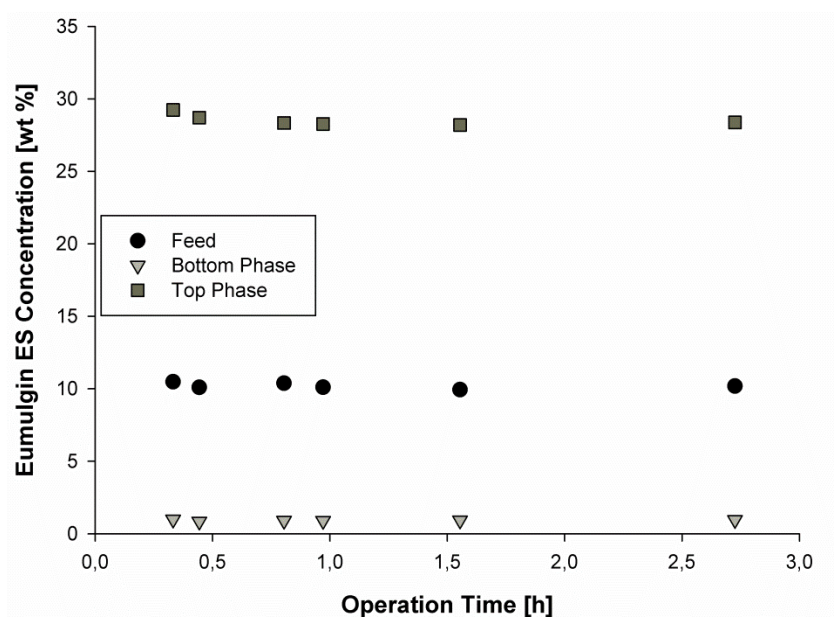
Figure 7.8: Continuous separation of the phase-forming surfactant in the magnetic extractor at a flow rate of 9 L/h. The feed contains an initial surfactant concentration of 10 wt %. The average surfactant concentration in the bottom phase is 0.9% and the average concentration in the top phase is 29 wt %.

Besides the 200 nm-sized magnetic sorbents that have been applied, several other magnetic particles were tested in the CME set-up for their separation efficiency at a particle concentration of 2 g/L. Table 7.2 summarizes the results of the experiments.

Table 7.2: Overview of particle types tested in the CME set-up and achieved separation efficiencies.

Particle Supplier	Base Matrix	Mean Size	Functionalization	Separation Efficiency	Flowrate
Merck Millipore	MagPrep Silica	25 nm	-	> 95 %	5 L/h
Merck Millipore	MagPrep Silica	100 nm	SO_3	> 99 %	5 L/h
NIIMT	p(NIPA-AAc) with embedded magnetite nanoparticles	200 nm	Acrylic acid	> 99 %	9 L/h
Chemagen	MPVA12	2000 nm	DEAP	> 99 %	9 L/h

From the data of Table 7.2 it can be seen that magnetic extraction is a versatile process, which can be applied to different magnetic particles which e.g., exhibit common functionalizations known from chromatography.

7.4.2 Part II: Continuous Protein Purification Using Magnetic Extraction

For proof of concept of continuous magnetic extraction of proteins in liter scale, purification of the antibody fragment Fab α33 from a crude heat extract of *E. coli* was investigated. The process parameters for the purification of Fab α33 by means of CME were obtained by the creation of a Fab α33 supernatant/Eumulgin ES phase diagram. The resulting diagram was similar to the one in [26]. The influence of the proteins is therefore negligible and the process parameters obtained from Table 2 were applied for the processing of the Fab α33 broth. In the sorption step, magnetic cation exchange particles were used in order to bind the target protein in the presence of the non-ionic surfactant Eumulgin ES. After 10 min of binding, the temperature was increased until T_T and the particles loaded with protein were enriched in the micelle-rich top phase leaving the magnetic extractor, while the effluent containing the micelle-poor phase contained most of the host cell proteins (HCP). In the washing step, the micelle-rich top phase was mixed with two volumes of sodium phosphate buffer. The solution was then again separated by magnetic extraction to remove contaminating HCP which remained in the top phase of the initial sorption step as a result of incomplete phase removal of the bottom phase. In the elution step, the Fab α33 was eluted from the particles by the addition of two volumes of 750mM sodium chloride elution buffer. The phases were separated again by magnetic extraction. In this step, the bottom, micelle-poor phase contained the eluted target protein, while the magnetic particles and the majority of the surfactant were discharged in the top phase. Table 7.3 summarizes the composition of the discharged bottom phases after the feed of the respective step was completely processed by CME.

Table 7.3: Summary of the volumes and concentrations of the bottom phases resulting from conductig the sorption, wash and elution steps in the CME.

Process step	Volume [L]	Particles [g/L]	Eumulgin ES [% wt]	DNA [mg/L]	Total protein [g/L]	Fab α33 [g/L]
Initial Solution	14.723	1.38	10	10.43	0.48	0.075
Sorption	11.39	0.006	2.83	7.08	0.178	0.05
Wash	7.773	0.017	1.67	3.82	0.072	0.03
Eluate	5.082	0.001	0.34	0.34	0.147	0.145
Recovery Rate[a]	-	115 %	67 %	73.4	52 %	175.7 %

[a]For calculation of the recovery rate, the sum of the mass flow of all bottom phases and the eluate top phase was compared to the initial mass flow in the feed

As can be seen from Table 7.3, the leaving bottom phases of the eluates in the CME contain only between 1 and 17 mg particles per liter. This indicates that the particles are concentrated in the top phases instead and processed to the next step. The remaining Eumulgin ES concentration in the eluate bottom phase is 0.34%. The DNA concentration is reduced from 10 mg/L to 0.3 mg/L. The HCP is additionally removed to a large extent. During the process, the total volume is consecutively decreased from 14.7 to 5.1 liters. To calculate the recovery rate, a mass balance which included all leaving bottom streams and the leaving eluate top phase was done. As can be seen from Table 3, the total Fab mass is overemphasized. This is probably due to the analytical inaccuracy of the densiometric procedure applied. Nevertheless, the results clearly show the purification and concentration capabilities of the CME process. Regarding the mass balance deviations in the case of total protein and DNA, it is probable that even after the elution step a fraction of the proteins and the DNA is still adsorbed to the magnetic carriers due to unspecific adsorption.

In order to visually confirm the purification of the Fab, the bottom phases were analyzed by SDS- PAGE. Figure 7.9 shows the SDS-PAGE analysis of the clarified bottom phases obtained from the CME process. The protein patterns are compared based on equal total amounts of protein in each lane.
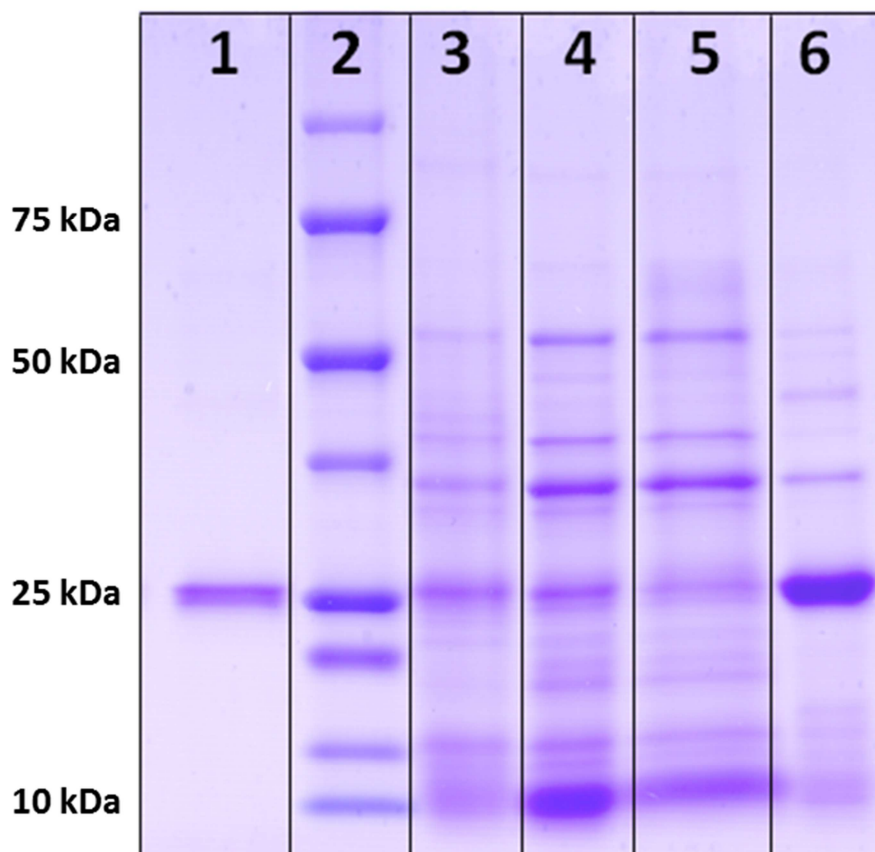
Figure 7.9: SDS-PAGE analysis of the purification process of Fab α33 by CME. Lane 1: Fab standard [1 µg]; 2: Protein standard; 3: *E. coli* Heat shock solution; 4: Sorption supernatant; 5: Wash; 6: Eluate. The total protein concentration in each lane was 3 µg.

It can be seen that Fab α33 is not removed completely from the sorption supernatant (lane 4 in Figure 7.9). Therefore, the yield of the protein binding could be further increased by improvement of the binding capacity of the particles or by increasing the total particle concentration in the system. This target-protein loss is, however, not an effect of the magnetic extraction process itself though, but a particle-related issue. Yet, considering the purity of the Fab α33 in the bottom phase of the eluate – lane 6 in the gels – it is clearly confirmed that the use of SO_3 particles in the CME process can be used to enrich the target protein.

Table 7.4 summarizes the final purification data by comparing the concentrations in the feed and the concentration of the leaving elution phase of the system.

Table 7.4: Comparison of the initial CME feed and the bottom phase of the elution step.

Particle removal	Surfactant removal	HCP removal	DNA removal	Fab Yield	Fab Purity	Purification factor
>99.9 %	>98 %	>95 %	>98 %	>67 %	>98 %	6.3

The numbers can be seen in comparison to an ATPE study on the continuous purification of an IgG using a packed column in combination with a mixer-settler [8]. Here, a total yield of 85% and a purity of 84% of the IgG molecule were achieved. No DNA depletion was reported. The advantage of the CME, cf. this state-of-the-art ATPE process, is the significantly increased purity which arises from the addition of the selective magnetic sorbents. The total yield in our process, however, could be further improved by optimization of a) the magnetic sorbents' capacity or concentration in the CME; or by b) the further optimization of the top to bottom phase discharge ratio (P). The incomplete separation of the top from bottom phase leads to Fab α33 being discharged in the top phase of the elution step and the decrease in the total Fab α33 yield. This problem, however, may be solved by simply introducing an additional CME process step, where the remaining Fab α33 is withdrawn in the bottom phase.

7.4.3 Review of the Recyclability of the CME Components – Surfactants and Particles

Reuse of the phase-forming component in an AMTPS is one striking advantage of AMTPS, cf. ATPS, because only the micelle-depleted phase is discharged in the course of the sorption, wash and elution steps. In the case of the CME, the micelle-rich phase of the eluate phase is removed together with the magnetic particles and can be reused in the course of a next sorption step. In order to calculate the theoretical amount of recyclable phase-forming component, samples were taken during the continuous operation of the CME during binding, wash, and elution. Table 7.5 compares the surfactant concentrations from the continuous mode with the surfactant concentrations after finishing the process step and discharging the separator content into the collection tank.

Table 7.5: Comparison of surfactant concentrations in the bottom phase during CME operation and after discharging the separator.

Process Step	Surfactant concentration	
	during operation	**after discharging the separator**
Binding	0.9 %	2.8 %
Wash	1.0 %	1.7 %
Elution	0.2 %	0.34 %

The surfactant concentrations at the end of each process step detected in the collection tanks of the bottom phases are slightly higher. This is explained by the large separation chamber bed volume to total volume ratio (e.g. 6.8 liters initial elution feed, cf. 2.8 liters separation chamber volume). After complete processing of the feed, the CME chamber has to be drained. In the course of this operation, comparatively much surfactant is lost in contrast to continuous operation mode due to incomplete phase separation. For large feed volumes or truly continuous operation, however, the impact of surfactant that is lost during this drainage would be insignificant; thus, the numbers given in Table 7.5 are more reasonable for real continuous processing. The amount of recyclable surfactant was calculated from the loss of surfactant in the bottom phases during the continuous operation of the magnetic extraction. Using this calculation, 87% of the total surfactant can be recycled in the top phase of the elution step. Additionally, the total particle loss after binding, washing, and elution amounted to approximately 1% of the initial particle amount. The remaining 99% can be applied to the next binding step of a consecutive CME. These results suggest that the reuse of both phase- forming surfactant and magnetic particles can be effectively achieved in the CME.

7.5 Conclusion

Continuous Magnetic Extraction has been introduced as a promising approach to a continuous low-cost bioseparation process. It is based on the processing of functional magnetic sorbents and their processing in AMTPS. Magnetic sorbents that partition exclusively to the micelle-rich phase of an AMTPS are separated in a novel extractor

based on a mixer and a magnetic field-enhanced flow-through phase separator. It was demonstrated that our pilot-scale CME can be operated at flow rates of several liters per hour at moderate temperatures with particle separation efficiencies of >99%. Additionally, the phase-forming non-ionic surfactant Eumulgin ES was continuously split into a micelle-rich and a micelle-depleted phase with separation rates >98%.

CME was applied for the capture of the antibody fragment Fab α33 from an industrial biosuspension. Magnetic cation exchange particles have been applied as magnetic sorbents. Using CME, the Fab α33 could be enriched in the eluate with a purification factor of approximately 6.3, a purity >98%, and a total yield of 67%.

Considering the particle separation performance, the complete purification process resulted in a recycling rate of >99% over three consecutively operated extractions, while 13% of the phase- forming surfactant was lost. The remaining phase-forming surfactant was collected together with the magnetic particles after the final elution step and, therefore, could be applied to the next continuous magnetic extraction.

7.6 References

[1] D. Low, R. O'Leary, N.S. Pujar, Future of antibody purification, Journal of Chromatography B-Analytical Technologies in the Biomedical and Life Sciences, 848 (2007) 48-63.

[2] P.A. Albertsson, Chromatography and Partition of Cells and Cell Fragments, Acta Chemica Scandinavica, 10 (1956) 148-148.

[3] C. Bordier, Phase-Separation of Integral Membrane-Proteins in Triton X-114 Solution, Journal of Biological Chemistry, 256 (1981) 1604-1607.

[4] H. Tani, T. Kamidate, H. Watanabe, Aqueous micellar two-phase systems for protein separation, Analytical Sciences, 14 (1998) 875-888.

[5] R. Hatti-Kaul, Aqueous two-phase systems - A general overview, Molecular Biotechnology, 19 (2001) 269-277.

[6] L.A. Sarubbo, L.A. Oliveira, A.L.F. Porto, J.L. Lima-Filho, G.M. Campos-Takaki, E.B. Tambourgi, Performance of a perforated rotating disc contactor in the continuous extraction of a protein using the PEG-cashew-nut tree gum aqueous two-phase system, Biochemical Engineering Journal, 16 (2003) 221-227.

[7] P. Vazquez-Villegas, O. Aguilar, M. Rito-Palomares, Study of biomolecules partition coefficients on a novel continuous separator using polymer-salt aqueous two-phase systems, Separation and Purification Technology, 78 (2011) 69-75.

[8] P.A.J. Rosa, A.M. Azevedo, S. Sommerfeld, W. Backer, M.R. Aires-Barros, Continuous aqueous two-phase extraction of human antibodies using a packed column, Journal of Chromatography B-Analytical Technologies in the Biomedical and Life Sciences, 880 (2012) 148-156.

[9] P. Trakultamupatam, J.F. Scamehorn, S. Osuwan, Scaling up cloud point extraction of aromatic contaminants from wastewater in a continuous rotating disk contactor. I. Effect of disk rotation speed and wastewater to surfactant ratio, Separation Science and Technology, 39 (2004) 479-499.

[10] T. Ingram, S. Storm, P. Glembin, S. Bendt, D. Huber, T. Mehling, I. Smirnova, Aqueous Surfactant Two-Phase Systems for the Continuous Countercurrent Cloud Point Extraction, Chemie Ingenieur Technik, 84 (2012) 840-848.

[11] S.A. Oelmeier, F. Dismer, J. Hubbuch, Application of an Aqueous Two-Phase Systems High-Throughput Screening Method to Evaluate mAb HCP Separation, Biotechnology and Bioengineering, 108 (2011) 69-81.

[12] G. Kopperschlager, G. Birkenmeier, Affinity partitioning and extraction of proteins, Bioseparation, 1 (1990) 235-254.

[13] A.M. Azevedo, P.A.J. Rosa, I.F. Ferreira, A.M.M.O. Pisco, J. de Vries, R. Korporaal, T.J. Visser, M.R. Aires-Barros, Affinity-enhanced purification of human antibodies by aqueous two-phase extraction, Separation and Purification Technology, 65 (2009) 31-39.

[14] M. Franzreb, M. Siemann-Herzberg, T.J. Hobley, O.R.T. Thomas, Protein purification using magnetic adsorbent particles, Applied Microbiology and Biotechnology, 70 (2006) 505-516.

[15] M. Suzuki, M. Kamihira, T. Shiraishi, H. Takeuchi, T. Kobayashi, Affinity Partitioning of Protein-a Using a Magnetic Aqueous 2-Phase System, Journal of Fermentation and Bioengineering, 80 (1995) 78-84.

[16] Q. Gai, F. Qu, T. Zhang, Y. Zhang, Integration of carboxyl modified magnetic particles and aqueous two-phase extraction for selective separation of proteins, Talanta, 85 (2011) 304-309.

[17] P. Wikstrom, S. Flygare, A. Grondalen, P.O. Larsson, Magnetic Aqueous 2-Phase Separation - a New Technique to Increase Rate of Phase-Separation, Using Dextran Ferrofluid or Larger Iron-Oxide Particles, Analytical Biochemistry, 167 (1987) 331-339.

[18] S. Flygare, P. Wikstrom, G. Johansson, P.O. Larsson, Magnetic Aqueous 2-Phase Separation in Preparative Applications, Enzyme and Microbial Technology, 12 (1990) 95-103.

[19] P.O. Larsson, Magnetically Enhanced Phase-Separation, Aqueous Two-Phase Systems, 228 (1994) 112-117.

[20] J.S. Becker, O.R.T. Thomas, M. Franzreb, Protein separation with magnetic adsorbents in micellar aqueous two-phase systems, Separation and Purification Technology, 65 (2009) 46-53.

[21] I. Fischer, M. Franzreb, Nanoparticle Mediated Protein Separation in Aqueous Micellar Two-Phase Systems, Solvent Extraction and Ion Exchange, 30 (2012) 1-16.

[22] W. McCabe, J. Smith, P. Harriot, Unit Operations of Chemical Engineering, Seventh Edition ed., McGraw-Hill, New York, 2005.

[23] D.T. Kamei, D.I.C. Wang, D. Blankschtein, Fundamental investigation of protein partitioning in two-phase aqueous mixed (nonionic/ionic) micellar systems, Langmuir, 18 (2002) 3047-3057.

[24] I. Fischer, M. Franzreb, Direct determination of the composition of aqueous micellar two-phase systems (AMTPS) using potentiometric titration-A rapid tool for detergent-based bioseparation, Colloids and Surfaces a-Physicochemical and Engineering Aspects, 377 (2011) 97-102.

[25] C.A. Schneider, W.S. Rasband, K.W. Eliceiri, NIH Image to ImageJ: 25 years of image analysis, Nature Methods, 9 (2012) 671-675.

[26] I. Fischer, C. Morhardt, S. Heissler, M. Franzreb, Partitioning Behavior of Silica-Coated Nanoparticles in Aqueous Micellar Two-Phase Systems: Evidence for an Adsorption-Driven Mechanism from QCM-D and ATR-FTIR Measurements, Langmuir, 28 (2012) 15789-15796.

8 Removal of the nonionic surfactant Eumulgin ES from protein solutions by means of adsorption and ultrafiltration

Ingo Fischer, Matthias Franzreb*

*: Corresponding author: Email: Matthias.Franzreb@kit.edu

8.1 Abstract

Aqueous Micellar Two-Phase Extraction (AMTPE) is a promising technique for large-scale protein purification, however, it is unavoidable that a certain surfactant load will remain in the product stream. Therefore, an industrial application of AMTPE requires efficient and economic ways for the removal of surfactants as a polishing step. In view of this demand, the removal of the nonionic surfactant Eumulgin ES has been investigated by means of fixed bed adsorption and cross-flow ultrafiltration. The critical micelle concentration of an aqueous Eumulgin ES solution is 3.8 mg/L with a hydrodynamic diameter of a micelle of approximately 15 nm at 22°C. The adsorption of Eumulgin ES to hydrophobic polystyrene beads leads to high loading capacities, but proteins also bind with high affinity to the beads, making the technique of limited use. A better way is to remove the surfactant by means of ultrafiltration through a hydrophobic polyethersulfone membrane. In the course of the filtration process a viscous micelle phase at the membrane forms, by which the flux through the membrane is decreased drastically. While elevated temperatures and salt concentrations decrease the flux and the overall separation performance, the opposite conditions lead to improved surfactant removal efficiencies. Cross-flow ultrafiltration is finally applied for the separation of Eumulgin ES from a proteinaceous soltution originating from a technical-scale AMTPE investigation. The filtration results in a total surfactant removal of >98.8% from the target protein solution within the rinsing with 8 bed volumes.

8.2 Introduction

Nonionic surfactants are amphiphilic molecules that contain at least one polar group and one nonpolar hydrophobic group. Due to this amphiphilic character, aqueous nonionic surfactant solutions exhibit special properties, for instance, when a certain surfactant concentration, denoted critical micelle concentration (cmc) is exceeded, the surfactants undergo spontaneous self-association and form ordered structures called micelles. Further increase in the surfactant concentration and/or temperature can lead to the splitting of the aqueous micellar solution into a micelle rich and a micelle poor phase, called aqueous micellar two-phase system (AMTPS) [1].

The range of applications and processes in which nonionic surfactants are utilized is tremendous. The spectrum spans the petrochemical, food, and cosmetics industry, agriculture as well as various microbiological and biotechnological processes [2]. An interesting application is the use of AMTPS for the selective separation of proteins by partitioning them between the micelle rich and micelle poor phase [3, 4].The target protein can then be withdrawn either from the micelle concentrated or the micelle depleted phase.

Due to the wide range of applications there is an increasing need for surfactant removal in the product streams or wastewaters of surfactant based processes. The process of choice is based on the physicochemical properties of the surfactants, especially the cmc and the micellar size which is directly related to the number of surfactant molecules in a micelle [5]. Surfactants with a high cmc can be removed by dialysis, as only single surfactant molecules diffuse through the dialysis membrane, or, more efficiently, by gel filtration as surfactants with high a cmc form small uniform micelles [6].

Surfactants with a low cmc form large micelles and thus their separation from other components like e.g. proteins by dialysis or gel filtrations is difficult. In this case, the successful removal of nonionic surfactants has been reported by adsorption to nonpolar polystyrene beads [7].

In larger scale, the separation of surfactants can also be performed by means of dead end or cross-flow ultrafiltration [8, 9]. In this case it is assumed, that single surfactant molecules are hereby separated from the micelles. For instance "Micellar Enhanced Ultrafiltration" (MEUF) utilizes the separation of ionic micelles from single ionic surfactant molecules for the removal of trace elements of heavy metal ions which are incorporated or sorbed to the micelles [10]. It has been reported, that the surfactant concentration in the permeates of ultrafiltration processes can slightly exceed the cmc when working with hydrophilic membranes [11, 12] and considerably in the case of hydrophobic membranes [13]. The knowledge of the properties of the applied surfactant, however, is crucial for the applied removal strategy.

In this work, process relevant properties of the non-ionic surfactant Eumulgin ES are revealed. The cmc and hydrodynamic radius of Eumulgin ES are studied. The removal of Eumulgin ES from aqueous solutions is investigated by comparing an adsorptive surfactant removal using nonpolar polystyrene beads and cross-flow ultrafiltration. Additionally, the influence of the temperature and salt concentration to the ultrafiltration of the surfactant is examined.

Eumulgin ES has earlier been used as phase forming surfactant in the course of magnetic extraction [14], an affinity based separation of proteins by the combination of functionalized magnetic particles and aqueous micellar two-phase systems (AMTPS). The final process step of magnetic extraction results in a purified protein solution with an undesired remaining Eumulgin ES concentration. It is demonstrated that the remaining surfactant can be removed by means of ultrafiltration from this proteinaceous solution with the target protein retained in the retentate.

8.3 Material and Methods

8.3.1 Chemicals

All chemicals were from p. A. grade. Water was deionized and purified in a Millipore Milli-Q Ultrapure system. Disodium-hydrogen phosphate and sodium-chloride were supplied by Carl Roth (Karlsruhe, Germany). Citric acid monohydrate was purchased from Merck

Millipore (Darmstadt, Germany). The proteins ovalbumin (Molecular weight: 44.2 kDa, grade >98%) and lysozyme from chicken egg white (Molecular weight: 14.6 kDa ~70000 units/mg) were purchased from Sigma-Aldrich (St. Louis, USA-MO). The nonionic surfactant Eumulgin ES ($C_{12}/C_{14}PEO_5PPO_5$ or PPG-5-Laureth-5, CAS-No.: 68439-51-0) was purchased from Cognis (Düsseldorf, Germany).

8.3.2 Methods

The critical micelle concentration was measured with a DCAT 11 system (Dataphysics, Filderstadt, Germany). A glass beaker was filled with 60ml milliQ water, sodium phosphate at pH 7 or sodium citrate at pH 3. A stock solution was prepared with a concentration of 0.3 g/L Eumulgin ES. Small volumes of the stock solution were added to the pure solution and the surface tension at the air-water interface was detected subsequently by the De-Nouy ring method using a Pt/Ir ring. The surface tension was plotted versus the surfactant concentration and the cmc was derived from the point of transition from exponential decline of the surface tension to linear decline.

The hydrodynamic diameter of an Eumulgin ES micelle was determined by dynamic light scattering (DLS) by means of a Zetasizer 5000 (Malvern Instruments GmbH, Herrenberg, Germany). A 0.5% Eumulgin ES solution was used in 20mM sodium-phosphate pH 7 and 20mM sodium citrate, pH 3. For the calculation of the DLS, the viscosity and refractive index of water was used and the influence of Eumulgin ES on both parameters neglected.

8.3.2.1 Adsorptive methods using hydrophobic beads

Porous hydrophobic polystyrene beads "BioBeads SM2" were purchased from BioRad (Hercules, USA-CA). Eumulgin ES binding studies were performed in 1.5 ml microcentrifuge tubes in a total volume of 1.5 ml and a constant BioBead concentration. The beads were equilibrated in 20mM sodium-phosphate buffer at pH 6.8 and incubated in an ultrasonic bath for 10 minutes in order to remove air that was entrained in the pores of the beads. The Eumulgin ES concentrations were prepared in a range from 0.1 g/L to 75 g/L in 20mM sodium-phosphate buffer at pH 6.8.

Adsorption was performed for 4 hours in a thermomixer (Eppendorf, Hamburg, Germany) at 25° C and 1400 rpm.

After the adsorption step, the beads were removed by centrifugation and the particle-free supernatants were subsequently analyzed for their Eumulgin ES concentration. The amount of protein adsorbed to the particles was calculated by the mass balance:

$$q = \frac{V_0 \cdot (c_0 - c_S)}{m_B}$$

[Eq. 8.1]

where q (mg/g) is the amount of bound protein onto the particle, m_B (g) the amount of BioBeads, V_0 is the volume of the experiment and c_0 and c_S are the concentrations of the surfactant in the supernatant before and after the adsorption.

Adsorption equilibrium was achieved in 4 hours (data not shown) and the experimental data obtained from the adsorption experiments were fitted to the Langmuir model:

$$q = q_{max} \cdot \frac{c}{K_L + c}$$

[Eq. 8.2]

with q_{max} (mg/g) representing the maximum binding capacity of the beads and K_L (in g/L) the Langmuir constant. The values for the Langmuir parameters were calculated using SigmaPlot (vers. 11.0, Systat Software, Inc., 2008).

Additionally, the adsorption of the two model proteins lysozyme and ovalbumine onto the BioBeads was characterized in the same way, in order to compare the binding constants of the proteins to the beads. The Eumulgin ES concentration in the supernatants was determined by potentiometric titration. The protein concentration was determined by UV-Spectroscopy using a Nanodrop ND-1000 (Thermo Fisher Scientific, Waltham, USA-MA) photometer.

8.3.2.2 Removal of the surfactant using cross-flow filtration

Ultrafiltration experiments were performed using Vivaflow 50 tangential flow cassettes with a diafiltration reservoir (Sartorius Stedim, Göttingen, Germany). The matrix of the

membranes was of polyethersulfone (PES) with an active membrane area of 50 cm² and a molecular weight cut-off (MWCO) of 30 kDa.

The feed was circulated across the membrane with a Masterflex L/S pump (Cole Palmer, IL-US). The cross-flow velocity was set to 450 ml/min. A pressure indicator was integrated to monitor the pressure at the retentate side of the membrane. During all filtrations the pressure remained constant at 0.2-0.25 mPa. The permeate outlet was connected to a fraction collector (Super Frac, GE-Healthcare, Uppsala, Sweden). Fractions of the permeate were collected on a time resolved basis. The permeate flow was calculated by the collected volumes in the fraction collector. The vacuum-sealed reservoir was connected to a buffer tank. Because of the withdrawal of permeate, the volume in the reservoir decreased and a vacuum was generated in the reservoir. Due to this vacuum, buffer was drawn from the large tank to the reservoir. In this mode, the total volume circulating the membrane remained constant. The reservoir and buffer tank was set up in a temperature controlled water bath (RC 20 S, Lauda, Germany). The initial Eumulgin ES concentration was 1 % and the total volume in the reservoir was 200 ml. The water bath was set to 6°C or to 35°C to determine the influence of the temperature to the filtration. Additionally, so as to investigate the influence of NaCl to the filtration performance, a 1% Eumuglin ES solution set up containing 1 M NaCl and a 0.1% Eumulgin ES solution containing 500 mM NaCl were studied.

The permeate samples from the membrane filtration experiments were analyzed for their surfactant concentrations by total organic carbon (TOC) and for their salt concentration by conductometry. The total removal of surfactant was then calculated according to equation:

$$R = \left(\frac{\sum_{i=1}^{n} c_i \cdot V_i}{c_0 \cdot V_o} \right) * 100 \qquad \text{[Eq. 8.3]}$$

With c_0 and V_0 the initial volume and concentration of the surfactant solution and c_i and V_i the collected volumes and concentrations in the collected permeates.

Assuming the flux through the ultrafiltration membrane is not limited by concentration polarization at low pressures, it can be described by the Hagen-Poiseuille pore model:

$$J = \frac{\varepsilon d_P^2 P_T}{32 \Delta \chi \mu}$$

[Eq. 8.4]

Where J is the flow rate through the membrane, ε is the surface porosity, d_P the channel diameter, P_T is the applied transmembrane pressure, $\Delta\chi$ is the length of the channel and μ is the viscosity of the permeating fluid [15].

8.3.2.3 Surfactant removal from proteinaceous solution

In order to demonstrate the surfactant removal from solutions representative for bioseparation processes a proteinaeous solution has been applied in the ultrafiltration set-up. A Vivaflow 50 tangential flow cassette with a MWCO of 10 kDa was used. The experimental set-up was similar to the one described above. The proteinaceous solution originated from a large-scale magnetic extraction experiment. The principle of magnetic extraction is described elsewhere [14, 16]. An initial solution of 104 ml volume was applied with an Eumulgin ES concentration of 3.4 g/L. The protein concentration was determined by SDS-PAGE and densiometric analysis.

8.3.3 Analytics

Total organic carbon in the samples was detected via the Multi N/C 2000 (Analytik Jena, Jena, Germany). The samples were prepared by adding 15 µl hydrochloric acid and purging the sample with N_2 to remove inorganic carbon. The total surfactant concentration was calculated from the TOC content; the carbon mass makes up for 63.8 % of the total mass of the nonionic surfactant Eumulgin ES.

Potentiometric titration was performed using the NIO surfactant electrode (Metrohm, Birkenfeld, Germany) as described elsewhere [17]. A sample was weighed into a glass beaker and 10 mL of barium chloride solution (c= 0.1 M) and 60 mL of water were added. This solution was then titrated with a sodium-tetraphenylborate solution using the Metrohm NIO electrode. As result the end-point volume was recorded. The surfactant

mass fraction was then obtained by comparing the end point volume with the end point volumes of known Eumulgin ES mass fractions using linear regression.

Protein concentrations were measured spectrophotometrically at 280 nm using a Nanodrop® ND-1000 (Thermo Fisher Scientific, Waltham, USA-MA) photometer. For chicken ovalbumin and lysozyme the mass extinction coefficients of a 10 mg/ml solution were determined to be 5.5 and 26.4, respectively.

The sodium chloride detection was performed by conductivity detection using a Knick 702 conductometer (Knick, Berlin, Germany). A calibration curve was made with known sodium chloride standards, and the sodium chloride concentration in the permeate fractions was calculated accordingly.

In course of the experiments with proteinaceous solutions ,the depletion of the target protein was determined by densiometric analysis following SDS PAGE. The protein-loaded SDS gels were Coomassie Blue-stained and scanned as TIFF image files. The images were afterwards analyzed using the software ImageJ® [18]. From the quotient of the intensities of the samples the total protein loss was calculated. The protein concentrations were hereby kept within the range of linear correlation between protein amount and band intensity on the gel.

8.4 Results and Discussion

8.4.1 Critical Micelle Concentration

The cmc was determined with the De-Nouy Ring method. Small amounts of Eumulgin ES were added gradually to an aqueous solution and the surface tension was measured. The cmc was determined in milliQ water, in sodium citrate at pH 3 and in sodium phosphate at pH 7. However, the influence of the pH was negligible, resulting in a practically identical the shape of the curves (data not shown). In figure 1 the decline of the surface tension is plotted versus the total Eumulgin ES concentration in Eumulgin ES sodium phosphate at pH 7. The surface tension decreases exponentially up to a concentration of 3.8 mg/L Eumulgin ES. Further addition of surfactant leads to a linear decrease in the

surface tension. The concentration at the point of transition from exponential to linear decline is described as the cmc [19, 20].
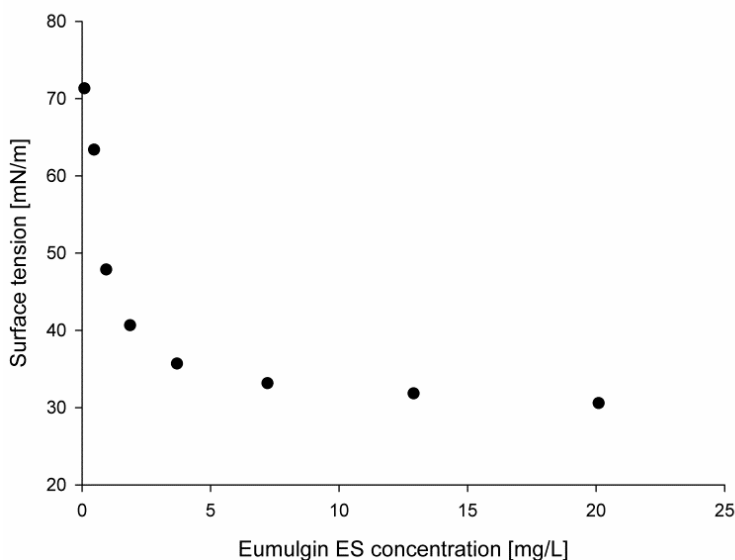
Figure 8.1: Surface tension diagram of Eumulgin ES. The transition from exponential decay to linear decay in the surface tension at 3.8 mg/L marks the cmc.

8.4.2 Hydrodynamic Diameter

The size of Eumulgin ES micelles in a 0.5% Eumulgin ES solution was investigated in presence of sodium phosphate and sodium citrate using DLS. DLS is a well applied tool method for the investigation of micelle radii, as it can be assumed that micelles in aqueous solutions act like hard-spheres in a Newtonian fluid [21-23]. It was assumed that there was little influence of the concentration of Eumulgin ES on the hydrodynamic radius as it was shown by neutron scattering that the size of a micelle of nonionic surfactants does not vary significantly at concentrations below the binodale at constant temperatures [24]. Table 8.1 shows the results obtained from the DLS measuring. The hydrodynamic diameter of the micelles is approximately 15 nm. It is not influenced by the pH level, which confirms the nonionic nature of Eumulgin ES because in the case of ionic surfactants, a change in the pH changes hydrodynamic radius occurs due to electrostatic repulsion of the surfactant molecules [25]. The micelle diameter of approximately 15 nm is in good agreement to a single surfactant molecule, which was calculated to 5.5 nm.

Table 8.1: Sizes of the hydrodynamic radius of Eumulgin ES micelles at pH3 and pH 7 at 22°C.

Buffer	Hydrodynamic radius [nm]	Standard deviation [nm]
Sodium phosphate, pH 3	14.8	0.8
Sodium citrate, pH 7	15.2	1.6

8.4.3 Eumulgin ES removal

8.4.3.1 Adsorption

The adsorptive behavior of Eumulgin ES onto porous hydrophobic polystyrene beads was investigated. The surfactant is adsorbed to the beads because of the hydrophobic tail. Due to the porous character of the beads, the adsorption equilibrium was reached after 4 hours. When the experimental data are fitted to the langmuir model, BioBeads SM2 exhibit a high loading capacity of 574 mg/g, but an unfavorable binding constant of K_L = 7.43 g/L for Eumulgin ES for the experimental conditions. The experimental data and the Langmuir regression plot are shown in Figure 8.2.
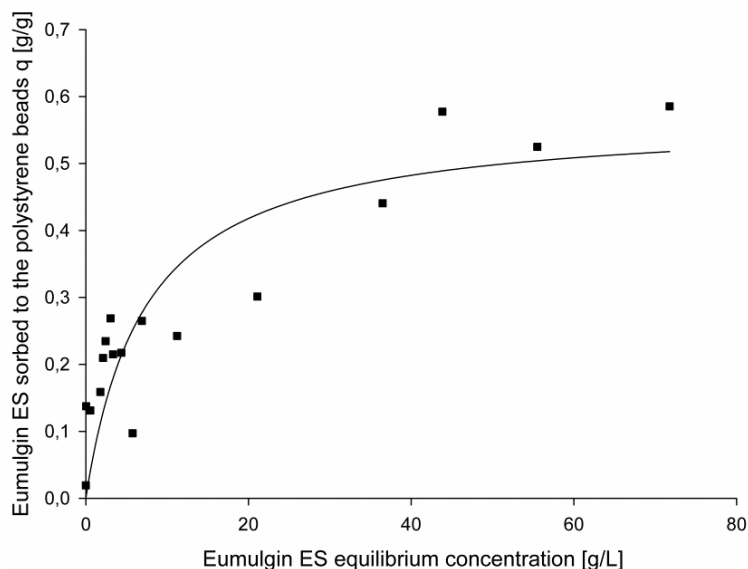
Figure 8.2. Adsorption isotherm at 25°C of Eumugin ES onto BioBeads. ES. The solid curve is created by fitting the experimental data to the Langmuir model resulting in a K_L value of 7.43 g/L and q_{max} of 574 mg/g.

The sorption of the two commonly known proteins lysozyme and ovalbumine onto the biobeads was investigated. Figure 8.3 depicts the sorption isotherms of these proteins.
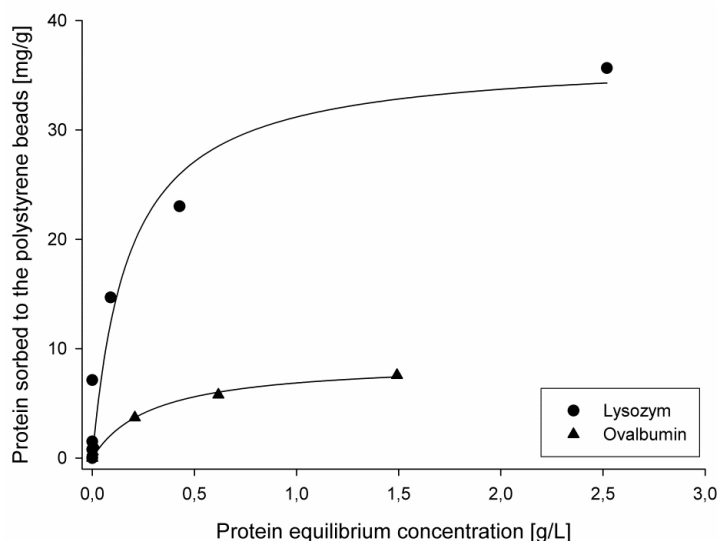
Figure 8.3. Sorption Isotherms of lysozyme and ovalbumin onto polystyrene BioBeads. The straight lines represent a Langmuir regression fits for both proteins. The Langmuir regression results in K_L=0.17 g/L and q_{max}=36.7 mg/g for lysozyme and for ovalbumin K_L= 0.29 g/L and q_{max}=8.8 mg/g.

A Langmuir regression analysis results for Lysozyme in in K_L=0.17 g/L and q_{max}=36.7 mg/g and for ovalbumin K_L= 0.29 g/L and q_{max}=8.8 mg/g. The low q_{max} value of proteins c.f. Eumulgin ES can be related to the average pore size of 9 nm of the beads. As single surfactant molecules can enter the pores, the proteins are too large and only adsorb onto the particle surface. Table 2 summarizes the obtained parameters for the Biobeads.

Table 8.2: Sorption properties of BioBeads for Eumulgin ES and the commonly used proteins Lysozyme and Ovalbumin

Substance	K_L [g/L]	q_{max} [mg/g]
Eumulgin ES	7.43	574
Lysozyme	0.17	36.7
Ovalbumine	0.29	8.8

Considering an adsorptive surfactant removal process for the further purification of an AMTPE solution BioBeads SM exhibit unfavorable sorption properties. On the one hand, the q_{max} value of the beads favors their usage, c.f. the low q_{max} values of proteins. On the other hand, the K_L values of the proteins are more than one order of magnitude smaller. This leads to an immense loss of target as proteins preferably sorb to the particles.
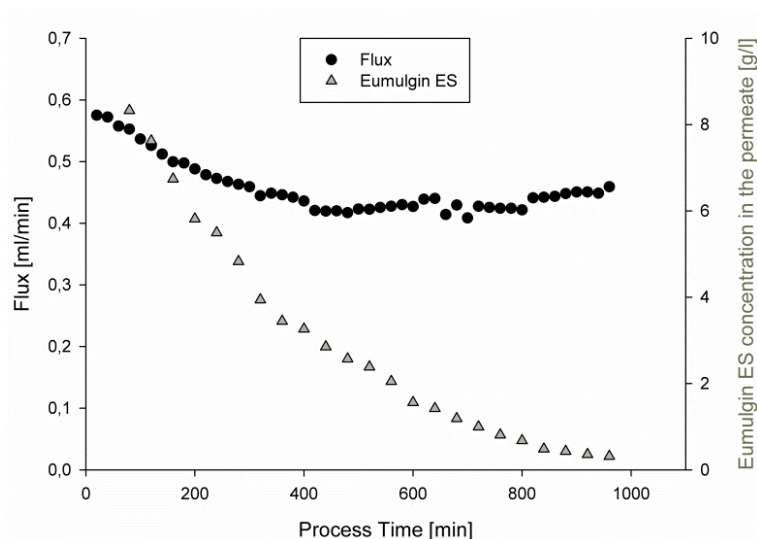
8.4.3.2 Ultrafiltration

In order to investigate the ultrafiltration behavior of the nonionic surfactant Eumulgin ES, particular surfactant characteristics as the molecular weight of a micelle and the cmc are of importance. In Table 8.3 these critical process parameters of Eumulgin ES are summarized. Based on the simplification that an Eumulgin ES micelle is a spherical sphere with the density of Eumulgin ES, the molecular weight of such a micelle was calculated to 412 kDa for a radius of a single outstrechted surfactant molecule. From the measurement of the hydrodynamic radius of 15 nm, the average molecular weight of a spherical micelle is calculated to 1042 kDa.

Table 8.3: Properties of Eumulgin ES.

Density	982 kg/m³
Molecular weight	696 g/mol
Critical micelle concentration	3.8 mg/L
Calculated length of an outstretched single molecule	5.5 nm
Calculated molecular weight of spherical micelle with a radius of 5.5 nm[a]	412 kDa
Hydrodynamic diameter obtained by DLS	15 nm
Calculated average molecular weight of a micelle with a radius of 7.5nm[a]	1042 kDa

[a]based on the assumption of spherical micelles having the density of Eumulgin ES.

A VivaFlow 50 membrane module with an MWCO of 30 kDa was applied for the filtration of the nonionic surfactant Eumulgin ES. The ultrafiltration has been performed in reservoir mode, with amount of fresh buffer being added to the retentate equal to the amount removed by filtration. In this mode, the total volume circulating the membrane remained constant at 200 ml. A 1 % Eumulgin ES starting concentration was used. The circulating fluid was placed in a water bath in order to keep the temperature constant. Two temperatures were applied: 6°C in order to prevent the system from phase separating and 35°C in order to perform the filtration at two phase conditions. Both experiments were compared on a total process time basis and were run for 960 minutes at 6 °C and respectively 1140 minutes at 35 °C. In Figure 8.4, the flux and surfactant concentration in the permeates are plotted versus the process time for the filtration at 6°C.

Figure 8.4. Ultrafiltration of an 1% Eumulgin ES solution using 30 kDa membrane at 6 °C. The flux through the membrane is constant and the Eumulgin ES concentration in the permeate declines exponentially.

The flux of pure water through the membrane was 24 ml/min. The flux decreases drastically to 0.6 ml/min when the surfactant is brought in contact with the membrane. Yet, a constant flux of 0.5 ml/min through the membrane is achieved. The Eumulgin ES concentration in the permeates decreases exponentially. All Eumulgin ES concentrations in the permeates are largely higher than the cmc. This shows that the Eumulgin ES molecules pass the membrane unhamperedly. It is noticeable, that although the temperature of the reservoir was kept constant at 6°C the circulating liquid becomes turbid in the course the experiment.

Flux and Eumulgin ES concentrations in the permeate for an ultrafiltration at 35°C are depicted in Figure 8.5. As can be seen, the flux declines to 0.2 ml/min, while the surfactant concentration in the permeates slightly increases from 1 g/L to 3 g/L.
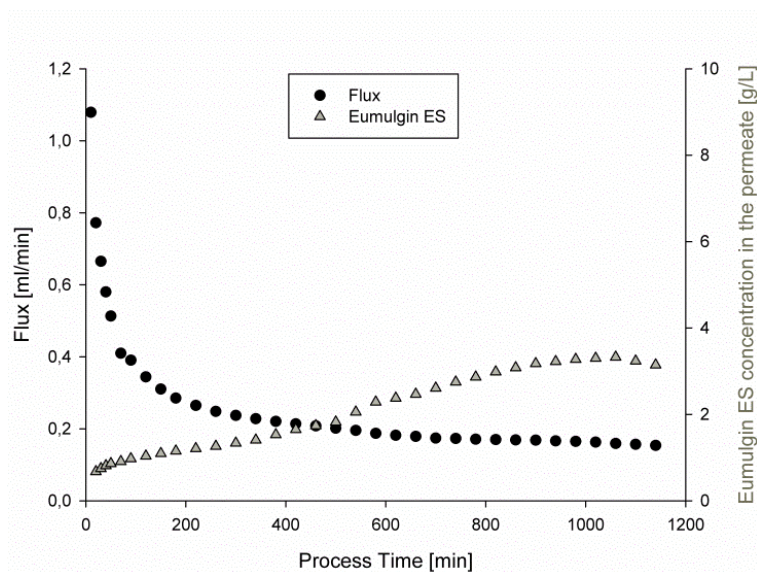
Figure 8.5. Ultrafiltration of Eumulgin ES in a 30 kDa membrane at 35°C. The flux decreases exponentially and Eumulgin ES concentration in the permeates increase slightly.

Based on the calculations in Table 8.3, spherical Eumulgin ES micelles are too large to pass the 30 kDa membrane. Yet, as shown in the Figure 8.4 and Figure 8.5 the concentrations of the permeates are higher than the cmc. A concentration profile above the cmc in the permeates has been reported for PES membranes [13] and was explained by adsorption of the surfactants to the hydrophobic membrane pores.

The reduction of the flux especially at elevated temperatures can also be explained by an extension of the concentration polarization model described by Jonsson [27]. According to this model surfactants accumulate at the filtrate side of the membrane and form micelles. As the micelle concentration is further increased a phase boundary is created and the flux and surfactant through the membrane is dependent on this micelle concentration at the membrane [27]. In this model the surfactants form monodisperse micelles and the surfactant concentration in the filtrate can be below or above the cmc. It is well known however, that nonionic surfactants tend to form large micelles when exceeding a certain concentration or temperature [28]. An increase in temperature or significant increase of surfactant concentration at the membrane surface is therefore likely to lead to the formation of large micelles and thus to the creation of an AMTPS with two phases at the membrane. The principle is shown in Figure 8.6.
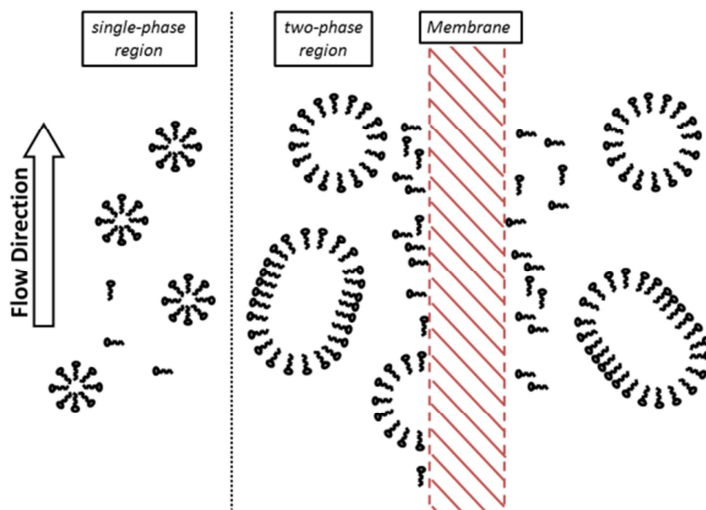
Figure 8.6: Concentration polarization of nonionic surfactants. At the filtrate side of the ultrafiltration membrane the concentration of the nonionic surfactant in the feed c_F is above the cmc. Close to the membrane, a dense micelle rich phase is formed containing large micelles and surfactant monomers. The surfactants molecules can pass the membrane resulting in a concentration c_P at the permeate side which is much higher than the cmc and in some cases even higher than the average surfactant concentration on the retentate side (see Figure 8.9).

The creation of these large micelles at the surface of the membrane leads to an increase in the viscosity. According to Equation 8.4 the increase of the viscosity leads to the decrease of the flux. This effect is confirmed from comparing the flux in Figure 8.7 and Figure 8.8 for the different temperatures: At higher temperatures, the micellar growth is more pronounced, thus the viscosity is increased - and the flux through the membrane is decreased. The formation of an AMTPS can also be confirmed by the occurrence of a turbid ("cloudy") phase during the filtration at 6°C. This occurrence was also described elsewhere [11].

The total surfactant removal in the filtration experiments at 6°C and 35°C calculated according to Equation 8.3 was compared. Figure 8.7 and Figure 8.8 present the resulting diagram for 6°C and 35° respectively for a total process time of 960 minutes and 1140 minutes. 68.4% of the surfactant is removed at 6°C and the total volume is exchanged twice. As can be seen from Figure 8.7 the fraction of removed surfactant reaches saturation.
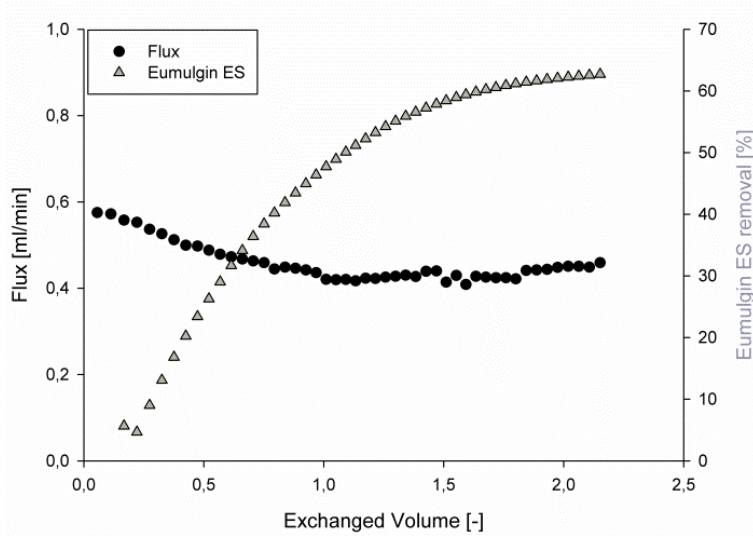
Figure 8.7. Ultrafiltration of Eumulgin ES in a 30 kDa membrane at 6°C for 960 minutes. The removal of surfactant is calculated by the concentrations in the permeate. 68.4 % of the surfactant is removed by exchanging the total volume two times.

During the filtration at 35°C the total volume that was exchanged 1.2 times. 24 % of the total Eumulgin ES was removed in the course of the filtration and the fraction of removed surfactant did not reach saturation.
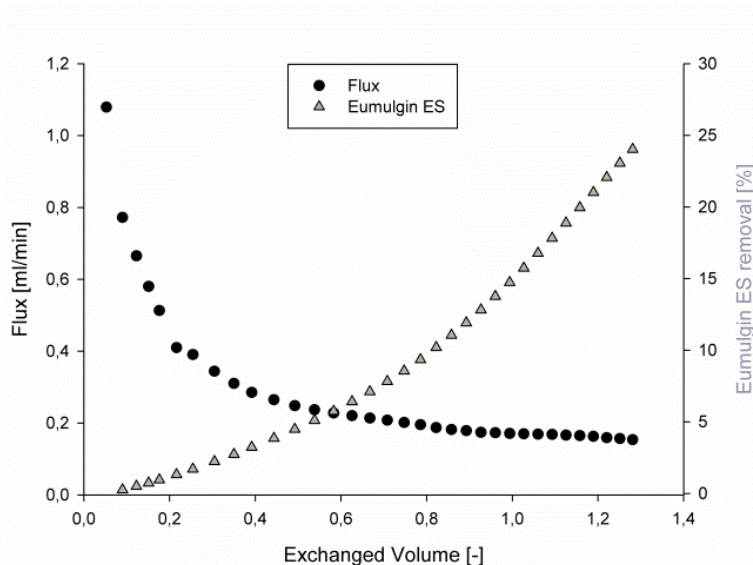
Figure 8.8. Ultrafiltration of Eumulgin ES in a 30 kDa membrane at 35°C for 1140 minutes. The removal of surfactant is calculated by the concentrations in the permeate. 24% of the surfactant is removed by exchanging the total volume two times.

The remaining Eumulgin ES concentration in the circulating streams was additionally determined to investigate the amount of Eumulgin ES that was accumulated to the

membrane. Table 8.4 summarizes the results for the Eumulgin ES filtration at 6°C and 35°C.

Table 8.4: . Process parameters for the ultrafiltration of a 1% Eumulgin ES solution using a 30 kDa PES membrane.

Temperature [°C]	6°C	35°C
Process Time[h]	960 min	1140 min
Exchanged Volume [-]	2.2	1.2
Eumulgin ES Removal [%]	68.4%	24%
Circulating Eumulgin ES concentration in the retentate	0.32 g/L	3.4 g/L
Removal calculated from the circulating concentration	96.5 %	67.4 %
Calculated amount of Eumulgin ES at the membrane surface	28.1 %	43.4 %

From the retentate concentration, the amount of separated surfactant at 6°C is calculated to 96.5%, while it is 67.4% for 35°C. The amount of surfactant accumulated at the membrane was calculated by analyzing the total Eumulgin ES amount in permeate c.f. the retentate. For 6°C 28.1% of the surfactant is still attached to the membrane, and 43.4% for 35°C respectively. This is in concordance to the theory of expanded micelle polarization, as in case of the filtration at 35°C the micelles formed are larger that at 6°C and more Eumulgin ES is adsorbed to the ultrafiltration membrane due to hydrophobic interaction [29].

Summarizing the separation performance, filtration at 6°C is preferred to filtration at 35°C. Applying the same experimental conditions, the flux is increased and the amount of surfactant removed is significantly higher than at 35°C.

8.4.3.3 Effect of NaCl on the filtration performance

In order to investigate the influence of salt to the filtration, Eumulgin ES solutions of 1% and 0.1 % respectively were prepared containing 1 M and 0.5 M NaCl. The solutions were filtered by a 30 kDa PES membrane while the temperature was kept constant at 6 °C. Figure 8.9 shows the resulting concentrations of NaCl, Eumulgin ES and flux through the membrane for the filtration of a 1 % Eumulgin ES, 1 M NaCl solution and Figure 8.10 the same data for a 0.1 % Eumulgin ES, 0.5 M NaCl filtration.
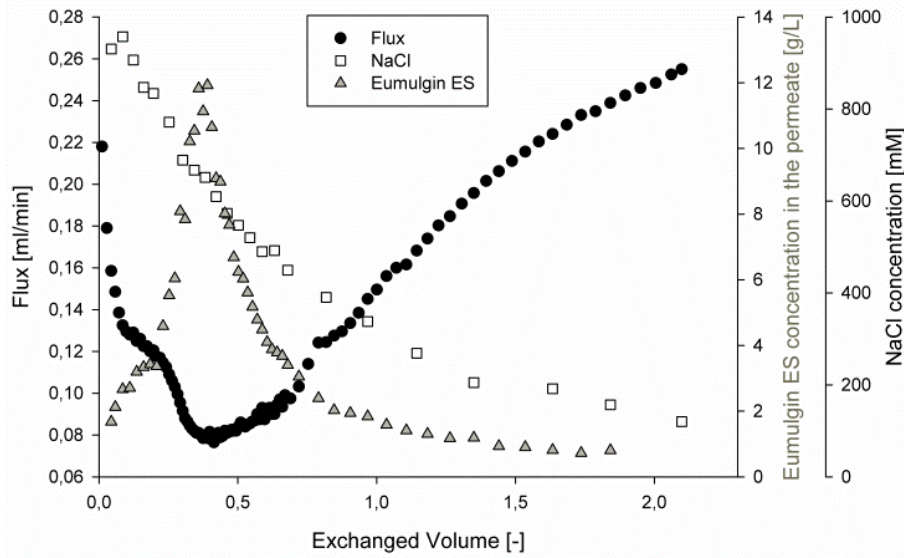
Figure 8.9: Ultrafiltration of a 1% Eumulgin ES solution in 1M NaCl using a 30 kDa membrane at 6°C. The flow rate decreases to a minimum, while the Eumulgin ES concentration increases to a maximum. With ongoing removal of the salt, the flow rate increases and the Eumulgin ES concentration in the permeates declines
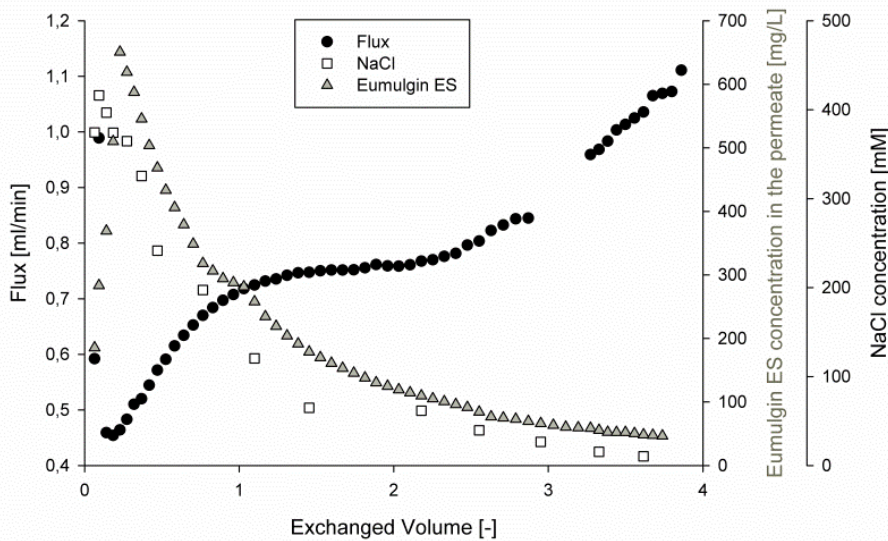
Figure 8.10: Ultrafiltration of a 0.1% Eumulgin ES solution in 0.5M NaCl using a 30 kDa membrane at 6°C. The flow rate decreases to a minimum, while the Eumulgin ES concentration increases to a maximum. As the NaCl is filtered through the membrane, the flow rate increases and the Eumulgin ES concentration in the permeates declines

Figure 8.9 and Figure 8.10 exhibit the very same trends: the flow rate decreases up to a minimum and is then increasing again with decreasing salt concentration. The Eumulgin ES concentration increases with decreasing flow rate and decreases with increasing flow

rate, while the salt concentration is unaffected of both, flow rate and surfactant concentration. These results can be explained by the extended surfactant polarization: NaCl lowers the cmc of nonionic surfactants and shifts the phase diagram (or the cloud point) of AMTPS to lower temperatures [30]. The effect of salt onto the phase separation curve is schematically shown in Figure 11 for a constant filtration temperature T_F. Due to the initial NaCl concentration at the membrane, large micelles form and the viscosity reaches a maximum at concentration c_0 in Figure 8.11. Consequently, the flux through the membrane reaches a minimum due to the high viscosity of the micelle rich phase at the membrane. While the NaCl is filtered through the membrane the cmc is consequently increased and the phase separation curve is shifted upwards. This results in a lower surfactant concentration at the membrane (c_1 in Figure 8.11) and consequently, the viscosity decreases and the Eumulgin ES flux through the membrane increases.
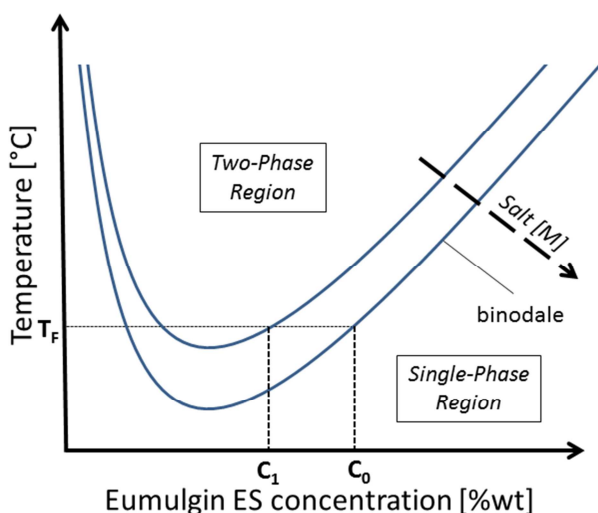
Figure 8.11: Scheme of the influence of salt onto the phase diagram of an Eumulgin ES AMTPS. The binodale separates the single phase region from the two-phase region. With increasing salt concentration, the binodale is lowered. When the salt is removed (by filtration) the binodale is lifted and the boundary concentration c_0 of the surfactant rich phase is reduced to c_1 at a constant temperature T_F.

In summary, NaCl has a temporal effect on the filtration performance of the filtration of Eumulgin ES, but as the salt is removed due to the filtration process, the effect is neutralized.

8.4.4 Removal of Eumulgin ES from a proteinaceous solution

Finally, the applicability of cross-flow ultrafiltration for the removal of Eumulgin ES from a proteinaceous solution was investigated. In this case, the initial solution originated from the application of magnetic extraction for the separation and subsequent enrichment of a 50 kDa target protein in the micelle poor phase of an Eumulgin ES based AMTPS. The remaining Eumulgin ES concentration in the product stream of this process was 0.34 g/L. A 10 kDa PES filter was used in order to retain the target protein in the retentate. In a total process time of 13 hours the volume was exchanged 8.4 times. Only in the permeate the surfactant concentration was determined by TOC measurements, as the retentate also contained the target protein, which would have interfered with the TOC measurement. Figure 8.12 shows the course of the surfactant removal as a function of the exchanged volume. The surfactant can be removed by means of the 10 kDa PES with a concentration of 0.04 g/L remaining and thus resulting in a total surfactant removal of >98.8%.
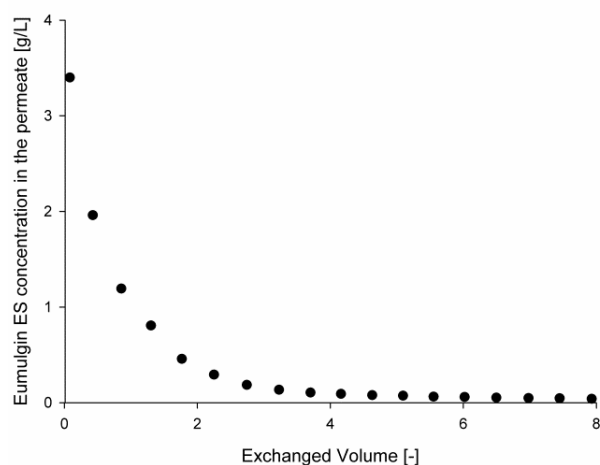
Figure 8.12: Removal of Eumuglin ES as polishing step of a surfactant based separation process

The protein concentration in the retentate was monitored by the comparison of the initial solution and the solution after the filtration by means of coomassie blue stained SDS PAGE and following densiometric analysis. Figure 8.13 shows the resulting SDS gel. From the difference of the band intensity, the loss of the target protein was roughly estimated to 49.8 %. This may be on the one hand attributed to the thermal instability of the protein, which probably has a pronounced effect at the long process time of 13.4 hours.

In addition to this, the shear stress from the cross-flow at the filter surface may also have led to the denaturation of the target protein. The band pattern on the SDS gel in Figure 8.13 however reveals, that the proteins are retained from the 10 kDa filter, and therefore, are separated from Eumulgin ES.

Although room for improvement of the total protein recovery is given, the filtration demonstrates that the separation of the phase forming surfactants from a protein as polishing step in a magnetic extraction process can be achieved by cross-flow ultrafiltration.
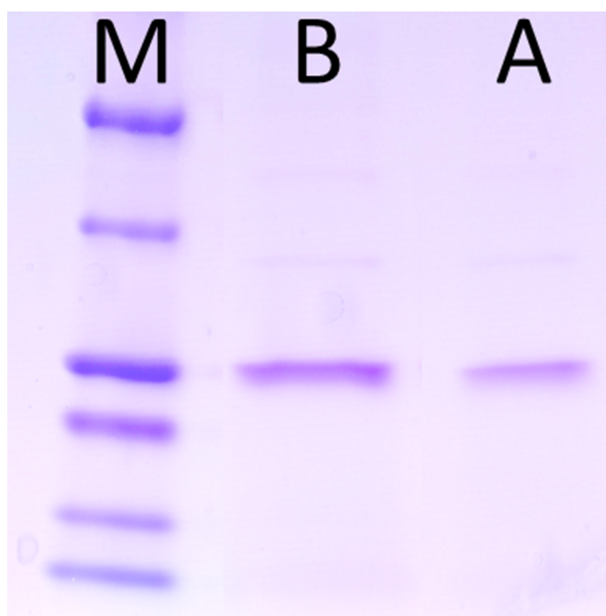
Figure 8.13. SDS PAGE analysis of the target protein in the initial solution and the retentate after ultrafiltration applying a 10 kDa PES membrane at a process time of 13.4 hours. M: Protein standard; B: Protein solution before filtration; A: Protein solution after filtration. Approximately 50 % of the target protein is lost during filtration.

8.5 Conclusion

The properties of the nonionic surfactant Eumulgin ES, the cmc and the hydrodynamic diameter have been investigated. Furthermore, the removal of Eumulgin ES from aqueous solutions has been discussed. The results show, that at high Eumulgin ES concentrations filtration is the method of choice because the surfactant can be removed through the membrane and thus filtration is favorable c.f. adsorptive techniques. During filtration, a micelle rich phase forms at the ultrafiltration membrane, described as surfactant

concentration polarization. The extent of this polarization is directly influenced by the temperature as well as from the presence of sodium chloride. The creation of the micelle rich phase at the membrane leads to an increase of the viscosity and therefore to a decrease of the flux through the membrane. Although the flux is decreased, the nonionic surfactant Eumulgin ES can be removed by ultrafiltration with concentrations in the permeate much higher than the cmc. Low temperatures and NaCl concentrations are favorable as they counteract the formation of the surfactant concentration polarization at the membrane surface. Using cross-flow ultrafiltration, the separation of a protein from an Eumulgin ES containing solution was achieved by holding the target protein back in the retentate and removing the surfactant with the permeate with a total surfactant removal of >98.8 %. Although 50% of the target protein was lost in the first experiments, the surfactant removal by means of ultrafiltration as polishing step in a bioseparation process was demonstrated.

8.6   References

[1] C. Bordier, Phase-Separation of Integral Membrane-Proteins in Triton X-114 Solution, Journal of Biological Chemistry, 256 (1981) 1604-1607.

[2] A. Singh, J.D. Van Hamme, O.P. Ward, Surfactants in microbiology and biotechnology: Part 2. Application aspects, Biotechnology Advances, 25 (2007) 99-121.

[3] H. Tani, T. Kamidate, H. Watanabe, Micelle-mediated extraction, Journal of Chromatography A, 780 (1997) 229-241.

[4] C.O. Rangel-Yagui, A. Pessoa, D. Blankschtein, Two-phase aqueous micellar systems - An alternative method for protein purification, Brazilian Journal of Chemical Engineering, 21 (2004) 531-544.

[5] J.L. Rigaud, D. Levy, G. Mosser, O. Lambert, Detergent removal by non-polar polystyrene beads - Applications to membrane protein reconstitution and two-dimensional crystallization, European Biophysics Journal with Biophysics Letters, 27 (1998) 305-319.

[6] T.M. Allen, A.Y. Romans, H. Kercret, J.P. Segrest, Detergent Removal during Membrane Reconstitution, Biochimica Et Biophysica Acta, 601 (1980) 328-342.

[7] P.W. Holloway, Simple Procedure for Removal of Triton X-100 from Protein Samples, Analytical Biochemistry, 53 (1973) 304-308.

[8] M. Schwarze, D.K. Le, S. Wille, A. Drews, W. Arlt, R. Schomacker, Stirred cell ultrafiltration of aqueous micellar TX-100 solutions, Separation and Purification Technology, 74 (2010) 21-27.

[9] D. Doulia, I. Xiarchos, Ultrafiltration of micellar solutions of nonionic surfactants with or without alachlor pesticide, Journal of Membrane Science, 296 (2007) 58-64.

[10] A.A. Mungray, S.V. Kulkarni, A.K. Mungray, Removal of heavy metals from wastewater using micellar enhanced ultrafiltration technique: a review, Central European Journal of Chemistry, 10 (2012) 27-46.

[11] J.S. Yang, K. Baek, J.W. Yang, Crossflow ultrafiltration of surfactant solutions, Desalination, 184 (2005) 385-394.

[12] R. Urbanski, E. Goralska, H.J. Bart, J. Szymanowski, Ultrafiltration of surfactant solutions, Journal of Colloid and Interface Science, 253 (2002) 419-426.

[13] H. Byhlin, A.S. Jonsson, Influence of adsorption and concentration polarisation on membrane performance during ultrafiltration of a non-ionic surfactant, Desalination, 151 (2003) 21-31.

[14] I. Fischer, M. Franzreb, Nanoparticle Mediated Protein Separation in Aqueous Micellar Two-Phase Systems, Solvent Extraction and Ion Exchange, 30 (2012) 1-16.

[15] I. Xiarchos, D. Doulia, V. Gekas, G. Tragardh, Polymeric ultrafiltration membranes and surfactants, Separation and Purification Reviews, 32 (2003) 215-278.

[16] J.S. Becker, O.R.T. Thomas, M. Franzreb, Protein separation with magnetic adsorbents in micellar aqueous two-phase systems, Separation and Purification Technology, 65 (2009) 46-53.

[17] I. Fischer, M. Franzreb, Direct determination of the composition of aqueous micellar two-phase systems (AMTPS) using potentiometric titration-A rapid tool for detergent-based bioseparation, Colloids and Surfaces a-Physicochemical and Engineering Aspects, 377 (2011) 97-102.

[18] C.A. Schneider, W.S. Rasband, K.W. Eliceiri, NIH Image to ImageJ: 25 years of image analysis, Nature Methods, 9 (2012) 671-675.

[19] T. Arai, K. Takasugi, K. Esumi, Micellar properties of nonionic saccharide surfactants with amide linkage in aqueous solution, Colloids and Surfaces a-Physicochemical and Engineering Aspects, 119 (1996) 81-85.

[20] M.R. Vidal-Paruta, L.D. King, Critical Micelle Concentration of Nonionic Surfactants in Water and Carbon Tetrachloride, J Pharm Sci, 53 (1964) 1217-1220.

[21] H.C. Teh, G.H. Ong, S.C. Ng, L.M. Gan, Light-Scattering from Triton X-100 in Water-Isopropanol Solutions, Physics Letters A, 78 (1980) 487-490.

[22] M. Corti, V. Degiorgio, Light-Scattering Study on Micellar Properties of a Nonionic Surfactant, Optics Communications, 14 (1975) 358-362.

[23] K. Streletzky, G.D.J. Phillies, Temperature-Dependence of Triton X-100 Micelle Size and Hydration, Langmuir, 11 (1995) 42-47.

[24] M. Zulauf, K. Weckstrom, J.B. Hayter, V. Degiorgio, M. Corti, Neutron-Scattering Study of Micelle Structure in Isotropic Aqueous-Solutions of Poly(Oxyethylene) Amphiphiles, Journal of Physical Chemistry, 89 (1985) 3411-3417.

[25] A. Rahman, C.W. Brown, Effect of Ph on the Critical Micelle Concentration of Sodium Dodecyl-Sulfate, Journal of Applied Polymer Science, 28 (1983) 1331-1334.

[26] G. Kopperschlager, G. Birkenmeier, Affinity partitioning and extraction of proteins, Bioseparation, 1 (1990) 235-254.

[27] A.S. Jonsson, B. Jonsson, H. Byhlin, A concentration polarization model for the ultrafiltration of nonionic surfactants, Journal of Colloid and Interface Science, 304 (2006) 191-199.

[28] Y.J. Nikas, C.L. Liu, T. Srivastava, N.L. Abbott, D. Blankschtein, Protein Partitioning in 2-Phase Aqueous Nonionic Micellar Solutions, Macromolecules, 25 (1992) 4797-4806.

[29] I. Xiarchos, D. Doulia, Interaction behavior in ultrafiltration of nonionic surfactant micelles by adsorption, Journal of Colloid and Interface Science, 299 (2006) 102-111.

[30] T. Gu, P.A. Galeragomez, Clouding of Triton-X-114 - the Effect of Added Electrolytes on the Cloud Point of Triton-X-114 in the Presence of Ionic Surfactants, Colloids and Surfaces a-Physicochemical and Engineering Aspects, 104 (1995) 307-312.

9 Conclusion and Outlook

In the course of this thesis a process was designed that allows the continuous separation of magnetic particles in an AMTPS, while the particles themselves serve as carriers of a particular target protein – continuous magnetic extraction. Initially, proper process analytics were established. The proof of concept was subsequently demonstrated by the separation of lysozyme from ovalbumin using magnetic cation exchange particles. The process was finally applied to purify the antibody fragment Fab α33 produced by an *E. coli* fermentation. The minimal particle and surfactant loss during the continuous operation demonstrated its potential as unit operation in downstream processing.

As only one exemplar of the equipment was built, it allowed the continuous processing of only one step, either binding, wash or elution. Therefore, the effluent streams had to be collected and the stream containing the product had to be reinjected into the set-up in the course of the next step. In order to establish a real continuous process these steps should be performed in parallel, minimizing the idle times of the collected streams. Therefore, a cascade of magnetic extraction units should be installed where the flow rates as well as the dosing of buffers will have to be adjusted in a complex regulative process. In order to guarantee the stability of a long term magnetic extraction process, an increased recyclability of both, the magnetic particles and the surfactants should be pursued.

In the course of the demonstrated separation, the applied stream had been clarified by centrifugation before continuous magnetic extraction was performed. Therefore, a future task will be the separation of feedstocks containing high loads of solid contaminants. Especially hydrophobic contaminations, e.g. cell debris, are likely to partition into the micelle rich phase of the Eumulgin ES based AMTPS. It has to be investigated if the removal of such contaminations from the magnetic phase can be performed by adjusting the weir (or the flow rate) so that only the particles floating at the top of the surfactant rich phase are withdrawn, while the contaminated surfactant phase will have to be discharged together with the contaminations in the binding step. In this scenario a certain

amount surfactant will be lost, the sparing out of a solid-liquid separation process, however, is worth this loss.

It was also shown that the partitioning behavior of the magnetic sorbents in the AMTPS is directly related to the adsorption of the surfactants to the particle surface. These findings can be exploited in order to create tailor-made magnetic beads. The phase forming surfactant should be covalently bound to the magnetic particle – or, if sufficient, only its hydrophobic residue that extends into the feed solution. Such a particle should partition into the micelle rich phase independent of the buffer conditions. An ideal magnetic particle would accordingly be of hybrid nature - exhibiting specific functional ligands to capture the target protein on the one hand and phase forming surfactants as an anchor for the micelle rich phase on the other hand.

10 References

[1] I. Safarik, M. Safarikova, Magnetic techniques for the isolation and purification of proteins and peptides, Biomagn Res Technol, 2 (2004) 7.

[2] M. Franzreb, M. Siemann-Herzberg, T.J. Hobley, O.R.T. Thomas, Protein purification using magnetic adsorbent particles, Applied Microbiology and Biotechnology, 70 (2006) 505-516.

[3] I. Langmuir, The Adsorption of Gases on Plane Surfaces of Glass, Mica and Platinum, J. Am. Chem. Soc., 40 (1918) 1361–1403.

[4] A. Meyer, Einsatz magnettechnologischer Trennverfahren zur Aufbereitung von Molkereiprodukten, PhD Thesis, 2004, Institute of Functional Interfaces, University of Karlsruhe (TH)

[5] M. Franzreb, Magnettechnologie in der Verfahrenstechnik wässriger Medien, Habilitationsschrift, 2003, Institute of Functional Interfaces, Universtiy of Karlsruhe (TH)

[6] J. Svoboda, Magnetic Methods for the Treatment of MInerals, New York, 1987.

[7] L. Michalowski, U. Heinecke, J. Schneider, H. Wich, Magnettechnik: Grundlagen und Anwendungen, Fachbuchverlag Leipzig, Leipzig, 1995.

[8] J.A. Oberteufer, Magnetic Separation - Review of Principles, Devices, and Applications, Ieee Transactions on Magnetics, Ma10 (1974) 223-238.

[9] J.J. Hubbuch, D.B. Matthiesen, T.J. Hobley, O.R.T. Thomas, High gradient magnetic separation versus expanded bed adsorption: a first principle comparison, Bioseparation, 10 (2001) 99-112.

[10] J.J. Hubbuch, O.R.T. Thomas, High-gradient magnetic affinity separation of trypsin from porcine pancreatin, Biotechnology and Bioengineering, 79 (2002) 301-313.

[11] A. Heeboll-Nielsen, W.S. Choe, A.P.J. Middelberg, O.R.T. Thomas, Efficient inclusion body processing using chemical extraction and high gradient magnetic fishing, Biotechnology Progress, 19 (2003) 887-898.

[12] A. Heeboll-Nielsen, M. Dalkiaer, J.J. Hubbuch, O.R.T. Thomas, Superparamagnetic adsorbents for high-gradient magnetic fishing of lectins out of legume extracts, Biotechnology and Bioengineering, 87 (2004) 311-323.

[13] A. Heeboll-Nielsen, S.F.L. Justesen, T.J. Hobley, O.R.T. Thomas, Superparamagnetic cation-exchange adsorbents for bioproduct recovery from crude process liquors by high-gradient magnetic fishing, Separation Science and Technology, 39 (2004) 2891-2914.

[14] C. Hoffmann, Einsatz magnetischer Separationsverfahren zur biotechnologischen Produktaufarbeitung, PhD Thesis, 2002, Institute of Functional Interfaces, University of Karlsruhe (TH)

[15] N. Ebner, Einsatz von Magnettrenntechnologie bei der Bioproduktaufarbeitung, PhD Thesis, 2006, Institute of Functional Interfaces, University of Karlsruhe (TH)

[16] A. Meyer, D.B. Hansen, C.S.G. Gomes, T.J. Hobley, O.R.T. Thomas, M. Franzreb, Demonstration of a strategy for product purification by high-gradient magnetic fishing: Recovery of superoxide dismutase from unconditioned whey, Biotechnology Progress, 21 (2005) 244-254.

[17] A. Meyer, S. Berensmeier, M. Franzreb, Direct capture of lactoferrin from whey using magnetic micro-ion exchangers in combination with high-gradient magnetic separation, Reactive & Functional Polymers, 67 (2007) 1577-1588.

[18] C. Müller, Magnettechnologische Reinigung von Gonadotropin aus Pferdeserum, PhD Thesis, 2011, Institute of Functional Interfaces, Karlsruhe Institute of Technology

[19] J. Lindner, K. Wagner, C. Eichholz, H. Nirschl, Efficiency Optimization and Prediction in High-Gradient Magnetic Centrifugation, Chemical Engineering & Technology, 33 (2010) 1315-1320.

[20] M.W. Beijerinck, Über eine Eigentümlichkeit der löslichen Stärke, Zentralblatt für Bakteriologie, Parasitenkunde und Infektionskrankheiten, 2 (1896) 697-699.

[21] P.A. Albertsson, Chromatography and Partition of Cells and Cell Fragments, Acta Chemica Scandinavica, 10 (1956) 148-148.

[22] P.A. Albertsson, Partition of Cell Particles and Macromolecules, John Wiley and Sons, New York, 1986.

[23] B. Montalvo-Hernandez, M. Rito-Palomares, J. Benavides, Recovery of crocins from saffron stigmas (Crocus sativus) in aqueous two-phase systems, Journal of Chromatography A, 1236 (2012) 7-15.

[24] N. Pietruszka, I.Y. Galaev, A. Kumar, Z.K. Brzozowski, B. Mattiasson, New polymers forming aqueous two-phase polymer systems, Biotechnology Progress, 16 (2000) 408-415.

[25] N.J. Bridges, K.E. Gutowski, R.D. Rogers, Investigation of aqueous biphasic systems formed from solutions of chaotropic salts with kosmotropic salts (salt-salt ABS), Green Chemistry, 9 (2007) 177-183.

[26] J. Huddleston, A. Veide, K. Kohler, J. Flanagan, S.O. Enfors, A. Lyddiatt, The Molecular-Basis of Partitioning in Aqueous 2-Phase Systems, Trends in Biotechnology, 9 (1991) 381-388.

[27] M.J. Boland, Aqueous two-phase extraction and purification of animal proteins, Molecular Biotechnology, 20 (2002) 85-93.

[28] M.R. Helfrich, M. El-Kouedi, M.R. Etherton, C.D. Keating, Partitioning and assembly of metal particles and their bioconjugates in aqueous two-phase systems, Langmuir, 21 (2005) 8478-8486.

[29] A.B. Mageste, L.R. de Lemos, G.M.D. Ferreira, M.D.H. da Silva, L.H.M. da Silva, R.C.F. Bonomo, L.A. Minim, Aqueous two-phase systems: An efficient, environmentally safe and economically viable method for purification of natural dye carmine, Journal of Chromatography A, 1216 (2009) 7623-7629.

[30] F. Luechau, T.C. Ling, A. Lyddiatt, Primary capture of high molecular weight nucleic acids using aqueous two-phase systems, Separation and Purification Technology, 66 (2009) 202-207.

[31] S.G. Walker, A. Lyddiatt, Processing of nanoparticulate bioproducts: application and optimisation of aqueous two-phase systems, Journal of Chemical Technology and Biotechnology, 74 (1999) 250-255.

[32] A.M. Azevedo, A.G. Gomes, P.A.J. Rosa, I.F. Ferreira, A.M.M.O. Pisco, M.R. Aires-Barros, Partitioning of human antibodies in polyethylene glycol-sodium citrate aqueous two-phase systems, Separation and Purification Technology, 65 (2009) 14-21.

[33] V.G. Lacerda, A.B. Mageste, I.J.B. Santos, L.H.M. da Silva, M.D.H. da Silva, Separation of Cd and Ni from Ni-Cd batteries by an environmentally safe methodology employing aqueous two-phase systems, Journal of Power Sources, 193 (2009) 908-913.

[34] Y. Xu, M.A. Souza, M.Z.R. Pontes, M. Vitolo, A. Pessoa, Liquid-liquid extraction of enzymes by affinity aqueous two-phase systems, Brazilian Archives of Biology and Technology, 46 (2003) 741-750.

[35] J.A. Asenjo, B.A. Andrews, Aqueous two-phase systems for protein separation: A perspective, Journal of Chromatography A, 1218 (2011) 8826-8835.

[36] F. Ruiz-Ruiz, J. Benavides, O. Aguilar, M. Rito-Palomares, Aqueous two-phase affinity partitioning systems: Current applications and trends, Journal of Chromatography A, 1244 (2012) 1-13.

[37] P.G. Mazzola, A.M. Lopes, F.A. Hasmann, A.F. Jozala, T.C.V. Penna, P.O. Magalhaes, C.O. Rangel-Yagui, A. Pessoa, Liquid-liquid extraction of biomolecules: an overview and update of the main techniques, Journal of Chemical Technology and Biotechnology, 83 (2008) 143-157.

[38] K. Naganagouda, V.H. Mulimani, Aqueous two-phase extraction (ATPE): An attractive and economically viable technology for downstream processing of Aspergillus oryzae alpha-galactosidase, Process Biochemistry, 43 (2008) 1293-1299.

[39] W. McCabe, Smith, J., Harriot, P., Unit Operations of Chemical Engineering, Seventh ed., McGraw-Hill, New York, 2005.

[40] H. Tani, T. Kamidate, H. Watanabe, Aqueous micellar two-phase systems for protein separation, Analytical Sciences, 14 (1998) 875-888.

[41] Y.X. Huang, G.M. Thurston, D. Blankschtein, G.B. Benedek, The Effect of Salt Identity and Concentration on Liquid Liquid-Phase Separation in Aqueous Micellar Solutions of C-8-Lecithin, Journal of Chemical Physics, 92 (1990) 1956-1962.

[42] C.L. Liu, Y.J. Nikas, D. Blankschtein, Partitioning of Proteins Using 2-Phase Aqueous Surfactant Systems, Aiche Journal, 41 (1995) 991-995.

[43] H. Tani, A. Matsuda, T. Kamidate, H. Watanabe, Extraction of proteins based on phase separation in aqueous triblock copolymer surfactant solutions, Analytical Sciences, 13 (1997) 925-929.

[44] H. Tani, Y. Suzuki, A. Matsuda, T. Kamidate, Enhancement of the excluded-volume effect in protein extraction using triblock copolymer-based aqueous micellar two-phase systems, Analytica Chimica Acta, 429 (2001) 301-309.

[45] D.T. Kamei, J.A. King, D.I.C. Wang, D. Blankschtein, Separating lysozyme from bacteriophage P22 in two-phase aqueous micellar systems, Biotechnology and Bioengineering, 80 (2002) 233-236.

[46] F.H. Quina, W.L. Hinze, Surfactant-mediated cloud point extractions: An environmentally benign alternative separation approach, Industrial & Engineering Chemistry Research, 38 (1999) 4150-4168.

[47] D. Blankschtein, G.M. Thurston, G.B. Benedek, Phenomenological Theory of Equilibrium Thermodynamic Properties and Phase-Separation of Micellar Solutions, Journal of Chemical Physics, 85 (1986) 7268-7288.

[48] S. Puvvada, D. Blankschtein, Molecular-Thermodynamic Approach to Predict Micellization, Phase-Behavior and Phase-Separation of Micellar Solutions .1. Application to Nonionic Surfactants, Journal of Chemical Physics, 92 (1990) 3710-3724.

[49] H. Lam, M. Kavoosi, C.A. Haynes, D.I.C. Wang, D. Blankschtein, Affinity-enhanced protein partitioning in decyl beta-D-glucopyranoside two-phase aqueous micellar systems, Biotechnology and Bioengineering, 89 (2005) 381-392.

[50] D. Blankschtein, Y.X. Huang, G.M. Thurston, G.B. Benedek, Salt Effects on Liquid Liquid-Phase Separation in Aqueous Micellar Solutions of the Zwitterionic Surfactant C8-Lecithin, Langmuir, 7 (1991) 896-897.

[51] D. Blankschtein, G.M. Thurston, G.B. Benedek, Theory of Phase-Separation in Micellar Solutions, Physical Review Letters, 54 (1985) 955-958.

[52] D.T. Kamei, D.I.C. Wang, D. Blankschtein, Fundamental investigation of protein partitioning in two-phase aqueous mixed (nonionic/ionic) micellar systems, Langmuir, 18 (2002) 3047-3057.

[53] H. Tani, T. Kamidate, H. Watanabe, Micelle-mediated extraction, Journal of Chromatography A, 780 (1997) 229-241.

[54] H. Watanabe, H. Tanaka, Nonionic Surfactant as a New Solvent for Liquid-Liquid - Extraction of Zinc(Ii) with 1-(2-Pyridylazo)-2-Naphthol, Talanta, 25 (1978) 585-589.

[55] C. Bordier, Phase-Separation of Integral Membrane-Proteins in Triton X-114 Solution, Journal of Biological Chemistry, 256 (1981) 1604-1607.

[56] A. Sanchezferrer, R. Bru, F. Garciacarmona, Phase-Separation of Biomolecules in Polyoxyethylene Glycol Nonionic Detergents, Critical Reviews in Biochemistry and Molecular Biology, 29 (1994) 275-313.

[57] J.F. Liu, J.B. Chao, R. Liu, Z.Q. Tan, Y.G. Yin, Y. Wu, G.B. Jiang, Cloud Point Extraction as an Advantageous Preconcentration Approach for Analysis of Trace Silver Nanoparticles in Environmental Waters, Analytical Chemistry, 81 (2009) 6496-6502.

[58] E.K. Paleologos, D.L. Giokas, M.I. Karayannis, Micelle-mediated separation and cloud-point extraction, Trac-Trends in Analytical Chemistry, 24 (2005) 426-436.

[59] R.A. Ramelmeier, G.C. Terstappen, M.R. Kula, The partitioning of cholesterol oxidase in Triton X-114-based aqueous two-phase systems, Bioseparation, 2 (1991) 315-324.

[60] G.C. Terstappen, A.J. Geerts, M.R. Kula, The Use of Detergent-Based Aqueous 2-Phase Systems for the Isolation of Extracellular Proteins - Purification of a Lipase from Pseudomonas-Cepacia, Biotechnology and Applied Biochemistry, 16 (1992) 228-235.

[61] G.C. Terstappen, R.A. Ramelmeier, M.R. Kula, Protein Partitioning in Detergent-Based Aqueous 2-Phase Systems, Journal of Biotechnology, 28 (1993) 263-275.

[62] T. Minuth, H. Gieren, U. Pape, H.C. Raths, J. Thommes, M.R. Kula, Pilot scale processing of detergent-based aqueous two-phase systems, Biotechnology and Bioengineering, 55 (1997) 339-347.

[63] T. Minuth, J. Thommes, M.R. Kula, A closed concept for purification of the membrane-bound cholesterol oxidase from Nocardia rhodochrous by surfactant-based cloud-point extraction, organic-solvent extraction and anion-exchange chromatography, Biotechnology and Applied Biochemistry, 23 (1996) 107-116.

[64] K. Selber, F. Tjerneld, A. Collen, T. Hyytia, T. Nakari-Setala, M. Bailey, R. Fagerstrom, J. Kan, J. van der Laan, M. Penttila, M.R. Kula, Large-scale separation and production of engineered proteins, designed for facilitated recovery in detergent-based aqueous two-phase extraction systems, Process Biochemistry, 39 (2004) 889-896.

[65] T. Saitoh, H. Tani, T. Kamidate, T. Kamataki, H. Watanabe, Polymer-Induced Phase-Separation in Aqueous Micellar Solutions of Alkylglucosides for Protein Extraction, Analytical Sciences, 10 (1994) 299-303.

[66] Y.J. Nikas, C.L. Liu, T. Srivastava, N.L. Abbott, D. Blankschtein, Protein Partitioning in 2-Phase Aqueous Nonionic Micellar Solutions, Macromolecules, 25 (1992) 4797-4806.

[67] C.O. Rangel-Yagui, H. Lam, D.T. Kamei, D.I.C. Wang, A. Pessoa, D. Blankstein, Glucose-6-phosphate dehydrogenase partitioning in two-phase aqueous mixed (nonionic/cationic) micellar systems, Biotechnology and Bioengineering, 82 (2003) 445-456.

[68] K.H. Kroner, H. Hustedt, S. Granda, M.R. Kula, Technical Aspects of Separation Using Aqueous 2-Phase Systems in Enzyme Isolation Processes, Biotechnology and Bioengineering, 20 (1978) 1967-1988.

[69] P. Vazquez-Villegas, O. Aguilar, M. Rito-Palomares, Study of biomolecules partition coefficients on a novel continuous separator using polymer-salt aqueous two-phase systems, Separation and Purification Technology, 78 (2011) 69-75.

[70] F. Luechau, T.C. Ling, A. Lyddiatt, Physical characterisations of a single-stage Kuhni-type aqueous two-phase extraction column, Biochemical Engineering Journal, 50 (2010) 90-98.

[71] P.A.J. Rosa, A.M. Azevedo, S. Sommerfeld, W. Backer, M.R. Aires-Barros, Continuous aqueous two-phase extraction of human antibodies using a packed column, Journal of Chromatography B-Analytical Technologies in the Biomedical and Life Sciences, 880 (2012) 148-156.

[72] P. Trakultamupatam, J.F. Scamehorn, S. Osuwan, Scaling up cloud point extraction of aromatic contaminants from wastewater in a continuous rotating disk contactor. I. Effect of disk rotation speed and wastewater to surfactant ratio, Separation Science and Technology, 39 (2004) 479-499.

[73] P. Trakultamupatam, J.F. Scamehorn, S. Osuwan, Scaling up cloud point extraction of. aromatic contaminants from wastewater in a continuous rotating disk contactor. II. Effect of operating temperature and added electrolyte, Separation Science and Technology, 39 (2004) 501-516.

[74] P. Taechangam, J.F. Scamehorn, S. Osuwan, T. Rirksomboon, Continuous Cloud Point Extraction of Volatile Organic Contaminants from Wastewater in a Multi-Stage Rotating Disc Contactor: Effect of Structure and Concentration of Solutes, Separation Science and Technology, 43 (2008) 3601-3623.

[75] T. Ingram, S. Storm, P. Glembin, S. Bendt, D. Huber, T. Mehling, I. Smirnova, Aqueous Surfactant Two-Phase Systems for the Continuous Countercurrent Cloud Point Extraction, Chemie Ingenieur Technik, 84 (2012) 840-848.

[76] G. Kopperschlager, G. Birkenmeier, Affinity partitioning and extraction of proteins, Bioseparation, 1 (1990) 235-254.

[77] G. Takerkart, E. Segard, M. Monsigny, Partition of Trypsin in 2-Phase Systems Containing a Diamidino-Alpha,Omego-Diphenylcarbamyl Poly (Ethylene-Glycol) as Competitive Inhibitor of Trypsin, Febs Letters, 42 (1974) 218-220.

[78] S.D. Flanagan, S.H. Barondes, Affinity Partitioning - Method for Purification of Proteins Using Specific Polymer-Ligands in Aqueous Polymer 2-Phase Systems, Journal of Biological Chemistry, 250 (1975) 1484-1489.

[79] M.C. Tejedor, C. Delgado, M. Grupeli, J. Luque, Affinity Partitioning of Erythrocytic Phosphofructokinase in Aqueous 2-Phase Systems Containing Poly(Ethylene Glycol)-Bound Cibacron Blue - Influence of Ph, Ionic-Strength and Substrates Effectors, Journal of Chromatography, 589 (1992) 127-134.

[80] L.L. Cheng, M. Joelsson, G. Johansson, Combination of Polymer-Bound Charged Groups and Affinity Ligands for Extraction of Enzymes by Partitioning in Aqueous 2-Phase Systems, Journal of Chromatography, 523 (1990) 119-130.

[81] S. Fernandes, H.S. Kim, R. Hatti-Kaul, Affinity extraction of dye- and metal ion-binding proteins in polyvinyl pyrrolidone-based aqueous two-phase system, Protein Expression and Purification, 24 (2002) 460-469.

[82] A.M. Azevedo, P.A.J. Rosa, I.F. Ferreira, A.M.M.O. Pisco, J. de Vries, R. Korporaal, T.J. Visser, M.R. Aires-Barros, Affinity-enhanced purification of human antibodies by aqueous two-phase extraction, Separation and Purification Technology, 65 (2009) 31-39.

[83] P.A.J. Rosa, A.M. Azevedo, I.F. Ferreira, J. de Vries, R. Korporaal, H.J. Verhoef, T.J. Visser, M.R. Aires-Barros, Affinity partitioning of human antibodies in aqueous two-phase systems, Journal of Chromatography A, 1162 (2007) 103-113.

[84] B.A. Andrews, D.M. Head, P. Dunthorne, J.A. Asenjo, PEG Activation and Ligand Binding for the Affinity Partitioning of Proteins in Aqueous Two-Phase Systems, Biotechnology Techniques, 4 (1990) 49-54.

[85] M. Lu, F. Tjerneld, Interaction between tryptophan residues and hydrophobically modified dextran. Effect on partitioning of peptides and proteins in aqueous two-phase systems, Journal of Chromatography A, 766 (1997) 99-108.

[86] M.R. Gavasane, V.G. Gaikar, Aqueous two-phase affinity partitioning of penicillin acylase from E-coli in presence of PEG-derivatives, Enzyme and Microbial Technology, 32 (2003) 665-675.

[87] C.K. Lee, W.D. Su, Nonionic surfactant-mediated affinity cloud-point extraction of vancomycin, Separation Science and Technology, 34 (1999) 3267-3277.

[88] T.T. Franco, A.T. Andrews, J.A. Asenjo, Conservative chemical modification of proteins to study the effects of a single protein property on partitioning in aqueous two-phase systems, Biotechnology and Bioengineering, 49 (1996) 290-299.

[89] T.T. Franco, A.T. Andrews, J.A. Asenjo, Use of chemically modified proteins to study the effect of a single protein property on partitioning in aqueous two-phase systems: Effect of surface hydrophobicity, Biotechnology and Bioengineering, 49 (1996) 300-308.

[90] K. Berggren, A. Veide, P.A. Nygren, F. Tjerneld, Genetic engineering of protein-peptide fusions for control of protein partitioning in thermoseparating aqueous two-phase systems, Biotechnology and Bioengineering, 62 (1999) 135-144.

[91] S. Fexby, A. Nilsson, G. Hambraeus, F. Tjerneld, L. Bulow, Partitioning and characterization of tyrosine-tagged green fluorescent proteins in aqueous two-phase systems, Biotechnology Progress, 20 (2004) 793-798.

[92] L. Ekblad, J. Kernbichler, B. Jergil, Aqueous two-phase affinity partitioning of biotinylated liposomes using neutral avidin as affinity ligand, Journal of Chromatography A, 815 (1998) 189-195.

[93] A.A. Bhide, R.M. Patel, J.B. Joshi, V.G. Pangarkar, Affinity Partitioning of Enzymes Using Unbound Triazine Dyes in Peg/Phosphate System, Separation Science and Technology, 30 (1995) 2989-3000.

[94] T. de Gouveia, B.V. Kilikian, Bioaffinity extraction of glucoamylase in aqueous two-phase systems using starch as free bioligand, Journal of Chromatography B, 743 (2000) 241-246.

[95] S. Teotia, R. Lata, M.N. Gupta, Chitosan as a macroaffinity ligand - Purification of chitinases by affinity precipitation and aqueous two-phase extractions, Journal of Chromatography A, 1052 (2004) 85-91.

[96] S. Fernandes, G. Johansson, R. Hatti-Kaul, Purification of recombinant cutinase by extraction in an aqueous two-phase system facilitated by a fatty acid substrate, Biotechnology and Bioengineering, 73 (2001) 465-475.

[97] S. Teotia, M.N. Gupta, Purification of phospholipase D by two-phase affinity extraction, Journal of Chromatography A, 1025 (2004) 297-301.

[98] A.M. Lopes, A. Pessoa, C.D. Rangel-Yagui, Can affinity interactions influence the partitioning of glucose-6-phosphate dehydrogenase in two-phase aqueous micellar systems?, Quimica Nova, 31 (2008) 998-1003.

[99] T. Saitoh, W.L. Hinze, Use of Surfactant-Mediated Phase-Separation (Cloud Point Extraction) with Affinity Ligands for the Extraction of Hydrophilic Proteins, Talanta, 42 (1995) 119-127.

[100] P.O. Hedman, J.G. Gustafsson, Protein Adsorbents Intended for Use in Aqueous 2-Phase Systems, Analytical Biochemistry, 138 (1984) 411-415.

[101] B. Mattiasson, T.G.I. Ling, Efforts to Integrate Affinity Interactions with Conventional Separation Technologies - Affinity Partition Using Biospecific Chromatographic Particles in Aqueous 2-Phase Systems, Journal of Chromatography, 376 (1986) 235-243.

[102] A. Kondo, T. Kaneko, K. Higashitani, Purification of Fusion Proteins Using Affinity Microspheres in Aqueous 2-Phase Systems, Applied Microbiology and Biotechnology, 40 (1993) 365-369.

[103] Y.J. Kwon, R. Hatti-Kaul, Protein separation using metal ion-bound particles in aqueous two-phase system, Biotechnology Techniques, 13 (1999) 145-148.

[104] M. Roobol-Boza, V. Dolby, M. Doverskog, A. Barrefelt, F. Lindqvist, U.C. Oppermann, K.K. Van Alstine, F. Tjerneld, Membrane protein isolation by in situ solubilization, partitioning and affinity adsorption in aqueous two-phase systems - Purification of the human type 1 11 beta-hydroxysteroid dehydrogenase, Journal of Chromatography A, 1043 (2004) 217-223.

[105] C.A. Ku, J.D. Henry, J.B. Blair, Affinity-Specific Protein Separations Using Ligand-Coupled Particles in Aqueous 2-Phase Systems .2. Recovery and Purification of Pyruvate-Kinase and Alcohol-Dehydrogenase from Saccharomyces-Cerevisiae, Biotechnology and Bioengineering, 33 (1989) 1089-1097.

[106] C.A. Ku, J.D. Henry, J.B. Blair, Affinity-Specific Protein Separations Using Ligand-Coupled Particles in Aqueous 2-Phase Systems .1. Process Concept and Enzyme Binding-Studies for Pyruvate-Kinase and Alcohol-Dehydrogenase from Saccharomyces-Cerevisiae, Biotechnology and Bioengineering, 33 (1989) 1081-1088.

[107] M. Suzuki, M. Kamihira, T. Shiraishi, H. Takeuchi, T. Kobayashi, Affinity Partitioning of Protein-a Using a Magnetic Aqueous 2-Phase System, Journal of Fermentation and Bioengineering, 80 (1995) 78-84.

[108] Q. Gai, F. Qu, T. Zhang, Y. Zhang, Integration of carboxyl modified magnetic particles and aqueous two-phase extraction for selective separation of proteins, Talanta, 85 (2011) 304-309.

[109] P. Wikstrom, S. Flygare, A. Grondalen, P.O. Larsson, Magnetic Aqueous 2-Phase Separation - a New Technique to Increase Rate of Phase-Separation, Using Dextran Ferrofluid or Larger Iron-Oxide Particles, Analytical Biochemistry, 167 (1987) 331-339.

[110] P.O. Larsson, Magnetically Enhanced Phase-Separation, Aqueous Two-Phase Systems, 228 (1994) 112-117.

[111] S. Flygare, P. Wikstrom, G. Johansson, P.O. Larsson, Magnetic Aqueous 2-Phase Separation in Preparative Applications, Enzyme and Microbial Technology, 12 (1990) 95-103.

[112] J.S. Becker, Einsatz magnetischer Extraktionsphasen zur Bioproduktaufarbeitung, PhD Thesis, 2009, Institute of Functional Interfaces, University of Karlsruhe (TH)

[113] H. Walter, D.E. Brooks, D. Fisher, Partitioning in aqueous two-phase systems: theory, methods, uses, and application to biotechnology, Academic Press, Orlando, Florida, 1985.

[114] M.A. Hoeben, R.G.J.M. van der Lans, L.A.M. van der Wielen, Kinetic model for separation of particle mixtures by interfacial partitioning, Aiche Journal, 50 (2004) 1156-1168.

[115] S.M. Baxter, P.R. Sperry, Z.W. Fu, Partitioning of Polymer and Inorganic Colloids in Two-Phase Aqueous Polymer Systems, Langmuir, 13 (1997) 3948-3952.

[116] X. Zeng, K. Osseo-Asare, Partitioning behavior of silica in the Triton X-100/dextran/water aqueous biphasic system, Journal of Colloid and Interface Science, 272 (2004) 298-307.

[117] X. Zeng, J. Quaye, K. Osseo-Asare, Partition of hematite in the Triton X-100/Dextran aqueous biphase system, Colloids and Surfaces a-Physicochemical and Engineering Aspects, 246 (2004) 135-145.

[118] H.S. Garewal, Procedure for Estimation of Microgram Quantities of Triton X-100, Analytical Biochemistry, 54 (1973) 319-324.

[119] A. Barber, C.C.T. Chinnick, P.A. Lincoln, The Analysis of Mixtures of Surface-Active Quaternary Ammonium Compounds and Polyethylene Oxide Type of Non-Ionic Surface-Active Agents, Analyst, 81 (1956) 18-25.

[120] L.S. Lagutina, K.F. Sholts, Turbidimetric method for quantitative determination of Triton X-100 with silicotungstic acid, Applied Biochemistry and Microbiology, 38 (2002) 294-297.

[121] S. Rajakumari, M. Srinivasan, R. Rajasekharan, Spectrophotometric method for quantitative determination of nonionic, ionic and zwitterionic detergents, Journal of Biochemical and Biophysical Methods, 68 (2006) 133-137.

[122] Metrohm, Titrimetric/potentiometric determination of non-ionic surfactants based on polyoxyethylene adducts using the NIO electrode, Application Bulletin 230/1 e.

[123] M. Sak-Bosnar, Z. Grabaric, B.S. Grabaric, Surfactant sensors in biotechnology part 1 - Electrochemical sensors, Food Technology and Biotechnology, 42 (2004) 197-206.

[124] M. Sak-Bosnar, D. Madunic-Cacic, R. Matesic-Puac, Z. Grabaric, Sensitive potentiometric method for determination of micromolar level of polyethoxylated nonionic surfactants in effluents, Tenside Surfactants Detergents, 44 (2007) 11-18.

[125] M. Sak-Bosnar, D. Madunic-Cacic, N. Sakac, O. Galovic, M. Samardzic, Z. Grabaric, Potentiometric sensor for polyethoxylated nonionic surfactant determination, Electrochimica Acta, 55 (2009) 528-534.

[126] J.X. Zhao, W. Brown, Adsorption of a Nonionic Surfactant (C(12)E(7)) on Carboxylated Styrene-Butadiene Copolymer Latex-Particles Using Dynamic Light-Scattering and Adsorption-Isotherm Measurements, Journal of Colloid and Interface Science, 169 (1995) 39-47.

[127] W. Brown, J.X. Zhao, Adsorption of Sodium Dodecyl-Sulfate on Polystyrene Latex-Particles Using Dynamic Light-Scattering and Zeta-Potential Measurements, Macromolecules, 26 (1993) 2711-2715.

[128] F. Ravera, E. Santini, G. Loglio, M. Ferrari, L. Liggieri, Effect of nanoparticles on the interfacial properties of liquid/liquid and liquid/air surface layers, Journal of Physical Chemistry B, 110 (2006) 19543-19551.

[129] S. Paria, K.C. Khilar, A review on experimental studies of surfactant adsorption at the hydrophilic solid-water interface, Advances in Colloid and Interface Science, 110 (2004) 75-95.

[130] J. Brinck, F. Tiberg, Adsorption behavior of two binary nonionic surfactant systems at the silica-water interface, Langmuir, 12 (1996) 5042-5047.

[131] J. Brinck, B. Jonsson, F. Tiberg, Kinetics of nonionic surfactant adsorption and desorption at the silica-water interface: One component, Langmuir, 14 (1998) 1058-1071.

[132] R. Abe, K. Kuno, Adsorption of Polyoxyethylated Nonylphenol on Carbon Black in Aqueous Solution, Kolloid-Zeitschrift and Zeitschrift Fur Polymere, 181 (1962) 70-&.

[133] J.M. Corkill, J.F. Goodman, J.R. Tate, Adsorption of Non-Ionic Surface-Active Agents at Graphon/Solution Interface, Transactions of the Faraday Society, 62 (1966) 979-&.

[134] F. Tiberg, Physical characterization of non-ionic surfactant layers adsorbed at hydrophilic and hydrophobic solid surfaces by time-resolved ellipsometry, Journal of the Chemical Society-Faraday Transactions, 92 (1996) 531-538.

[135] L.M. Grant, F. Tiberg, W.A. Ducker, Nanometer-scale organization of ethylene oxide surfactants on graphite, hydrophilic silica, and hydrophobic silica, Journal of Physical Chemistry B, 102 (1998) 4288-4294.

[136] L.M. Grant, T. Ederth, F. Tiberg, Influence of surface hydrophobicity on the layer properties of adsorbed nonionic surfactants, Langmuir, 16 (2000) 2285-2291.

[137] M. Schonhoff, O. Soderman, Z.X. Li, R.K. Thomas, Internal dynamics and order parameters in surfactant aggregates: A 2H NMR study of adsorption layers and bulk phases, Langmuir, 16 (2000) 3971-3976.

[138] G. Despert, J. Oberdisse, Formation of micelle-decorated colloidal silica by adsorption of nonionic surfactant, Langmuir, 19 (2003) 7604-7610.

[139] J. Oberdisse, Fragmented structure of adsorbed layer of non-ionic surfactant on colloidal silica, Physica B-Condensed Matter, 350 (2004) E913-E916.

[140] J. Oberdisse, Small angle neutron scattering and model predictions for micelle-decorated colloidal silica beads, Physical Chemistry Chemical Physics, 6 (2004) 1557-1561.

[141] D. Lugo, J. Oberdisse, M. Karg, R. Schweins, G.H. Findenegg, Surface aggregate structure of nonionic surfactants on silica nanoparticles, Soft Matter, 5 (2009) 2928-2936.

[142] R.F. Tabor, J. Eastoe, P. Dowding, Adsorption and Desorption of Nonionic Surfactants on Silica from Toluene Studied by ATR-FTIR, Langmuir, 25 (2009) 9785-9791.

[143] J.J.R. Stalgren, J. Eriksson, K. Boschkova, A comparative study of surfactant adsorption on model surfaces using the quartz crystal microbalance and the ellipsometer, Journal of Colloid and Interface Science, 253 (2002) 190-195.

[144] X. Liu, D. Wu, S. Turgman-Cohen, J. Genzer, T.W. Theyson, O.J. Rojas, Adsorption of a Nonionic Symmetric Triblock Copolymer on Surfaces with Different Hydrophobicity, Langmuir, 26 (2010) 9565-9574.

[145] D.M. Nevskaia, A. GuerreroRuiz, J.D.D. LopezGonzalez, Adsorption of polyoxyethylenic surfactants on quartz, kaolin, and dolomite: A correlation between surfactant structure and solid surface nature, Journal of Colloid and Interface Science, 181 (1996) 571-580.

[146] J. Drzymala, E. Mielczarski, J.A. Mielczarski, Adsorption and flotation of hydrophilic and hydrophobic materials in the presence of hydrocarbon polyethylene glycol ethers, Colloids and Surfaces a-Physicochemical and Engineering Aspects, 308 (2007) 111-117.

[147] P.J. Anielak, K, Adsorpion of Nonionic Surfactants on Synthetic Adsorbents, Physical Chemistry, (1990).

[148] G.P. Vanderbeek, M.A.C. Stuart, The Hydrodynamic Thickness of Adsorbed Polymer Layers Measured by Dynamic Light-Scattering - Effects of Polymer Concentration and Segmental Binding Strength, Journal De Physique, 49 (1988) 1449-1454.

[149] P.W. Holloway, Simple Procedure for Removal of Triton X-100 from Protein Samples, Analytical Biochemistry, 53 (1973) 304-308.

[150] T.M. Allen, A.Y. Romans, H. Kercret, J.P. Segrest, Detergent Removal during Membrane Reconstitution, Biochimica Et Biophysica Acta, 601 (1980) 328-342.

[151] A.S. Michaels, New Separation Techniques for the CPI, Chemical Engineering Progress, 64 (1968).

[152] M.C. Porter, Concentration Polarization with Membrane Ultrafiltration, Industrial & Engineering Chemistry Product Research and Development, 11 (1972) 234-&.

[153] H. Schott, Ultrafiltration of Nonionic Detergent Solutions, Journal of Physical Chemistry, 68 (1964) 3612-&.

[154] M. Schwarze, D.K. Le, S. Wille, A. Drews, W. Arlt, R. Schomacker, Stirred cell ultrafiltration of aqueous micellar TX-100 solutions, Separation and Purification Technology, 74 (2010) 21-27.

[155] J.S. Yang, K. Baek, J.W. Yang, Crossflow ultrafiltration of surfactant solutions, Desalination, 184 (2005) 385-394.

[156] J.H. Markels, S. Lynn, C.J. Radke, Cross-Flow Ultrafiltration of Micellar Surfactant Solutions, Aiche Journal, 41 (1995) 2058-2066.

[157] A.A. Mungray, S.V. Kulkarni, A.K. Mungray, Removal of heavy metals from wastewater using micellar enhanced ultrafiltration technique: a review, Central European Journal of Chemistry, 10 (2012) 27-46.

[158] R. Urbanski, E. Goralska, H.J. Bart, J. Szymanowski, Ultrafiltration of surfactant solutions, Journal of Colloid and Interface Science, 253 (2002) 419-426.

[159] H. Byhlin, A.S. Jonsson, Influence of adsorption and concentration polarisation on membrane performance during ultrafiltration of a non-ionic surfactant, Desalination, 151 (2003) 21-31.

[160] V.A.K. Anthati, K.V. Marathe, Selective Separation of Copper (Ii) and Cobalt (Ii) from Wastewater by Using Continuous Cross-Flow Micellar-Enhanced Ultrafiltration and Surfactant Recovery from Metal Micellar Solutions, Canadian Journal of Chemical Engineering, 89 (2011) 292-298.

[161] D. Doulia, I. Xiarchos, Ultrafiltration of micellar solutions of nonionic surfactants with or without alachlor pesticide, Journal of Membrane Science, 296 (2007) 58-64.

[162] A.S. Jonsson, B. Jonsson, H. Byhlin, A concentration polarization model for the ultrafiltration of nonionic surfactants, Journal of Colloid and Interface Science, 304 (2006) 191-199.

[163] Y. Kaya, C. Aydiner, H. Barlas, B. Keskinler, Nanofiltration of single and mixture solutions containing anionics and nonionic surfactants below their critical micelle concentrations (CMCs), Journal of Membrane Science, 282 (2006) 401-412.

[164] I. Xiarchos, D. Doulia, Interaction behavior in ultrafiltration of nonionic surfactant micelles by adsorption, Journal of Colloid and Interface Science, 299 (2006) 102-111.

[165] M. Henschke, L.H. Schlieper, A. Pfennig, Determination of a coalescence parameter from batch-settling experiments, Chemical Engineering Journal, 85 (2002) 369-378.

[166] T. Voeste, K. Weber, B. Hiskey, G. Brunner, Liquid–Solid Extraction, in: Ullmann's Encyclopedia of Industrial Chemistry, Wiley-VCH Verlag GmbH & Co. KGaA, 2000.

[167] M. Henschke, Dimensionierung liegender Flüssig-flüssig Abscheider anhand diskontinuierlicher Absetzversuche, Fortschritt-Berichte VDI, Reihe 3 (Verfahrenstechnik), Nr. 379, VDI Verlag, Düsseldorf, 1995.

[168] Y. Zimmels, Sedimentation, in: Ullmann's Encyclopedia of Industrial Chemistry, Wiley-VCH Verlag GmbH & Co. KGaA, 2000.

[169] S.A.K. Jeelani, R. Hosig, E.J. Windhab, Kinetics of low Reynolds number creaming and coalescence in droplet dispersions, Aiche Journal, 51 (2005) 149-161.

[170] S. Samanta, P. Ghosh, Coalescence of bubbles and stability of foams in aqueous solutions of Tween surfactants, Chemical Engineering Research & Design, 89 (2011) 2344-2355.

[171] D. Rautenberg, E. Blaß, Koaleszenz von Einzeltropfen an geneigten Platten in Flüssigkeiten, Chemie Ingenieur Technik, 55 (1983) 643-643.

[172] H.W. Brandt, K.-H. Reissinger, J. Schröter, Moderne Flüssig/Flüssig-Extraktoren–Übersicht und Auswahlkriterien, Chemie Ingenieur Technik, 50 (1978) 345-354.

[173] E. Müller, R. Berger, E. Blass, D. Sluyts, A. Pfennig, Liquid–Liquid Extraction, in: Ullmann's Encyclopedia of Industrial Chemistry, Wiley-VCH Verlag GmbH & Co. KGaA, 2000.

[174] K.-H. Reissinger, J. Schröter, W. Bäcker, Möglichkeiten und Probleme bei der Auslegung von Extraktoren, Chemie Ingenieur Technik, 53 (1981) 607-614.

[175] E.U. Schlünder, F. Thurner, Destillation, Absorption, Extraktion, Georg Thieme Verlag, Stuttgart, 1986.

[176] M. Bohnet, Separation of Immiscible Liquids, Chemie Ingenieur Technik, 48 (1976) 177-189.

[177] L. Schlieper, M. Chatterjee, M. Henschke, A. Pfennig, Liquid-liquid phase separation in gravity settler with inclined plates, Aiche Journal, 50 (2004) 802-811.

11 Appendix

## 11.1 Opitmization of the Continous Magnetic Extraction

The optimum process parameters for the operation of the CME were determined by a Design of Experiments (DoE) approach in order to optimize the surfactant and particle separation efficiency. From these boundary conditions a matrix was created for the selected process parameters T_S, $\dot{V}_I$ and C_R. Magnetic extraction experiments were performed with the process parameters from Table 11.1 and the separation efficiencies S_S and S_P have been determined. Table 11.1 summarizes the factors and results from the DoE experiments.

Table 11.1: Defined factors and responses from the DoE experiments. S_S and S_P have been calculated according Equations 7.5 and 7.6.

Factors			Responses	
T_S [°C]	$\dot{V}_I$ [L/h]	C_R*100 [%]	S_S [%]	S_P [%]
30	9[a]	33	93,8	99,3
30	5,4	33	97,7	99,7
30	15	33	88,9	93,3
30	9	20[b]	90,8	97,5
40	9	20	93,7	97,7
30	5,4	12,5	91,4	98,1
30	15	12,5	86,1	89,3
35	9	33	97,3	99,6
35	5,4	20	96,6	99,9
35	15	20	92,8	94,9
35	9	12,5	92,9	99,1
40	5,4	12,5	96,8	99,9
40	15	12,5	90,7	95,4
40	5,4	33	98,3	99,9
40	15	33	95,5	96,5
35	9	20	92,7	98,5
35	9	20	92,3	98,3
35	9	20	92,4	98,2

[a]the initially $\dot{V}_I$ prescribed by the DoE software has been adjusted from 10.5 L/h to 9 L/h; [b]the initially C_R prescribed by the DoE software has been adjusted from 22.75 to 20. This adjustment, however, was taken into account when the evaluation of the results was done.

A multilinear regression (MLR) on S_R and S_P was performed using the software MODDE Umetrics Inc., San Jose, US-CA). The main parameters were identified and the parameters with insignificant influence were eliminated. The goodness of the fit was $R^2_{S,P}$=0.8 and $R^2_{S,S}$=0.84 respectively. The according response plots for the particle separation efficiency and surfactant separation efficiency can be seen in Figure 11.1 and Figure 11.2. The goodness of prediction which estimates the predictive power of the model was calculated to $Q^2_{S,P}$=0.6 and $Q^2_{S,S}$=0,73. The numbers indicate that, although the DoE model is based on linear and quadratic correlations between the chosen factors, the model provides satisfying insight for a prediction of the separation efficiencies in the examined range.
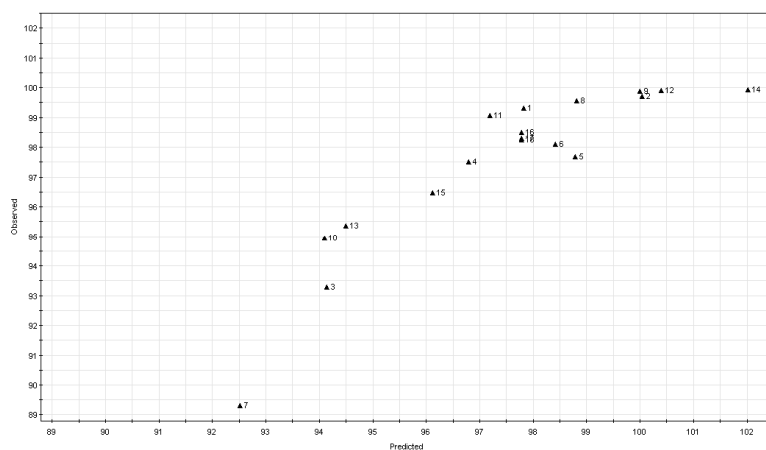
Figure 11.1: Response plot for the particle separation model.
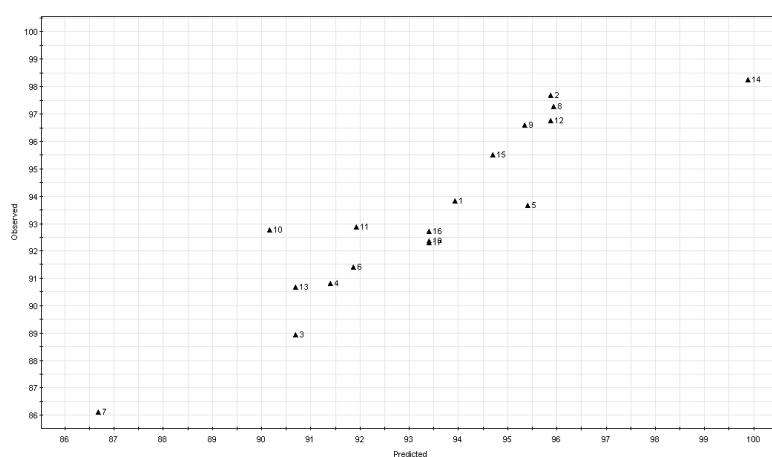
Figure 11.2: Response plot for the surfactant separation model.

Figure 11.3 and Figure 11.4 show the resulting contour plots for S_S and S_P. Both plots exhibit the same trends.
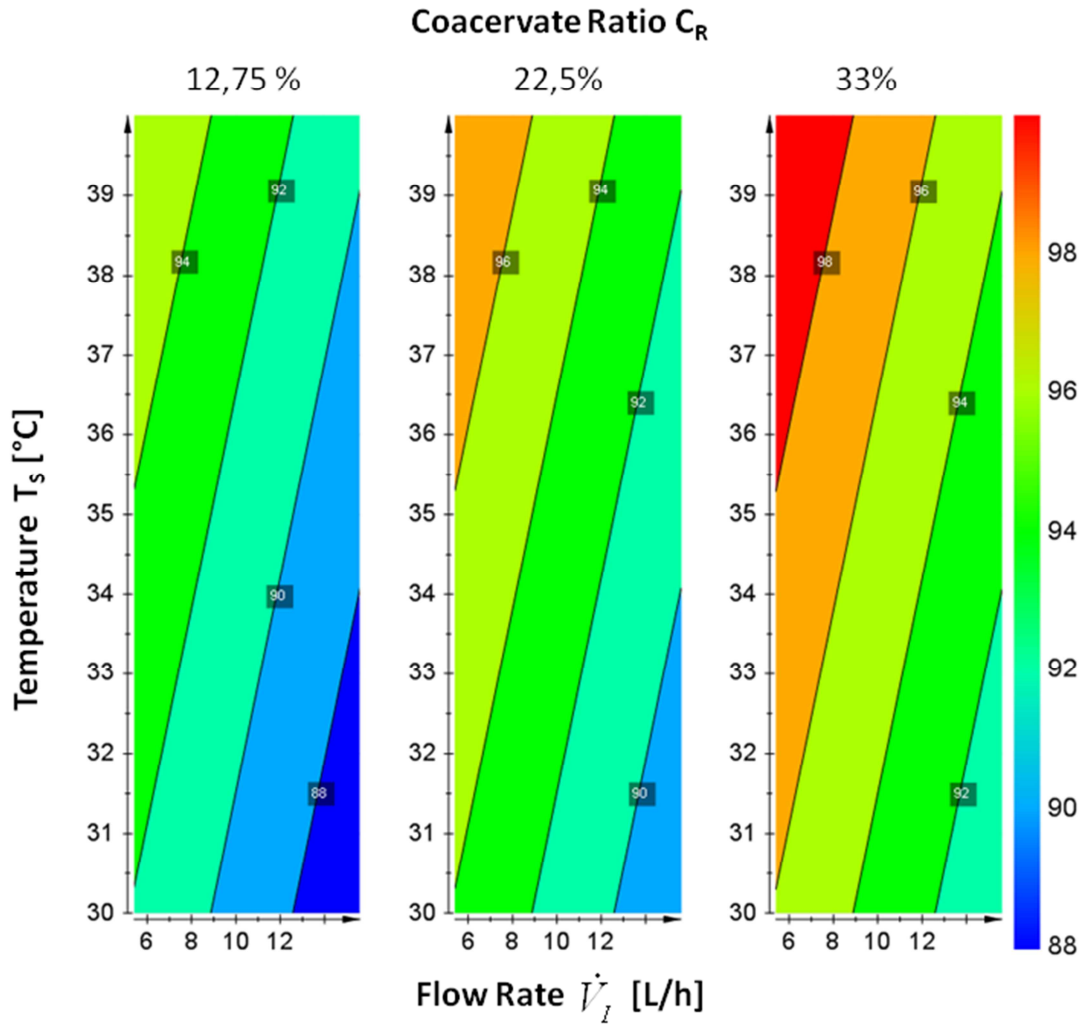
Figure 11.3. Prediction plot of the surfactant separation efficieny in the magnetic extractor calculated by the DoE software MODDE. The correlation between T_S, $\dot{V}_I$ and C_R is linear and can be described the equation: $S_P=2.03\ T_S -2.75\dot{V}_I +2.04C_R$
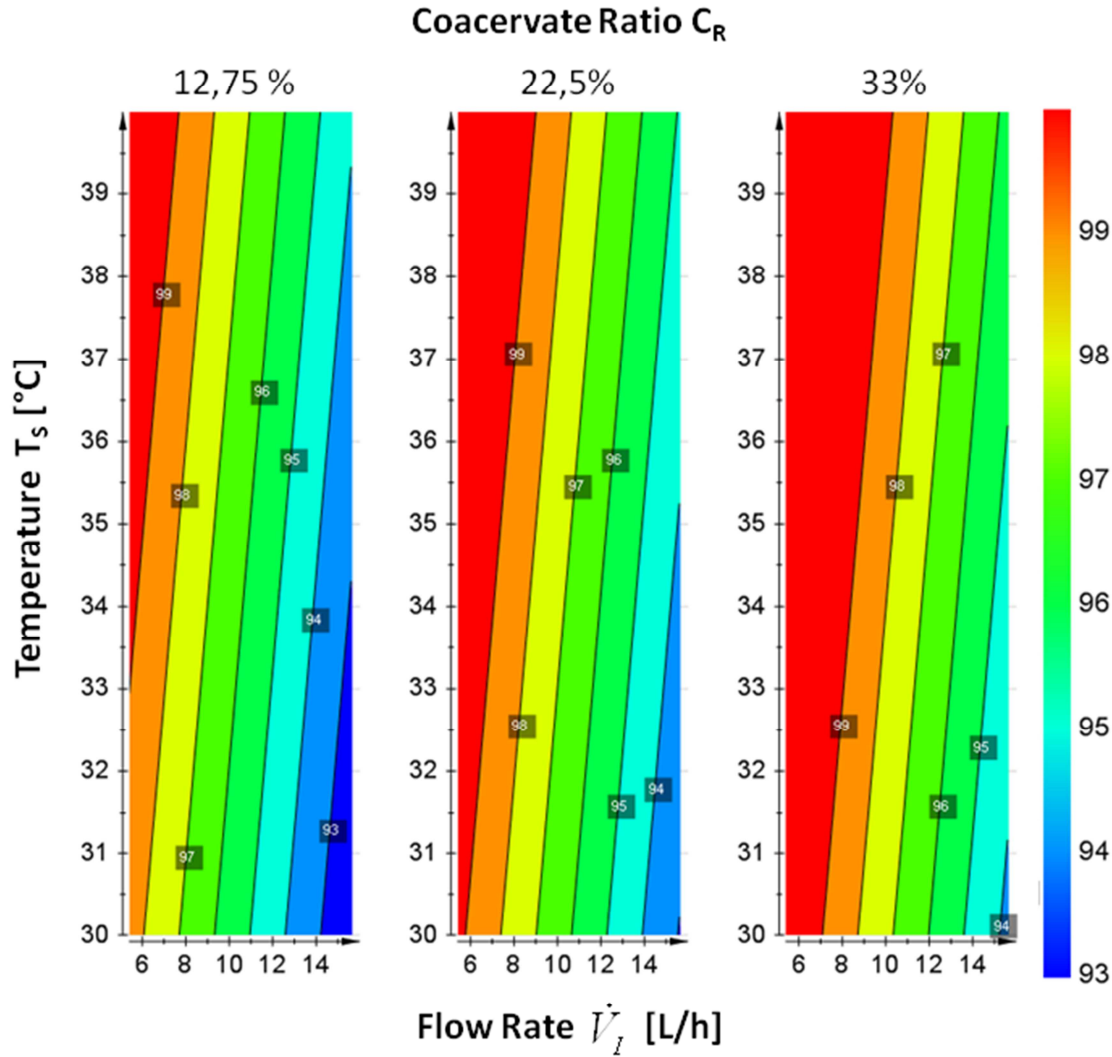
Figure 11.4. Prediction plot of the particle separation efficieny in the magnetic extractor generated by the DoE software MODDE. The correlation between T_S, $\dot{V}_I$ and C_R is linear and can be described the equation $S_S=0.99T_S -3.13\dot{V}_I +0.81C_R$

The dependency of the separation efficiencies with respect to C_R, T_S and $\dot{V}_I$ can be described by the following equations:

$$S_P=0.99T_S + 0.81C_R - 3.13\,\dot{V}_I \tag{Eq. 11.1}$$

$$S_S=2.03T_S + 2.04C_R - 2.75\,\dot{V}_I \tag{Eq. 11.2}$$

From the equations it can be seen that, while the impact of $\dot{V}_I$ is practically equal for S_S and S_P the impact of T_S and C_R is stronger on S_S than on S_P. This may be attributed to the fact, that the particles are directly influenced by the magnetic field, thus reducing the importance of other parameters. Yet, in both cases, the separation efficiencies are mostly

influenced by the flow rate. Elevated temperatures are favourable for the process, however, it is likely that increasing T_S is unfavourable in terms of thermal stability of a target protein. An increase in the C_R also leads to an increase of S_S and S_R. But the increase of C_R coincidently reduces $\dot{V}_B$, which in the case of the elution step, will lead to increased product loss. Nevertheless, the results show that a S_P of >99.9% can be achieved and the magnetic extractor can be operated continuously at several liters per hour. The choice of the process parameters has conclusively to be a compromise between loss of surfactant and particles and yield of the target protein.

11.2 Quantification of Eumulgin ES by means of Spectophotometry

In Figure 11.5 the absorbance at 213 nm is plotted versus the Eumulgin ES concentration. The relationship between concentration and absorbance is linear. Following Lambert-Beer´s Law the molar absorbance coefficient can be calculated to: $\varepsilon_{\lambda=216}$=17.9 L mol^{-1} cm^{-1}, respectively $\varepsilon_{\lambda=216}$=0.03 L g^{-1} cm^{-1}.
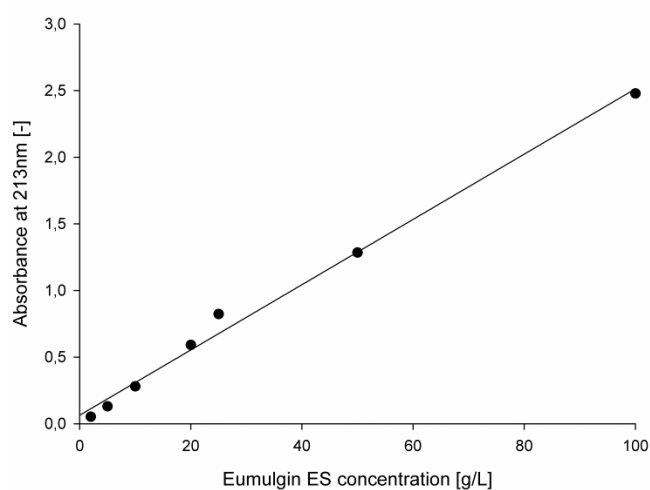
Figure 11.5. Absorbance of Eumulgin ES vs concentration. The relation is linear following Lambert Beer´s Law.

For concentrations of Eumulgin ES below 200 mg/L, the absorbance at 213 nm increases drastically, as can be seen in Figure 4.
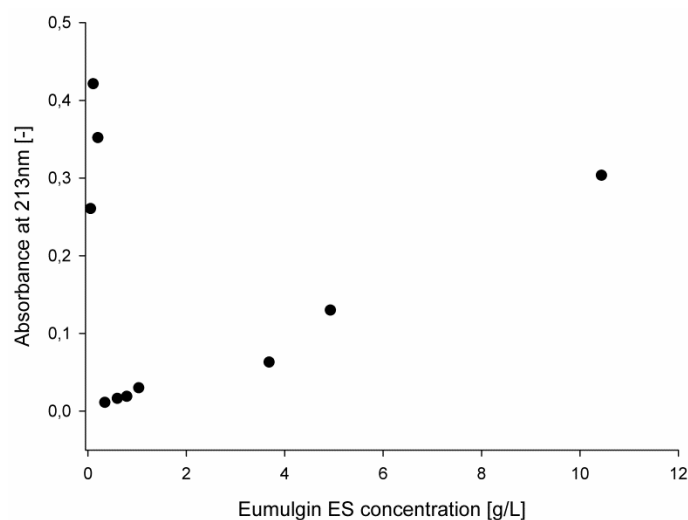
Figure 11.6. Absorbance of Eumulgin ES at concentrations from 0.005% to 1.1%. At 0.02%wt, the absorbance of Eumulgin ES increases drastically.

The phenomenon occurs at a concentration which is 50 times the cmc determined by measuring the decline of the surface tension (results shown in chapter 8.4.1). According to the theory of cmc determination by measuring the surface tension, at these concentrations the air-liquid surface is covered with surfactant molecules and micelles start to form. The observed effect may then either be explained by a structural change in the micelle structure or shape, or the minimum in absorbance may be related to the moment where micelles being to form, although it is 50 times the cmc determined by the surface tension method.

11.3 Influence of Eumulgin ES onto Protein Quantification

The total protein concentration was determined by a micro bichinoninic acid (BCA) assay kit (Pierce, Rockford, US-IL) with the usage of an automated robotic station Cobas Mira (Roche Diagnostics, Basel, CH). In order to establish reliable protein quantification, the influence of Eumulgin ES onto the absorbance has been investigated. In Figure 11.7, the change of the absorbance signal for increasing Eumulgin ES concentration in the assay buffer was investigated.
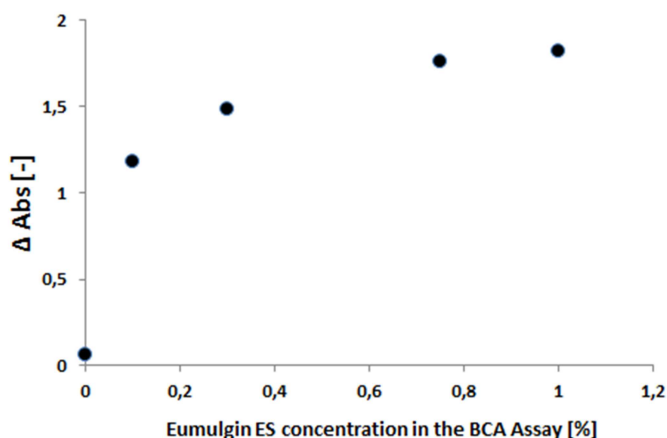
Figure 11.7. Change of Absorbance in the BCA Assay from the addition of Eumulgin ES to the Assay Reagent

As can be seen, the addition of Eumulgin ES leads to a drastic increase in the absorbance. This change in absorbance makes the determination of the protein concentration of a sample containing an unknown Eumulgin ES concentration difficult. The course of the change, however, reaches saturation at Eumulgin ES concentrations above 1 %. For this reason, 1 % Eumulgin ES was added to the BCA assay buffer. The determination of the total protein was therefore always performed in the region above saturation. Although the total absorbance in this region is above 1.5, the automatic robotic station allowed reliable quantification of protein concentrations.

11.4 Abbreviations

Abbreviation	Meaning
Abs	Absorbance
ADH	Alcohol Dehydrogenase
AFM	Atomic Force Microscopy
AMTPS	Aqueous Micellar Two-phase System
ATPE	Aqueous Two-phase Extraction
ATPS	Aqueous Two-phase System
ATR	Attenuated Total Reflectance
BSA	Bovine Serum Albumin
cf.	compared for
CME	Continuous Magnetic Extraction
CPE	Cloud Point Extraction
DNA	Desoxyribonucleic acid
DoE	Design of Experiments
DTAB	Dodecyltrimethylammonium Bromide
DTU	Technical University of Denmark
E. coli	Escherichia coli
FTIR	Fourier Transfrom Infrared Spectroscopy
GFP	Green Fluorescent Protein
HGMF	High Gradient Magnetic Fishing
HGMS	High Gradient Magnetic Separation
IgG	Immunoglobulin G
kDa	kilo Dalton
ME	Magnetic Extraction
MEC	Magnetic Field Enhanced Centrifuge
MEP	Magnetic Extraction Phases
MEUF	Micellar Enhanced Ultrafiltration
MLR	Multilinear Regression

MME	Micelle Mediated Extraction
MWCO	Molecular Weight Cut-off
PEG	Polyethylene Glycol or Polyethylene Oxide
QCM-D	Quartz Crystal Microbalance with Dissipation
SDS	Sodium Dodecyl Sulfate
TOC	Total Organic Carbon
UF	Ultrafiltration
UV-VIS	Ultraviolet-visible

11.5 Symbols

11.5.1   Phyisical Constants

μ_0	$1.257*10^{-6}$ V s A^{-1} m^{-1}	permeability constant of the vacuum
g	9.807 m s^{-2}	gravitational constant
k	$1.38065 * 10^{-23}$ J K^{-1}	Boltzman constant

11.5.2   Latin Symbols

A	m^2	area
B	T	magnetic flux density
B_{sub}	T	magnetic flux density in a substance
B_{vac}	T	magnetic flux density in vacuum
C	J	attractive intermicellar free energy
c	kg/L	concentration
C	kg s cm^{-2}	mass sensitivity constant
c*	kg/L	equilibrium concentration
c_B	kg/L	bulk concentration
c_P	kg/L	particle concentration
d	m	diameter

D	$m^2\,s^{-1}$	diffusion coefficient
D	-	dissipation
D_M	-	demagnetisation factor
d_P	m	pore diameter
E	J	energy
F	J	free (interfacial) energy
f	s^{-1}	frequency
F_B	N	buoyant force
F_F	N	frictional force
F_G	N	gravitational force
F_M	N	magnetic force
G	J	Gibbs energy
H	$A\,m^{-1}$	magnetic field strength
H_C	$A\,m^{-1}$	coecitive field strength
J	T	magnetic polarisation
J	$m\,s^{-1}$	flux
J_S	T	saturation polarization
K	-	partitioning coefficient
K_{HR}	-	correction factor according to Hadamard and Rybcynski
K_L	g/L	Langmuir constant
M	$A\,m^{-1}$	magnetisation
m	kg	mass
M_P	$A\,m^{-1}$	particle magnetisation
n		overtone
N	mol	amount of substance
p	$N\,m^{-2}$	pressure
q	kg/kg	loading
q^*	kg/kg	equilibrium loading
q_0	kg/kg	initial loading
q_{max}	kg/kg	maximum loading

R	-	volume ratio
R	m	radius
t	m	film thickness
T	K	absolute temperature
T	°C	temperature
T_C	°C	lower consolute critical temperature
t_{Eff}	m	effective film thickness
v	$m\ s^{-1}$	velocity
V_P	m^3	particle volume
v_{st}	m/s	velocity of a particle calculated by the Stokes´law
w	-	mass fraction

11.5.3   Greek Symbols

$\Delta\mu$	J	free energy advantage from for micellar growth
μ_R	-	magnetic material dependent permeability
δ	m	thickness of a gel layer adjacent to a membrane
ε	-	hold-up
ε	$L\ g^{-1}\ cm^{-1}$	molar absorption coefficient
η	$kg\ m^{-1}\ s^{-1}$	dynamic viscosity
κ	-	magnetic volume susceptibility
λ	nm	wavelength
σ	$J\ m^{-2}$	interfacial tension / interfacial energy
τ	-	tortuosity
ϕ	-	volume fraction
χ	m	channel length trough a membrane
χ	-	mole fraction
ρ	$kg\ m^{-3}$	density

11.6 Indices

*	thermodynamic equilibrium
0	Initial
Ads	adsorption
aq	aqueous phase
B	buoyancy
B	bottom phase
B	bulk
C	coercitive
c	convection
c	continuous phase
C	critical
co	coacervate phase
d	diffusion
d	disperse phase
Eff	effective film
EV	excluded volume
EV	excluded volume
G	gravity
g	gel
HR	Hadamard, Rybcynski
i	intrinsic
i	initial
M	magnetic
mat	matter
max	maximum
P	pore
PB	particle-bottom

PT	particle-top
R	remanence
R	friction
S	saturation
sub	substance
T	top phase
TP	top-bottom
V	volumetric
vac	vacuum

12 Curriculum Vitae

INGO FISCHER

*18. August 1982 in Pforzheim

AUSBILDUNG

06/2009- 09-2012	**Karlsruher Institut für Technologie (KIT)**
	Anfertigung einer Dissertation über das Thema „Design and Application of Continuous Magnetic Extraction" unter Prof. Dr. –Ing. Matthias Franzreb
10/2003 – 03/2009	**Universität Karlsruhe (TH)**
	Studium der Fachrichtung Bioingenieurwesen, Abschlussnote 1,8
	Diplomarbeit über das Thema: „Untersuchung der mikrobiellen Gemeinschaft auf marinen Schwämmen (Porifera) mittels Denaturierender Gradienten Gelelektrophorese" unter Prof. Dr. Christoph Syldatk
	Hauptfächer: Bioverfahrenstechnik, Technische Biologie
1994 - 2002	**Lise-Meitner Gymnasium, Königsbach**
	Abschluss: Allgemeine Hochschulreife, Abschlussnote: 1,8
	Leistungskurse: Englisch, Biologie

AUSLANDSAUFENTHALTE

02 – 04 / 2012	**University of Birmingham**
	Sechswöchiger Gastforscheraufenthalt im Rahmen der Dissertation im Department for Biochemical Engineering unter Prof. O.R.T Thomas

PRAKTIKA

10 / 2006 – 03 / 2007	**Mitenyi Biotec, Bergisch Gladbach**
	Department R&D Reagents
	Abteilung für rekombinante Proteine

PERSÖNLICHE WEITERBILDUNGSMAßNAHMEN

11/2011   **Grundlagen der Mitarbeiterführung**

07/2011   **Lab View –Core 1**

04/2011   **Scientific Presentation**

11/2010   **Grundlagen des Projektmanagements**

BISHER AUS DER PROMOTION HERVORGEGANGENE VERÖFFENTLICHUNGEN

AUFSÄTZE IN ZEITSCHRIFTEN

Partitioning behavior of silica-coated nanoparticles in Aqueous Micellar Two-Phase Systems: Evidence for an adsorption driven mechanism from QCM-D and ATR-FTIR measurements - Fischer, I., Morhardt, C., Heissler, S., Franzreb, M (2012), Langmuir 28(45): 15789-15796

Nanoparticle Mediated Protein Separation in Aqueous Micellar Two-Phase Systems - Fischer I., Franzreb. M. (2010), Solvent Extraction and Ion Exchange 30 (2012), 1-16

Magnetische Extraktion – Ein neuartiger Ansatz zur technischen Aufreinigung von Biomolekülen durch magnetische Nanopartikel - Fischer I., Franzreb. M. (2012), Chemie Ingenieur Technik, 84, 1291-1292.

Determination of the Composition of Aqueous Micellar Two-phase Systems (AMTPS) Using Potentiometric Titration - A Rapid Tool for Detergent-based Bioseparation - Fischer, I., Franzreb, M. (2010), Colloids and Surfaces A: Physicochemical and Engineering Aspects 377 (2011), 1-3, 97-102

KONFERENZ BEITRÄGE

Continous Magnetic Extraction - A novel method for the large-scale separation of functional magnetic nanosorbents- Fischer, I. Franzreb, M. – ESBES+ISPPP2012, Istanbul, Türkei**,**

Magnetische Extraktion - Ein neuartiger Ansatz zur technischen Aufreinigung von Biomolekülen durch magnetische Nanopartikel – Fischer, I., Franzreb, M., Dechema Jahrestagung 2012, Karlsruhe

Magnetic Extraction – Magnetic Particle Mediated Protein Separation in Aqueous Micellar Two Phase – Fischer, I., Franzreb, M., Dechema Himmelfahrtstagung 2012, Freiburg

Magnetic Extraction – Magnetic Particle Mediated Protein Separation in Aqueous Micellar Two Phase Systems - Fischer, I., Franzreb, M., Biopartitioning and Purification 2011, Puerto Vallarta, Mexiko

POSTER   **Magnetic Extraction – Magnetic Particle Mediated Protein Separation in Aqueous Micellar Two Phase Systems** – Fischer, I., Franzreb, M., ECAB 2011, Berlin

Einfluss der Tensidsorption an Grenzflächen auf das Verteilungsverhalten nanoskaliger Biosorbentien in wässrigen mizellaren Zweiphasensystemen - Fischer, I., Morhardt, C. Franzreb, M., Dechema Himmelfahrstagung 2011, Potsdam

Advanced Magnetic nano-particles deliver smart Processes and Products for Life – Franzreb, M., Cerff, M., Fischer, I., Lindner, J., Müller, T., Scholz, A., Nanofutures 2010, Portugal